CHEMISTRY DIVISION
ANNUAL PROGRESS REPORT
FOR PERIOD ENDING MAY 20, 1970

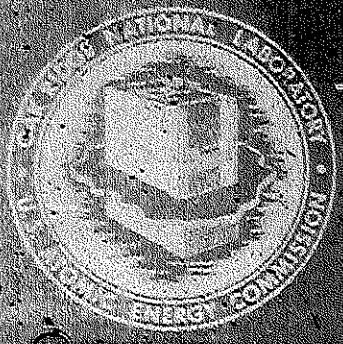

OAK RIDGE NATIONAL LABORATORY
operated by
UNION CARBIDE CORPORATION
for the
U.S. ATOMIC ENERGY COMMISSION

BLANK PAGE

Printed in the United States of America. Available from Clearinghouse for Federal Scientific and Technical Information, National Bureau of Standards, U.S. Department of Commerce, Springfield, Virginia 22151
Price: Printed Copy $3.00; Microfiche $0.65

BLANK PAGE

CHEMISTRY DIVISION ANNUAL PROGRESS REPORT
May 20, 1968
ORNL-4306

Errata

P. 2, 1st column, line 6:

To sentence ending "$\sigma(^{237}Np) = 1.2$ mb", add "for the production of ^{236}Pu."

P. 2, 1st column, last line:

For "$I(^{43}Nb)$" read "$I(^{93}Nb)$".

P. 2, 2nd column, line 4:

For "$I(^{94}Nb) = 122 \pm 10$ barns", read "$I(^{94}Nb) = 142 \pm 10$ barns.

P. 75, 1st column, Eq. (8):

For the numerical constant "0.606" on the right hand side, read "0.303".

P. 75, 1st column, line 3 from bottom:

For "0.88" read "1.76".

P. 75, 1st column, last line:

Delete remainder of paragraph with sentence beginning "This 'discrepancy' is a ..."

P. 108, 1st column, line 17 from bottom:

For "enhanced solubility" read "enhanced insolubility".

P. 110, 2nd column, Eq. (3):

Should read

$$\frac{\partial C_o(\underline{x},\underline{t})}{\partial \underline{t}} = D_o \frac{\partial^2 C_o(\underline{x},\underline{t})}{\partial \underline{x}^2} - \frac{\underline{j}_o}{\underline{n}F\delta} \cdot \frac{C_o(\underline{x},\underline{t})}{C_o^0}$$

P. 111, 2nd column, line 2 above Eq. (9):

For "$[\Delta\phi(x)]$" read "$[\Delta\Phi(x)]$".

NOTICE

The attached is an expanded table of contents for ORNL-4306

Titles of Individual Reports in Chemistry Division Annual Progress Report for Period Ending May 20, 1968, ORNL-4306

*This contribution will be found in sect. 2, "Chemistry and Physics of Transuranium Elements."

*This contribution will be found in sect. 2, "Chemistry and Physics of Transuranium Elements."

†A report based on work performed in the Chemistry Division under the Water Research Program.

*This contribution will be found in sect. 2, "Chemistry and Physics of Transuranium Elements."

ORNL-4306

Contract No. W-7405-eng-26

CHEMISTRY DIVISION ANNUAL PROGRESS REPORT

for Period Ending May 20, 1968

E. H. Taylor, Director
Sheldon Datz, Associate Director
Ralph Livingston, Associate Director
B. H. Ketelle, Assistant Director

G. E. Moore, Editor of Annual Report

SEPTEMBER 1968

OAK RIDGE NATIONAL LABORATORY
Oak Ridge, Tennessee
operated by
UNION CARBIDE CORPORATION
for the
U. S. ATOMIC ENERGY COMMISSION

BLANK PAGE

Reports previously issued in this series are as follows:

ORNL-2386	Period Ending June 20, 1957
ORNL-2584	Period Ending June 20, 1958
ORNL-2782	Period Ending June 20, 1959
ORNL-2983	Period Ending June 20, 1960
ORNL-3176	Period Ending June 20, 1961
ORNL-3320	Period Ending June 20, 1962
ORNL-3488	Period Ending June 20, 1963
ORNL-3679	Period Ending June 20, 1964
ORNL-3832	Period Ending May 20, 1965
ORNL-3994	Period Ending May 20, 1966
ORNL-4164	Period Ending May 20, 1967

Contents

*This contribution will be found in sect. 2, "Chemistry and Physics of Transuranium Elements."

*This contribution will be found in sect. 2, "Chemistry and Physics of Transuranium Elements."

†A report based on work performed in the Chemistry Division under the Water Research Program.

*This contribution will be found in sect. 2, "Chemistry and Physics of Transuranium Elements."

Introduction

A problem that arises in any report such as this is how much and in what way it should be organized. It should be helpful to the reader if similar work is reported together, but then the question arises as to what aspect of similarity should be controlling. Should all spectroscopy appear together or all work on the heavy elements, spectroscopy included? Traditionally, this report has been organized mostly by subfields of chemistry, Radiation Chemistry and Nuclear Chemistry, for example, but some sections have reflected an organizational grouping around a common objective, as exemplified recently in Isotope Chemistry and earlier in Reactor Chemistry. Research based on particular techniques, such as optical spectroscopy, calorimetry, ESR, and others have usually been collected under Chemical Physics, although in some cases the motivation has been the controlling factor, and spectroscopy employed to predict or understand isotopic separation factors has been placed with Isotope Chemistry.

No inspiration to resolve this dilemma has appeared this year, even with a new editor, but calling attention to it may of itself assist readers in locating topics of interest. We hope the somewhat fuller use of cross reference in the Table of Contents will be useful for the same purpose. A change from last year's report is the inclusion of a ninth section for contributions from the now-flourishing Transuranium Research Laboratory. These appeared last year under Nuclear Chemistry and Chemical Physics. This year, they drag with them some coauthors whose normal place is in another section.

Some collaborative work with other divisions and some work supported by agencies other than AEC are described here either only in outline or not at all. One can find record of these contributions by Chemistry Division staff in the list of publications, and, of course, they are covered more fully in other reports. Similarly, review articles and other publications based on earlier work appear only in that list.

The report is not closely edited for uniformity of style and scope, but we hope that it covers the work of the Division at a level somewhere between a collection of abstracts and a collection of journal articles. Topics not yet ready for publication are normally covered somewhat more fully than others. We know from their suggestions that some readers would appreciate fuller coverage even of our completed work in order to get around publishing delays and the difficulty (for some) of obtaining journals. This has never been practical, however, and it is rapidly becoming less so. Particularly in nuclear physics, but also in many other fields, the rate of acquisition of useful data has become so great that every subject investigated results in a relatively large publication. The series of abstracts reported under Nuclear Chemistry illustrates this trend. The availability of fast computers compounds this problem; they make it possible efficiently to extract much more information from the same data than was formerly possible. When rapid acquisition of data and rapid data treatment are combined, as in nuclear physics or in diffraction, the result is almost frightening.

The year being reported is the first one throughout which the Transuranium Research Laboratory was in operation. Both the chemical and the nuclear side of the program have made interesting starts. For example, an aqueous solution of a curium complex ion (β-diketone) showed fluorescence that indicated the presence of energy levels probably suitable for laser action. Preparations are under way to exploit this if possible. And, on the nuclear side, two new isotopes of neptunium, ^{229}Np and ^{230}Np, were discovered and partially characterized. In general, facilities for the preparation and analysis of compounds of these elements are adequate, and studies of them by optical spectroscopy and by x-ray dif-

fraction are well started. Thermochemical measurements will be started shortly, and equipment for magnetic studies is being assembled. The high-resolution conversion-electron spectrometer is ready except for a coolant booster pump, and the magnetic mass separator is contracted for.

Although not blessed with such obvious new opportunities as the research on transuranium elements, our other programs continue to broaden and refine our knowledge of chemistry and sometimes turn up wholly new observations. Thus the scattering of fast potassium ions or atoms by D_2 was found to lead to vibrational excitation, dissociation, and ionization. In Radiation Chemistry, a restudy, with modern techniques, of a classic research on the radiolysis of aliphatic acids is producing very detailed results that should improve our understanding of energy transfer. In the field of solution chemistry, measurements and computation are being applied to solutions of two or more solutes. Improved systematization of our knowledge, if not improvement of our understanding, is already apparent. Two programs concerned with the same old substance, water, are producing data of exceptional range and quality, and are at the stage where we shall soon see how far interpretation can be carried. The measurements are of x-ray diffraction and of near-infrared absorption over a wide range of temperature; they include not only water but other liquids and solutions. The generality of photolysis (with additives) for the production of organic free radicals is obvious in the ever-widening range of radicals for which ESR spectra are being obtained and interpreted.

As mentioned last year, it seems useful to call attention here to those items which have some present or potential applicability to other fields. We note, therefore, the following: (1) The continuing development of dynamically formed membranes under the auspices of the Office of Saline Water. Further work has been done on membrane-forming materials, on supports, and on applications to pollution; such membranes have also been used to test theoretical equations developed earlier to describe membrane behavior. (2) Both processes for separation of ^{13}C continue to look promising, and an old ghost, a liquid-liquid process for uranium isotope separation, was laid to rest again. (3) The low-background gamma-ray spectrometer for study of returned moon samples was completed, shipped to Houston, and found to be indeed the world's lowest-background spectrometer.

To some, at least, of the "original" members of the Division, the Laboratory is still a temporary collection of young physicists, chemists, and engineers who will disperse some day soon to the normal world of university and industrial positions. It is implausible, therefore, that one of us has now retired, but this is the case. Since Max Bredig has edited this report for many years, I should like to take note here of his many services to the Division, to the Laboratory, and to the science of chemistry. It is fortunate that his retirement is only an administrative discontinuity, for his chemical knowledge, judgment, and insight are irreplaceable.

1. Nuclear Chemistry

THE NEUTRON CAPTURE THERMAL CROSS SECTION AND RESONANCE INTEGRAL OF ^{252}Cf

J. Halperin C. E. Bemis, Jr.
J. R. Stokely

See p. 22.

THE NEUTRON CAPTURE RESONANCE INTEGRAL OF THE 6.75-DAY ^{237}U

J. Halperin J. H. Oliver
C. R. Baldock R. W. Stoughton

Measurements have been made of the resonance integral of the 6.75-day ^{237}U in irradiations in the ETR at Idaho. An integrated resonance flux-time product of $\sim 7 \times 10^{19}$ neutrons per unit lethargy was achieved in a thermal-neutron-filtered irradiation. The resonance flux was measured using thin foils of dilute cobalt-aluminum alloy and is based upon I (^{59}Co) = 75 barns.

A sample of ^{236}U containing initially 48 ppm of ^{238}U was irradiated in a 3-mm-thick cadmium cylinder until approximately half of the ^{113}Cd in the filter had been converted to ^{114}Cd. The uranium product was examined in a two-stage mass spectrometer. Singly charged uranium metal ions were produced by surface ionization from rhenium filaments and measured with a 14-stage electron multiplier. A preliminary value for I (^{237}U) of 1200 ± 200 barns can be reported.

MEASUREMENTS OF THE $(n,2n)$ CROSS SECTIONS OF ^{233}U, ^{235}U, AND ^{237}Np

J. Halperin L. E. Idom
C. R. Baldock J. H. Oliver
R. H. Rainey[1]

Two irradiations have been carried out at the ETR in Idaho to measure the integral $(n,2n)$ cross sections of ^{233}U, ^{235}U, and ^{237}Np. Due to low yields and the difficulties introduced by competing reactions, no previous measurements appear to have been made (at this late date) of these cross sections to enable the prediction of reaction rates in fission neutron spectra. The consequence of production of $(n,2n)$ products for both ^{233}U and ^{237}Np is to increase the problems associated with the handling of uranium in chemical processing and thermal diffusion plants. The formation of members of the $4n$ decay series (^{236}Pu or ^{232}U) ultimately gives rise to ^{208}Tl (2.61-Mev gamma).

The irradiations were carried out in cylindrical cadmium containers of 120-mil wall thickness. The cadmium, by filtering the thermal neutrons, served to minimize competing reactions and the high burnup which would otherwise have taken place. Since the $(n,2n)$ reactions have a threshold of approximately 6 Mev, the reaction rates of interest were unaffected by the presence of the cadmium.

Following irradiation, the uranium samples were purified by a TBP extraction procedure. The ^{233}U samples were electrodeposited on platinum plates and alpha pulse analyzed to evaluate the ^{232}U formed during the irradiation. The ^{235}U samples were assayed by mass analysis using a two-stage mass spectrometer. The ^{237}Np samples containing ^{236}Pu were assayed using a TTA (2-thenoyltrifluoroacetone) extraction procedure so that the low-specific-activity ^{237}Np could be measured in the presence of the relatively large amount of ^{238}Pu. The ^{236}Pu was determined by alpha pulse spectroscopy. The fission neutron spectrum was monitored by the (n,p) reactions in ^{46}Ti and ^{54}Fe. The 84-day ^{46}Sc and the 303-day ^{54}Mn activities were measured by gamma-ray spectroscopy. The fission flux spectrum was

[1]Chemical Technology Division.

evaluated on the basis of a 9.0- and 65-mb cross section for ^{46}Ti and ^{54}Fe respectively.[2]

At the present time preliminary values can be reported for the $(n,2n)$ cross sections of $\sigma_{n,2n}$ (^{233}U) = 3.5 mb, σ (^{235}U) = 24 mb, and σ (^{237}Np) = 1.2 mb. The neptunium cross section does not include the partial cross section leading to the formation of the >5000-year ^{236}Np, which is thought to be small.[3] The estimated uncertainty in these values is about 25%. S. Pearlstein[4] has made calculations of the values of a large number of $(n,2n)$ cross sections using a statistical model of nuclear reactions. His estimates, which may be compared with the above values, are $\sigma_{n,2n}$ (^{233}U) = 3.3 mb, $\sigma_{n,2n}$ (^{235}U) = 15 mb, and $\sigma_{n,2n}$ (^{237}Np) = 1.3 mb.

THE THERMAL NEUTRON CAPTURE CROSS SECTIONS AND RESONANCE INTEGRALS OF ^{93}Nb AND ^{94}Nb

R. E. Druschel J. Halperin

In a continuation of measurements previously reported,[5] the values for the thermal cross sections and resonance integrals of both ^{93}Nb and ^{94}Nb have been refined. Additional irradiations have been made, and more detailed treatment of the data has been carried out. The experimental procedures have been previously described[5] and need not be repeated here.

The value of the 2200-m/sec cross section σ_0 (^{93}Nb) = $1.1_5 \pm 0.1$ barns has been calculated from the measured thermal cross section assuming the usual $1/v$ dependence upon energy. This thermal value is in good agreement with that of Tattersall *et al.*,[6] $\sigma_0 = 1.17 \pm 0.2$ barns, and Pomerance,[7] $\sigma_0 = 1.10 \pm 0.5$ barns. The resonance integral was measured as I (^{93}Nb) = $9.2_5 \pm 0.6$ barns, which is somewhat larger than that reported by Schuman,[8] $I = 8.4$ barns.

Similarly the 2200 m/sec value σ_0 (^{94}Nb) = 16.8 ± 1.5 barns and I (^{94}Nb) = 122 ± 10 barns were measured in this experiment. These values may be compared with values of 5 barns and 15 ± 4 barns reported for the thermal cross section by Schuman[8] and Douglas,[9] respectively, and a value[8] of $I = 500 \pm 200$ reported for the resonance integral.

The application of ^{93}Nb and ^{94}Nb to the monitoring of neutron irradiations involving relatively high burnups is of interest due to the low neutron cross section of ^{93}Nb. However, the relatively high cross section of ^{94}Nb implies a moderate correction due to its burnup. For irradiations that are not too long compared with the 35-day ^{95}Nb, the ^{94}Nb burnup can be determined directly from the measured ^{95}Nb. For longer irradiations, the ^{94}Nb burnup can be taken into account from the cross-section parameters.

THE REACTOR CROSS SECTION OF ^{204}Tl

R. E. Druschel H. A. O'Brien[10]
J. Halperin

The reactor cross section of ^{204}Tl has been measured in an irradiation in the HFIR. Since ^{204}Tl is a pure beta emitter of relatively long half-life, its production as a power source is of some interest, and the optimization of its production is dependent upon the evaluation of its cross section.

A sample of isotopically pure ^{203}Tl had been prepared earlier in an irradiation of ^{202}Hg forming the 47-day ^{203}Hg, which had been "milked" to produce ^{203}Tl containing only 0.1% ^{205}Tl. (Natural thallium is 70% abundant in ^{205}Tl.) Thallium-204 is produced upon irradiating ^{203}Tl, and the subsequent production of ^{205}Tl gives a direct measure of the cross section of ^{204}Tl (see expression 1):

$$^{203}\mathrm{Tl}\ (n,\gamma)\ ^{204}\mathrm{Tl} \xrightarrow[3.8\ \text{years}]{\beta^-} (n,\gamma)\ ^{205}\mathrm{Tl}\ . \qquad (1)$$

[2] C. H. Hogg and L. P. Weber, "Fast-Neutron Dosimetry at the MTR-ETR Site," *Symposium on Radiation Effects and Neutron Dosimetry*, p. 133 (1962).

[3] J. R. Stehn, *Neutron Cross Sections*, BNL-325, 2d ed., Suppl. 2, Vol. III, *Z = 88 to 98* (1965).

[4] S. Pearlstein, *Nucl. Sci. Eng.* 23, 238 (1965).

[5] R. E. Druschel and J. Halperin, *Chem. Div. Ann. Progr. Rept. May 20, 1967*, ORNL-4164, p. 2.

[6] R. B. Tattersall, H. Rose, S. K. Pattendon, and D. Jowitt, *J. Nucl. Energy* A12, 32 (1960).

[7] H. Pomerance, *Phys. Rev.* 83, 671 (1951).

[8] R. P. Schuman, IDO-16760, p. 13 (1961).

[9] D. L. Douglas, A. C. McWherter, and R. P. Schuman, *Phys. Rev.* 92, 369 (1953).

[10] Isotopes Division.

Table 1.1. Cross-Section Measurement of ^{204}Tl

	Sample				Initial Sample
	1-A	1-B	2-A	2-B	
Mass analysis, %					
^{203}Tl	93.78 ± 0.05	93.85 ± 0.02	96.98 ± 0.04	97.83 ± 0.02	99.900 ± 0.002
^{204}Tl	5.81 ± 0.04	5.76 ± 0.02	2.81 ± 0.03	2.03 ± 0.02	
^{205}Tl	0.410 ± 0.020	0.393 ± 0.008		0.134 ± 0.007	0.100 ± 0.002
Thermal flux, neutrons cm^{-2} sec^{-1}	11.8×10^{14}	11.2×10^{14}	5.66×10^{14}	3.78×10^{14}	
σ_{eff} (^{203}Tl), barns	14.6	15.2	14.7	15.0	
σ_{eff} (^{204}Tl), barns	21.4	22.0		21.5	

In order to produce sufficient ^{205}Tl, in this second-order reaction, so that its determination would not be masked by the original ^{205}Tl, two capsules were irradiated in the HFIR to an integrated flux-time product of $\sim 4 \times 10^{21}$ and $\sim 1.5 \times 10^{21}$ neutrons/cm^2 respectively. Dilute samples of cobalt-aluminum alloy were used to monitor the neutron flux. Following the irradiation the thallium was chemically purified and mass analyzed.[11] The data are summarized in Table 1.1.

The effective cross sections for both ^{203}Tl and ^{204}Tl measured in the experiment are listed in the last two rows of the table. The ratio of thermal to resonance flux is estimated to be $\phi_{th}/\phi_r = 13$ in this experiment, and the effective cross section for ^{204}Tl was measured as $\sigma_{eff}(^{204}Tl) = 21.6 \pm 2$ barns. The fact that the effective cross sections for both ^{203}Tl and ^{204}Tl were constant between the two capsules implies that the ratio of ϕ_{th} to ϕ_r was also relatively constant in these irradiations. However, the resonance contribution to the ^{204}Tl cross section can be estimated to be small, since the first resonance in ^{204}Tl has been reported[12] at 123 ev.

In support of the measurement of ^{204}Tl, a remeasurement was carried out of the thermal cross section and resonance integral of ^{203}Tl. This irradiation using cadmium filters was carried out in the hydraulic tube of the ORR and irradiated to an integrated flux-time product of $\sim 2 \times 10^{20}$ neutrons/cm^2. Following the irradiation the thallium was assayed by mass analysis.[11] The value of the 2200-m/sec cross section was determined to be 11.0 ± 0.5 barns, in good agreement with the value 11.4 ± 0.9 barns reported by Pomerance.[13] The resonance integral was measured as 39.5 ± 2 barns, which is in good agreement with 40 ± 5 barns reported by Konks and Shapiro.[14]

STUDIES OF MIXING OF COLLECTIVE BANDS IN ^{152}Sm AND ^{154}Gd

L. L. Riedinger[15] Noah R. Johnson
J. H. Hamilton[16]

One test required of any model which attempts to describe collective nuclear phenomena is to find if it can adequately predict the gamma-ray branching ratios of energy levels resulting from these collective effects. The simple adiabatic model of an axially symmetric deformed nucleus has been found to be grossly inadequate in this respect.[17] Nonadiabatic coupling of the intrinsic

[11] We are grateful to R. L. Walker and D. H. Smith of the Analytical Chemistry Division for these analyses.

[12] R. P. Schuman, J. R. Berreth, and G. E. Stokes, WASH-1056, p. 94 (March 1965).

[13] H. Pomerance, *Phys. Rev.* 83, 641 (1951).

[14] V. A. Konks and F. L. Shapiro, *Soviet Phys. JETP (English Transl.)* 20, 531 (1965).

[15] Oak Ridge Graduate Fellow from Vanderbilt University under appointment from Oak Ridge Associated Universities.

[16] Vanderbilt University, Nashville, Tenn.

[17] G. Alaga, K. Alder, A. Bohr, and B. R. Mottelson, *Kgl. Danske Videnskab. Selskab, Mat.-Fys. Medd.* 29, No. 9 (1955).

and rotational motions of the nucleus causes the wave functions of the vibrational and rotational bands of states to mix, which leads to corrections in the predicted gamma-ray branching ratios. These corrections are proportional to spin-independent ratios of matrix elements, which are called mixing parameters. To avoid invoking a detailed theory to predict these matrix elements, one usually tests the above treatment by finding if a consistent set of mixing parameters can be fitted to the experimental branching ratios from the vibrational bands.

We have studied the radioactive decays of ^{152}Eu (12.4 years) and ^{154}Eu (16 years) in an attempt to determine accurately the branching ratios of members of the β- and γ-vibrational bands in the deformed daughter nuclei ^{152}Sm and ^{154}Gd. Extensive gamma-ray singles and gamma-gamma coincidence measurements have been performed using Ge(Li) and NaI detectors and 1600-, 4096-, and 20,000-channel pulse-height analyzers. Some preliminary results for these two nuclei were reported last year at this time.[18] However, further experiments involving 20- and 35-cm^3 Ge(Li) detectors (the preliminary data were taken with a 6-cm^3 detector) have yielded a more detailed picture of band mixing in these two nuclei.

In both ^{152}Sm and ^{154}Gd, we have observed the seven possible transitions from the 2^+, 3^+, and 4^+ members of the γ band to the 0^+, 2^+, and 4^+ members of the ground-state rotational band. The experimental ratios of reduced $E2$ transition probabilities [$B(E2)$ ratios] are calculated from the gamma-ray intensities. These ratios for the various levels of the γ-vibrational band are shown in column 3 of Table 1.2. Note that single primes on spins denote members of the γ band. From each experimental $B(E2)$ ratio, the mixing parameter, Z_γ, is determined and listed in column 5. This parameter describes the amount of mixing of the wave functions of the γ and ground-state bands which must be involved in order to bring agreement between the adiabatic-model prediction in column 4 and the particular experimental $B(E2)$ ratio. A constant Z_γ value for each $B(E2)$ ratio of a given nucleus would indicate that mixing of the γ and ground-state bands is sufficient to explain the $B(E2)$ ratios. However, it appears that there are small fluctuations in the various Z_γ values, especially in view of the low value determined from the $(4' \rightarrow 2)/(4' \rightarrow 4)$ ratio in ^{154}Gd. Thus, it becomes necessary to include in the model prediction of $B(E2)$ another correction term which results from mixing of the wave functions of the β and γ bands. The corresponding mixing parameter, $Z_{\beta\gamma}$, is then determined from the experimental ratios and given in column 6. There is no value for the $(3' \rightarrow 4)/(3' \rightarrow 2)$ ratio in each nucleus. Since a β-vibrational band has no 3^+ member, there can be no β-band admixture into the 3^+ of the γ band. In view of the large errors on the $Z_{\beta\gamma}$ values, one can conclude that a constant $Z_{\beta\gamma}$ has been obtained for each γ band. In other words, including such mixing has enabled us to legitimately fit the data with a consistent set of mixing parameters. Previous to these experiments, the observed branching ratios for these and other deformed nuclei could be fitted to theory using only the Z_γ correction term. The present work yields one of the first pieces of quantitative evidence for the existence of mixing between the wave functions of the β and γ bands.

Next, let us consider the β-vibrational band. The six gamma-ray transitions from the 0^+, 2^+, and 4^+ members of the β band to the 0^+, 2^+, and 4^+ members of the ground-state band have been observed in both ^{152}Sm and ^{154}Gd. The various experimental $B(E2)$ ratios are given in column 3 of Table 1.3; the double primes indicate members of the β band. The parameter Z_β, which describes mixing of the β and ground-state bands, is determined from each ratio and given in column 5. A very large discrepancy in the values is evident for each nucleus. If the effect of β-γ band mixing is included by using $Z_{\beta\gamma}$ from Table 1.2, a new estimate of Z_β results for each ratio, as given in column 6. In this case, correction for mixing of the β and γ bands has not brought internal consistency, as in the γ band. This is the first case in which such widely varying Z_β values have been found and has been reported earlier by us[19] and by Liu *et al.*[20] In both ^{152}Sm and ^{154}Gd, the differing values would be brought into agreement

[18] L. L. Riedinger, N. R. Johnson, and J. H. Hamilton, *Chem. Div. Ann. Progr. Rept. May 20, 1967*, ORNL-4164, p. 12.

[19] L. L. Riedinger, Noah R. Johnson, and J. H. Hamilton, *Phys. Rev. Letters* 19, 1243 (1967).

[20] Y-t Liu, O. B. Nielsen, P. Salling, and O. Skilbreid, *Bull. Acad. Sci. U.S.S.R., Phys. Ser. (English Transl.)* 31, 69 (1967).

Table 1.2. Experimental and Theoretical Ratios of Reduced $E2$ Transition Probabilities from Members of the γ Band in ^{152}Sm and ^{154}Gd

Nucleus	$\frac{I' \to I_1}{I' \to I_2}$ [a]	$\frac{B(E2; I' \to I_1)}{B(E2; I' \to I_2)}$ Experiment	Theory[b]	Z_γ [c]	$Z_{\beta\gamma}$
				$\times 10^{-2}$	$\times 10^{-2}$
^{152}Sm	$\frac{4' \to 4}{4' \to 2}$	11.2 ± 1.9	2.92	8.1 ± 0.8	−(0.2 ± 0.4)
	$\frac{3' \to 4}{3' \to 2}$	1.00 ± 0.05	0.40	7.7 ± 0.5	
	$\frac{2' \to 2}{2' \to 4}$	10.0 ± 1.4	20.0	6.7 ± 1.8	−(0.4 ± 0.8)
	$\frac{2' \to 2}{2' \to 0}$	2.38 ± 0.18	1.43	8.8 ± 1.4	−(0.8 ± 1.0)
^{154}Gd	$\frac{4' \to 4}{4' \to 2}$	6.41 ± 0.97	2.92	5.1 ± 0.9	1.2 ± 0.4
	$\frac{3' \to 4}{3' \to 2}$	1.05 ± 0.06	0.40	8.2 ± 0.5	
	$\frac{2' \to 2}{2' \to 4}$	7.34 ± 0.95	20.0	11.4 ± 2.3	1.2 ± 0.8
	$\frac{2' \to 2}{2' \to 0}$	2.30 ± 0.12	1.43	8.3 ± 0.9	0 ± 0.8

[a] States with primes are in the γ-vibrational band and those without primes are in the ground-state rotational band.
[b] Predictions from adiabatic symmetric-rotor model.
[c] Calculated assuming that β-γ band mixing is negligible.

if the $E2$ intensity of the $2'' \to 2$ transition were only about one-half of the observed singles intensity. However, our gamma-gamma coincidence measurements indicate that all of the singles intensity belongs to the $2'' \to 2$ transition in each case. Also, the angular correlation experiments of Hamilton *et al.*[21] and of McGowan *et al.*[22] indicate that the $2'' \to 2$ transition is essentially pure $E2$ in character for ^{154}Gd and ^{152}Sm respectively.

One thus concludes that the variation in Z_β values is real and unexplainable by mixing of any known excitation into the β-vibrational band. Contrary to the evidence from the γ-band $B(E2)$ ratios, these results for the β band indicate that the perturbational treatment of an intrinsic-rotational coupling is probably invalid for ^{152}Sm and ^{154}Gd. This may possibly be connected to the fact that these nuclei are in the transition region from spherical to highly deformed shapes and are not good symmetric rotors to first order, with the result that these so-called β-vibrational states contain large admixtures of other states which are at this time unknown. It is obvious that detailed branching ratios from members of β bands in more strongly deformed nuclei are much needed at this time.

[21] J. H. Hamilton, A. V. Ramayya, L. C. Whitlock, and A. Meulenberg, *Phys. Rev. Letters* 19, 1484 (1967).
[22] F. K. McGowan, R. O. Sayer, and P. H. Stelson, to be published.

Table 1.3. Experimental and Theoretical Ratios of Reduced $E2$ Transition Probabilities from Members of the β Band in ^{152}Sm and ^{154}Gd

Nucleus	$\frac{I'' \rightarrow I_1}{I'' \rightarrow I_2}$ [a]	$\frac{B(E2; I'' \rightarrow I_1)}{B(E2; I'' \rightarrow I_2)}$ Experiment	$\frac{B(E2; I'' \rightarrow I_1)}{B(E2; I'' \rightarrow I_2)}$ Theory[b]	Z_β Without β–γ Mixing	Z_β With β–γ Mixing
				$\times 10^{-2}$	$\times 10^{-2}$
^{152}Sm	$\frac{2'' \rightarrow 4}{2'' \rightarrow 2}$	2.80 ± 0.87	1.8	1.8 ± 1.4	1.7 ± 1.4
	$\frac{2'' \rightarrow 0}{2'' \rightarrow 2}$	0.15 ± 0.02	0.7	8.8 ± 0.6	9.1 ± 0.6
	$\frac{2'' \rightarrow 4}{2'' \rightarrow 0}$	18.3 ± 6.0	2.6	5.5 ± 1.0	5.6 ± 1.0
	$\frac{4'' \rightarrow 2}{4'' \rightarrow 4}$	0.06 ± 0.03	1.1	5.4 ± 0.4	5.7 ± 0.5
^{154}Gd	$\frac{2'' \rightarrow 4}{2'' \rightarrow 2}$	3.15 ± 0.30	1.8	2.3 ± 0.5	2.6 ± 0.5
	$\frac{2'' \rightarrow 0}{2'' \rightarrow 2}$	0.12 ± 0.02	0.7	9.7 ± 0.5	9.0 ± 0.6
	$\frac{2'' \rightarrow 4}{2'' \rightarrow 0}$	25.2 ± 3.7	2.6	6.5 ± 0.4	6.3 ± 0.4
	$\frac{4'' \rightarrow 2}{4'' \rightarrow 4}$	0.09 ± 0.06	1.1	5.1 ± 0.6	4.4 ± 0.7

[a] States with double primes are in the β-vibrational band and those without primes are in the ground-state rotational band.

[b] Predictions from adiabatic symmetric-rotor model.

DECAY PROPERTIES OF ^{158}Eu

L. L. Riedinger[23] Noah R. Johnson
J. H. Hamilton[24]

Our studies of the deformed nuclei ^{152}Sm and ^{154}Gd have shown that the usual theoretical descriptions of energy levels arising from β and γ vibrations of the nucleus are very inadequate in these two cases.[25] It is very important to find if these discrepancies still exist for nuclei that are more strongly deformed. Therefore, we have undertaken an experimental study of the levels in ^{158}Gd (which is more strongly deformed than ^{154}Gd as a result of having four more neutrons) as populated by radioactive decay of ^{158}Eu (46 min).

Radioactive sources were prepared through the (d,α) reaction involving 14-Mev deuterons and a target of Gd_2O_3 enriched in mass 160. Sources of europium were then chemically separated from other rare-earth activities by a procedure similar to that used by Daniels and Hoffman.[26] This

[23] Oak Ridge Graduate Fellow from Vanderbilt University under appointment from Oak Ridge Associated Universities.

[24] Vanderbilt University, Nashville, Tenn.

[25] L. L. Riedinger, Noah R. Johnson, and J. H. Hamilton, preceding contribution in this section.

[26] W. R. Daniels and D. C. Hoffman, *Phys. Rev.* 147, 845 (1966).

separation is based on the precipitation as hydroxides of all the other rare earths in the III oxidation state while europium is reduced to and held in the II state. Sources were usually ready for counting within 50 min after the bombardment. Gamma-ray singles experiments involving 20- and 35-cm^3 Ge(Li) detectors and 1600-, 4096-, and 20,000-channel pulse-height analyzers have been performed. Gamma-gamma coincidence experiments are planned for the future.

Due to the short half-life of the ^{158}Eu decay and the time-consuming chemical separation that is necessary, there has been very little previous work on this nucleus. In the most recent work,[26] involving a small-volume Ge(Li) and NaI detector, 23 gamma rays were attributed to the decay of ^{158}Eu, and some were placed in a level scheme of ^{158}Gd through NaI-NaI coincidence experiments. Although the results of our experiments are in a preliminary form, we are able to assign 41 gamma rays to the ^{158}Eu decay through half-life considerations. The preliminary energies (kev) of these gamma rays, with the ones not seen by Daniels and Hoffman[26] marked with asterisks, are: 80, 180, 528.3, 606.5, 699*, 743.2, 770*, 777*, 780*, 816*, 824*, 853*, 871*, 897.7, 907*, 923, 944.2, 953*, 963, 977.2, 987*, 1005, 1107.7, 1116*, 1142, 1185, 1187, 1263.8, 1293*, 1312*, 1324*, 1348, 1429, 1885*, 1945, 2025*, 2139, 2247*, 2369*, 2449*, and 2747. In addition, there are seven others which we can only tentatively assign to the ^{158}Eu decay: 828*, 1034*, 1063*, 1234*, 1301*, 2263*, and 2515*. It is anticipated that future experiments will help clarify the decay scheme of this nucleus and in particular will yield much needed information on the β- and γ-vibrational bands of ^{158}Gd.

DECAY PROPERTIES OF 66-min ^{110}In

Noah R. Johnson H. W. Boyd[27]

The decay properties of 66-min ^{110}In have been investigated by the use of NaI, Ge(Li), and anthracene detectors. Sources of the 4-hr parent activity ^{110}Sn were prepared by ion exchange techniques following the $(\alpha,4n)$ reaction on enriched ^{110}Cd. Since the spectra of ^{110}Sn are quite simple, these sources were usually used directly in order to provide a much longer effective half-life for ^{110}In. In some experiments, however, it was necessary to have pure ^{110}In sources; these were prepared by an ion exchange "milking" procedure.

Previous studies of this nucleus were made primarily with NaI spectrometers. In the present investigation numerous new transitions have been observed as a result of using the highly improved resolution of Ge(Li) detectors and of an NaI three-crystal pair spectrometer. In addition, many new subtle features have been revealed in our detailed coincidence studies with a multiparameter analyzer. Prominent ^{110}In gamma rays have been observed at 655.9, 817.3, 1001.9, 1127.5, 1424.2, 1475.3, 1512.7, 1785, 2128.9, 2210.6, 2256.7, 2316.3, 2418.2, 2650.7, 2810, 2946.7, 3074, 3470, 3600, and 3780 kev. In addition, there are indications of several more transitions of low intensity.

In the beta-ray measurements, care was taken to eliminate the possibility of summing of the kinetic energy of the positrons with annihilation quanta in the anthracene detector. Two NaI detectors were placed at 180° to the anthracene crystal while being shielded from the source. A gate demanding a triple coincidence between 511-kev quanta in the NaI detectors and beta rays in the anthracene detector gave a clean beta-ray distribution with a maximum energy end point at 2.14 Mev.

At this point we have many new details on the levels in ^{110}Cd. However, it is expected that as soon as the analysis of all our coincidence data is completed, the new information – in conjunction with the information on this same nucleus being obtained at Washington University[28] – will provide one of the best documented of the even-even cadmium level schemes, which are currently of considerable theoretical interest.

DECAY OF ^{135}Pr AND THE NEW ISOTOPE ^{135}Nd

A. R. Brosi B. H. Ketelle

A new radioactive isotope of neodymium has been produced and identified as ^{135}Nd. It decays

[27] ORAU summer participant. Permanent address: West Georgia College, Carrollton, Ga.

[28] A collaborative effort on the decay of ^{110}In is presently being carried out with Prof. Demetrios Sarantites of Washington University.

by positron and gamma-ray emission to ^{135}Pr. Two gamma rays which decay with 12-min half-lives and energies of 205 and 442 kev have been observed. The mass and element assignments of the new isotope are based on the fact that it is produced by bombarding ^{136}Ce with 35-Mev ^{3}He ions. At this energy ^{3}He ions can give a ^{136}Ce(^{3}He,4n) ^{135}Nd reaction. When an ion exchange rare-earth separation was performed on the target material the new isotope was found in the neodymium fraction. The mass and element assignments were confirmed by the fact that characteristic gamma rays of ^{135}Pr and ^{135}Ce grew into the neodymium fraction. The growth curves of the 83-kev and 296-kev gamma rays emitted in the decay of ^{135}Pr were consistent with a parent half-life of 12 min.

Measurements with a lithium-drifted germanium detector showed that ^{135}Pr has a much more complex decay scheme than that previously published. About 30 gamma rays were observed, most of which fit into a tentative energy level scheme for ^{135}Ce.

In measurements made with NaI gamma detectors there has been an apparent discrepancy in the way in which the ~297-kev level in ^{135}Ce is depopulated. When it is formed in the decay of the 20-sec ^{135}Ce isomer there is an intense cascade through an 83-kev level with very little crossover. On the other hand, when it is formed in the positron decay of ^{135}Pr there is a low-intensity cascade with a much more intense crossover transition. Measurements made with a lithium-drifted germanium detector now indicate that the sum of the energies of the gammas in cascade, 213.7 kev plus 83.2 kev equal to 296.9 kev, is somewhat greater than 296.4 kev, the energy of the apparent crossover gamma ray. This evidence indicates that there are two levels with different spins which have the same energy within a fraction of a kilovolt. Whereas both levels are populated by positron decay from the $^{5}/_{2}^{+}$ ground state of ^{135}Pr, only the upper level is populated by the isomeric transition from the $^{11}/_{2}^{-}$ level in ^{135}Ce. Probable spin assignments are $^{5}/_{2}^{+}$ for the upper level and $^{3}/_{2}^{+}$ for the lower level.

DECAY OF THE ^{89}Zr ISOMERS

E. L. Robinson[29] R. C. Hagenauer[30]
E. Eichler

We have studied the gamma-ray spectra from 78-hr ^{89g}Zr and 4-min ^{89m}Zr with 20-cm^3 and 35-cm^3 Ge(Li) detectors. The 78-hr species was prepared by the reaction ^{89}Y(p,n). We obtained the 4-min isomer from the decay of 70-min ^{89m}Nb, which was made by ^{90}Zr(p,2n). The ^{89}Nb was adsorbed on a Dowex 1 anion exchange column, and samples of ^{89m}Zr were periodically eluted. In this way the 4-min half-life was effectively extended to 70 min. The precisely determined gamma-ray energies, including three new transitions, are included in the level scheme of Fig. 1.1. These radiations have recently been reported by Hinrichsen.[31] We also present, for comparison, the ^{89}Y levels identified by reaction spectroscopy.[32]

DECAY OF ^{89}Nb AND ^{89m}Nb

R. C. Hagenauer[33] E. Eichler
G. D. O'Kelley

A study of the decay scheme of ^{89}Nb and ^{89m}Nb was made using 20-cm^3 and 35-cm^3 Ge(Li) detectors. We prepared sources by irradiating $^{90}ZrO_2$ with 27-Mev protons. Niobium was separated by dissolving the powder in concentrated HF and eluting the zirconium from a Dowex 1 anion exchange column with 9 *M* HCl–2 *M* HF. We then counted the part of the column containing the niobium.

---

[29]Visiting Scientist from the Department of Physics, University of Alabama, Birmingham.

[30]ORAU Graduate Fellow from the University of Tennessee.

[31]P. F. Hinrichsen, *Bull. Am. Phys. Soc.* 13, 583 (1968).

[32]P. F. Hinrichsen, S. M. Shafroth, and D. M. Van Patter, to be published.

[33]ORAU Predoctoral Fellow from the University of Tennessee.

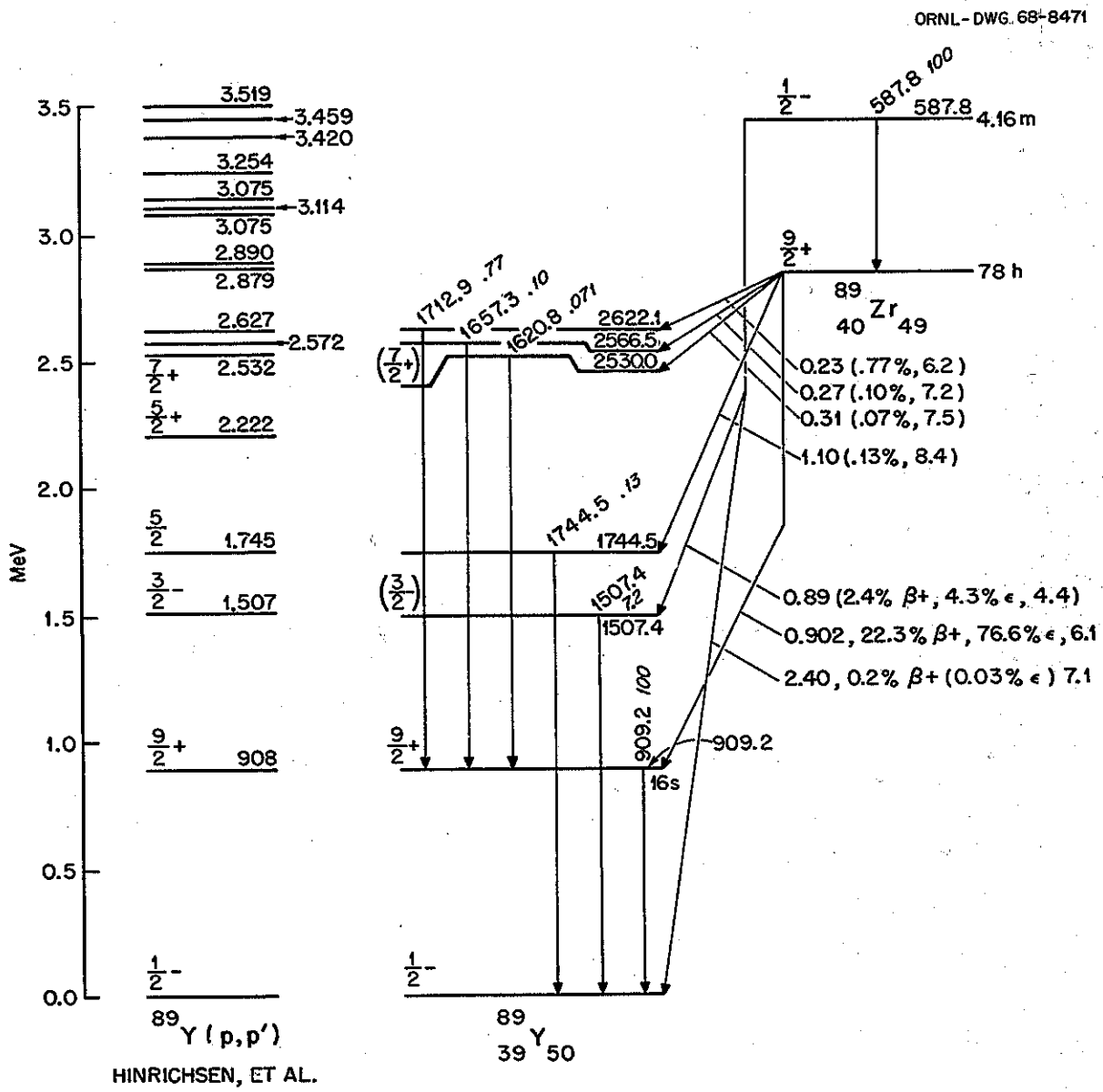

Fig. 1.1. Decay Scheme of ^{89}Zr Isomers. Levels observed by ^{89}Y(p,p') by Hinrichsen *et al.*[4] are included.

A 7.5 × 7.5 cm NaI crystal was used with a 20-cm^3 Ge(Li) detector to make gamma-gamma coincidence measurements. We performed beta-ray measurements using an anthracene crystal in coincidence with two NaI detectors to measure only positron radiation.

We found approximately 60 gamma rays ranging from 480 kev to 3960 kev associated with 2-hr ^{89}Zr. Forty of these have not been reported in the literature.[34] A half-life 68 ± 2 min was found for a 588-kev and 770-kev gamma. We suspect these follow the decay of ^{89m}Nb. This half-life

[34] E. K. Hyde and J. M. Nitschke, *Nucl. Chem. Div. Ann. Rept. 1965*, UCRL-16580, p. 88.

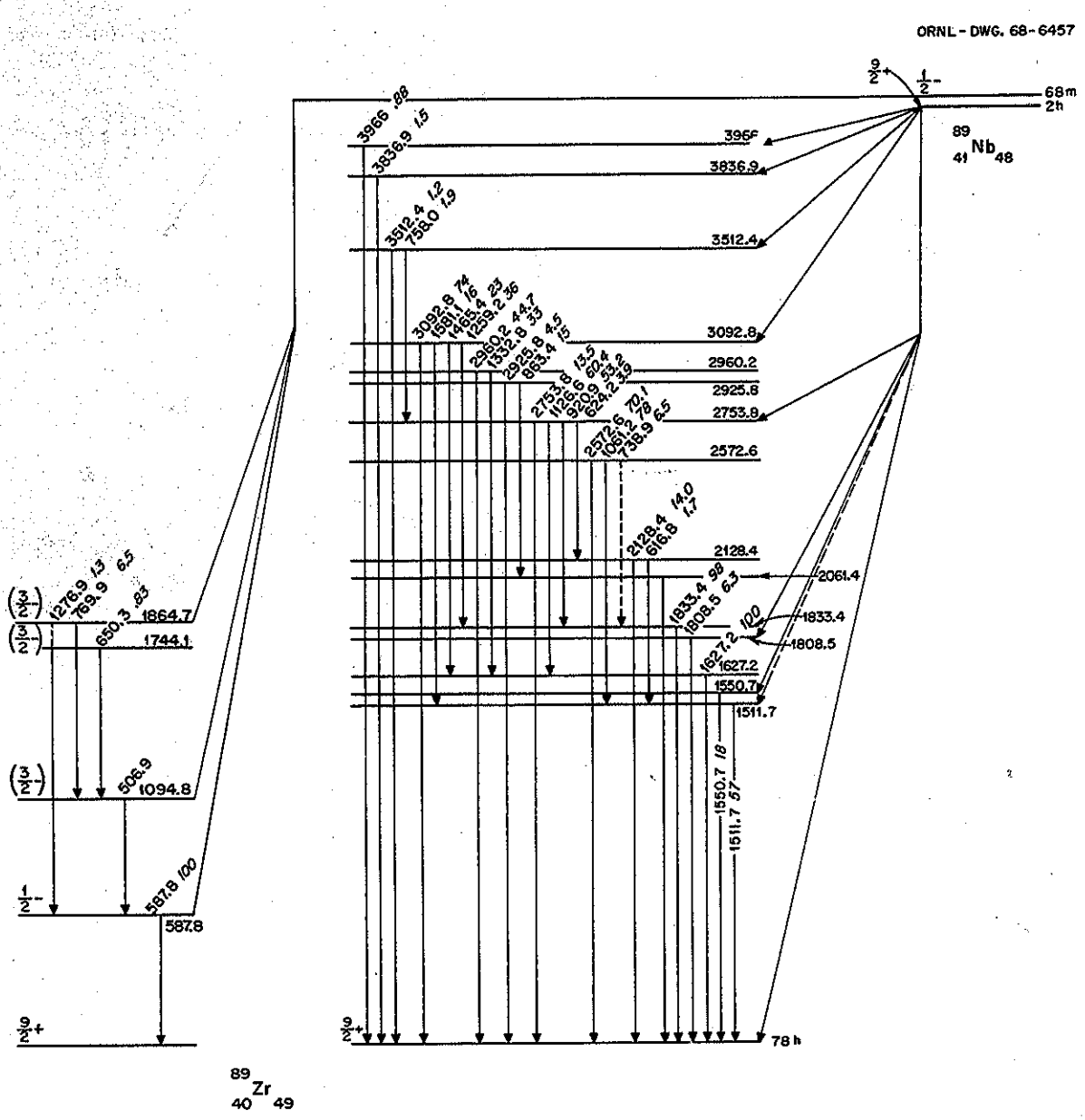

Fig. 1.2. Tentative Decay Scheme of the ^{89}Nb Isomers.

is consistent with the 66 ± 4 min half-life determined by Flegenheimer,[35] but not with the 42-min determination by Butement and Qaim.[36]

Initial gamma-gamma coincidence studies along with energy sum agreements have made possible a tentative decay scheme as shown in Fig. 1.2. Some of these levels correspond to those seen by Ball and Fulmer.[37]

[35] A. Hanser and J. F. Flegenheimer, *Radiochim. Acta* 5, 120 (1966).

[36] F. D. S. Butement and S. M. Qaim, *J. Inorg. Nucl. Chem.* 26, 1481 (1964).

[37] J. B. Ball and C. B. Fulmer, to be published.

THE DECAY OF 10.5-hr ^{245}Pu AND 2.08-hr ^{245}Am

A. H. Wapstra C. E. Bemis, Jr.

See p. 23.

INVESTIGATION OF THE DECAY OF ^{172}Hf AND ^{172}Lu

M. F. Roche R. L. Hahn
K. S. Toth C. E. Bemis, Jr.
T. H. Handley

See p. 26.

THE ALPHA DECAY OF ^{253}Cf AND ^{254}Cf

C. E. Bemis, Jr. J. Halperin

See p. 28.

NEW NEPTUNIUM ISOTOPES, ^{229}Np AND ^{230}Np

R. L. Hahn M. F. Roche
K. S. Toth

See p. 29.

PARTIAL ALPHA HALF-LIVES OF ^{242}Pu AND ^{244}Pu

J. Halperin C. E. Bemis, Jr.
R. Eby

See p. 31.

SEARCH FOR ^{88}Mo AND ^{89}Mo

R. C. Hagenauer[38] E. Eichler
G. D. O'Kelley

We have carried out a search for the neutron-deficient nuclei ^{88}Mo and ^{89}Mo. This program was begun when we failed to find the 20- and 7-min periods reported by Butement and Qaim[39] for ^{88}Mo and ^{89}Mo respectively. We have used the following reactions: ^{92}Mo($p,p3n$), ^{93}Nb($p,5n$), and ^{90}Zr(^{3}He,$4n$) to make ^{89}Mo and the analogous reactions with an additional emitted neutron for ^{88}Mo. We have utilized rapid chemical separations for molybdenum, including remote operation procedures, enabling us to begin chemistry in the cyclotron target room immediately after the end of bombardment. In all cases we have failed to see the 20- or 7-min period.[39]

In addition, there was no evidence of new activities that could be ascribed to ^{89}Mo or ^{88}Mo. This failure could be in part due to abnormally small reaction cross sections, although estimates based on a statistical-model Monte Carlo calculation[40] do not support this supposition.

SEARCH FOR THE NEW NUCLIDE ^{247}Pu

C. E. Bemis, Jr. J. Halperin

See p. 31.

LEVELS IN Nb AND Tc NUCLEI FROM THE (p,ny) REACTION

E. Eichler J. K. Dickens[41]
R. A. Kuebbing[42]

Our utilization of in-beam gamma-ray spectroscopy in conjunction with the (p,n) reaction has borne new fruit this year. The nuclei ^{92}Nb, ^{94}Nb, ^{94}Tc, ^{95}Tc, ^{96}Tc, ^{97}Tc, and ^{98}Tc have been studied. In addition to the basic excitation function technique, we have studied gamma-gamma coincidence spectra to aid the level assignments. The pulsed beams of the tandem and 6-Mev Van de Graaff accelerators have enabled us to measure the half-lives of several delayed states in these nuclei.

As an example of typical (p,ny) results, we show in Fig. 1.3 a series of gamma-ray spectra from

---

[38] ORAU Graduate Fellow from the University of Tennessee.

[39] F. D. S. Butement and S. M. Qaim, *J. Inorg. Nucl. Chem.* 26, 1491 (1964).

[40] I. Dostrovsky, Z. Fraenkel, and G. Friedlander, *Phys. Rev.* 116, 683 (1959).

[41] Neutron Physics Division.

[42] ORAU Graduate Fellow from Case Western Reserve University.

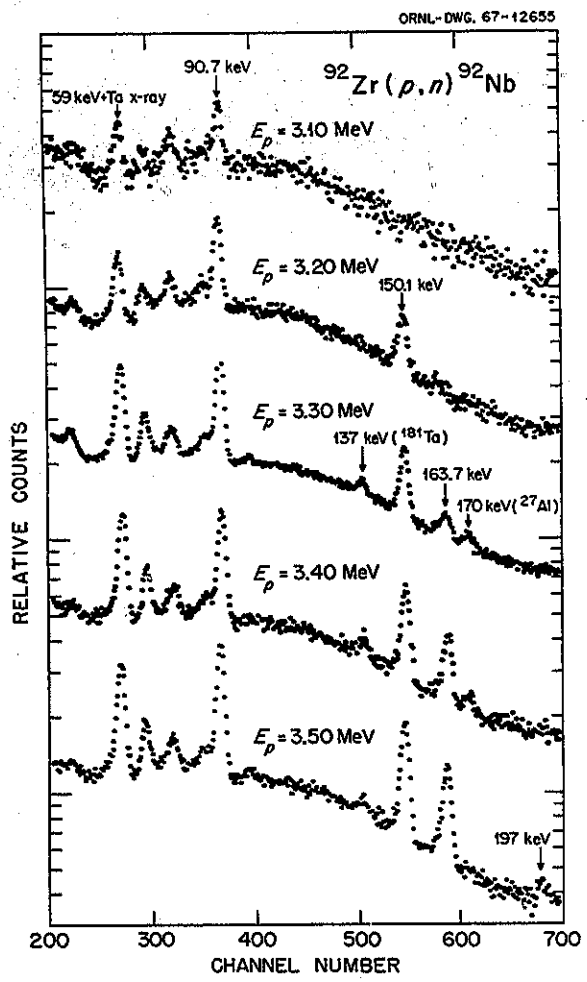

Fig. 1.3. Gamma-Ray Spectra from $^{92}Zr(p,n\gamma)^{92}Nb$ at E_p = 3.10 to 3.50.

$^{92}Zr(p,n\gamma)^{92}Nb$ taken at successively higher proton energies. The level scheme constructed from such data is given in Fig. 1.4 along with level spectra inferred from earlier (p,d) and (d,t) and recent $(^3He,d)$ measurements. We also present several theoretical predictions of the ^{92}Nb levels. The low-lying 2^- level seen in ^{92}Nb (and other odd-odd nuclei in this region) is probably due to the configuration $(\pi p_{1/2})(\nu d_{5/2})$. Since it must decay to a member of the $(\pi g_{9/2})(\nu d_{5/2})$ family, the $E1$ transition should be strongly l-forbidden. In confirmation, we have evidence that the lifetime is approximately 10 μsec.

SEARCH FOR $E0$ RADIATION IN THE DECAY OF THE TWO-PHONON 0^+ STATE IN ^{80}Kr

R. A. Kuebbing[43] K. J. Casper[44]
E. Eichler

The isomers 4.5-hr ^{80m}Br and 18-min ^{80}Br decay by beta emission to the excited states of ^{80}Kr and ^{80}Se. We have measured the electron spectrum, using an Si(Li) detector, in coincidence with the beta rays, attempting to find the $E0$ radiation in the decay of the first excited 0^+ state to the ground state in ^{80}Kr. The sources were prepared by thermal neutron capture on enriched $NH_4{}^{79}Br$. The interference of ^{82}Br produced by $^{81}Br(n,\gamma)$ has been shown to be negligible. We are presently working on reducing interdetector scattering.

NUCLEAR REACTION SPECTROSCOPY WITH THE TRANSURANIUM ELEMENTS

R. L. Hahn K. S. Toth
E. Newman M. F. Roche

See p. 33.

ANGULAR DISTRIBUTION OF ^{64}Cu NUCLEI FROM THE $^{65}Cu(^3He,\alpha)$ REACTION

N. T. Porile I. Fujiwara
R. L. Hahn

See p. 33.

FRAGMENT ENERGY CORRELATION MEASUREMENTS IN THE FISSION OF ^{233}U, ^{235}U, AND ^{238}U BY 7- TO 13-Mev PROTONS

R. L. Ferguson Frances Pleasonton[46]
S. C. Burnett[45] F. Plasil[46]
H. W. Schmitt[46]

Fission fragment mass and kinetic energy distributions and mass-vs-energy correlations have

[43] ORAU Graduate fellow from Case Western Reserve University.

[44] Cleveland State University.

[45] Oak Ridge Graduate Fellow from the University of Tennessee under appointment from the Oak Ridge Associated Universities.

[46] Physics Division.

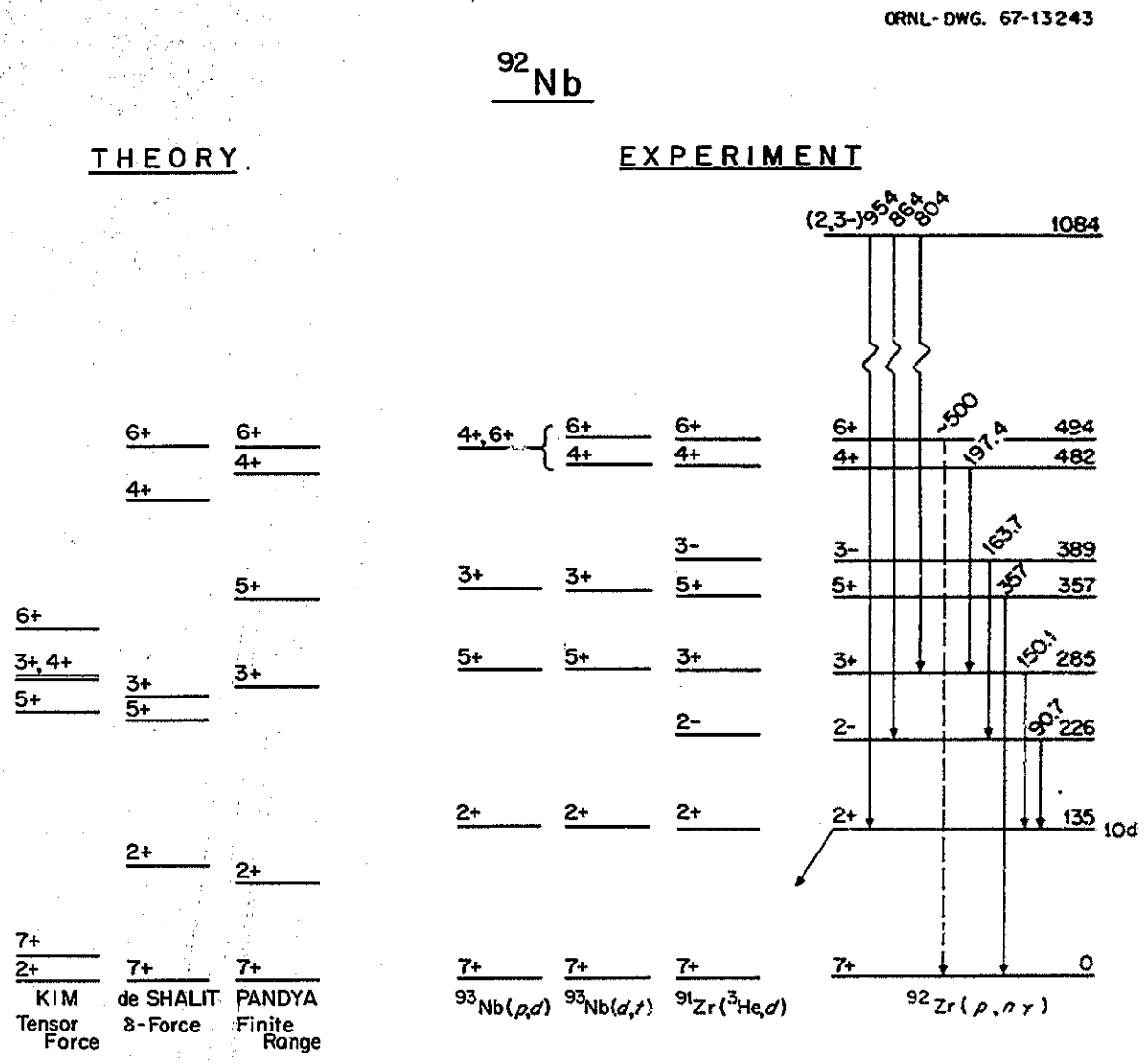

Fig. 1.4. Comparison of Experimental and Theoretical ^{92}Nb Level Schemes.

recently been thoroughly studied at this laboratory for thermal-neutron-induced fission of several fissile nuclides and for spontaneous fission of ^{252}Cf.[47–49] For moderate excitation energies, however, too few data are available to develop completely the systematics of mass and energy distributions and their correlations as functions of compound nucleus excitation energy. In order to obtain information for such a development, the kinetic energies of correlated fission fragments were measured, using silicon surface barrier detectors, for proton-induced fission of uranium isotopes. Initial results of the experiments are summarized here in terms of fragment

[47] H. W. Schmitt, J. H. Neiler, and F. J. Walter, *Phys. Rev.* 141, 1146 (1966).

[48] J. H. Neiler, F. J. Walter, and H. W. Schmitt, *Phys. Rev.* 149, 894 (1966).

[49] F. Pleasonton, *Phys. Div. Ann. Progr. Rept. Dec. 31, 1967*, ORNL-4230, p. 88.

mass and kinetic energy distributions. These properties are presented as functions of target isotope and proton bombarding energy.

The ORNL tandem accelerator was used to bombard thin targets of ^{233}U, ^{235}U, and ^{238}U with a proton beam, the energy of which was varied from 7 to 13 Mev in 1- or 1.5-Mev steps. The apparatus used was essentially identical to that shown in Fig. 1 of ref. 49.

A summary of the various detector configurations is given in Table 1.4. Bombardment data are summarized in Table 1.5, which lists beam characteristics and total numbers of fission events observed for all targets and projectile energies. Beam currents were limited to $\lesssim 150$ na to reduce accidental coincidences between scattered protons and fission fragments to less than 5% of the fragment count rate, except in the 7-, 8-, and 9-Mev ^{235}U experiments. In these latter runs, pileup may have been as high as 40%. However, the scattered protons deposit an average of only ~ 1 Mev of energy in the fragment detectors. Therefore, the average perturbation on the fragment energies is small. The effect on fragment mass distributions should be even less important since pileup occurs approximately equally in both detectors and would tend to cancel in the equation:

$$\mu_1 = \frac{AE_{K2}}{E_{K1} + E_{K2}} ,$$

where A is the compound nucleus mass, μ_1 is the provisional fragment mass, and the E_K's are fragment kinetic energies. Analysis of the data

Table 1.4. Summary of Detector Configurations

Target	Detector 1		Detector 2	
	Active Area (cm^2)	Distance to Target (cm)	Active Area (cm^2)	Distance to Target (cm)
^{233}U	2.0	9.7	3.0	6.2
^{235}U	2.5	10.0	5.0	10.0
^{238}U	2.0	9.7	5.0	5.8

Table 1.5. Summary of Bombardment Data

Target	Proton Energy (Mev)	Beam Diameter (cm)	Beam Current (na)	Total Fission Events
^{233}U	7.0	0.5	150	12,071
	8.5	0.5	150	67,842
	10.0	0.5	125	64,653
	11.5	0.5	150	68,600
	13.0	0.5	50	73,641
^{235}U	7.0	1.0	1800	11,442
	8.0	1.0	1500	24,280
	9.0	1.0	825	44,941
	10.0	1.0	160	58,657
	11.0	1.0	95	73,970
	12.0	1.0	100	70,300
	13.0	1.0	53	71,963
^{238}U	8.0	0.5	150	38,717
	9.0	0.5	150	49,071
	10.0	0.5	150	48,310
	11.0	0.5	50	48,151
	12.0	0.5	33	47,373
	13.0	0.5	20	48,562

followed the method described in ref. 47, except that the processing was carried only far enough to obtain the distribution of events in μ and E_K, the total fragment kinetic energy – that is, the $N(\mu, E_K)$ array and the functions immediately derivable from it. Corrections for the emission of neutrons from the fragments will, of course, affect these functions. The effects of neutron emission are indicated in Fig. 1.5 for three systems for which the neutron emission functions are known.[50,51] These effects are seen to be small and are expected to change only slowly with bombarding energy and target isotope. Furthermore, since details of the neutron emission are not known for all fission systems described here, the provisional mass functions are taken to be adequate approximations of the true functions for purposes of comparison.

Figure 1.5 shows examples of the distributions obtained from these experiments. In the left-hand portion, for $^{233}U(p_{8.5\ Mev},f)$, are given the fragment mass yield $N(\mu)$ (bottom panel), average total kinetic energy $E_K(\mu)$ (middle panel), and the root mean square width $\sigma_{E_K}(\mu)$ of the total kinetic energy distribution (top panel). The open circles in these plots indicate the results of correcting for neutron emission as mentioned above. The same functions are shown for $^{233}U(p_{13\ Mev},f)$ and $^{238}U(p_{12\ Mev},f)$ in the center and right-hand portions respectively.

[50] S. C. Burnett, R. L. Ferguson, F. Plasil, and H. W. Schmitt, *Phys. Div. Ann. Progr. Rept. Dec. 31, 1967*, ORNL-4230, p. 83.

[51] S. C. Burnett, R. L. Ferguson, F. Plasil, and H. W. Schmitt, private communication.

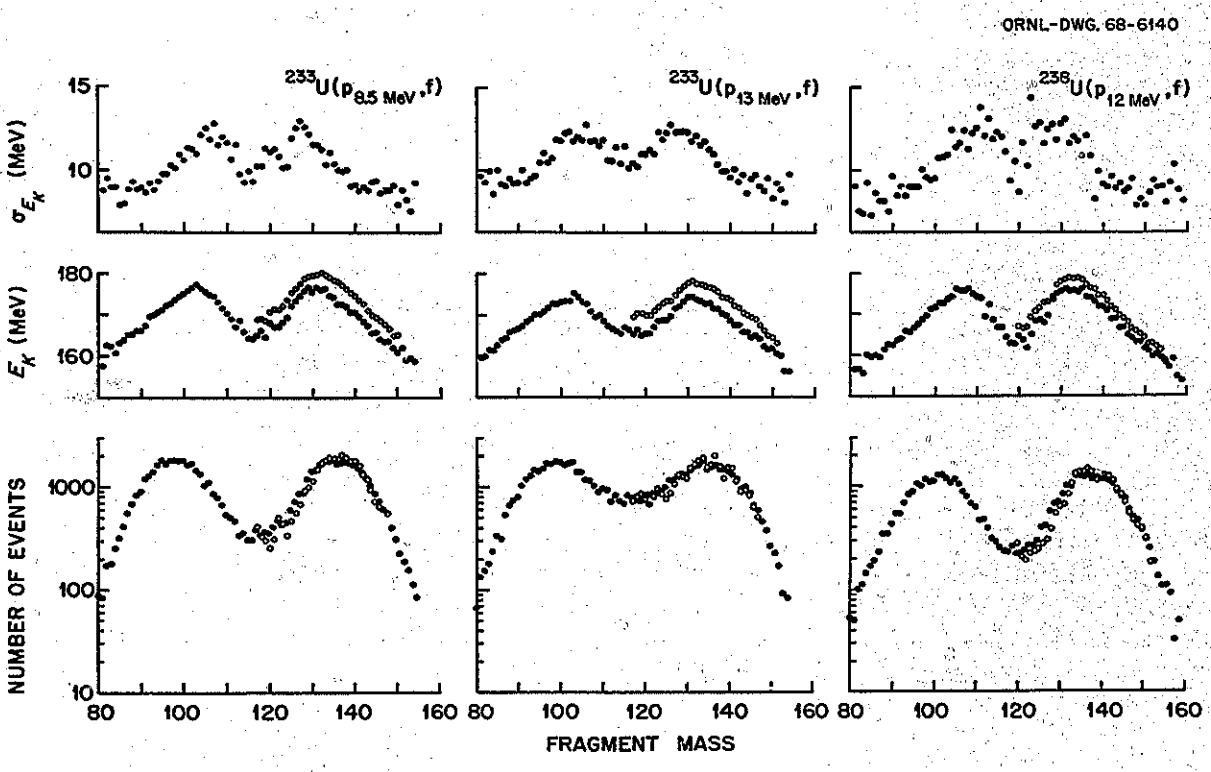

Fig. 1.5. Fragment Mass Yield $N(\mu)$ (bottom panels), Average Total Kinetic Energy $E_K(\mu)$ (middle panels), and rms Width of the Kinetic Energy Distribution $\sigma_{E_K}(\mu)$ (top panels) for 8.5-Mev Proton Fission of ^{233}U in the Left-Hand Portions, 13-Mev Proton Fission of ^{233}U in the Center Portion, and 12-Mev Proton Fission of ^{238}U in the Right-Hand Portions. The open circles indicate results of applying a correction for neutron emission.

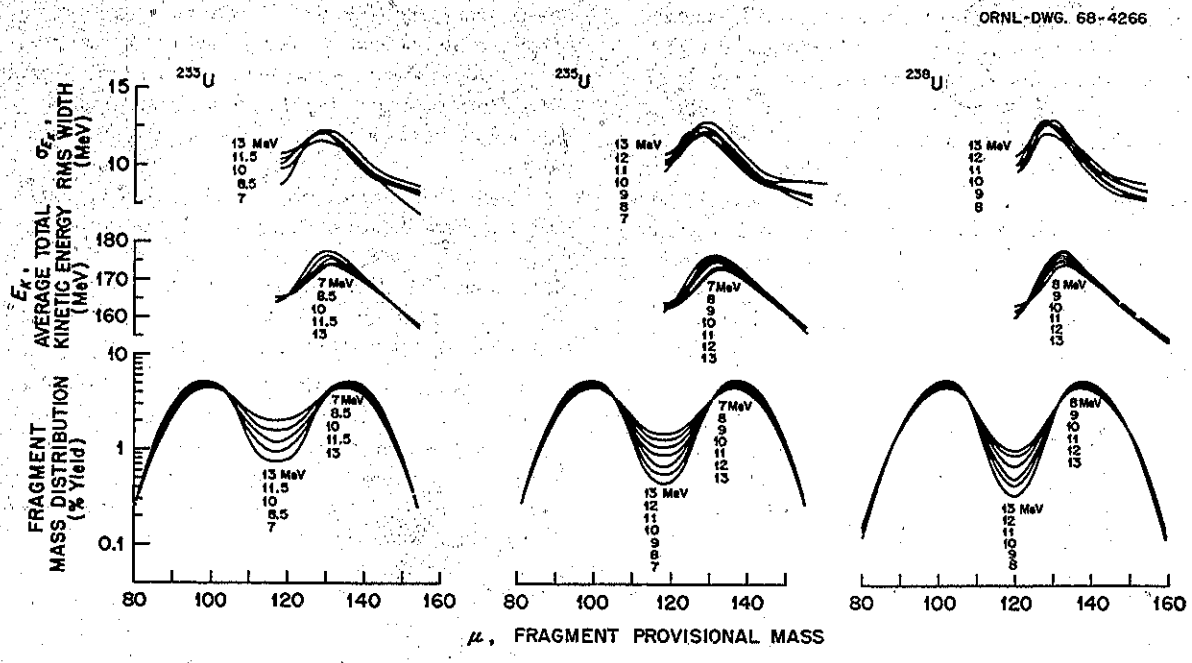

Fig. 1.6. Composite Curves Showing Fragment Mass Yield $N(\mu)$ (bottom panels), Average Total Kinetic Energy $E_K(\mu)$ (middle panels), and rms Width of the Kinetic Energy Distribution $\sigma_{E_K}(\mu)$ (top panels) for Proton-Induced Fission of ^{233}U in the Left-Hand Portions, of ^{235}U in the Center Portions, and of ^{238}U in the Right-Hand Portions. Curves are labeled with the energy (in Mev) of the protons inducing fission.

A summary of all the results is presented in Fig. 1.6. To obtain the data shown here, the observed values at complementary masses were averaged by reflecting the points through $\mu = A/2$ and by drawing smooth curves through the resulting points. Mass distributions are normalized to 200% yield. The format of this figure is the same as for Fig. 1.5, with the results for ^{233}U in the left-hand portion, ^{235}U in the center portion, and ^{238}U in the right-hand portion.

Salient features of the results are:

1. the double-peaked mass distributions, with the filling in of the valley as the bombarding energy increases;
2. the dip in E_K for symmetric mass division and the decrease of the maximum E_K with increasing bombarding energy;
3. the near congruity (within measurement uncertainties) of the $\sigma_{E_K}(\mu)$ functions for all proton bombarding energies, for each target isotope.

Finally, Fig. 1.7 recapitulates the variations in the mass distributions with excitation energy. The ratio of yield at the peaks of the distribution to that in the valley is plotted vs excitation energy

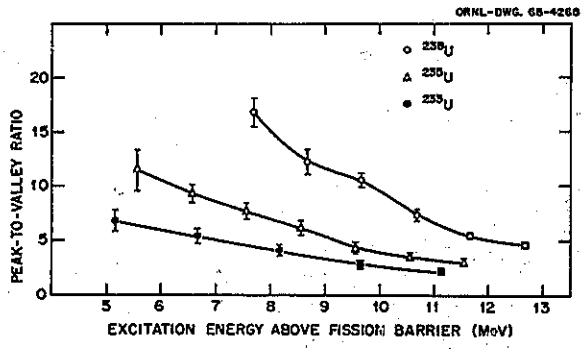

Fig. 1.7. Fragment Mass Yield Peak-to-Valley Ratios for Proton-Induced Fission of ^{233}U, ^{235}U, and ^{238}U as a Function of Compound Nucleus Excitation Energy Above the Fission Barrier.

above the fission barrier for all three target isotopes. Values of the excitation energy were calculated from semiempirical masses[52] and estimated fission barriers,[53] neglecting the effects of any prefission neutron emission. It can be seen that the values of this ratio and the steepness of its variation with excitation energy are inversely related to the fissility parameters of the target isotopes.

FRAGMENT ENERGY CORRELATION MEASUREMENTS IN 30-Mev PROTON-INDUCED FISSION OF ^{232}Th

F. Plasil[54] H. W. Schmitt[54]
R. L. Ferguson Frances Pleasonton[54]

In a continuing study of the characteristics of medium-excitation fission, we have determined the fragment mass and kinetic energy correlations for the fission of several heavy elements bombarded by medium-energy protons from ORIC. Reported here are preliminary results for 30-Mev proton-induced fission of ^{232}Th. This system has proven to be particularly interesting since it exhibits the three-peaked structure which has been observed only in a rather restricted range of excitation energies and fissioning nuclei.[55] Such distributions can be readily decomposed into two components, one representative of symmetric fission and one representative of asymmetric fission. One can then determine the properties of these components and possibly study the fission processes giving rise to them.

The experimental method and procedures of analysis used were essentially identical to those summarized in the previous paper. In Fig. 1.8 we present a contour plot of the correlations between fragment mass μ and total kinetic energy E_K. The data were smoothed by summing events over 5 Mev × 5 amu boxes and were symmetrized by reflecting points across the $\mu = 116.5$ symmetry plane.

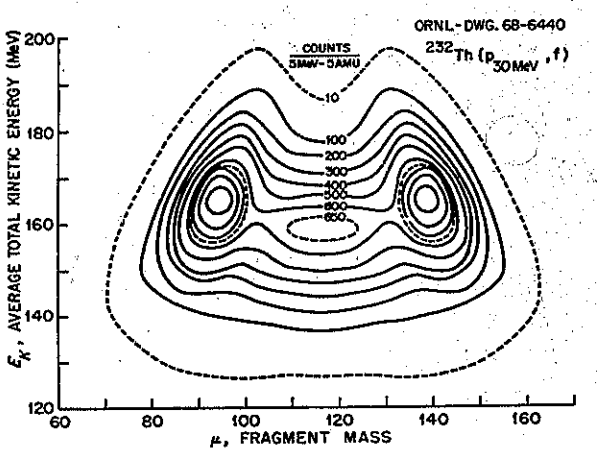

Fig. 1.8. Fragment Mass and Kinetic Energy Correlations for 30-Mev Proton-Induced Fission of ^{232}Th.

The two peaks corresponding to asymmetric fission occur at $\mu = 94.5$, $E_K = 165$ and at $\mu = 138.5$, $E_K = 165$; the peak corresponding to symmetric fission occurs at $\mu = 116.5$, $E_K = 159$. In addition, it can be seen that at the highest kinetic energies ($E_K \gtrsim 185$ Mev) the predominant mass division results in the formation of fragments with $\mu \tilde{=} 132$ and their complements with $\mu \tilde{=} 101$. However, at lower energies the most probable division shifts toward more asymmetric masses. The greatest probability for symmetric mass splits occurs at an energy ~6 Mev lower than that at which the asymmetric peaks are found.

In an attempt to elucidate the systematic behavior of such features as these, we have begun detailed investigations of several fission systems, including further study of ^{232}Th bombarded with protons of other energies. Interpretation of the results of these experiments, in the context of an appropriate model, should provide useful information on many of the long-standing problems of fission.

NUCLEAR CHARGE DISTRIBUTION IN FISSION: INDEPENDENT YIELD OF ^{134}I FROM SPONTANEOUS FISSION OF ^{252}Cf

D. E. Troutner

See p. 34.

[52] V. E. Viola and G. T. Seaborg, *J. Inorg. Nucl. Chem.* 28, 697 (1966).

[53] V. E. Viola and B. D. Wilkins, *Nucl. Phys.* 82, 65 (1966).

[54] Physics Division.

[55] See, for example, E. K. Hyde, *Nuclear Properties of the Heavy Elements*, vol. III, *Fission Phenomena*, pp. 289 ff, Prentice-Hall, Englewood Cliffs, New Jersey, 1964.

MASS YIELDS OF ^{101}Mo AND ^{102}Mo FROM SPONTANEOUS FISSION OF ^{252}Cf

R. M. Harbour D. E. Troutner

See p. 35.

A SEARCH FOR ^{101}Nb FROM THERMAL-NEUTRON FISSION OF ^{235}U

R. M. Harbour D. E. Troutner

See p. 36.

GAS-JET SYSTEM FOR RAPID COLLECTION OF RECOIL NUCLEI

R. L. Hahn

See p. 37.

THE $\pi\sqrt{2}$ DOUBLE-FOCUSING ELECTRON SPECTROMETER

C. E. Bemis, Jr.

See p. 38.

THE TRANSURANIUM RESEARCH LABORATORY ISOTOPE SEPARATOR

L. D. Hunt C. E. Bemis, Jr.

See p. 40.

LOW-LEVEL GAMMA-RAY SPECTROMETER FOR LUNAR SAMPLES[56]

G. D. O'Kelley V. A. McKay[59]
P. R. Bell[57] R. T. Roseberry[59]
J. S. Eldridge[58] R. E. Wintenberg[59]

Introduction

The development of a high-sensitivity, low-background gamma-ray spectrometer for assay of lunar samples continued along the general lines described in the previous report.[60] The prototype spectrometer was completed at ORNL, and valuable preliminary data were obtained. Recently, a very similar system was installed at the Lunar Receiving Laboratory (LRL) in Houston, Texas, and initial performance data were determined.

A simplified diagram of the physical arrangement of the detectors is shown in Fig. 1.9. This final design evolved through a series of detector and anticoincidence mantle studies carried out in connection with the prototype system, and it is generally similar to the conceptual design previously shown.[61]

Detectors

Two NaI(Tl) scintillation detectors were obtained[61] for evaluation. One detector was a cylindrical rod of NaI(Tl) 9 in. in diameter × 5 in. long attached to four phototubes of low radioactivity (RCA developmental type C70145, now assigned type number 4521). The other detector used a NaI(Tl) crystal of identical size, but with a 4-in. thickness of pure NaI as a gamma-absorbing light guide interposed between the scintillator and the photomultiplier tubes (see Fig. 1.9). A comparison between data obtained with the two detectors demonstrated conclusively that, although the detector with the light guide had poorer resolution (full width at half maximum counting rate) by about 1% at 662 kev, the reduction in photomultiplier-induced background justified the use of a pure NaI light guide.

Studies using the complete ORNL prototype also showed that a significant part of the background spectrum was due to radioactive contamination in the materials used to enclose the detector crystals. New detectors for the LRL counting facility are under construction using only materials selected for low radioactive contamination.

---

[56] Sponsored by the National Aeronautics and Space Administration through interagency agreements with the U.S. Atomic Energy Commission.

[57] Thermonuclear Division; present address: NASA Manned Spacecraft Center, Houston, Tex.

[58] Analytical Chemistry Division.

[59] Instrumentation and Controls Division.

[60] *Chem. Div. Ann. Progr. Rept. May 20, 1967*, ORNL-4164, p. 20.

[61] Harshaw Chemical Co., Cleveland, Ohio.

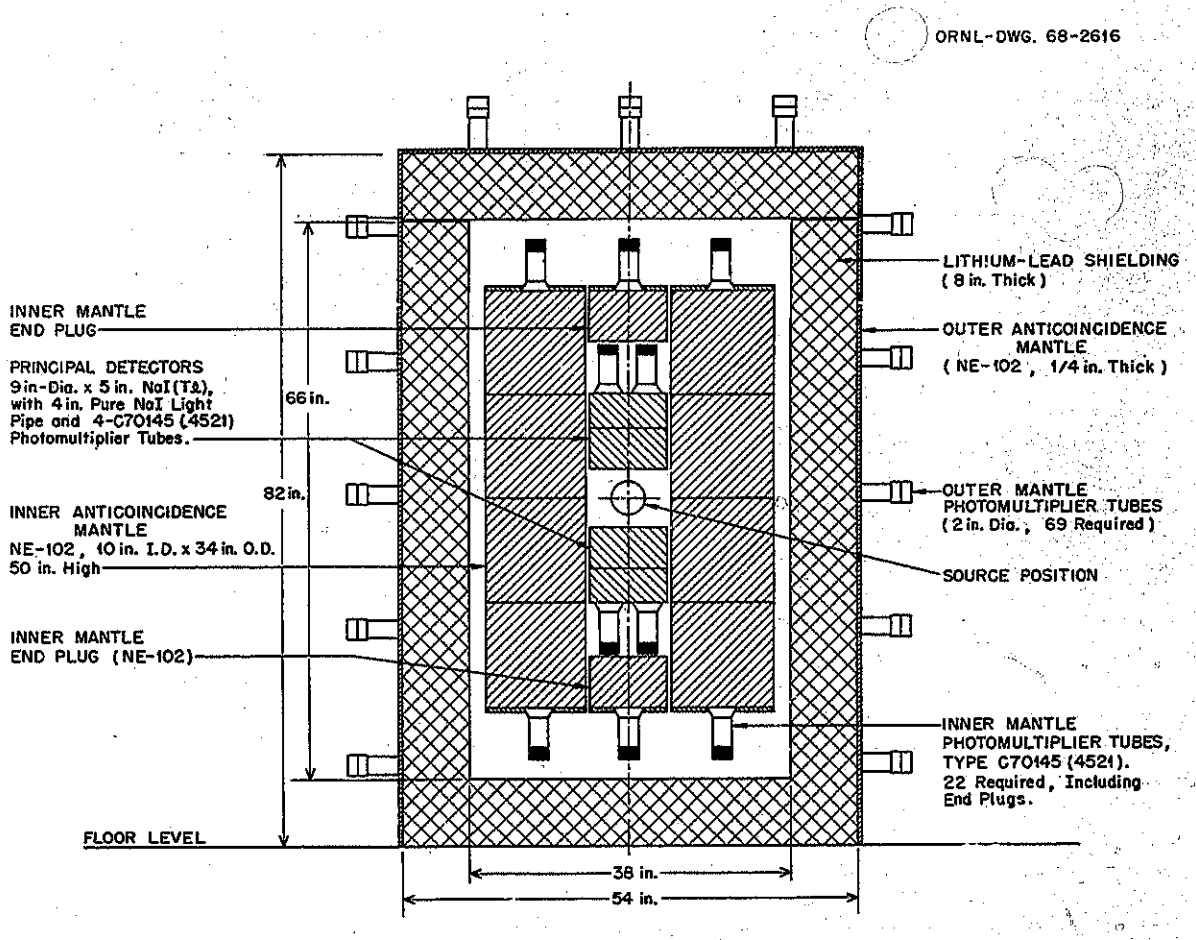

Fig. 1.9. Simplified Drawing of the Final Design for the Low-Background Gamma-Ray Spectrometers. Both the ORNL prototype and the Lunar Receiving Laboratory spectrometers were operated as shown, except the lower principal detector has no 4-in. pure NaI light pipe.

Anticoincidence Mantles

Both the prototype and the final LRL systems use an inner anticoincidence mantle of NE-102 plastic scintillator 34 in. OD by 10 in. ID and 50 in. high. Such a mantle is used both to suppress background events in the two principal detectors and to improve the NaI(Tl) detector response by suppressing events in the principal detectors for which some energy was lost through Compton scattering. The inner mantle sensitivity was adjusted so photons of energy greater than 40 kev would initiate an anticoincidence signal. Experience with the prototype suggested that an even lower threshold energy would be desirable; however, routine operation below 40 kev was precluded due to phototube noise.

The outer anticoincidence mantle should only be sensitive to mesons and should have only minimal gamma-ray sensitivity. Measurements carried out with a single 2-in.-diam photomultiplier tube mounted on 18-in. squares of NE-102 plastic scintillator of several thicknesses showed that a thickness of 0.25 in. was adequate for meson detection. Accordingly, the passive detector shield is covered on five sides with a meson-sensitive mantle of 0.25-in.-thick NE-102 viewed by 69 photomultiplier tubes located approximately 18 in. apart.

Detection efficiency for mesons was evaluated by constructing a "meson telescope," consisting of two coincident NaI(Tl) detectors located on opposite sides of a typical mantle section. When the mantle was operated in anticoincidence it was found to reject every coincident event seen by the meson telescope, even when the telescope geometry viewed mantle areas most remote from the photomultiplier tubes. Thus, the outer mantle design appears completely satisfactory.

Shielding

The passive shield for the ORNL prototype spectrometer was constructed as outlined previously.[60] The "lead concrete," composed of Chemtree-82 (a commercial lead cement[62]), mixed lead shot, LiF, and water, was poured into the basic mechanical shield structure, which was reinforced with wooden forms. Pouring of the shield was completed in late June 1967; however, release of water was slower than expected, and the mixture was slow to harden. As a precaution, detectors were not installed in the prototype system until two months had elapsed and some temporary bracing had been installed to prevent the inner liner of the shield from buckling.

After our experience with the prototype, the LRL shield was constructed with better provision for draining. The LRL shield was poured in December 1967 and was put into service in March 1968.

System Performance

As noted previously,[60] an elaborate electronic system is required to identify and record either noncoincident ("singles") events or gamma-gamma coincidence events. In addition, recording of events in either principal detector must be inhibited any time that a signal is received from either the inner or outer mantle amplifiers, or at any time these amplifiers may be overloaded to the extent that they cannot report the occurrence of a signal. When the outer mantle alone registers an event, the logic circuitry should disable recording of signals from the principal detectors only for the time required for absorption of meson-induced neutrons in the lithium-loaded lead shield (<100 μsec). If, on the other hand, both inner and outer mantles register simultaneously, then the inhibit time should be made much greater, since such an event is characteristic of a meson-induced neutron, which may produce 2.2-Mev gamma rays from the $^1H(n,\gamma)$ reaction after a long slowing-down time. A logic system to meet all of the above requirements has been constructed, which uses a combination of commercial modules and special-purpose logic units designed and fabricated at ORNL. Reliability of the system has been excellent.

Some representative data recorded with the ORNL prototype system are shown in Fig. 1.10. The upper NaI(Tl) detector used a pure NaI light guide to reduce photomultiplier-induced back-

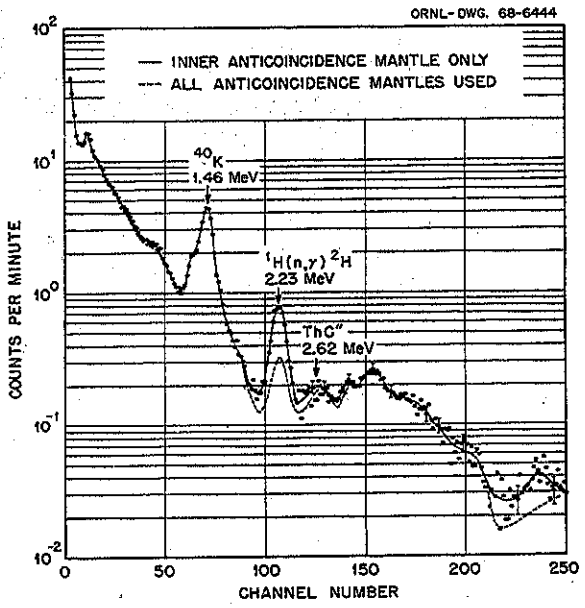

Fig. 1.10. Background Data Obtained with the ORNL Prototype System Arranged as in Fig. 1.9 and Located Inside a Room with Concrete Walls 24 in. thick in Building 4500N, ORNL. Background spectra shown are for two 9 × 5 in. NaI(Tl) principal detectors with their outputs summed (active detector volume ~10,400 cc). Dashed curve shows the effect of the outer anticoincidence mantle on suppression of the 2.2-Mev gamma ray from capture of meson-induced neutrons in the hydrogen of the inner mantle scintillator.

[62] Chemtree Corp., Central Valley, N.Y.

ground, but the lower detector had no light guide. Since both detector contributions were summed together, the principal contamination lines at 1.46 Mev (^{40}K) and 2.62 Mev (Th C″) were contributed predominantly by the lower detector. The structure above 3.2 Mev may be due to alpha-particle groups from uranium and thorium contamination in the NaI(Tl) crystals or in material close to them. The background in the energy interval 100 to 2000 kev – a useful criterion because it is independent of the 2.2-Mev peak intensity – is about 350 counts/min for the two detectors [an active NaI(Tl) volume of 10,400 cc]. With pure NaI light guides to shield both detectors and carefully chosen cladding materials, it should be possible to reduce the above background by another 30 to 40 counts/min. The most notable result of such improvements should be the reduction of the ^{40}K peak at 1.46 Mev, which is of paramount importance since the determination of small amounts of ^{40}K will be a very important use of this equipment.

The role of the outer anticoincidence mantle in reducing the neutron capture peak at 2.2 Mev is also illustrated in Fig. 1.10. It is apparent that the capture peak was greatly reduced when the outer mantle was employed.

The two detectors used in the prototype studies have been temporarily installed in the LRL system, which is located 60 ft underground with a 40-ft overburden of earth to reduce the cosmic ray flux. Preliminary background measurements in the interval 100 to 2000 kev yielded about 340 counts/min; however, the area of the neutron capture peak with all anticoincidence mantles operative was only about 0.4 count/min, compared with 1.5 counts/min for the best conditions so far obtained on the ORNL prototype, located about 840 ft above mean sea level.

2. Chemistry and Physics of Transuranium Elements

THE NEUTRON CAPTURE THERMAL CROSS SECTION AND RESONANCE INTEGRAL OF ^{252}Cf

J. Halperin C. E. Bemis, Jr.
J. R. Stokely[1]

The optimization of the production of ^{252}Cf in the HFIR has prompted an interest in the measurement of the neutron cross section of ^{252}Cf. The rate of formation of the higher einsteinium isotopes and their optimization are similarly affected by this value.

The 2.65-year ^{252}Cf captures neutrons to form the 17.6-day ^{253}Cf, which beta decays to the 20.5-day alpha-decaying ^{253}Es, as shown in expression 1:

$$^{252}Cf(n,\gamma)^{253}Cf \xrightarrow[\beta^-]{17.6\ \text{days}} {}^{253}Es \xrightarrow[\alpha]{20.5\ \text{days}} {}^{249}Bk \xrightarrow[\beta^-]{314\ \text{days}} \quad (1)$$

Following irradiation the ^{253}Es alphas were measured to evaluate the formation of the 253 mass chain. The alpha assay proved to be more accurate than a mass analysis that was also made. The mass analysis suffered from the disadvantages of the small samples and low 253 mass content.

Two samples containing ~50 ng each of ^{252}Cf were deposited upon aluminum foil and irradiated in the hydraulic tube of the ORR using a cadmium filter technique. A cadmium cylinder of 40-mil wall thickness, 10 mm in diameter and 10 mm high, was used as a neutron filter. Thin foils of a cobalt-aluminum alloy containing 0.151% cobalt were irradiated with the samples to provide a measure of the neutron flux.[2] The californium was irradiated for 60 hr in a constant thermal neutron flux of 1.57×10^{14} neutrons cm^{-2} sec^{-1} in a position where the ratio of the thermal flux to the resonance flux per unit lethargy was 8.31.

Following irradiation, the californium samples were dissolved in an HCl medium to which was added lanthanum carrier. Sodium hydroxide precipitation of $La(OH)_3$ separated the actinides from the aluminum present, and LaF_3 precipitation then separated the product from most other non-rare-earth contaminants. The sample in a 20% ethanol–saturated HCl medium was passed through a cation exchanger which separated the actinides from lanthanide contaminants. Finally a "But" column separation (a Dowex 50 column with an α-hydroxyisobutyric acid eluent) was carried out to remove the californium fraction from other actinides. The californium fraction was then electrodeposited upon a platinum plate.

The growth of the ^{253}Es 6.64-Mev alphas compared with the 6.12-Mev alphas of ^{252}Cf was measured in an alpha-ray spectrometer using a silicon detector with ~15 kev resolution. Equation 2 describes the growth of ^{253}Es from the separated sample of ^{253}Cf:

$$\frac{A_{93}}{A_{82}} = \frac{A^0_{83}}{A^0_{82}} \frac{\lambda_{93}(e^{-\lambda_{83}t} - e^{-\lambda_{93}t})}{(\lambda_{93} - \lambda_{83})e^{-\lambda_{82}t}} . \quad (2)$$

The subscript denotes the nuclide. The first digit indicates the last digit of the atomic number, and the second digit indicates the last digit of the atomic mass. (Thus the subscript 83 specifies $^{253}_{98}Cf$.) A indicates the activity, λ the radioactive

[1] Analytical Chemistry Division.

[2] We are indebted to R. E. Druschel for his help in preparing the capsule for irradiation and evaluating the neutron monitors.

decay constant, t the time after the californium-einsteinium separation and the superscript "0" refers to the time $t = 0$.

The formation of ^{253}Cf during the time of the irradiation T and the decay period τ following may be written to an adequate approximation as in Eq. 3:

$$\frac{A_{83}}{A_{82}} = \frac{\lambda_{83}}{\lambda_{82}} \frac{\phi\sigma_{82}(1 - e^{-\Lambda_{83}T})e^{-\lambda_{83}\tau}}{\Lambda_{83}\, e^{-\lambda_{82}(t+\tau)}}. \qquad (3)$$

Here $\Lambda = \lambda + \phi\sigma$, the removal rate constant while in the reactor, T is the irradiation time (at constant power level), and τ is the time following removal from the reactor (or until the chemical separation of californium and einsteinium is effected). Depending upon whether the described experiment is cadmium filtered or not, the parameters ϕ and σ are to be interpreted as ϕ_r, the resonance flux per unit lethargy, and I, the resonance integral, or as ϕ_{th}, the thermal neutron flux, and σ_{eff}, the effective reactor cross section, respectively. The resonance integral $I = \int \sigma\, dE/E$ is taken with a lower limit characterized by the neutron filter, which is 0.54 ev in the current experiment. The thermal flux ϕ_{th} is equated to the Maxwellian component of the thermal flux spectrum. The sub-cadmium reaction rate is given by the product $\phi_{th}\sigma_{th}$, where σ_{th} can be evaluated from the measured σ_{eff} through the expression $\sigma_{th} = \sigma_{eff} - (\phi_r/\phi_{th})I$. On the assumption of a $1/v$ energy dependence of the cross section in the thermal region, the value of σ_0, the 2200 m/sec cross section, can be deduced from σ_{th} using the expression $\sigma_0 = \sigma_{th}/(1 + k\phi_r/\phi_{th})$, where k is a constant dependent upon the neutron temperature of the flux distribution and was taken to be $k = 0.42$ in the current experiment.[3]

The results of the experiment are summarized in Table 2.1. The resonance integral is $42._7 \pm 4$ barns. The value of σ_0, the 2200 m/sec cross section, is $19._9 \pm 3$ barns. However, there is evidence that ^{253}Cf has a substantial fission cross section.[4] In this experiment the effect is minor but not negligible. For example, a fission cross section of 3000 barns would increase the reported value to σ_0 (^{252}Cf) = $21._1$ barns.

The value of the thermal cross section reported here can be contrasted to values of the capture cross section of ^{252}Cf ranging from 7 to 60 barns previously reported.[4,5] The resonance integral of 43 barns measured here may be compared with the value of 42 barns reported by Smith[6] *et al.* and <80 barns by Gordon and Weinstock.[7]

THE DECAY OF 10.5-hr ^{245}Pu AND 2.08-hr ^{245}Am

A. H. Wapstra[8] C. E. Bemis, Jr.

Sources of 10.5-hr ^{245}Pu have been prepared by short neutron irradiations in the Oak Ridge Re-

[3] R. W. Stoughton and J. Halperin, *Nucl. Sci. Eng.* 6, 100 (1959).

[4] J. E. Bigelow, personal communication.

[5] J. A. Smith, C. J. Banick, R. L. Folger, H. P. Holcomb, and I. B. Richter, *Reactor Cross Sections for Pu-242–Cf-252*, E. I. du Pont de Nemours and Co., Aiken, S.C., Savannah River Lab., DP-MS-67-111 (Feb. 28, 1968).

[6] R. L. Folger, J. A. Smith, L. C. Brown, R. F. Overman, and H. P. Holcomb, *Foil Measurements on Integral Cross Sections of Higher Mass Actinides*, E. I. du Pont de Nemours and Co., Aiken, S.C., DP-MS-67-112 (March 1, 1968).

[7] L. M. Gordon and E. V. Weinstock, paper 77, ACS Meeting, San Francisco, April 1, 1968.

[8] Present address, Instituut voor Kernphysisch Onderzoek, Amsterdam, Netherlands.

Table 2.1. The Cross Section of ^{252}Cf

Sample	A_{93}/A_{82} at Separation	N_{83}/N_{82} at Discharge (ppm)	I (barns)	σ_{eff}[a] (barns)	σ_{th} (barns)	σ_0 (barns)
Cd filtered	0.00891	162 ± 5	$42._5 \pm 4$			
Unfiltered	0.0461	837 ± 20[b]		$26._0 \pm 3$	$20._9 \pm 3$	$19._9 \pm 3$

[a] Calculated on the basis of negligible burnout of ^{253}Cf due to fission; that is, σ_F (^{253}Cf) <500 barns.

[b] A mass assay gave 750 ± 150 ppm.

search Reactor of electromagnetically enriched samples of 8.28×10^7-year ^{244}Pu (75% ^{244}Pu, 25% ^{242}Pu). Equilibrium sources of ^{245}Pu and the daughter product, ^{245}Am, were used in an investigation of the decay of these species. A 35-cm^3 Ge(Li) detector system coupled to a 4096-channel analyzer was used to measure the gamma-ray spectrum. The resolution of the spectrometer system under the condition of these measurements was 2.48 kev (FWHM) for 1.332-Mev gamma rays. Using calibrated sources, the absolute and relative full-energy peak efficiency curve was measured for the energy range of interest. Mean full-energy peak channel numbers were converted to energies using standard gamma-ray sources together with an integral linearity curve determined for the spectrometer system. The nonlinearity correction for the system, determined both from gamma-ray standards and using a precision pulser, was never more than ±0.5 channel for channel numbers between 100 and 4096.

Table 2.2. Gamma-Ray Energies (E_γ) and Relative Intensities (I_γ) Observed in the Decay of ^{245}Pu-^{245}Am

Present Work		Previous Work[a,b]		Present Work		Previous Work[a,b]	
E_γ(kev)	I_γ	E_γ(kev)	I_γ	E_γ(kev)	I_γ	E_γ(kev)	I_γ
240.84 ± 0.07	1.0 ± 0.2[c]	240	5.6 ± 1.1	530.6 ± 0.3	0.2 ± 0.1		
252.72 ± 0.07	33 ± 3[c]	252.3	100	549.2 ± 0.6	0.2 ± 0.1		
277.0 ± 0.5	0.10 ± 0.05			560.03 ± 0.04	32 ± 3	560.1 ± 0.5	30 ± 2
280.29 ± 0.07	7.6 ± 0.8	280.2 ± 0.5	6 ± 1	591.6 ± 0.3	1.0 ± 0.2	591.8 ± 0.5	1.1 ± 0.3
293.2 ± 0.5	0.10 ± 0.05			593.7 ± 0.6	0.2 ± 0.1		
295.60 ± 0.15	0.45 ± 0.1[c]	296	3.6 ± 1.1	598.8 ± 0.3	0.7 ± 0.2	600 ± 1	0.4 ± 0.2
299.8 ± 0.7	0.1 ± 0.05			624.4 ± 0.4	1.3 ± 0.2	624 ± 1	1.3 ± 0.3
308.11 ± 0.07	29 ± 3	308.0 ± 0.5	23 ± 2	630.04 ± 0.07	16 ± 2	629.9 ± 0.5	
327.31 ± 0.07	150 ± 15	327.2 ± 0.5	100	642	< 0.2	642 ± 1	0.6 ± 0.3
333.1 ± 0.3	0.2 ± 0.1			657.2 ± 0.7	0.8 ± 0.4		
341.00 ± 0.15	0.6 ± 0.1	341 ± 1	0.8 ± 0.1	660.2 ± 0.10	5.0 ± 0.7	660.2 ± 0.5	4 ± 1
348.73 ± 0.07	5.7 ± 0.6	349 ± 1	5.0 ± 1	662.2 ± 0.7	0.5 ± 0.2		
357.90 ± 0.20	0.37 ± 0.10			669.28 ± 0.10	2.0 ± 0.3	669.5 ± 0.5	1.7 ± 0.3
376.58 ± 0.07	19 ± 2	376.5 ± 0.5	20 ± 2	687.6 ± 0.8	0.2 ± 0.1	687 ± 2	0.6 ± 0.3
381.9 ± 0.3	0.25 ± 0.1[d]			691	< 0.2	691 ± 2	0.5 ± 0.3
387.88 ± 0.10	1.7 ± 0.4	388 ± 1	0.8 ± 0.3	696.8 ± 0.4	0.5 ± 0.15	697 ± 1	0.7 ± 0.2
392.7 ± 0.4	0.4 ± 0.3			701.7 ± 0.3	0.4 ± 0.15	703 ± 2	0.5 ± 0.2
395.87 ± 0.15	0.6 ± 0.2			707.98 ± 0.20	1.6 ± 0.25	708 ± 2	1.8 ± 0.2
411.74 ± 0.10	2.9 ± 0.3	412 ± 1	3 ± 1	712	< 0.2	712 ± 2	0.3 ± 0.1
423.2 ± 0.3	< 0.2	423 ± 1	0.3 ± 0.1	730.40 ± 0.20	1.1 ± 0.15	730 ± 2	1.0 ± 0.3
428.51 ± 0.10	3.1 ± 0.3	428 ± 0.5	2.5 ± 0.5	733.5 ± 0.4	0.5 ± 0.2		
439.0 ± 1.0	0.2 ± 0.1			737.96 ± 0.20	1.3 ± 0.3	738 ± 2	1.7 ± 0.3
445.34 ± 0.10	1.8 ± 0.3	445.2 ± 0.5	1.6 ± 0.4	740.2 ± 0.7	0.8 ± 0.3		
450.0 ± 1.0	0.2 ± 0.1			743.70 ± 0.20	0.9 ± 0.2		
475.1 ± 0.6	0.35 ± 0.15			750.1 ± 1.0	0.1 ± 0.1	749 ± 2	0.3 ± 0.1
479.8 ± 1.0	0.12 ± 0.06			758.2 ± 0.8	0.2 ± 0.1		
481.9 ± 1.0	0.08 ± 0.04			762.73 ± 0.10	4.2 ± 0.4	763 ± 1	3 ± 1
486.3 ± 0.6	0.2 ± 0.1			766.59 ± 0.15	2.1 ± 0.3	767 ± 1	1.7 ± 0.5
491.50 ± 0.07	16 ± 1.5	492 ± 1	15 ± 2	776.66 ± 0.20	1.2 ± 0.2	776 ± 2	1.4 ± 0.4
511.5 ± 1.0	0.2 ± 0.1			781.55 ± 0.30	0.4 ± 0.15		
514.6 ± 0.2	1.0 ± 0.2			786.54 ± 0.15	2.2 ± 0.3	787 ± 1	1.7 ± 0.2
518.2 ± 0.5	0.3 ± 0.1	515(complex)	1.2 ± 0.3	796.37 ± 0.17	1.5 ± 0.4	796 ± 2	2 ± 1
525.08 ± 0.15	1.6 ± 0.2	525 ± 1	1.2 ± 0.3	799.87 ± 0.10	9.3 ± 1.0	800 ± 1	10 ± 2

Table 2.2 (Continued)

Present Work		Previous Work[a,b]		Present Work		Previous Work[a,b]	
E_γ(kev)	I_γ	E_γ(kev)	I_γ	E_γ(kev)	I_γ	E_γ(kev)	I_γ
817.04 ± 0.10	5.0 ± 0.5	817 ± 2	4.0 ± 0.5	972.6 ± 0.5	0.5 ± 0.2		
821.9 ± 0.7	0.5 ± 0.15	821 ± 2	0.5 ± 0.2	975 ± 1	1.5 ± 1.0	977 ± 2	3.0 ± 0.5
824	< 0.2	824 ± 2	0.7 ± 0.3	977.2 ± 0.2	2.3 ± 1.0		
833.14 ± 0.10	3.1 ± 0.3	833 ± 2	3.0 ± 0.5	982.4 ± 0.7	0.5 ± 0.2		
840.56 ± 0.10	7.6 ± 0.8	841 ± 2	6.0 ± 0.5	987.60 ± 0.10	7.8 ± 0.8	988 ± 2	6.5 ± 1.0
859.53 ± 0.15	3.0 ± 0.3	860 ± 2	2.7 ± 0.3	996.0 ± 0.3	1.2 ± 0.2	996 ± 2	0.8 ± 0.2
868.8 ± 0.4	0.7 ± 0.2	870 ± 2	0.7 ± 0.2	1001.0 ± 1.0	0.15 ± 0.10		
870.5 ± 0.5	0.4 ± 0.2			1005.1 ± 0.3	1.6 ± 0.6	1005 ± 3	1.2 ± 0.3
874.16 ± 0.20	0.8 ± 0.2	874 ± 2	0.7 ± 3	1007.31 ± 0.15	2.4 ± 0.6	1008 ± 3	2.5 ± 0.5
879.6 ± 0.4	0.3 ± 0.1	879 ± 2	0.4 ± 0.2	1013.2 ± 0.3	0.6 ± 0.2		
887.14 ± 0.15	4.2 ± 0.5	887 ± 2	3.0 ± 0.5	1018.33 ± 0.15	6.1 ± 0.8	1019 ± 2	5 ± 1
899.3 ± 1.0	0.2 ± 0.1	899 ± 3	0.4 ± 0.2	1023.32 ± 0.20	3.2 ± 0.6	1024 ± 2	2.0 ± 0.5
901.9 ± 0.8	0.3 ± 0.15			1028.2 ± 1.0	0.10 ± 0.04		
910.46 ± 0.07	8.2 ± 0.8	911 ± 2	7 ± 1	1036.2 ± 0.8	0.05 ± 0.02		
917.0 ± 0.5	0.5 ± 0.15	917 ± 3	0.5 ± 0.2	1040.2 ± 1.2	0.04 ± 0.02		
923.0 ± 0.6	0.3 ± 0.1			1042.4 ± 0.8	0.09 ± 0.03	1042 ± 3	0.10 ± 0.05
925.4 ± 1.0	0.10 ± 0.05	926 ± 3	0.10 ± 0.05	1051.3 ± 0.08	0.03 ± 0.01		
930.3 ± 0.6	0.3 ± 0.15	931 ± 3	0.10 ± 0.05	1079.1 ± 1.0	0.03 ± 0.01		
938.4 ± 0.2	6.0 ± 1.0			1083.9 ± 0.5	0.20 ± 0.04	1084 ± 3	0.10 ± 0.05
941.0 ± 1.0	1.5 ± 1.0	938 ± 2	7 ± 1	1093.7 ± 0.7	0.08 ± 0.03		
945.2 ± 0.5	0.3 ± 0.1	946 ± 3	0.10 ± 0.05	1097.9 ± 0.7	0.10 ± 0.03		
953 ± 1.5	0.10 ± 0.05			1111.9 ± 0.5	0.32 ± 0.04	1112 ± 3	0.3 ± 0.1
957.59 ± 0.15	5.8 ± 0.6	958 ± 2	5.0 ± 0.5	1138.5 ± 0.5	0.25 ± 0.04	1138 ± 3	0.2 ± 0.1
964.0 ± 0.7	0.25 ± 0.1			1166.3 ± 0.5	0.30 ± 0.04	1166 ± 3	0.3 ± 0.1
968.5 ± 0.7	0.2 ± 0.1						

[a] W. R. Daniels, D. C. Hoffman, F. O. Lawrence, and C. J. Orth, *Nucl. Phys.* A107, 569 (1968).

[b] M. E. Bunker, D. C. Hoffman, C. J. Orth, and J. W. Starner, *Nucl. Phys.* A97, 593 (1967).

[c] ^{245}Am decay.

[d] ^{243}Pu decay.

The gamma-ray energies and intensities together with the results of previous workers[9,10] are listed in Table 2.2. Approximately 66 of the observed 105 transitions in the decay of 10.5-hr ^{245}Pu have been placed in a level scheme for ^{245}Am. Three distinct rotational bands based on the Nilsson single-particle states, the $5/2^+[642]$, the $5/2^-[523]$, and $7/2^+[633]$, have been observed with band head energies at 0, 27.90, and 327.31 kev respectively. Moments of inertia, $\hbar^2/2I$, have been calculated from the energies of the rotational states and are 3.4, 6.0, and 7.3 kev for the orbitals $5/2[642]$, $5/2[523]$, and $7/2[633]$ respectively. Four or more rotational members were observed in each of the three bands.

Energy levels and assignments are listed in Table 2.3. Coincidence experiments together with high resolution conversion electron measurements using the ORNL 35-cm iron-free electron spectrometer are planned to further investigate the decay scheme.

[9] W. R. Daniels, D. C. Hoffman, F. O. Lawrence, and C. J. Orth, *Nucl. Phys.* A107, 569 (1968).

[10] M. E. Bunker, D. C. Hoffman, C. J. Orth, and J. W. Starner, *Nucl. Phys.* A97, 593 (1967).

Table 2.3. Energy Levels and Assignments in ^{245}Am Observed in the Decay of ^{245}Pu

Energy (kev)	Assignment (I,π)	Comments
0	$5/2^+$	$5/2[642]$ band head
19.20	$7/2^+$	$K = 5/2$
27.90	$5/2^-$	$5/2[523]$ band head
47.03	$9/2^+$	$K = 5/2$
70.30	$7/2^-$	$K = 5/2$
87.66	$11/2^+$	$K = 5/2$
124.45	$9/2^-$	$K = 5/2$
134.45	$13/2^+$	$K = 5/2$
190.80	$11/2^-$	$K = 5/2$
327.31	$7/2^+$	$7/2[633]$ band head
395.77	$9/2^+$	$K = 7/2$
475.54	$11/2^+$	$K = 7/2$
562.8	$13/2^+$	$K = 7/2$
887.4	$(7/2^+)$	
921.0		
957.5	$(9/2^+)$	
987.5		
1024.1		
1065.2		
1070.4		
1185.6		

INVESTIGATION OF THE DECAY OF ^{172}Hf AND ^{172}Lu

M. F. Roche[11] R. L. Hahn
K. S. Toth[11] C. E. Bemis, Jr.
T. H. Handley[12]

Long-lived ^{172}Hf (~5 years) was produced by bombarding lutetium oxide with protons accelerated in the Oak Ridge Isochronous Cyclotron. After a year the hafnium fraction was chemically separated from the irradiated lutetium. At that time the only radioactivity remaining in the hafnium fraction was due to the decay of ^{172}Hf. In this manner, by waiting a few months, a source of ^{172}Lu (6.7 days), in equilibrium with its hafnium parent, became available for decay studies.

The gamma rays from this source were counted for ten days with a 35-cm^3 Ge(Li) crystal spectrometer connected to a 4096-channel analyzer. Under these conditions, the resolution was 2.4 kev full width at half maximum for the 1002.5-kev gamma ray in the spectrum. The resultant gamma-ray spectrum from the decay chain $^{172}Hf \rightarrow {}^{172}Lu \rightarrow {}^{172}Yb$, covering the energy range from 90 to 2266 kev, is shown in Fig. 2.1. The combination of high counting rate of the sample (~10 μC) and high resolution of the spectrometer made possible the identification of many new gamma rays in the decay of ^{172}Lu.

The measured photon intensities were combined with published conversion-electron data[13] to obtain *K*-shell internal conversion coefficients (ratio of *K*-shell conversion-electron intensity to gamma-ray intensity). The resulting values are plotted in Fig. 2.2 and compared with the calculated conversion coefficients of Sliv and Band.[14] It is seen that most of the experimental values are consistent with predicted values for *M*1 and *E*2 transitions, as is expected for states in deformed even-even nuclei. However, some of the transitions appear to be *E*1 in character, confirming the presence of negative-parity levels in ^{172}Yb.[15,16]

Because naturally occurring ^{174}Hf has been observed to undergo alpha decay with a half-life of 2×10^{15} years, a search for possible alpha decay in ^{172}Hf was also undertaken. A limit of $> 10^{12}$ years for this decay mode was determined.

A level scheme incorporating the new information from this work and that from previously proposed decay schemes is currently being constructed for the decay $^{172}Lu \rightarrow {}^{172}Yb$.

[11] Electronuclear Division.

[12] Analytical Chemistry Division.

[13] B. Harmatz, T. H. Handley, and J. W. Michelich, *Phys. Rev.* 123, 1758 (1961).

[14] L. A. Sliv and I. M. Band, *Gamma Rays*, Acad. Sci. USSR, Moscow-Leningrad (1961); also p. 1639 in *Alpha-, Beta- and Gamma-Ray Spectroscopy*, vol. 2, K. Siegbahn (ed.), North-Holland Publ. Co., Amsterdam, 1965.

[15] J. G. Prather, unpublished thesis, Utah State University, 1967.

[16] O. H. Otteson and R. G. Helmer, *Phys. Rev.* 164, 1485 (1967).

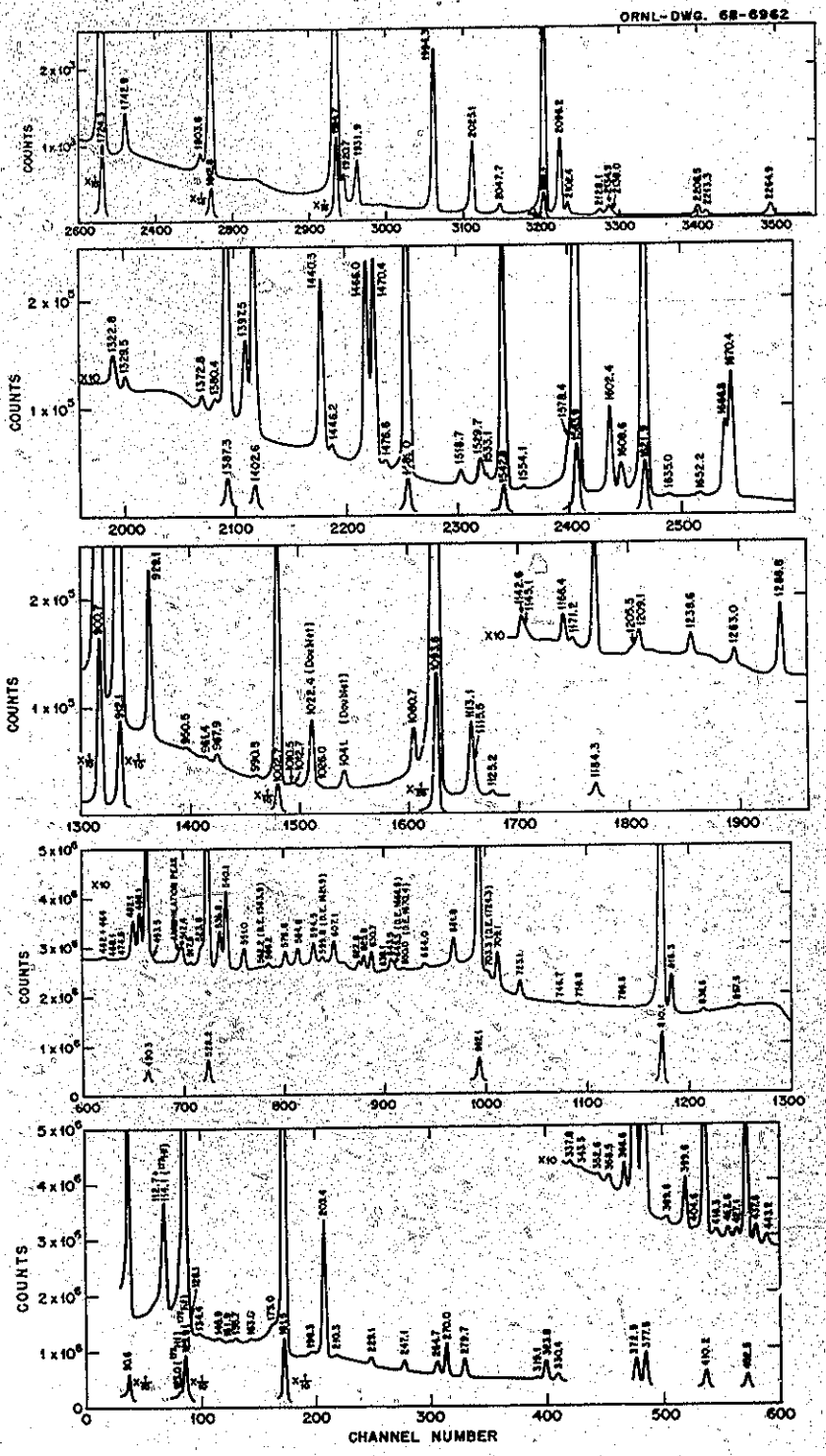

Fig. 2.1. Gamma-Ray Spectrum Obtained with a High-Resolution Ge(Li) Gamma-Ray Spectrometer from an Equilibrium Mixture of ^{172}Hf and ^{172}Lu.

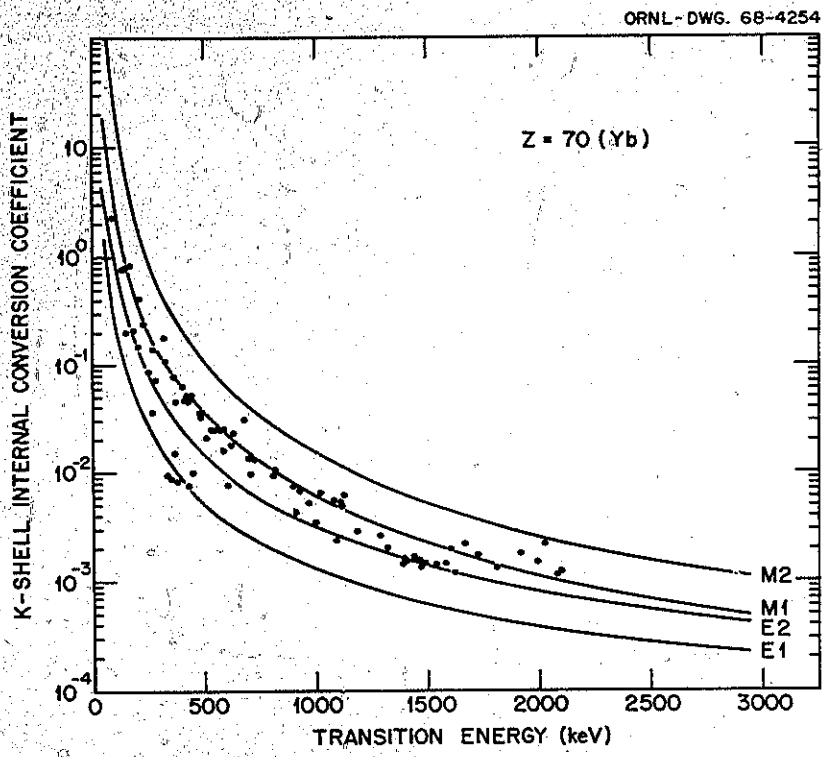

Fig. 2.2. Comparison of Experimentally Determined K-Shell Internal Conversion Coefficients with Those Calculated by Sliv and Band.[4]

THE ALPHA DECAY OF ^{253}Cf AND ^{254}Cf

C. E. Bemis, Jr. J. Halperin

The alpha branching decay of 60.5 ± 0.2 day ^{254}Cf has been observed with high-resolution surface-barrier detectors. A small sample of californium, irradiated in the High Flux Isotope Reactor for a flux-time product of 1.3×10^{22} neutrons/cm^2 (69.7×100 Mwd), was electromagnetically enriched in ^{254}Cf using the Livermore isotope separator.[17] The section of the aluminum collector plate corresponding to mass 254 was removed, and the alpha spectrum together with the total number of fission events was measured using cooled surface-barrier detectors at an energy resolution of ~10 kev (FWHM). After applying a small correction, ~0.01%, to the number of fission events due to ^{252}Cf which was present in the sample, the resulting alpha/fission ratio for ^{254}Cf is $(3.10 \pm 0.16) \times 10^{-3}$. The partial alpha half-life for ^{254}Cf corresponding to this ratio is 53.4 ± 2.7 years.

Using the alpha-particle energies for the main groups of ^{252}Cf (6.119 Mev), ^{254}Es (6.437 Mev), and ^{253}Es (6.640 Mev), which were also present in the sample, as calibration points, the measured alpha decay energy for ^{254}Cf to the ground state of ^{250}Cm is 5.834 ± 0.003 Mev.

In order to avoid the two-stage isotope separation process that would be involved in producing ^{250}Cm via the double neutron capture route using ^{248}Cm as the target, a more profitable method may be the irradiation of ^{252}Cf to produce ^{254}Cf, which would then be allowed to decay. The nuclide ^{250}Cm is produced via alpha decay of ^{254}Cf. The yields of the two methods are quite comparable considering the efficiencies of the isotope separation processes.

[17] We are indebted to E. K. Hulet and R. J. Dupzyk of Lawrence Radiation Laboratory, Livermore, for performing this isotope separation.

The alpha decay of ^{253}Cf has also been observed in these measurements. From the collector position corresponding to mass 253, alpha particles with an energy of 5.979 ± 0.005 Mev were observed. This energy corresponds to an alpha transition to the $^{7}/_{2}^{+}$[613] state in ^{249}Cm, as previously reported.[18] No other alpha transitions with an intensity greater than 5% of the 5.979-Mev transition were observed that could be ascribed to ^{253}Cf decay. This result is also in accord with the previous result.[18]

NEW NEPTUNIUM ISOTOPES, ^{229}Np AND ^{230}Np

R. L. Hahn M. F. Roche[19]
K. S. Toth[19]

The study and correlation of the decay properties of isotopes of the heavy elements is of great interest since these elements are of almost unique importance for the investigation of the phenomena of fission, spontaneous fission decay, and alpha decay. A program was recently begun to synthesize new neutron-deficient transuranium isotopes by bombarding enriched heavy-element targets with projectiles accelerated in the Oak Ridge Isochronous Cyclotron (ORIC). Detection of the alpha particles emitted in the decay of these new nuclear species was selected as the means of identification because: (1) an alpha-particle energy combined with a particular decay half-life is an extremely specific mode of identification, (2) background problems due to beta-gamma contamination are essentially eliminated, and (3) the study of the alpha spectra of these new isotopes adds to the knowledge of alpha-decay systematics in the heavy-element region.

In the first series of experiments a ^{233}U (99.99%) target was bombarded with protons to produce neptunium isotopes by (p,xn) reactions. Product nuclei, recoiling out of the thin target, were collected on a beryllium catcher foil placed behind the target. To facilitate the detection of short-lived radionuclides and at the same time guarantee containment of the ^{233}U alpha activity, the experiments were performed on-line at ORIC. After irradiation, a remotely controlled arrangement was used to transfer the catcher foil from behind the target to a position in front of an Si(Au) detector. Alpha spectra were stored in a 1600-channel analyzer whose memory was utilized in an 8- by 200-channel mode. Data could then be taken at eight different times after bombardment and half-lives determined for all the observed alpha peaks.

An initial survey of nuclides produced in proton bombardments from 24 to 56 Mev established that two new alpha groups had indeed been observed. The optimum bombarding energies, 32 and 42 Mev, were then selected for the production of ^{230}Np and ^{229}Np by means of $(p,4n)$ and $(p,5n)$ reactions. Because of the large probability for fission, which competes with neutron evaporation from the compound nucleus, low counting rates were encountered. To compensate for the low counting statistics,

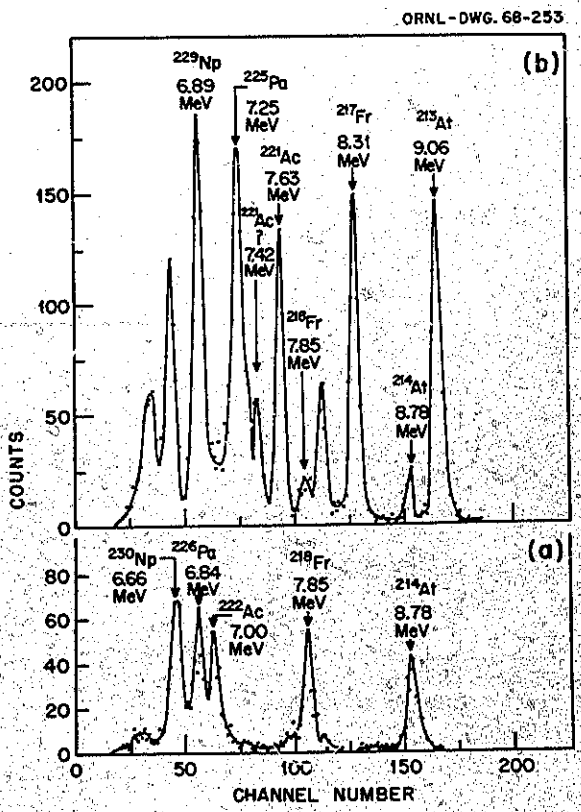

Fig. 2.3. Alpha-Particle Spectra Measured in Proton Bombardments of ^{233}U. (*a*) At 32 Mev the new isotope ^{230}Np and its α-decay daughters are seen. (*b*) The spectrum at 42 Mev shows new isotope ^{229}Np and its descendants.

[18] Combined Radiochemistry Group, *Phys. Rev.* 148, 1192 (1966).

[19] Electronuclear Division.

multiple bombardments were made at each of the two energies, and the data from successive irradiations were summed.

The two sections of Fig. 2.3 show the spectra observed at 32 and 42 Mev. In addition to the ^{230}Np (6.66-Mev) and ^{229}Np (6.89-Mev) peaks, the alpha-decay daughters present in the two decay chains are also seen and identified. The low-intensity peak at 7.42 Mev in part *b* of the figure is tentatively assigned to the alpha decay from ^{221}Ac to an excited state in ^{217}Fr.

The half-lives of ^{230}Np and ^{229}Np were found to be 4.6 ± 0.3 and 4.0 ± 0.2 min respectively. Transient equilibrium in the decay chains is achieved rapidly after the two parents are produced because the half-lives of the descendants are much shorter than those of the parents. However, the half-life of ^{226}Pa (the alpha-decay daughter of ^{230}Np) is 1.8 min, so that by proper choice of irradiation and counting intervals, it is possible to observe the 1.8-min growth followed by the 4.6-min decay of each of the daughter nuclides in the ^{230}Np chain, as is shown in Fig. 2.4. Part *a* presents curves for the parent ^{230}Np and for a composite of the data for all its daughters, while part *b* shows points for each daughter separately.

Table 2.4 summarizes the new information gathered in this study and compares it with previously known data. The alpha-particle energies for ^{230}Np, ^{229}Np, and ^{225}Pa are new. Energies calculated from the $Q(\alpha)$ values obtained by Viola and Seaborg[20] in their study of decay

[20] V. E. Viola, Jr., and G. T. Seaborg, *J. Inorg. Nucl. Chem.* 28, 697, 741 (1966).

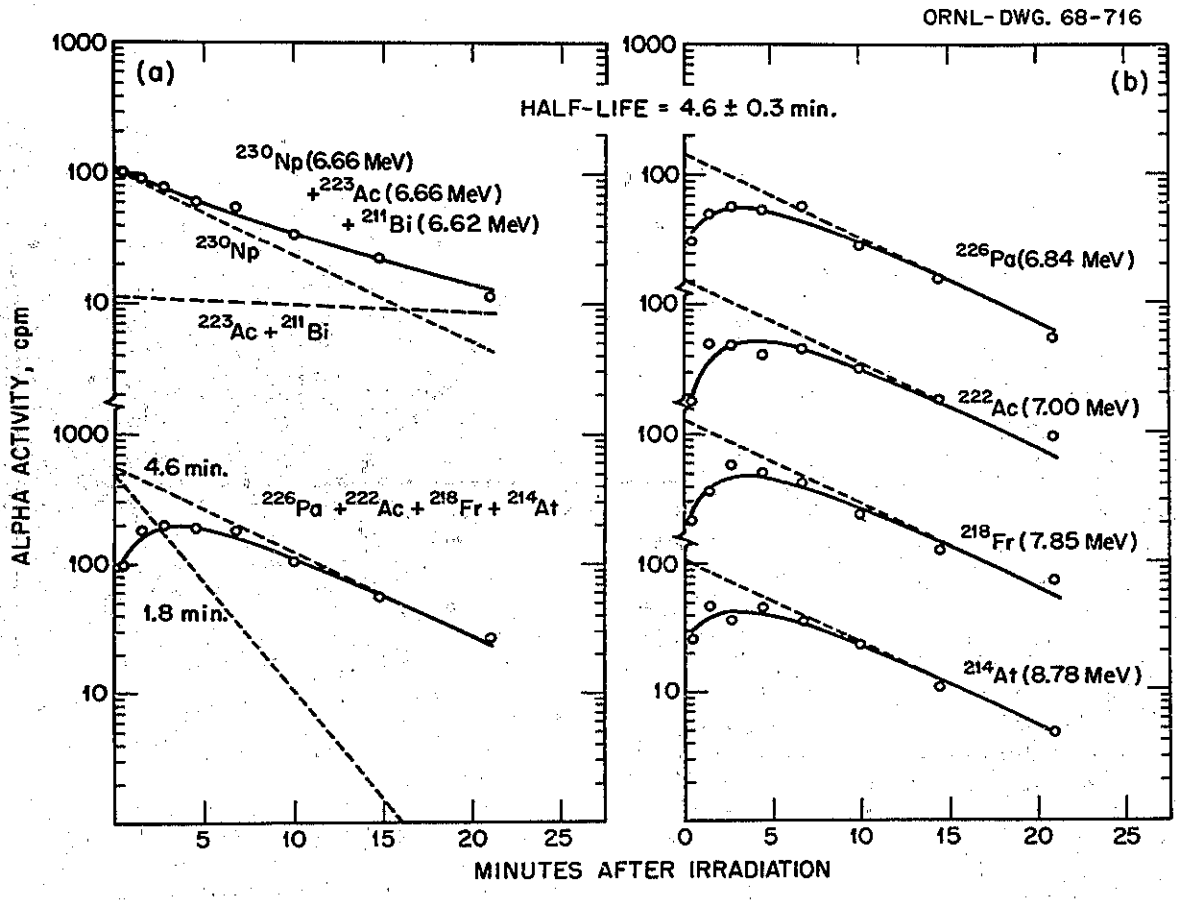

Fig. 2.4. Least-Squares Fits to the Decay Data Taken at 32 Mev. The growth of the 1.8-min ^{226}Pa decay chain following the decay of 4.6-min ^{230}Np is clearly demonstrated. Unlabeled peaks arise from other decay chains.

Table 2.4. Summary of New Alpha-Decay Information

Nuclide	Alpha-Particle Energies (Mev)		
	Present Study (±0.02)	Calculated[a]	Literature[b]
^{230}Np	6.66	6.65	
^{229}Np	6.89	6.98	
^{225}Pa	7.25	7.29	
^{221}Ac	7.63 (~70%) 7.42 (~30%)		7.6
^{217}Fr	8.31		8.3
^{213}At	9.06		9.2

[a]V. E. Viola, Jr., and G. T. Seaborg, *J. Inorg. Nucl. Chem.* 28, 697, 741 (1966).
[b]C. M. Lederer, J. M. Hollander, and I. Perlman, *Table of Isotopes*, Wiley, New York, 1967.

systematics are in agreement with the experimental ones. Furthermore, the earlier alpha-particle energies[21] of the products following ^{229}Np were reported only to within 0.1 Mev, so that the energies reported herein to ±0.02 Mev represent a significant improvement in precision.

PARTIAL ALPHA HALF-LIVES OF ^{242}Pu AND ^{244}Pu

J. Halperin C. E. Bemis, Jr.
R. Eby[22]

A refinement in the analysis of the ^{242}Pu and ^{244}Pu half-life experiments[23] has been made.

For the ^{242}Pu alpha half-life measurements, mixed samples of ^{239}Pu and ^{242}Pu were prepared for mass analysis and for alpha spectral analysis. Using a value of 24,401.5 ± 21.2 years for the ^{239}Pu alpha half-life, the resulting values for the partial alpha half-life of ^{242}Pu are given in Table 2.5. The adopted value for the ^{242}Pu alpha half-life is $(3.869 \pm 0.016) \times 10^5$ years.

Samples of plutonium, highly enriched in ^{244}Pu (~75%) were mass analyzed and the ratio of ^{242}Pu alpha events to ^{244}Pu alpha events measured using the system previously reported.[23] The results of two determinations using two samples of different ^{244}Pu concentration are presented in Table 2.6. Using the adopted value of $(3.869 \pm 0.016) \times 10^5$ years for the ^{242}Pu alpha half-life, a value of $(8.28 \pm 0.10) \times 10^7$ years was determined for the ^{244}Pu partial alpha half-life. The result for ^{244}Pu is in substantial agreement with previous determinations by other workers.[24]

Results of these experiments are being prepared for publication.

SEARCH FOR THE NEW NUCLIDE ^{247}Pu

C. E. Bemis, Jr. J. Halperin

A series of experiments designed to produce and identify the unknown nuclide ^{247}Pu have been performed.

Approximately 500 μg of plutonium, isotopically enriched in ^{244}Pu (76.94% ^{244}Pu, 22.88% ^{242}Pu) was irradiated in the High Flux Isotope Reactor for a total flux-time product of $\sim 1.3 \times 10^{22}$ neutrons/cm^2 (69.7 × 100 Mwd). Following the irradiation, the plutonium product was chemically recovered by an $La(OH)_3$ precipitation, an LaF_3 precipitation, and an ion exchange separation on

[21]C. M. Lederer, J. M. Hollander, and I. Perlman, *Table of Isotopes*, Wiley, New York, 1967.
[22]Analytical Chemistry Division.
[23]C. E. Bemis and J. Halperin, *Chem. Div. Ann. Progr. Rept. May 20, 1967*, ORNL-4164, p. 3.
[24]P. R. Fields *et al.*, *Nature* 212, 131 (1966).

Table 2.5. Summary of Results for ^{242}Pu

Sample	Activity Ratio,[a] A_{242}/A_{239}	Mass Ratio,[a] N_{239}/N_{242}	^{242}Pu Half-Life (years)
			$\times 10^5$
A	0.74747 ± 0.00111	0.08417 ± 0.00076	3.879 ± 0.035
B	0.26232 ± 0.00063	0.23637 ± 0.00194	3.936 ± 0.034
C	2.1758 ± 0.00395	0.02905 ± 0.00025	3.861 ± 0.033
D	0.15226 ± 0.00050	0.41683 ± 0.00242	3.845 ± 0.026
Weighted average[b]			3.869 ± 0.016

[a]The errors assigned represent the standard deviation.

[b]The average value was determined by weighting the individual values according to their standard deviation (statistical weights).

Table 2.6. Summary of Results for ^{244}Pu

Sample	Activity Ratio,[a] A_{244}/A_{242}	Mass Ratio,[a] N_{244}/N_{242}	^{244}Pu Half-Life (years)
			$\times 10^7$
1	0.01344 ± 0.00024	2.926 ± 0.030	8.40 ± 0.18
2	0.01582 ± 0.00018	3.363 ± 0.027	8.22 ± 0.12
Weighted average[b]			8.28 ± 0.10

[a]The errors assigned represent the standard deviation.

[b]The average value was determined by weighting the individual values according to their standard deviation (statistical weights).

Dowex 1 in an HCl medium. A mass analysis[25] of the purified product (10.6% ^{242}Pu, 89% ^{244}Pu, 108 ppm ^{246}Pu at reactor discharge) together with the measured plutonium chemical yield indicated that approximately 0.05 μg of ^{246}Pu was recovered.

Small samples of the recovered plutonium containing 3.5 ng of ^{246}Pu were irradiated at a flux of $\sim 5 \times 10^{13}$ neutrons cm^{-2} sec^{-1} for times ranging from 2 to 10 min in the pneumatic tube facility in the Oak Ridge Research Reactor. The irradiated plutonium was carried through an LaF_3 precipitation cycle to remove fission products and loaded on a Dowex 1 anion exchange column in 10 *M* HCl which was positioned in front of a 35-cc Ge(Li) detector. The resolution of the spectrometer system was measured to be 2.5 kev (FWHM) for 1.33-Mev gamma rays. The ^{245}Am and ^{246}Am daughter products were continually eluted off the column during the course of the experiment, which consisted in taking a series of short successive gamma-ray spectra in order to identify new transitions which might be ascribed to the beta decay of ^{247}Pu.

From systematics, ^{247}Pu is expected to have a ground-state configuration of $\frac{1}{2}^+[620]$ in the

[25]We are indebted to R. Eby for performing these measurements.

Nilsson model and to have a total beta-decay energy of about 2.1 Mev. Predictions from systematics and information on the decay[26] of 24-min ^{247}Am indicate a ground-state configuration for ^{247}Am of either $\frac{5}{2}^+[642]$ or $\frac{5}{2}^-[623]$. The beta decay of ^{247}Pu may be expected to populate the $\frac{3}{2}^-[521]$ and the $\frac{1}{2}^-[521]$ proton states in ^{247}Am at energies of about 100 and 900 kev, respectively, which would lead to a predicted half-life for ^{247}Pu in the range of a few minutes.

We have searched for unidentified gamma rays in the range 200 to 100 kev in our experimental spectra without success. If we assume irradiation to near saturation for ^{247}Pu, an upper limit to the (n,γ) cross section for ^{246}Pu of 250 mb may be set from the absence of gamma rays in our spectra, or conversely, if the (n,γ) cross section is as high as 1 barn, the ^{247}Pu half-life is less than ~1 min.

A very low (n,γ) cross section for ^{246}Pu is expected in analogy with other closed-shell or semimagic nuclei. These experiments will be continued after the installation of an isotope separator, which would increase the sensitivity of our experiments by a factor of 100.

NUCLEAR REACTION SPECTROSCOPY WITH THE TRANSURANIUM ELEMENTS

R. L. Hahn
K. S. Toth[27]
E. Newman[27]
M. F. Roche[27]

Nuclear reaction spectroscopy involves the measurement of the energies and angular distributions of the light particles emitted during a nuclear reaction. It is a powerful experimental technique that has contributed significantly to our knowledge in areas such as nuclear reaction mechanisms, nuclear structure, optical-model parameters, and nuclear radii and deformations.

To test the feasibility of applying this technique to the study of the transuranides, a preliminary study was recently begun of the ^{238}U(^{3}He, d)^{239}Np reaction at the Oak Ridge Isochronous Cyclotron. The ^{3}He kinetic energy was 50 Mev. Because of the high resolution required to separate the closely spaced energy levels in the actinide elements (~ few tens of kilo-electron volts), the broad-range magnetic spectrograph at ORIC, with a typical energy resolution of ~0.05%, was used in the experiment. The deuterons emitted from the thin uranium target at 15° to the incident beam were magnetically analyzed in the spectrograph and focused onto plates coated with photographic emulsion. Total bombardment time was 10 hr, at an average beam intensity of ~0.05 μa.

A very preliminary scan of the developed plates indicates that a large number of deuteron tracks were recorded during the irradiation. Detailed reading of the plates to obtain energy spectra of the deuterons (in units of number of tracks per 0.5 mm along the plate) is currently being performed. Future analysis of the data will have as its main purpose the characterization of proton single-particle levels in the deformed nuclei of the transuranium elements.

ANGULAR DISTRIBUTION OF ^{64}Cu NUCLEI FROM THE ^{65}Cu(^{3}He,α) REACTION

N. T. Porile[28]
I. Fujiwara[28]
R. L. Hahn

Measurement of the average projected ranges of the recoil products formed in a nuclear reaction yields information about the linear momentum transferred in the reaction that can be compared with the predictions of various models of nuclear interactions. A recent study[29] of this type of the reactions of ^{3}He particles with ^{65}Cu indicated that the ^{65}Cu(^{3}He,2n) reaction proceeds predominantly by compound nucleus formation, but that more than one mechanism apparently contributes to the ^{65}Cu(^{3}He,α) reaction.

To obtain more detailed information about the ^{65}Cu(^{3}He,α)^{64}Cu reaction, the angular distributions of the ^{64}Cu recoil product were measured at energies from 12 to 32 Mev. The irradiations were performed with the external ^{3}He beam of the Argonne National Laboratory 60-in. cyclotron. The ^{64}Cu nuclei that recoiled out of the thin target were collected in aluminum foils placed at known angles with respect to the incident beam.

---

[26] C. J. Orth, W. R. Daniels, B. H. Erkkila, F. O. Lawrence, and D. C. Hoffman, *Phys. Rev. Letters* 19, 128 (1967).

[27] Electronuclear Division.

[28] Chemistry Department, Purdue University, Lafayette, Ind.

[29] S. B. Saha and N. T. Porile, *Phys. Rev.* 151, 907 (1966).

Standard radiochemical separations followed by assay of the ^{64}Cu nuclei with beta proportional counters were employed to obtain values of the differential cross section for formation of ^{64}Cu as a function of laboratory angle θ. Such an angular distribution, measured at 16.7 Mev, is shown in Fig. 2.5, where the open circles represent the experimental points.

To aid in interpreting these data, calculated angular distributions for ^{64}Cu were generated by using either of two distinctly different models for the nuclear reaction $^{65}Cu(^3He,\alpha)^{64}Cu$. In the direct-interaction model, the $(^3He,\alpha)$ reaction proceeds via the pickup by the incident ^3He of a ^{65}Cu neutron, leaving the resulting ^{64}Cu nucleus in its ground state. If instead the ^3He particle and ^{65}Cu nucleus amalgamate to form an excited ^{68}Ga compound nucleus, ^{64}Cu can be formed by the evaporation of an alpha particle or of two neutrons and two protons. The angular distributions for ^{64}Cu calculated with direct-reaction theory[30] and compound-nucleus theory[31] are shown in Fig. 2.5 as the dashed and dot-dashed curves respectively. It is quite clear from the figure that neither reaction mechanism taken alone can account for the experimental results. Indeed, the direct pickup mode appears to be most important at angles where the compound nuclear contribution is small, and vice versa. Inclusion of both reaction mechanisms, as is shown by the sum curve (solid line) in Fig. 2.5, is required to fit the observed data.

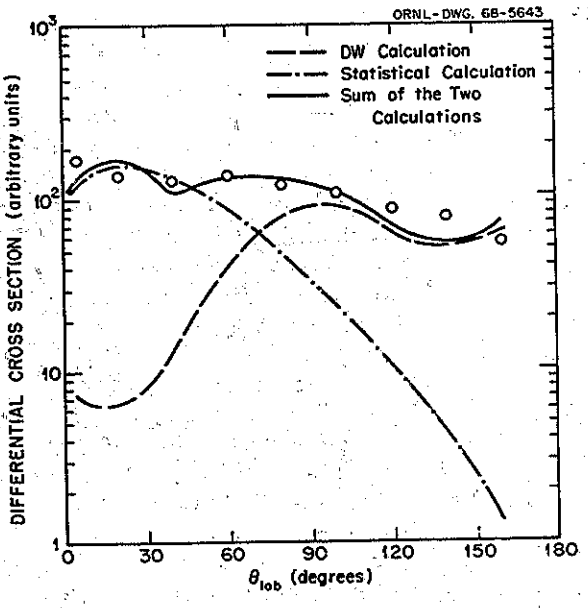

Fig. 2.5. Comparison of Theory with the Experimental Angular Distribution (open circles) of ^{64}Cu Recoil Nuclei from the Reaction $^{65}Cu(^3He,\alpha)^{64}Cu$ Measured at 16.7 Mev. The solid curve is the sum of the calculated direct neutron pickup (dashed curve) and compound-nucleus (dot-dashed curve) contributions to the reaction.

NUCLEAR CHARGE DISTRIBUTION IN FISSION: INDEPENDENT YIELD OF ^{134}I FROM SPONTANEOUS FISSION OF ^{252}Cf

D. E. Troutner[32]

The most probable nuclear charge (Z_p) produced as a function of mass in the fission of ^{252}Cf can be measured using the characteristic K x rays of the fission fragments.[33–35] Since x-ray yields are known to be a function of Z,[36] the derived Z_p can be erroneous. Uncertainties are also introduced by low mass resolution. Ideally, in radiochemical experiments, however, the Z of each fission product is identified chemically, and the masses are identified by radioactivity measurements. In this work radiochemical techniques were used to measure the independent (i.e., formed directly by fission) yield of ^{134}I in the fission of ^{252}Cf.

This is part of a series of experiments which has been initiated to measure independent yields of several products of ^{252}Cf fission. From a knowledge of these yields, it should be possible to compare nuclear charge distribution from ^{252}Cf fission with that from ^{233}U, ^{235}U, and ^{239}Pu fission and to compare Z_p's for ^{252}Cf fission de-

[30] R. H. Bassel, R. M. Drisko, and G. R. Satchler, ORNL-3240 (1966); R. L. Hahn, *Nucl. Phys.* A101, 545 (1967).

[31] N. T. Porile and G. B. Saha, *Phys. Rev.* 158, 1027 (1967).

[32] Visiting Scientist from Department of Chemistry, University of Missouri, Columbia.

[33] L. E. Glendenin and J. P. Unik, *Phys. Rev.* 140, B1301 (1965).

[34] S. S. Kapoor, H. R. Bowman, and S. G. Thompson, *Phys. Rev.* 140, B1310 (1965).

[35] S. R. Dolce, W. M. Gibson, and T. D. Thomas, *Bull. Am. Phys. Soc.* 11, 335 (1966).

[36] R. L. Watson, H. R. Bowman, and S. G. Thompson, *Phys. Rev.* 102, 1169 (1967).

termined by radiochemical methods with those determined by x-ray methods.

A 1-mil aluminum catcher foil was suspended ~0.02 in. above a ^{252}Cf source from which fragments from $\sim 1 \times 10^7$ fissions/min were collected. After exposure the foil was dissolved in HCl containing I^- carrier and the iodine separated from other fission products by H_2O_2 oxidation to I_2, which was extracted into CCl_4. The I_2 was reduced to I^-, purified, and collected as AgI. The AgI sample was counted on an NaI crystal. Decay curves were resolved graphically into components due to 53-min ^{134}I and 6.7-hr ^{135}I. Corrections were made for small backgrounds due to 2.3-hr ^{132}I and 20.8-hr ^{133}I.

Iodine-134, in addition to being produced directly by the fission process, is also produced by the beta decay of ^{134}Te. In order to correct for the ^{134}I produced by beta decay, runs were made of varying exposure and separation times. Five such runs were made with exposure times, T, of 10 to 40 min. The time interval, t, between end of exposure and time of separation ranged from 4 to 9 min. Following each of these was a second run of the same T but with a somewhat longer (52 to 103 min) time interval, t', between exposure and separation.

From a knowledge of T, t, t', and the ^{134}I radioactivity in the two samples, the independent yield of ^{134}I was calculated. Since the precursors of ^{135}I have very short half-lives, its radioactivity was used as an internal fission monitor to correct all samples to the same number of fissions.

The results of a preliminary analysis of the data are shown in Table 2.7. The uncertainties shown for the selected value include estimates of the systematic errors due to uncertainties of ±1 min in the half-lives of 42-min ^{134}Te and 53-min ^{134}I as well as the standard deviation of the average value of the calculated yields.

Table 2.7. Independent Yields of ^{134}I from Spontaneous Fission of ^{252}Cf

Run	Independent Yields of ^{134}I
1	0.29
2A	0.28
2B	0.27
3	0.25
4	0.26
Average value	0.27 ± 0.01
Selected value	0.27 ± 0.03

Assuming that nuclear charge distribution can be represented satisfactorily by a Gaussian with a width parameter σ of 0.59 ± 0.06,[37] Z_p is estimated to be 52.15 ± 0.10.

This value for Z_p is somewhat lower than the value 52.7 ± 1.0 reported for $A = 133.8$ by Glendenin[33] from the results of x-ray measurements. It is in better agreement with the value of ~52.0 estimated using the method of Wahl *et al.*,[38] suggesting that the empirical Z_p function developed by those workers for ^{235}U may be applicable to fission of ^{252}Cf.

MASS YIELDS OF ^{101}Mo AND ^{102}Mo FROM SPONTANEOUS FISSION OF ^{252}Cf

R. M. Harbour[39] D. E. Troutner[40]

Aluminum catcher foils were suspended above a ^{252}Cf source in a manner described previously.[41] After exposures ranging from 15 to 35 min the foils were dissolved in HCl containing Mo(VI) carrier, and molybdenum was separated and purified. The radioactivities of ^{99}Mo, ^{101}Mo, and ^{102}Mo were determined by beta counting. The same radioactivities were determined in samples of molybdenum purified from solutions of ^{235}U which had been irradiated with thermal neutrons. The results of a preliminary analysis of the data are shown in Table 2.8.

Taking the yields of ^{99}Mo, ^{101}Mo, and ^{102}Mo from ^{235}U fission[42] to be 6.1%, 5.0%, and 4.1%, respectively, and the yield of ^{99}Mo from ^{252}Cf

[37] A. E. Norris and A. C. Wahl, *Phys. Rev.* **146**, 926 (1966).

[38] A. C. Wahl, R. L. Ferguson, D. R. Nethaway, D. E. Troutner, and K. Wolfsberg, *Phys. Rev.* **126**, 1112 (1962).

[39] Department of Chemistry, University of Missouri, Columbia.

[40] Visiting Scientist from Department of Chemistry, University of Missouri, Columbia.

[41] D. E. Troutner, "Nuclear Charge Distribution in Fission: Independent Yield of ^{134}I from Spontaneous Fission of ^{252}Cf," this report.

[42] E. P. Steinberg and L. E. Glendenin, *Proc. U.N. Intern. Conf. Peaceful Uses At. Energy* **7**, 3 (1956).

Table 2.8. Relative Rates of Formation of ^{101}Mo and ^{102}Mo with Respect to ^{99}Mo from the Spontaneous Fission of ^{252}Cf and from the Thermal Neutron Fission of ^{235}U

	Rate of Formation ^{101}Mo / Rate of Formation ^{99}Mo (arbitrary units)		Rate of Formation ^{102}Mo / Rate of Formation ^{99}Mo (arbitrary units)	
	^{235}U	^{252}Cf	^{235}U	^{252}Cf
	30.0	53.0	14.7	29.8
	30.5	51.8	15.0	30.0
	30.4	50.2	14.4	30.1
Average	30.3 ± 0.1	51.9 ± 0.8	14.7 ± 0.2	30.0 ± 0.1

fission[43] to be 2.57%, the yields of ^{101}Mo and ^{102}Mo from ^{252}Cf are calculated to be 3.6 ± 0.1% and 3.5 ± 0.1% respectively. The errors shown include only the standard deviations of the measurements of ratios of radioactivities and do not include any uncertainties in the previously reported yields listed above as standards. These preliminary values suggest there may be a small fine-structure peak near mass 101 in ^{252}Cf fission similar to the one near mass 100 in ^{235}U fission. Experiments are in progress to measure yields of other mass chains for which no results have been reported.

A SEARCH FOR ^{101}Nb FROM THERMAL-NEUTRON FISSION OF ^{235}U

R. M. Harbour[44] D. E. Troutner[45]

As part of a series of experiments to measure fission yields of short-lived isotopes of niobium and molybdenum, attempts were made to measure the cumulative fission yield of ^{101}Nb. Orth and Smith[46] report the half-life of this nuclide to be 1 ± 0.2 min.

Samples of ^{235}U evaporated on magnesium foil were irradiated for a few seconds in the pneumatic tube facility of the ORR and the foils dissolved in HCl containing Fe(III) and Mo(VI) carriers. $Fe(OH)_3$ was precipitated from each solution by the addition of NH_3 and quickly filtered. Previous work[47] has shown that niobium and zirconium radioactivities are carried by the $Fe(OH)_3$. The $Fe(OH)_3$ precipitates were dissolved in HCl containing Zr(IV) and Mo(VI) carriers, zirconium and molybdenum purified by standard radiochemical procedures, and the radioactivities of ^{99}Mo and ^{101}Mo-^{101}Tc resulting from the decay of any ^{99}Nb or ^{101}Nb in the precipitate determined by beta counting. The radioactivity of ^{97}Zr in each sample was used as a fission monitor to correct all samples to the same number of fissions.

From a knowledge of the ^{101}Mo-^{101}Tc radioactivities in these samples and that in a sample in which all ^{101}Mo precursors were allowed to decay before separating and purifying molybdenum, it is possible to calculate the fraction of the mass 101 chain found in each $Fe(OH)_3$ precipitate.

Three pairs of runs were made. In one run of each pair $Fe(OH)_3$ was separated as quickly as possible. In the second run, $Fe(OH)_3$ was separated at 10 min after irradiation, so that any ^{101}Mo-^{101}Tc radioactivity in that precipitate was a measure of the incompleteness of the niobium-molybdenum separation. The first pair of runs

[43] W. E. Nervik, *Phys. Rev.* 119, 1685 (1960).

[44] Department of Chemistry, University of Missouri, Columbia.

[45] Visiting Scientist from Department of Chemistry, University of Missouri, Columbia.

[46] C. J. Orth and R. K. Smith, *J. Inorg. Nucl. Chem.* 15, 4 (1960).

[47] D. E. Troutner, R. L. Ferguson, and G. D. O'Kelley, *Phys. Rev.* 130, 1466 (1963).

Table 2.9. Fractions of Mass 101 and Mass 99 Chains Present as Niobium Found in Quickly Separated Fractions from the Slow Neutron Fission of ^{235}U

Run	Separation Time (min)	Fraction of Mass 101 Chain Found in $Fe(OH)_3$	Fraction of Mass 99 Chain Found in $Fe(OH)_3$	
			Observed	Calculation from ref. 47
3	2.0	0.0015 ± 0.0005	0.170	0.189
4	10.0	0.0010 ± 0.0003	0.023	0.021
5	2.0	0.0012 ± 0.0004	0.230	0.189
6	10.0	0.0030 ± 0.0010	0.028	0.021

indicated that ~3% of the chain was carried down as ^{101}Mo by the $Fe(OH)_3$. Accordingly, in the next two pairs of runs the $Fe(OH)_3$ was dissolved and then reprecipitated. A much better separation resulted. Since a ~60-min activity was present as an impurity in the molybdenum samples, additional purification of the molybdenum was performed in the third pair of runs. The ~60-min activity was reduced from a level equivalent to 0.3% of the chain to a level equivalent to 0.01% of the chain.

In the second and third pairs of runs, the fraction of the mass 99 chain found in the $Fe(OH)_3$ was also measured. The results of a preliminary analysis of the data are summarized in Table 2.9.

It appears that if the half-life of ^{101}Nb is 1 min, its fission yield must be quite small. Using the average value of runs 3 and 5 and the half-life of ^{101}Nb as 1 ± 0.2 min, the estimated yield is 0.007 ± 0.004 of the mass 101 chain. However, the ^{101}Mo radioactivity observed in runs 3 and 5 is approximately the same as that observed in runs 4 and 6, which indicates that the ^{101}Mo in runs 3 and 5 may be nothing more than the result of an incomplete niobium-molybdenum separation. Agreement of the fraction of the mass 99 chain found in each precipitate with the calculated fraction is evidence that niobium was indeed carried by the $Fe(OH)_3$. These experiments show, within the experimental uncertainty in the efficiency of the niobium-molybdenum separation, that a (1 ± 0.2)-min ^{101}Nb is not a product of fission of ^{235}U.

GAS-JET SYSTEM FOR RAPID COLLECTION OF RECOIL NUCLEI

R. L. Hahn

The remotely controlled system previously used to collect nuclei that recoil out of an irradiated target[48] suffers from two main disadvantages: (1) the cyclotron beam not only passes through the target, but through the beryllium catcher foil as well, producing undesirable background radioactivity; (2) the recoil nuclei are not slowed down before impinging upon the catcher foil and in some instances bury themselves in the catcher. Both of these effects serve to worsen the resolution of the alpha-particle spectrometer used to identify new alpha-emitting transuranium nuclides. In addition, the system is slow, requiring ~10 sec to convey the activity to the detector.

To overcome these difficulties, a new system based upon one first reported by Macfarlane and Griffioen[49] and used by others[50] has been designed and fabricated. The fundamental idea inherent in the design, as illustrated in Fig. 2.6, is that the recoil nuclei ejected from the target are stopped in an atmosphere of helium gas, which then carries the nuclides through a very

[48] See "New Neptunium Isotopes, ^{229}Np and ^{230}Np," this report.

[49] R. D. Macfarlane and R. D. Griffioen, *Nucl. Instr. Methods* 24, 461 (1963).

[50] Private communications from A. Ghiorso, K. Valli, and M. Nurmia.

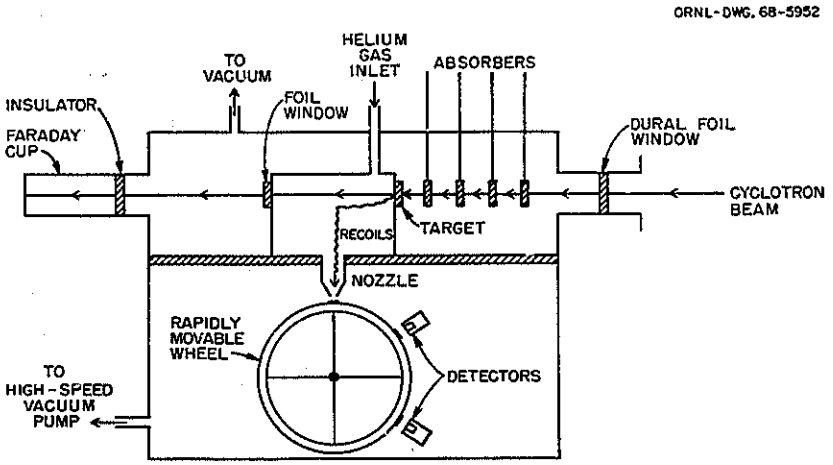

Fig. 2.6. Schematic Drawing of the Gas-Jet System. The entire assembly will be housed in a glove box maintained at less than atmospheric pressure.

small orifice and deposits them on a surface for assay. Thus the recoil catcher is not exposed to the cyclotron beam, nor do the recoils have sufficient kinetic energy to be buried in the catcher.

Because radioactive targets of the transuranium elements will be irradiated in this assembly, several containment features have been incorporated into the system. The entire assembly will be mounted in a glove box maintained at less than atmospheric pressure. High-efficiency filters will be installed in the vacuum lines. A dural foil will serve to isolate the system from the vacuum of the cyclotron; also a series of baffles and a high-speed pneumatically driven valve will protect the cyclotron in the rare event that some contamination might enter the beam pipe from the gas-jet system. Moreover, the radioactive targets will be housed in special holders to prevent contamination of the glove box or system.

In the present design, a rapidly driven wheel will convey the collected radioactivity to a series of detectors. It is expected that half-lives of the order of a few hundred milliseconds will be measured with this new system.

THE $\pi\sqrt{2}$ DOUBLE-FOCUSING ELECTRON SPECTROMETER

C. E. Bemis, Jr.

The construction of the 35-cm iron-free double-focusing spectrometer, as previously described,[51] is essentially complete. The instrument has been installed in the spectrometer building, and preliminary measurements of the focusing properties have been performed.

Calculations of the vector potential and magnetic field expansion coefficients have been made to determine the usefulness of the instrument at high momentum resolutions. Using the radial coil dimensions determined from x-ray radiographs of the individual coil layers, a set of optimum half separation distances for each of the three coil pairs has been determined. The achieved mean half separation distances from the plane of symmetry are given in Table 2.10 together with the mean coil radii and other coil data. The vector potential and magnetic field expansion coefficients for the completed assembly are given in Table 2.11 together with the theoretical values for perfect double focusing (sixth-order calculation) and the allowed deviations from theoretical which would cause an increase of about one-quarter line width at a resoltuion of 0.01%. The magnetic field expansion coefficients, a_n, correspond to the coefficients in the Taylor expansion of the axial field strength, B_z, a function of radius, r, in the symmetry plane as follows:

$$B_z(r) = B_0 \sum_{n=0}^{\infty} a_n \, (r/r_0 - 1) \, ,$$

[51] C. E. Bemis, *Chem. Div. Ann. Progr. Rept. May 20, 1967*, ORNL-4164, p. 4.

Table 2.10. Coil Dimensions for the ORNL 35-cm Iron-Free Electron Spectrometer

	Large Coils	Medium Coils	Small Coils
Number of layers per coil	4	3	2
Number of turns per layer	22	12	-10^a
Mean radius of all layers, cm	63.7246	33.8604	15.7693
Difference between mean radii of top and bottom coils, cm	0.0003	0.0010	0.0007
Mean half-separation of coils, cm	23.1676	27.2790	4.3481
Resistance per coil, ohms	0.1224	0.0249	0.0064

[a]The minus sign indicates that the current flows in the opposite sense to currents flowing in large and medium coils.

Table 2.11. Values of the Vector Potential (k_m) and Magnetic Field (a_n) Expansion Coefficients

m or n	a_n, Optimum Field Form	k_m, Optimum Field Form	k_m, Present Coil Assembly	Δk_m, Allowed Deviation from Optimum
1	−0.5000	1.0000	1.0000	
2	+0.3750	+0.5000	+0.4999	+0.0013
3	−0.2986	−0.2500	−0.2497	−0.0033
4	+0.2400	−0.5417	−0.5469	+0.15
5	−0.2017	+0.927	+1.332	−2.2
6	+0.1768	+3.56	+224.39	+97
7		−15.4	−121.2	−3500

where B_0 is the axial component of the field on the optic circle, $r = r_0$.

The excellent agreement between the achieved and theoretical values indicates that the spectrometer will indeed be useful at electron momentum resolution of 0.01% with transmission values approaching 0.1%.

The computer control system for the spectrometer is currently being installed. The computer, a Digital Equipment Corporation PDP-8, operates an 18-byte relay-operated voltage divider under program control which determines the current output to the spectrometer. The current is passed through one of four current-measuring resistors which are immersed in a constant-temperature oil bath. The voltage drop across the measuring resistor is determined using a manual six-dial potentiometer before each experiment commences. The current stability of the power supply and the stability of the current-measuring system have been measured as 3 to 4 ppm over a 4-hr period.

The vacuum and cooling systems have also been installed. The vacuum system performs satisfactorily, with a vacuum of 3×10^{-7} mm Hg being achieved in the spectrometer tank. At a focused electron energy of about 600 kev, the cooling system is able to maintain a temperature differential between the inlet and outlet of a large coil

layer to less than 1°C. A temperature differential of 1°C would correspond to a 2 ppm change in the spectrometer calibration constant (gauss cm amp^{-1}) due to thermal expansion effects in the coils.

An electron gun is currently being used to investigate any possible aberrations in the magnetic field and to determine optimal dimensions for resolution-defining baffles.

THE TRANSURANIUM RESEARCH LABORATORY ISOTOPE SEPARATOR

L. D. Hunt C. E. Bemis, Jr.

An electromagnetic isotope separator of the 90° homogeneous magnetic field sector type with a 150-cm mean radius is currently being constructed to our specifications by Danfysik A/S in Denmark. The useful mass range of the instrument is 1 to 265 atomic mass units for singly charged ions with an approximate mass range of 15% being in focus on the collector at any one time.

The mass resolution of the instrument, $m/\Delta m$ (FWHM), is expected to be greater than 2000 at total ion currents on the collector of approximately 50 μa. For total collector ion currents less than $\sim$50 μa, as is usually the case in practice, the mass resolution is expected to be somewhat better than 2000.

As the acceleration potential will be in excess of 80 kv for certain separations, equipment is being installed in the isotope separator laboratory that will maintain a relative humidity of less than 25%.

Particular care in the design of the separator has been given to vacuum problems. To ensure high isotopic enhancement factors, which may be related to the quality of the vacuum, all vacuum components have been fabricated from stainless steel and polished. Differential pumping at the ion source together with two 6-in. oil diffusion pumps with water-cooled baffles followed by liquid-nitrogen-cooled baffles is expected to provide a vacuum in the collection region of 2 to 8 $\times$ 10^{-7} mm Hg.

Devices for the collection of retarded ion beams will be included. Although the primary use of the instrument is expected to be for reactor- and cyclotron-produced transuranium element activities, isotopic enrichment and target preparation of all elements in the periodic table are planned.

INTRAMOLECULAR ENERGY TRANSFER IN ACTINIDE β-DIKETONES. EXCHANGE OF LANTHANIDE AND ACTINIDE IONS IN A CONVENIENT METHOD OF SCANNING ACTINIDE COMPLEXES FOR APPLICATION TO LIQUID LASERS

L. J. Nugent R. D. Baybarz[52]
J. R. Tarrant G. K. Werner[53]
J. L. Burnett O. L. Keller, Jr.

Intramolecular energy transfer has been demonstrated for the first time in actinide ion (A^{3+}) β-diketone complexes. The compounds are formed instantaneously in ethanol or acetonitrile solutions by exchange of A^{3+} with Tb^{3+} in $CsTb(HFA)_4$, where $(HFA)^-$ is the hexafluoroacetylacetonate anion. Before the introduction of the A^{3+} the 10^{-2} *M* $CsTb(HFA)_4$ solution exhibits the well-known sensitized fluorescence characteristic of various Tb^{3+} β-diketone complexes; namely, incident ultraviolet energy is strongly absorbed by the ligand, subsequently is transferred to the Tb^{3+} ion, and finally is emitted in two narrow, strong Tb^{3+} emission lines, one at 4881 A and the other at 5436 A. After the introduction of as little as 0.1 ng of $^{244}CmCl_3 \cdot xH_2O$ in 5 λ of ethanol, for example, to 5 λ of the $CsTb(HFA)_4$ solution, the Tb^{3+} emission lines are observed to diminish in intensity, and a new line, identified as the Cm^{3+} $J = 7/2 \rightarrow J = 7/2$ (ground state) transition, appears at 6051 A. Both the Tb^{3+} and the Cm^{3+} emission have essentially identical excitation spectra, so intramolecular energy transfer is clearly established for a curium-hexafluoroacetylacetonate complex. The measured decay time, quantum efficiency, and line width of the curium emission line suggest that this system will lase.

CHARGE-TRANSFER SPECTRA OF LANTHANIDE AND ACTINIDE TRIHALIDES IN SOLUTION

J. L. Burnett R. D. Baybarz[54]
L. J. Nugent

Charge-transfer absorption spectra are observed in the near-ultraviolet region for the lanthanide

[52]Chemical Technology Division.

[53]Physics Division.

[54]Chemical Technology Division.

halides $SmCl_3$, $SmBr_3$, $EuCl_3$, $EuBr_3$, $TmBr_3$, $YbCl_3$, and $YbBr_3$, each in anhydrous ethanol solution. The energy associated with the longest-wavelength absorption band in each case correlates closely with the sum of the known oxidation energy of the free halide ion ($X^- \rightarrow X + e^-$) and the known reduction energy of the aqueous lanthanide ion [$Ln^{3+}(aq) + e^-(aq) \rightarrow Ln^{2+}(aq)$]. Charge-transfer bands for the other lanthanides are not observed; on the basis of the above correlation they are expected to be too far in the ultraviolet for measurement in these experiments. Similar experiments were performed on the actinide (An^{3+}) halides $^{243}AmCl_3$, $^{243}AmBr_3$, $^{244}CmCl_3$, $^{244}CmBr_3$, $^{249}CfCl_3$, $^{249}CfBr_3$, $^{249}BkCl_3$, and $^{249}BkBr_3$. If it is considered feasible, the same measurements will be done on $^{253}EsCl_3$ and $^{253}EsBr_3$.

In the case of americium and curium the spectra were due to $f \rightarrow d$ transitions and absorption by radiolysis products – no charge transfer bands were seen. The berkelium spectra showed only a large uv absorption, while the californium spectra showed several peaks which are not interpreted as being due to radiolysis products. The assignments for these peaks have not yet been made.

SELF-ACTIVATED THERMOLUMINESCENCE IN SEVERAL LANTHANIDE- AND ACTINIDE-DOPED THORIUM DIOXIDE CRYSTALS

C. B. Finch[55] G. K. Werner[56]
L. J. Nugent M. M. Abraham[57]

Thermoluminescence in the temperature range 125 to 180°C has been found for ThO_2 crystals doped with Eu^{3+}, Gd^{3+}, Dy^{3+}, Er^{3+}, Tm^{3+}, Yb^{3+}, and $^{244}Cm^{3+}$. In each case the thermoluminescence emission spectrum is characteristic of the rare-earth tripositive ion and is identical to the spectrum obtained by ultraviolet excitation. It can be shown in the lanthanide cases that the energy released in the thermoluminescence process arises from the 4-Mev (1.39×10^{10} year half-life) alpha-particle emission from the 100% abundant naturally occurring ^{232}Th in the ThO_2. In the $^{244}Cm^{3+}$ case the thermoluminescence energy arises primarily from the more intense 6-Mev (18.1-year half-life) alpha-particle emission from $^{244}Cm^{3+}$. The alpha energy is primarily absorbed in the crystal (at room temperature), where it creates storage sites capable of releasing energy to excite the rare-earth ion at the elevated temperatures. The storage sites can also be created by 2537-A radiation, and they are slowly removed by visible light. Paramagnetic resonance measurements on the Tm^{3+}-doped crystals confirm that neither Tm^{2+} nor Tm^{4+} ions are present in the activated samples, indicating that the dipositive or tetrapositive ions are in general not involved in the energy transfer or storage process. The mechanism by which the energy is transferred is under study.

[55] Metals and Ceramics Division.
[56] Physics Division.
[57] Solid State Division.

PREPARATION AND CRYSTAL STRUCTURE OF CfOF

J. H. Burns J. R. Peterson

Californium oxyfluoride was prepared (by J. R. P.) at the Lawrence Radiation Laboratory, Berkeley, as part of a study of compounds of californium. Elsewhere, there has been extensive work in the preparation and x-ray study of lanthanide oxyfluorides as well as AcOF and PuOF.[58] In several of these compounds both a fluorite-type cubic structure and a rhombohedral distortion of it have been reported. Our crystal-structure determination was carried out both to establish the identity of the compound and to obtain accurate crystal parameters.

The isotope ^{249}Cf, stored on a resin bead, was used as starting material. Air ignition to Cf_2O_3 was followed by treatment with HF gas at about 700°C to form CfF_3 and the (accidental) admission of H_2O, which hydrolyzed the CfF_3 to CfOF. A single transparent, light-green crystal of about 30 μ diameter was formed. This sample was used for x-ray analysis.

Precession x-ray photographs and diffractometer measurements readily indicated that this crystal was face-centered cubic; the obvious choice of structure was the fluorite type, which was confirmed by the ultimate agreement reached between observed and calculated structure factors. All 530 forms (to $\sin \theta/\lambda = 0.69$) of the face-centered cubic reflections were measured by diffractometer

[58] W. H. Zachariasen, *Acta Cryst.* 4, 231 (1951).

using Mo $K\alpha$ radiation. Equivalent forms were averaged for a given reflection, tending to average out absorption effects due to nonregular shape but not accounting for dependence of absorption on 2θ angle. An approximate correction for the latter was applied but is limited in accuracy by lack of data on the linear absorption coefficient of californium. Seventeen independent structure factors were derived.

In the fluorite structure atomic positions are fixed by symmetry: californium is at the cation site and oxygen and fluorine are randomly distributed over the anion sites. Thus the only variable parameters are the unit cell dimension and isotropic temperature factors for the cation and average anion. The unit cell parameter was refined by least squares to fit seven measured 2θ angles near 57° (Mo $K\alpha$ = 0.70926 A). This gave an a_0 = 5.561 A with a standard error, σ, of 0.004 A. Temperature factors were adjusted by the method of least squares to fit the 17 observed structure factors. Values obtained were B(Cf) = 2.6 (σ = 0.2) A^2 and B(O, F) = 3.4 (σ = 0.3) A^2. The agreement index, based on fluorine, was 0.012.

From the unit cell dimension, the Cf-(O, F) distance is calculated to be 2.408 A, lying between the metal-(O, F) distances predicted for SmOF and EuOF.[59] A similar observation, that the Cf^{3+} radius is comparable with that of Eu^{3+}, has been reported[60] for the corresponding cubic sesquioxides.

CRYSTAL AND MOLECULAR STRUCTURE OF CESIUM TETRAKISHEXAFLUOROACETYLACETONATOEUROPATE(III) AND -AMERICATE(III)

J. H. Burns M. D. Danford

The two compounds designated $CsEu(HFA)_4$ and $CsAm(HFA)_4$, where HFA = hexafluoroacetylacetone, were found to crystallize with the same orthorhombic structure. Their unit cell dimensions, obtained by a least-squares fit to single-crystal measurements on a diffractometer, are as follows:

$CsEu(HFA)_4$	$CsAm(HFA)_4$
a = 8.660 ± 0.005 A	a = 8.62 ± 0.02 A
b = 21.75 ± 0.02	b = 21.93 ± 0.06
c = 17.43 ± 0.01	c = 17.45 ± 0.05

The space group is *Pbcn*, and the number of molecules per unit cell is 4.

Intensity data for use in determination of the structure were obtained with the computer-controlled x-ray diffractometer of the Transuranium Research Laboratory. About 1900 independent reflections were measured for $CsEu(HFA)_4$ and some 1050 for $CsAm(HFA)_4$. The latter crystal showed a continual degradation of intensity and crystallinity during the course of a week of data collection. Whether this damage is due to alpha radiation from the ^{243}Am or is the effect of x irradiation is not known, since similar degradation has been observed in $CsNd(HFA)_4 \cdot H_2O$ yet was not found in $CsEu(HFA)_4$.

The solution of the crystal structure was attained with the $CsEu(HFA)_4$ data by use of a Patterson map to locate the Cs, Eu, and O atoms and a succession of difference Fourier maps to elucidate the remainder of the structure. The heavy atoms are on a twofold axis in 4(c) positions, and the 26 other independent atoms are in general 8(*d*) sites of space group *Pbcn*. Hydrogen atoms were not located.

Refinement of the positional parameters of the 28 atoms of the structure and anisotropic thermal parameters for each was carried out by the method of least squares. After convergence of this iterative method the discrepancy index $R = \Sigma \big||F_0| - |F_c|\big| / \Sigma(F_0)$ was 0.06. In the case of $CsAm(HFA)_4$, refinement was limited to use of isotropic thermal parameters, since the data were judged to be insufficiently precise (due to the nature of the sample) to justify more elaborate treatment. The corresponding R index was 0.12.

The structure [to be discussed in terms of $CsEu(HFA)_4$, since $CsAm(HFA)_4$ is isomorphous] consists of an anionic species, $Eu(HFA)_4^-$, and Cs^+ ions interleaved at equal intervals along the a axis in a slightly zigzag chain. There are only F–F contacts between chains, no doubt accounting for the volatility of the compound. The europium atom is coordinated by eight O atoms at an average distance of 2.37 A in a dodecahedral array. The chelate rings span the dodecahedral

[59] H. A. Eick and D. B. Shinn, *Nucl. Sci. Abstr.* 21, 4483 (1967).

[60] J. R. Peterson and B. B. Cunningham, *Inorg. Nucl. Chem. Letters* 3, 327 (1967).

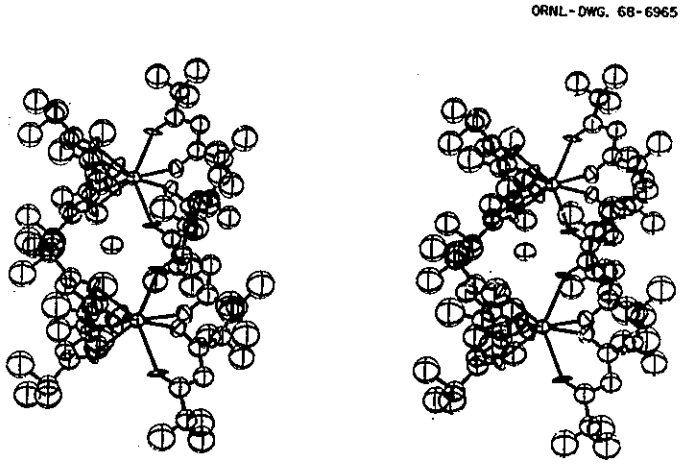

Fig. 2.7. A Stereographic Pair Showing One Cs^+ Ion and Its Two Neighboring $[Eu(HFA)_4]^-$ Ions.

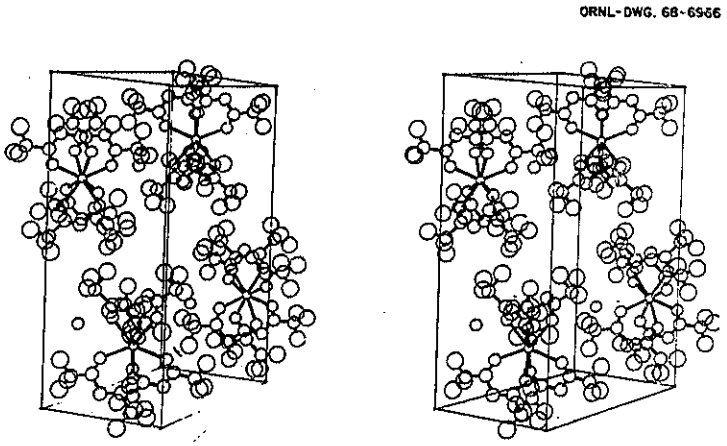

Fig. 2.8. A Stereographic Pair Which Illustrates the Packing of Molecules in One Unit Cell of $CsEu(HFA)_4$.

edges in a manner which produces an overall idealized D_2 symmetry for the anion. The six-membered chelate rings are essentially planar but folded along the O—O line by about 10°. Each Cs^+ ion has six contacts with O and six with F at average distances of 3.40 and 3.24 A respectively; these are equally distributed between two anions which the Cs^+ ion binds together.

Figure 2.7 shows the details of two $Eu(HFA)_4^-$ anions including the thermal motion represented by ellipsoids. Figure 2.8 shows one complete unit cell to illustrate the packing of molecules. The large thermal motions executed by the terminal fluorine atoms suggest that either hindered rotation of the CF_3 groups or a static disorder in their positions may exist.

PREPARATION AND PROPERTIES OF SOME RARE-EARTH AND AMERICIUM CHELATES

M. D. Danford J. H. Burns

Recent reports that yttrium forms a volatile anionic complex with hexafluoroacetylacetone (HFA)[61] and that rare earths form volatile chelates with 2,2,6,6-tetramethyl-3,5-heptanedione (THD)[62] have prompted us to investigate similar complexes with rare-earth elements and americium. Using essentially the published[61,62] methods of synthesis we have prepared a variety of chelates and performed measurements on them, which have included chemical analyses, volatility studies, and x-ray diffraction examination. Chemical analyses employed were Karl Fischer titrations for water, carbon and hydrogen analyses,[63] and spectrographic determination of the metals. A list of the compounds which have been characterized is given in Table 2.12 along with the crystallographic data obtained from single-crystal studies of each. Of these, the anhydrous compounds $CsEu(HFA)_4$ and $CsAm(HFA)_4$ were selected for crystal-structure determination as

[61] S. J. Lippard, *J. Am. Chem. Soc.* 88, 4300 (1966).

[62] K. J. Eisentraut and R. E. Sievers, *J. Am. Chem. Soc.* 87, 5256 (1965).

[63] J. R. Stokely, Analytical Chemistry Division.

Table 2.12. Crystallographic Data for Some Chelates of Rare Earths and Americium

Formula	Crystal System	Space Group	Unit Cell Dimensions (A)		
$CsLa(HFA)_4$	Triclinic	$P1$ or $P\bar{1}$	$a = 9.81$ $\alpha = 91°47'$	$b = 10.81$ $\beta = 106°42'$	$c = 17.06$ $\gamma = 114°57'$
$CsLa(HFA)_4 \cdot H_2O$	Monoclinic	$P2_1/c$	$a = 12.13$	$b = 20.84$ $\beta = 129°30'$	$c = 17.53$
$CsPr(HFA)_4 \cdot H_2O$	Monoclinic	$P2_1/c$	$a = 23.71$	$b = 18.76$ $\beta = 111°50'$	$c = 16.31$
$CsPr(HFA)_4 \cdot xH_2O$	Monoclinic	$P2_1/c$	$a = 12.56$	$b = 21.87$ $\beta = 127°53'$	$c = 17.74$
$CsNd(HFA)_4$	Orthorhombic	$Pbcn$	$a = 8.61$	$b = 21.87$	$c = 17.32$
$CsNd(HFA)_4 \cdot H_2O$	Monoclinic	$P2_1/c$	$a = 23.62$	$b = 18.78$ $\beta = 111°42'$	$c = 16.31$
$CsNd(HFA)_4 \cdot xH_2O$	Monoclinic	$P2_1/c$	$a = 12.51$	$b = 21.84$ $\beta = 127°43'$	$c = 17.72$
$CsEu(HFA)_4$	Orthorhombic	$Pbcn$	$a = 8.66$	$b = 21.65$	$c = 17.43$
$CsTb(HFA)_4$	Orthorhombic	$Pbcn$	$a = 8.67$	$b = 21.65$	$c = 17.48$
$CsAm(HFA)_4$	Orthorhombic	$Pbcn$	$a = 8.62$	$b = 21.93$	$c = 17.45$
$CsAm(HFA)_4 \cdot H_2O$	Monoclinic	$P2_1/c$	$a = 23.15$	$b = 18.78$ $\beta = 109°59'$	$c = 16.29$
$Eu(THD)_3$ from DMF[a]	Orthorhombic	$Pbca$	$a = 24.88$	$b = 22.71$	$c = 17.37$
$Nd(THD)_3$ from ether[a]	Monoclinic	$P2_1/c$	$a = 12.40$	$b = 28.20$ $\beta = 106°35'$	$c = 22.38$
$Am(THD)_3$	Monoclinic[b]				

[a] DMF = dimethylformamide. Different crystal forms were obtained from two solvents; hence the formula is in doubt.

[b] Powder diagram showed isomorphism with $Nd(THD)_3$.

discussed in the preceding paper. The number of water molecules per molecule of metal-organic compound is somewhat uncertain, as indicated in Table 2.12. The percentages of water, determined by Karl Fischer titrations, do not correspond to exactly one or two water molecules except for the compounds containing lanthanum and praseodymium. For $CsNd(HFA)_4 \cdot H_2O$ and the two isomorphous compounds containing praseodymium and americium the water of hydration will be ascertained by a crystal-structure analysis now under way. Sublimation of the compounds $CsLn(HFA)_4$, where Ln is one of the lanthanides of Table 2.12, was achieved at about 150° and a system pressure $\sim 10^{-2}$ mm with very little decomposition, but $CsAm(HFA)_4$ decomposed without subliming and formed AmF_3 at about 135°C. Both $Eu(THD)_3$ and $Am(THD)_3$ sublimed at about 105°C, system pressure 4×10^{-5} mm, with apparently little decomposition. The preparation of this volatile compound of americium is regarded as potentially of considerable practical importance.

3. Isotope Chemistry

SOLVENT EXTRACTION OF LITHIUM

D. A. Lee W. L. Taylor[1]
W. J. McDowell[2]

Further studies on the extraction of lithium ions using dibenzoylmethane (HDBM) and trioctylphosphine oxide (TOPO) in synergistic combination were completed. The distribution coefficient of lithium, $D_{Li} = [Li]_o/[Li]_a$, was determined as a function of equilibrium pH, chelating agent (HDBM) concentration, and adduct (TOPO) concentration. Variations of these relationships in the presence of competing alkali cations (including NH_4^+) were noted. Continuous variation studies also corroborated these results. From these data, molecular formulas for the extracted lithium species were proposed. A paper describing this work has been accepted for publication in the *Journal of Inorganic and Nuclear Chemistry*.

Formation of a 1:1 complex between the reagents HDBM and TOPO was indicated by dielectric constant measurements of various ratios of HDBM/TOPO in dodecane. A plot of dielectric constant vs mole fraction TOPO indicated a maximum deviation of the dielectric constant from ideality at approximately 0.5 mole fraction TOPO. Nuclear magnetic resonance measurements indicated that this complex was very weak. We estimated the value of the formation constant for this complex as 0.14, using the method described by Scruggs *et al.*[3]

The determination of the loading isotherms for lithium was made in the presence of various other alkali metal cations and ammonium ion. For systems supported with Na^+ and NH_4^+ the slope of the loading isotherm was 1, that is, the degree of association of the lithium species in the organic phase was the same as that in the aqueous phase. However, in systems supported by K^+, Rb^+, and Cs^+, the slope of the plots log $[Li]'_o$ vs log $[Li]_a$ were very nearly 2; thus, in these systems the extracted species were dimeric, and primed symbols indicate that a correction has been applied to take into account this association.

The dependence of the extraction coefficient on pH at constant HDBM, TOPO, Li, and supporting cation concentrations is shown in Fig. 3.1. The slope of 1 indicates first-power hydrogen ion dependence in all systems studied. The neutralization reaction which occurred at extraction thus involved one HDBM molecule and one lithium ion.

To determine the effect of HDBM concentration on the extraction coefficient, lithium concentration, pH, and TOPO concentration were held constant. For extraction systems in which sodium chloride was used as the supporting electrolyte, the slope of log D vs log HDBM was 1, as shown in Fig. 3.2. Thus, since HDBM is known to be monomeric in these solutions,[4-7] there was one HDBM molecule included in the extracted species for each lithium atom. This result suggests a compound of stoichiometry LiDBM·xTOPO. Similar behavior was observed in systems supported by ammonium chloride. For systems supported by heavier alkali metal salts (K, Rb, and Cs), log D'_{Li} vs log [HDBM] plots had slopes of ~2, thus

[1]ORAU Summer Participant 1966 from Mt. Vernon Nazarene College, Mt. Vernon, Ohio.

[2]Chemical Technology Division.

[3]R. L. Scruggs, T. Kim, and N. C. Li, *J. Phys. Chem.* 67, 2194 (1963).

[4]R. S. Rasmussen, D. D. Tunnicliff, and R. R. Brattain, *J. Am. Chem. Soc.* 71, 1068 (1949).

[5]G. A. Hammond, W. G. Borduin, and G. A. Guter, *J. Am. Chem. Soc.* 81, 4682 (1959).

[6]J. L. Burdett and M. T. Rogers, *J. Am. Chem. Soc.* 86, 2105 (1964).

[7]D. E. Williams, *Acta Cryst.* 21, 340 (1966).

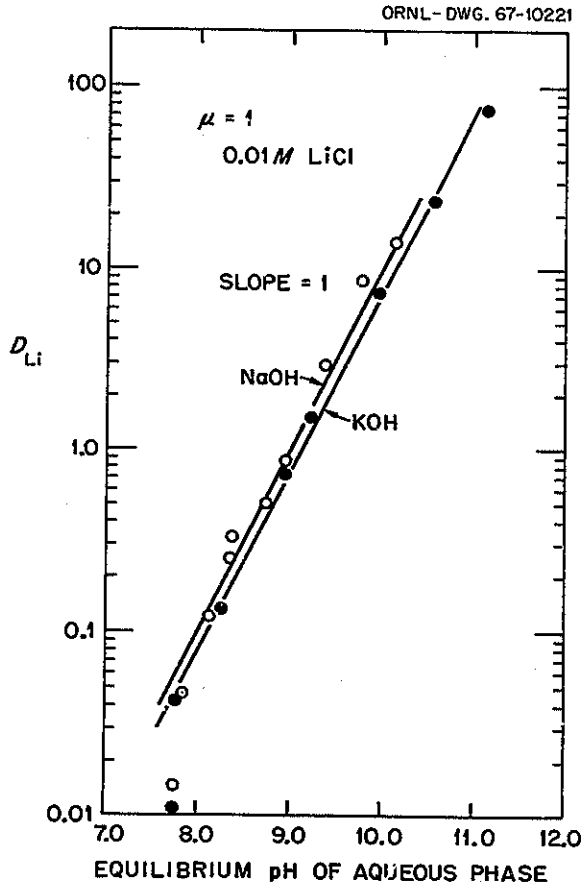

Fig. 3.1. Dependence of Extraction Coefficient on pH.

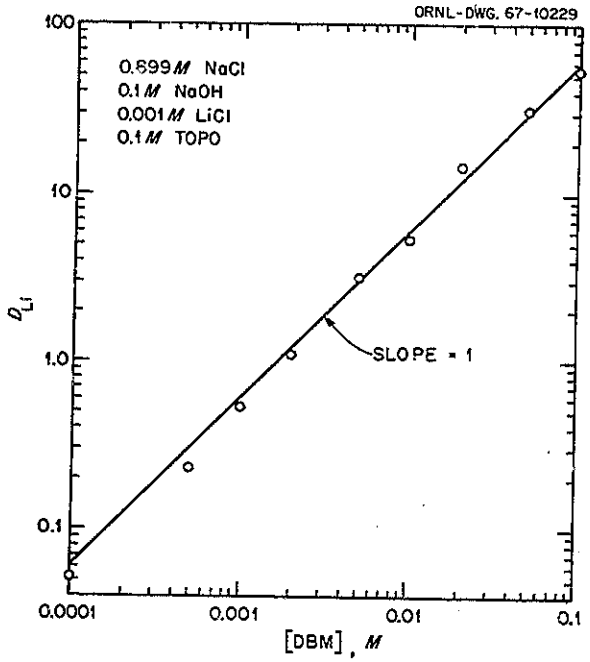

Fig. 3.2. Dependence of Extraction Coefficient on HDBM Concentration.

indicating two HDBM molecules per mole of lithium in the extracted species (Fig. 3.3). Since organic-phase lithium exists as a dimer in systems supported by the heavier alkali metal ions, the extracted lithium species contained four HDBM ligands. These results suggest a complex of stoichiometry $Li_2DBM_2 \cdot 2HDBM \cdot xTOPO$.

The effect of TOPO concentration on the extraction coefficient is shown in Fig. 3.4. Again, for systems supported by K^+, Rb^+, and Cs^+, the slopes of the plots of log D vs log [TOPO] were 2, indicating the consumption of two moles of TOPO per mole of extracted lithium. TOPO dependence with sodium as the supporting ion only approached the slope of 2, as given in Fig. 3.5. The deviation of the slope from 2 was probably due to competition for TOPO by sodium ions. Although the selectivity coefficient favors lithium 1000 to 1, the sodium concentration present was 1000 times greater than that of lithium. Thus the amount of sodium extracted was significant, and the concentration of TOPO available for extraction of lithium was somewhat less than that plotted in Fig. 3.5.

The foregoing results suggest that for sodium- and ammonium-supported systems the extracted species is a compound of stoichiometry LiDBM·2TOPO, and for systems supported by heavier alkali metals the extracted species is a compound of stoichiometry $Li_2DBM_2 \cdot 2HDBM \cdot 4TOPO$.

To aid further in the identification of the extracted lithium species, the method of continuous variations was applied. Extractions were made from systems in which the ratios of the concentrations of the reagents HDBM and TOPO were varied while the sum of their concentrations was held constant. In systems supported by K, Rb, and Cs ions, the maximum extraction coefficient for lithium occurred at 0.5 mole fraction TOPO. In systems supported by sodium ions, the maximum extraction

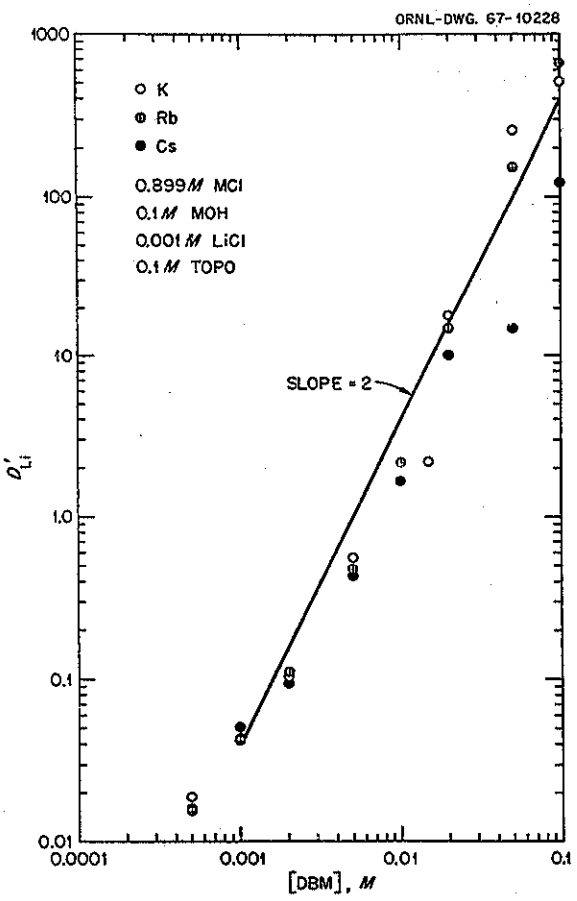

Fig. 3.3. Dependence of Extraction Coefficient on HDBM Concentration.

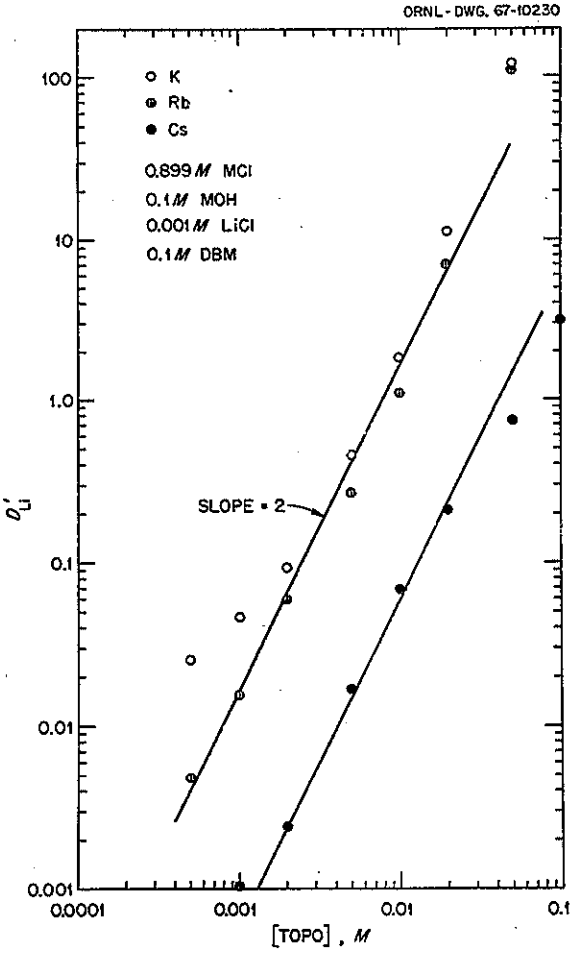

Fig. 3.4. Dependence of Extraction Coefficient on TOPO Concentration.

coefficient was much less definitive; however, an estimate of the peak near 0.66 mole fraction TOPO indicated two moles of TOPO per mole of HDBM in the extracted species. The results from the continuous variations studies are in agreement with the HDBM and TOPO reagent dependencies, both for the heavy alkali metal supporting salts and for the systems supported with sodium ions.

SEPARATION OF BORON ISOTOPES

A. A. Palko

The ANCO process[8] for separating boron isotopes is based on the chemical exchange reaction

$$C_6H_5OCH_3 \cdot {}^{11}BF_3(l) + {}^{10}BF_3(g) = C_6H_5OCH_3 \cdot {}^{10}BF_3(l) + {}^{11}BF_3(g) .$$

This process is economically superior to other methods for the separation of substantial quantities of high-purity boron isotopes.[9] However, this process could be improved further by substituting for anisole a donor which would yield a larger

[8] A. A. Palko, *Ind. Eng. Chem.* 51, 121 (1959).

[9] Letter, C. E. Larson to S. R. Sapirie; U.S. At. Energy Rept. KA-720 (Nov. 1, 1966).

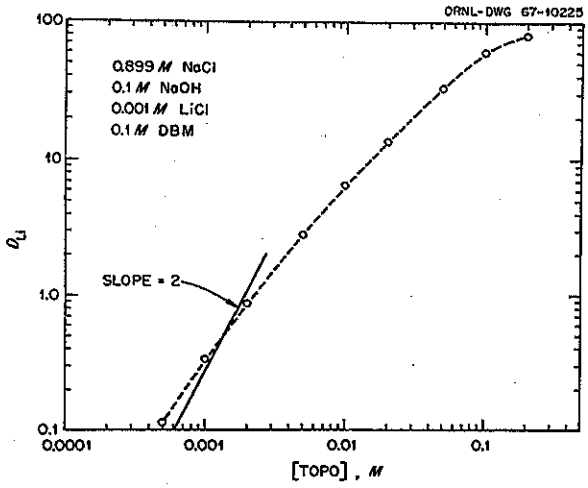

Fig. 3.5. Dependence of Extraction Coefficient on TOPO Concentration.

equilibrium constant for the isotopic exchange reaction and which would have even greater resistance to irreversible decomposition than anisole. According to a recently developed theory concerning the mechanism of the isotopic exchange reaction,[10] pentafluoroanisole[11] (PFA) should yield a larger equilibrium constant than anisole. Furthermore, PFA should be more resistant to attack by BF_3 than its unfluorinated analog. For these reasons we examined the technical feasibility of substituting PFA for anisole in the above isotopic exchange reaction.

At 800 torrs, 0.298, 0.156, and 0.009 mole of BF_3 per mole of PFA dissolved at −28.5, −21.0, and +24°C respectively. The freezing point of the solution was −30°C. Values for the isotopic equilibrium constant were 1.0365 and 1.0356 at −28.5 and −21°C.

Thus it appeared that PFA could be satisfactorily substituted for anisole from the standpoint of chemical stability and isotopic equilibrium constant. However, such a substitution was unacceptable with respect to the quantity of BF_3 which could be dissolved in PFA. In view of this handicap, it did not appear profitable to pursue the investigation further.

[10] A. A. Palko and J. S. Drury, *J. Chem. Phys.* 47, 2561 (1967).

[11] C. G. Jones, U.S. At. Energy Rept. K-1689 (April 1967).

FRACTIONATION OF CARBON ISOTOPES IN THE CUPROUS CHLORIDE–AMMONIUM CHLORIDE–CARBON MONOXIDE SYSTEM

A. A. Palko

Studies of the fractionation of carbon isotopes in the cuprous chloride–ammonium chloride–carbon monoxide system (COCO) have continued.[12] Several runs were made in the automatic bench-scale pilot plant, shown in Fig. 3.6, to measure isotopic fractionation as a function of time, flow rate, exchange column diameter, exchange column packing, and pH of the process solution. Reagent stabilities, refluxer efficiencies, and corrosion rates of various materials of construction were also investigated. Typical enrichment curves are shown in Fig. 3.7. Refluxer efficiencies were high; only 5 to 10 ppm of CO remained in the barren effluent from the product-end refluxer. The concentration of Cu_2Cl_2 and the pH of the solution remained essentially constant through each run.

[12] A. A. Palko, *Chem. Div. Ann. Progr. Rept. May 20, 1967*, ORNL-4164, p. 27.

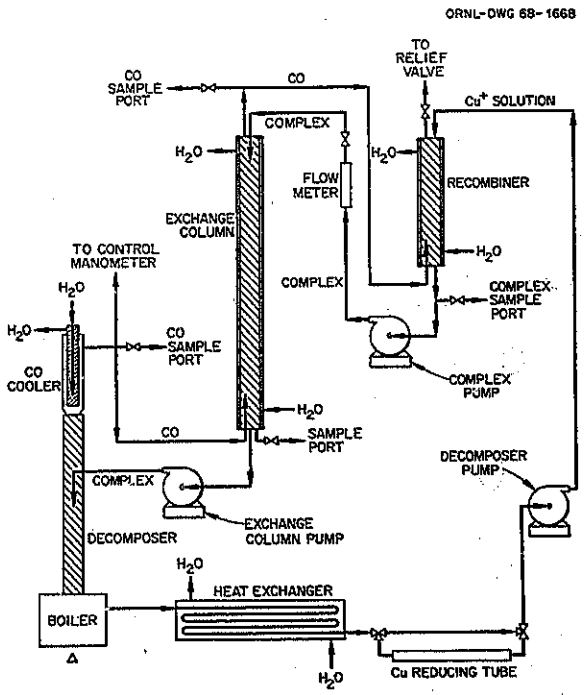

Fig. 3.6. Apparatus Used to Study the Cuprous Chloride–CO System.

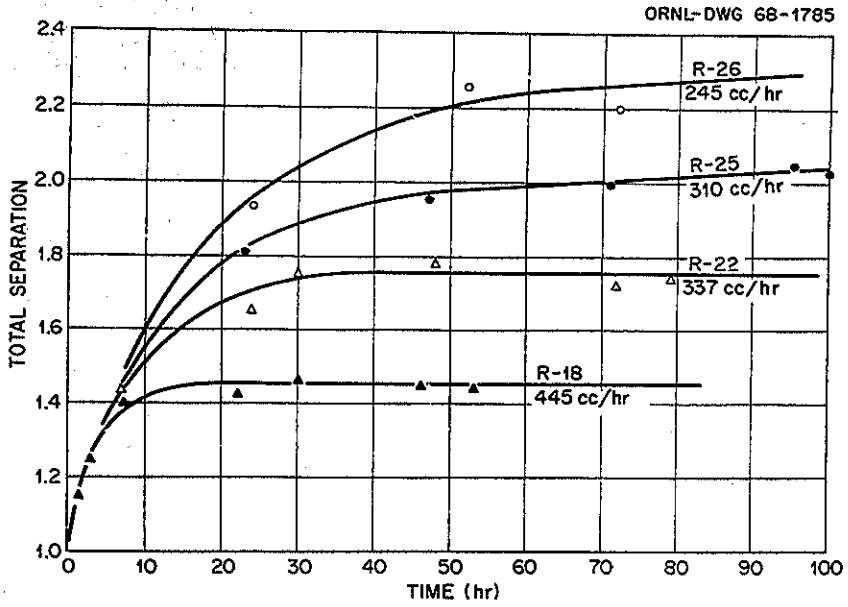

Fig. 3.7. Fractionation of Carbon Isotopes Using a 6-ft, $\frac{3}{4}$-in.-ID Exchange Column.

No oxidation of CO to CO_2 was observed. Attainment of isotopic equilibrium was rapid at all flow rates studied. Stage heights of less than $1\frac{1}{2}$ column diameters were readily attained. Except for some additional corrosion studies the laboratory examination of this system is complete. The process appears to be more attractive for the enrichment of multigram quantities of high-purity ^{13}C than previously described processes, although it is now threatened by the cyanide-cyanohydrin process described in the next report. The preparation of cost estimates for production plants of various sizes appears to be justified and will be undertaken when time permits.

A LIQUID-LIQUID SYSTEM FOR ENRICHMENT OF ^{13}C

L. L. Brown

As previously reported,[13] the chemical exchange reaction

$$R_2C(OH)\ {}^{12}CN(org) + {}^{13}CN^-(aq) = R_2C(OH)\ {}^{13}CN(org) + {}^{12}CN^-(aq)\ , \qquad (1)$$

where R represents H, an alkyl group, or an alkenyl group, results in an unusually large concentration of ^{13}C in the cyanohydrin species. Our studies of reaction (1) during this report period were devoted largely to obtaining a broader understanding of the factors involved in the exchange mechanism and in methods of refluxing each chemical species. The information obtained will aid in the design of a process for producing high-purity ^{13}C.

One major finding was that a portion of a ketone solvent may be converted to its cyanohydrin to serve as the exchange species. A variety of compounds having different side-chain structures were examined to see which yielded the largest isotopic separation factor. The isotopic separation factor is defined as

$$\alpha = \frac{(^{13}C/^{12}C)_{org}}{(^{13}C/^{12}C)_{aq}}$$

[13] L. L. Brown, *Chem. Div. Ann. Progr. Rept. May 20, 1967*, ORNL-4164, p. 28.

and equals the equilibrium constant for reaction (1). Except for mesityl oxide, which has an unsaturated side chain, the factors did not differ for the series of compounds examined. The separation factors at 25°C for these ketones were: methyl isopropyl, 1.040_1; methyl isobutyl (MIBK), 1.039_7; methyl amyl, 1.040_6; dibutyl, 1.039_8; and mesityl oxide, 1.029_7.

The exchange rate for reaction (1) must be rapid if the reaction is to be useful. We measured the rate of exchange of CN between normal acetone cyanohydrin in MIBK and $Na^{13}CN$ in water. The half-time of exchange was ~8 sec. This rate is adequate for any type of contactor which might be used in a commercial plant.

In order to establish an isotopic gradient in a chemical exchange column, it is necessary to reflux the chemical species in which the desired isotope concentrates. If an economical process is to result, it is usually necessary to reflux the other chemical species as well. In chemical exchange systems, reflux consists in converting the chemical species present in one phase to that form which is present in the opposite phase; that is, refluxing the product species in reaction (1) consists in converting $R_2C(OH)CN$ in methyl isobutyl ketone to CN^- in an aqueous solution. Thousands of moles of cyanohydrin must be refluxed for each mole of product obtained if high isotopic purities are achieved. It is thus mandatory that the reflux be accomplished by a simple, inexpensive reaction. Ideally, it is desirable to effect the reflux of each species by the simple addition or removal of heat. We have established the feasibility of refluxing the organic phase of reaction (1) by means of the reaction

$$R_2C(OH)CN(org) + Na_2CO_3(aq) =$$

$$R_2CO(org) + NaCN(aq) + NaHCO_3(aq) . \qquad (2)$$

Reaction (2) was displaced quantitatively to the right by passing the organic phase through a packed column countercurrent to the aqueous solution of Na_2CO_3, which had been heated to ~60°C.

Reflux of the waste stream requires the formation of cyanohydrin from an aqueous CN^- solution. From preliminary studies, it appeared that this could be accomplished by the following reaction:

$$NaCN(aq) + NaHCO_3(aq) + R_2CO(org) =$$

$$R_2C(OH)CN(org) + Na_2CO_3(aq) . \qquad (3)$$

Reaction (3) can be displaced to the right by passing the organic phase through a packed column countercurrent to a cooled aqueous solution of NaCN and $NaHCO_3$. The conditions required for the quantitative conversion of CN^- to the cyanohydrin are currently under study. When optimum conditions are established, it should be possible to integrate the exchange and reflux reactions so that the barren effluent generated in the refluxing of each isotopic species will serve as the reactant in the reflux reaction of the alternate species. Thus, there will be no net consumption of chemicals; only the addition or removal of heat will be required to reflux each stream. This system is indicated schematically in Fig. 3.8.

The cyanide-cyanohydrin exchange system (Cyanex system) continues to appear very attractive as a means of producing multigram quantities of high-purity ^{13}C at low unit cost.

VAPOR PRESSURE OF THE SYSTEM DIMETHYLAMINE–CARBON DIOXIDE

L. Landau C. R. Wilson[14]

Previous studies of the fractionation of carbon isotopes between CO_2 gas and alkylamine carbamate indicated a compositional anomaly for the dimethylamine carbamate. Analyses of this compound suggested a 1.8 mole ratio of amine to CO_2. Most other alkyl amines react with CO_2 to form a 2:1 complex. The exchange of carbon between dimethylamine carbamate and gaseous CO_2 also resulted in an unexpectedly low value for the isotopic fractionation factor. These observations suggested that the molecular species resulting from the addition of CO_2 to dimethylamine might be different from the species obtained with higher amines. To examine this possibility, we performed a detailed study of the vapor pressure of the system dimethylamine–carbon dioxide. Figure 3.9 shows the molar composition plotted against reciprocal temperature for several different vapor pressures.

These curves all show a maximum temperature for a composition of 64.2 mole % dimethylamine

[14]ORAU Summer Student Trainee from St. Mary's College of California.

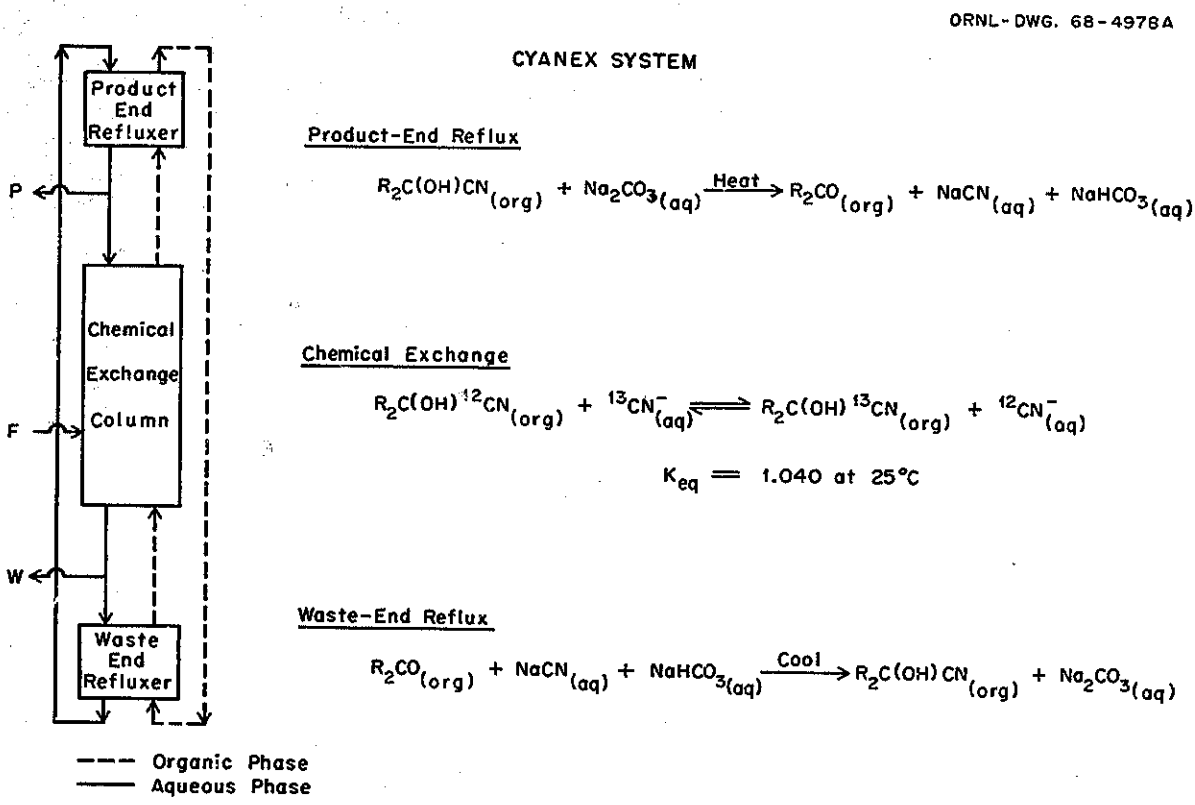

Fig. 3.8. A Liquid-Liquid System for Enrichment of ^{13}C.

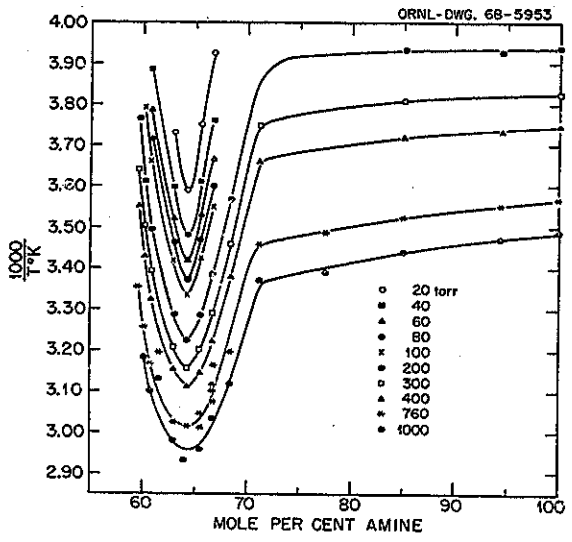

Fig. 3.9. The Vapor Pressure and Composition of Dimethylamine-CO_2.

over a pressure range from 20 torrs to 1000 torrs. This composition is equivalent to 1.8 moles of amine to 1 mole of CO_2 and indicates that the dimethylamine-CO_2 system is more complex than the other amine carbamate systems. Further investigation will be required to determine the nature of this complexity.

OXYGEN-17 FACILITY

D. Zucker

Extensive changes were made in the Oxygen-17 Facility during this report period. After 6.5 years of continuous operation a reboiler in the distillation cascade had to be replaced. The change was made necessary by the rapidly diminishing heat transfer capacity of the reboiler. In addition, the distillation column associated with the reboiler was repacked and fitted with a new, longer condenser.

The circulating water system which formerly served the jackets surrounding the distillation columns and the steam condensers was divided into two separate systems to allow greater operational control of these units.

Changes were made in the fittings of several thermal diffusion columns to minimize the inleakage of air and the outleakage of isotopically enriched oxygen. A second electrolysis cell and a two-column thermal diffusion cascade were added to the existing equipment. This revision is expected to double the ^{17}O output of the facility and to increase the purity of the ^{18}O product.

An alternate supply of 50-psig steam was provided from an adjacent building to eliminate the necessity of shutting down the thermal diffusion columns during occasional outages of the main steam supply.

New product withdrawal systems were designed and installed for the collection of all gaseous products. Former methods of collection utilized rubber tubing, which was found to degrade the quality of several gaseous streams, particularly the 99.8% ^{18}O and the 99.996% ^{16}O streams.

The alterations to the water distillation column and related equipment disrupted the isotopic gradient in that cascade and required a reduction in the product withdrawal rate. However, approximately 300 g of $H_2{}^{17}O$, $H_2{}^{18}O$, $^{18}O_2$, and $^{17}O_2$, having an aggregate value of $49,000, were transferred to Isotope Sales during the report period.

PHOTOCHEMICAL SEPARATION OF ISOTOPES

It is well known that an isotopically substituted molecule is capable of absorbing energy at a frequency different from that absorbed by an analogous molecule not containing the isotope of interest. This effect gives rise to the photochemical method of separating isotopes in which the desired isotopic species is selectively activated by irradiation with monochromatic light of the appropriate frequency. In principle, the activated species may then be separated from the undesired, unactivated species by means of a chemical reaction which occurs only with the activated molecules. This method, which is so attractive in principle, has met with little success in practice. In fact, despite numerous proposals and experimental trials, there are no practical applications of this technique.

In view of the many suggestions concerning the use of photochemical methods of separating isotopes, the Isotope Chemistry Group is undertaking a study of the problems associated with each step in the photochemical separation process. We intend to utilize spectroscopic data to compute the most favorable irradiation frequencies for given molecules. A study will then be made of conditions for excitation. Subsequently, other problems will be examined, such as finding a suitable reactant, minimizing chain reactions, and preventing energy transfer between activated and unactivated species.

The separation of chlorine isotopes was selected for examination first since spectroscopic data exist for $^{35}Cl_2$, $^{35}Cl^{37}Cl$, and $^{37}Cl_2$ by which the frequencies of various activated states may be computed.

Photochemical Separation of Chlorine Isotopes

W. H. Fletcher[15]

The argon ion laser has two strong emission lines, each of which contains about 40% of the total output. These are the lines at 4880 A and 5145 A. These lines lie at 20,486.7 cm^{-1} and 19,429.7 cm^{-1} respectively (vacuum frequencies). The first excited electronic state of Cl_2 produces absorption in this region, and these frequencies of radiation would produce molecules in the $v' = 18$ and $v' = 9$ vibrational states respectively. The rotational line frequencies for these and adjacent vibrational states have been computed for $^{35}Cl_2$, $^{35}Cl-{}^{37}Cl$, and $^{37}Cl_2$. One can find many lines of the last molecule which are separated from lines of the other two molecules by 1.5 to 2.0 cm^{-1}. This difference is sufficient so that a narrow laser line ($\sim$0.1 cm^{-1}) could be used to excite the heaviest molecule almost exclusively. Examination of the rotational frequencies around the two argon ion frequencies shows that all three molecules should be excited by the 20,486.7-cm^{-1} line, but the lower-frequency line could probably be used successfully in a selective excitation.

It would be possible to test the mechanism of separation by using the output of a wide-aperture

[15]Consultant, Department of Chemistry, University of Tennessee, Knoxville.

monochromator, but the total intensity available would be sufficient to make only enough products for a mass spectrographic analysis. The monochromator output would have the advantage of being tunable to any desired frequency.

CHEMICAL FRACTIONATION OF THE ISOTOPES OF URANIUM

A. C. Rutenberg

The isotopic equilibrium constant for the exchange of ^{235}U and ^{238}U between uranous ion in aqueous solution and uranous cupferride in chloroform was reported to be ~1.001 when it was first measured in 1947.[16] The value of $(K_{eq} - 1)$ is larger by one or two powers of 10 than that currently predicted for such a reaction. If the current estimate of the equilibrium constant is valid, there can be no question that it is technically and economically unfeasible to enrich ^{235}U to high purities by such a reaction. Since this question arises perennially, particularly among newcomers to the field of isotope separation, we have undertaken a redetermination of the equilibrium constant under conditions designed to yield the most precise values which present-day analytical techniques can achieve.

The experiment consisted in vigorously contacting equal volumes of two immiscible solutions, both 0.06 *M* in uranium. The immiscible phases consisted of an aqueous solution of UCl_4 in 1 *M* HCl, and uranous cupferride dissolved in chloroform. After separating the phases, the uranium was recovered from the desired phase, purified, reconverted to UCl_4, and used to prepare the two phases of the subsequent equilibration. We followed the aqueous phase through five equilibrations and the chloroform phase through four equilibrations. Samples from the starting uranium and the uranium recovered from the final equilibrations following both the aqueous and chloroform phases were submitted to the Isotopic Analysis Department of the Oak Ridge Gaseous Diffusion Plant for assay.

Preliminary results, based on analyses of the first few samples, indicated a value of ~1.00008 for the isotopic equilibrium constant. It thus appears economically and technically unfeasible to concentrate ^{235}U to high purities by chemical exchange reactions of the type examined.

When available, the final data will be analyzed statistically and will be published in the unclassified literature.

[16] R. W. Woodard *et al.*, *Chemical Separation of the Isotopes of Uranium*, Y-185, pp. 3–8 (August 1948; declassified with deletions Mar. 6, 1957).

MOLECULAR SPECTROSCOPY[17]

G. M. Begun A. C. Rutenberg
C. M. Haas[18]

The program to observe and interpret the vibrational spectra of isotopic and other interesting molecules has continued. The previously reported study[19] of the Raman and infrared spectra of the ^{10}B- and ^{11}B-substituted complexes of BF_3 with dimethyl sulfide was completed and published.[20] The results of the spectroscopic study[19] of the group IV-A and group V-A hexafluoride ions were also published.[21]

Bicyclo[1,1,0]butane consists of two cyclopropane rings sharing a common edge. The vibrational spectrum of this molecule has been reported in the literature[22] but not in sufficient detail to permit the successful completion of a force field analysis which one of us has undertaken. For this reason the Raman and infrared spectra of bicyclo[1,1,0]butane were observed. Figure 3.10 is a reproduction of the Raman spectrum. Wavelength, intensity, and polarization data for the principal lines are given in Table 3.1. In order to determine which, if any, lines in the Raman and infrared spectra are due to impurities, a sample of the material was fractionated by low-temperature distillation so that spectral comparisons could be made of the fractions. The force constant treatment is under way using computer techniques.

Solid I_2Cl_6 has been shown by x-ray data[23] to have a rare planar structure with two bridging

[17] W. H. Fletcher consulted on this work.

[18] Summer participant; address, Chemistry Department, University of Alabama.

[19] G. M. Begun and A. C. Rutenberg, *Chem. Div. Ann. Progr. Rept. May 20, 1967*, ORNL-4164, p. 31.

[20] G. M. Begun and A. A. Palko, *J. Chem. Phys.* 47, 967–70 (1967).

[21] G. M. Begun and A. C. Rutenberg, *Inorg. Chem.* 6, 2212–16 (1967).

[22] I. Haller and R. Srinivasan, *J. Chem. Phys.* 41, 2745 (1964).

[23] K. H. Boswijk and E. H. Wiebenga, *Acta Cryst.* 7, 417 (1954).

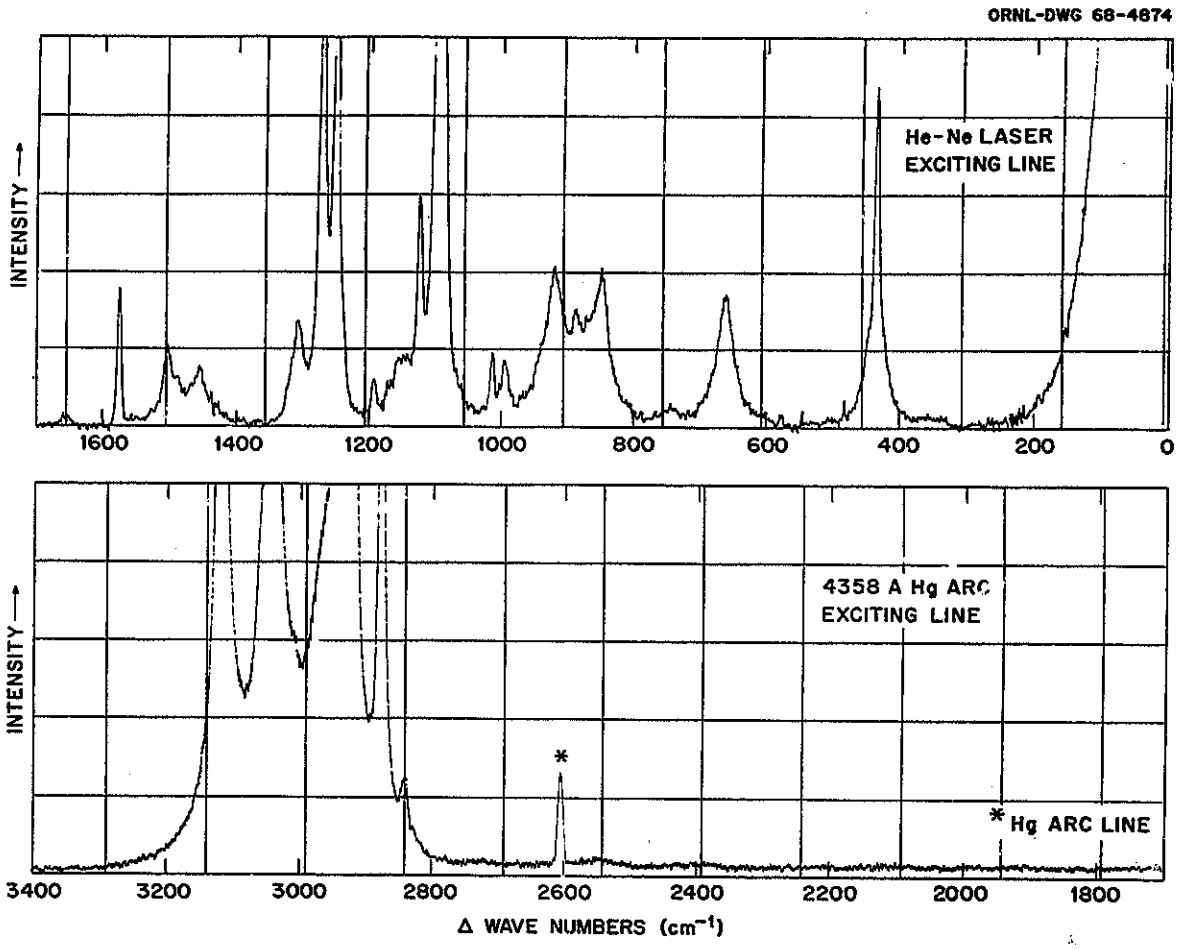

Fig. 3.10. Raman Spectrum of Liquid Bicyclo[1,1,0]butane.

chlorine atoms between the iodine atoms. Most compounds of this type (Al_2Cl_6, Ga_2Cl_6) have the bridging atoms in a plane perpendicular to the plane of the molecule. Since I_2Cl_6 is orange, it was not possible to obtain its spectrum with the conventional Raman equipment using the blue 4358-A mercury line for excitation. We have succeeded, however, in obtaining the Raman spectrum of solid I_2Cl_6 using a red laser (6328 A) for excitation. This spectrum is shown in Fig. 3.11. The planar structure of the molecule has a D_{2h} symmetry, and group theory leads to the following 18 vibrational modes:

$$4A_{1g} + 3B_{1g} + 1B_{2g} + 1B_{3g} + 1A_{1u} + 2B_{2u} + 3B_{2u} + 3B_{3u} .$$

Of these modes of vibration, the nine symmetric or "gerade" modes are expected to be Raman active, the A_{1u} mode should be inactive, and the other eight modes should be infrared active. Table 3.2 gives our observed Raman frequencies and their tentative assignments. Since we cannot obtain polarization data on powdered or microcrystalline samples, the assignments cannot be unequivocally established. We made a normal coordinate analysis of the molecule, and the calculated bond stretching and bond bending force constants reproduced the observed frequencies quite closely. These values are given in Table 3.3.

Table 3.1. Raman Lines of Bicyclo[1,1,0]butane (liquid)

Observed Bands (cm^{-1})	Relative Intensity	Polarization[a]	Observed Bands (cm^{-1})	Relative Intensity	Polarization[a]
331	0.2		1260	7	p
421	5	p	1294	1	p
648	4	dp	1443[b]	1	p
729	0.2	dp	1491	1	p
834	4	p	1563[b]	1	p
856[b]	1		1640	0.2	p
874[b]	0.5	p	2840[b]	0.3	p
906	5	dp	2876	5	p
982[b]	0.5	p	2924	17	p
1001	0.5	p	2954	0.2	
1077	1	p	2969	0.1	
1087	10	p	3008	0.1	
1111[b]	1	p	3036	6	dp
1137	0.5	dp	3054[b]	0.2	p
1180	0.2	p	3118	12	p
1239	7	p			

[a]p = polarized; dp = highly depolarized.

[b]These lines may be due to cyclobutene impurity.

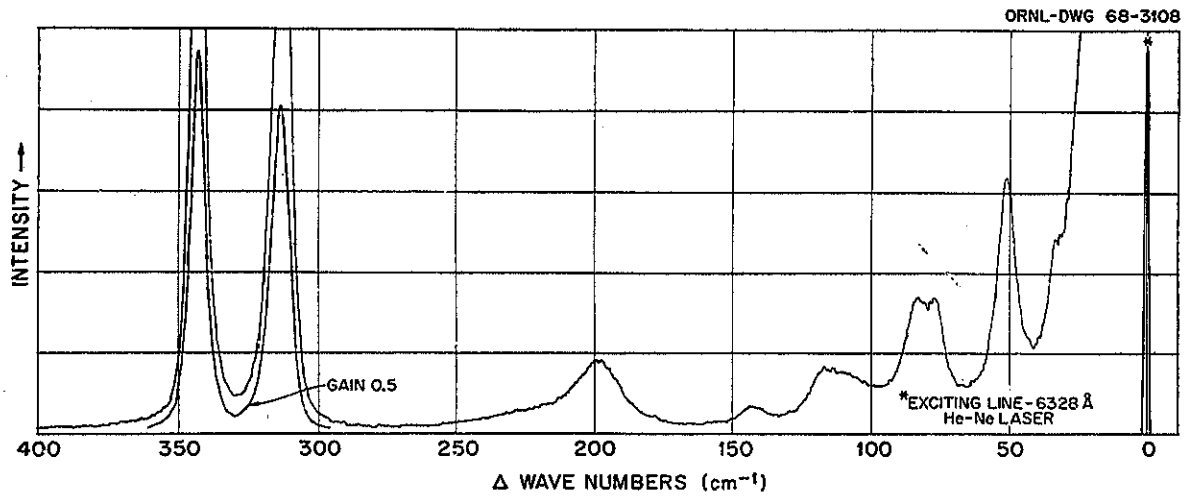

Fig. 3.11. Raman Spectrum of Solid I_2Cl_6.

Table 3.2. Raman Bands in Solid I_2Cl_6

Observed Bands (cm^{-1})	Relative Intensity	Assignment
32	0.2	Lattice vibration
51	3	$\nu_4 (A_{1g})$
77	0.8	$\nu_8 (B_{1g})$
83	0.8	$\nu_3 (A_{1g})$
110.5	0.2	$\nu_{15} (B_{3g})$
117.5	0.3	$\nu_{11} (B_{2g})$
142.0	0.1	$\nu_7 (B_{1g})$
199	1	$\nu_2 (A_{1g})$
313.5	8	$\nu_1 (A_{1g})$
343.6	10	$\nu_6 (B_{1g})$

Table 3.3. Preliminary Force Constants for I_2Cl_6 (millidynes/A)

$f_{I\text{-}Cl}$ (terminal I-Cl stretch)	1.7
$f_{I\text{-}Cl}$ (ring I-Cl stretch)	0.5
$f_\phi / r_1 r_2$ (Cl-I-Cl in-plane bend)	0.04
f_θ / r_2^2 (I-Cl-I in-plane bend)	0.03
f_γ / r_1^2 (I-Cl out-of-plane bend)	0.08

It may be seen that the ring or bridging I-Cl bonds are considerably weaker than the terminal bonds, and it is an approximation to assume in the force constant calculation that all four of these bonds are equivalent. This assumption was made because of the structural data which showed the bond distances to be nearly equal, but the instability of the complex indicates this may not be true. Further calculations are in progress.

ISOTOPIC MASS SPECTROMETRY

L. Landau

Samples of N_2, CO, and CO_2 derived from many different experiments were examined for isotopic fractionation using dual-collection techniques.

The isotopic compositions of other samples were determined by peak height measurements. Samples of O_2 from the Oxygen-17 Facility were so highly enriched in ^{17}O and ^{18}O that it was necessary to measure the heights of all m/e peaks to obtain meaningful results. Good analyses of BF_3 samples required the spectrometer to be baked out between samples. If analyzed by the usual ratio method, samples being compared would contaminate each other due to memory effects. It was necessary to analyze H_2 samples at m/e 2 and 3. These positions were so well resolved in our mass spectrometer that ions having these m/e ratios could not be collected simultaneously.

A total of over 600 samples were analyzed during this report period.

4. Radiation Chemistry

VIBRATIONALLY EXCITED OZONE IN THE PULSE RADIOLYSIS AND FLASH PHOTOLYSIS OF OXYGEN[1]

C. J. Hochanadel J. A. Ghormley J. W. Boyle

The kinetics of ozone formation in the pulse radiolysis and flash photolysis of gaseous oxygen were studied by measuring the change in optical absorption following the pulse or flash. The absorption spectrum immediately after the pulse was broader, and the peak was at longer wavelength (~2860 A) than that of ground-state ozone (~2560 A). The initial absorption is attributed to ozone in upper vibrational levels produced by $O + O_2 \rightleftharpoons O_3^{\ddagger}$. The overall third-order reaction $O + O_2 + M \longrightarrow O_3 + M$, where M is a third body, occurs by a sequence of steps. This was clearly shown by observing the kinetics at several wavelengths. At the longer wavelengths (e.g., 3130 A) some absorber was produced during the pulse. After the pulse the absorption first increased and then decayed. At the shorter wavelengths (<2800 A) the absorption built up continuously after the pulse and leveled off. As the reaction proceeds, with oxygen atoms converted to vibrationally excited ozone followed by stepwise deexcitation, the absorption increases and the spectrum shifts to shorter wavelengths. The relaxation time for deexcitation from the upper vibrational levels to the ground state is $\gtrsim 6 \times 10^{-6}$ sec in O_2 at 740 torrs and 24°C. Deexcitation requires at least 4.5×10^4 collisions. The third-order rate constant for oxygen atom disappearance is several times larger than that for formation of ozone in the ground vibrational state. This accounts for some of the discrepancy in the literature. Neither rate constant can be evaluated accurately by optical absorption measurements. However, measurements at 2800 A, where all vibrational levels appear to have about the same extinction coefficient, gave a value of $2.2 \times 10^8\ M^{-2}\ \text{sec}^{-1}$. This value should approximate the rate constant for oxygen atom disappearance, for which Kaufman and Kelso[2] determined $2.4 \times 10^8\ M^{-2}\ \text{sec}^{-1}$. Measurements at wavelengths below 2480 A gave an upper limit of the rate constant for formation of ground-state ozone of $1 \times 10^8\ M^{-2}\ \text{sec}^{-1}$.

[1]Summary of paper in press, in the *Journal of Chemical Physics*.

THE YIELD OF OZONE IN THE PULSE RADIOLYSIS OF GASEOUS OXYGEN AT VERY HIGH DOSE RATE. USE OF THIS SYSTEM AS A DOSIMETER

J. A. Ghormley C. J. Hochanadel J. W. Boyle

With the availability of field-emission high-energy electron sources that can produce pulsed beams at very high currents (several thousand amperes), it is feasible to study rapid reactions in gaseous systems by optical measurements, and it is therefore desirable to have a convenient gas-phase dosimeter. Ozone formation in oxygen provides a simple and accurate system for this purpose. Following an electron pulse (~30 nsec duration for our measurements) the ozone concentration builds up and reaches a steady value after about 30 μsec. Most of the ozone is generated after the electron pulse, and the back reaction is negligible. The ozone can be conveniently and accurately measured in situ by its absorption in the ultraviolet, thereby allowing measurement of the average dose absorbed in the volume occupied by the optical beam.

[2]F. Kaufmann and J. R. Kelso, *J. Chem. Phys.* 46, 4541 (1967).

A yield of ozone of 13.8 ± 0.7 molecules per 100 ev was measured in oxygen at 1 atm pressure at a dose rate of 10^{12} rads/sec. The absorbed dose was based on the energy absorbed in a thin aluminum calorimeter. While this yield is somewhat higher than a recently reported value[3,4] of 10.2 ± 0.6 determined from the initial rate of formation in radiolysis by cobalt gamma rays at low dose rate, it is clear that there is little or no dose-rate dependence over the range from 10^2 to 10^{12} rads/sec.

The a priori calculations of Fueki and Magee[5] indicated that the yield should be lower at this very high dose rate at this pressure. No dose-rate dependence is expected in the reactions of O atoms, since the known rate constants indicate that reaction of O atoms with oxygen to form ozone is favored over O atom combination or back reaction with ozone. Any dose-rate dependence would have had to enter through the fast reactions of the various ions, electrons, and excited species.

A HIGH-INTENSITY SQUARE-WAVE ANALYTICAL FLASH LAMP

R. V. Fitzsimmons[6] C. J. Hochanadel
J. A. Ghormley J. W. Boyle

Some work was done on developing a lamp to produce a high-intensity long-duration square-wave flash for high-resolution kinetic spectrophotometry. This would be used for observing the kinetics of individual vibrational states of diatomic molecules such as oxygen. The lamp was a xenon-filled quartz capillary 1 to 2 mm ID and 10 to 20 mm long connected with capacitors and inductors in a delay line circuit similar to that described by Fitzsimmons and Bair.[7] For the best flash, the emission in the visible had a rise time of 10 μsec and was constant within 3% for 60 μsec. The emission in the uv reached a maximum at about the same time as the visible but then decreased rapidly. At 2300 A the width at half height was only 20 μsec.

RADIATION-INDUCED OXIDATION OF CERIUM(III) IN DEAERATED SULFURIC ACID SOLUTIONS

R. W. Matthews[8] H. A. Mahlman
T. J. Sworski

Radiation-induced reduction of Ce(IV) in sulfuric acid solutions up to 8.0 *M* has been attributed to the following reaction mechanism:

$$H + Ce(IV) \longrightarrow H^+ + Ce(III)\ , \qquad (1)$$

$$H + O_2 \longrightarrow HO_2\ , \qquad (2)$$

$$HO_2 + Ce(IV) \longrightarrow H^+ + O_2 + Ce(III)\ , \qquad (3)$$

$$H_2O_2 + Ce(IV) \rightleftharpoons H^+ + HO_2 + Ce(III)\ , \qquad (4)$$

$$OH + Ce(III) \longrightarrow OH^- + Ce(IV). \qquad (5)$$

It has become generally accepted that there is no oxygen effect, except for any effect of oxygen on G_{H_2} and G_H, since the sequence of reactions (2) and (3) is equivalent to reaction (1).

For Ce(IV) reduction in air-saturated 0.4 *M* sulfuric acid, $G(Ce^{III})$ decreases with increase in Ce(III) concentration due to the dependence of $G_{H_2O_2}$ on Ce(III) concentration. Much to our surprise, we discovered an oxygen effect when we attempted to determine the dependence of $G(Ce^{III})$ on Ce(III) concentration for Ce(IV) reduction in deaerated 4.0 *M* sulfuric acid. While Ce(IV) is reduced linearly with dose in air-saturated 4.0 *M* sulfuric acid at any Ce(III) concentration, Ce(III) is oxidized in deaerated 4.0 *M* sulfuric acid containing 0.026 *M* Ce(III) as shown in Fig. 4.1. This is the first observation of overall Ce(III) oxidation by ^{60}Co radiation.

In the absence of initial Ce(IV), the concentration of Ce(IV) increases nonlinearly with dose to a maximum and then decreases to zero. The maximum concentration of Ce(IV) which is obtained increases with increase in either radiation intensity, as shown in Fig. 4.1, or sulfuric acid

[3] G. R. A. Johnson and J. M. Warman, *Discussions Faraday Soc.* 37, 87 (1964).

[4] J. T. Sears and J. W. Sutherland, *J. Phys. Chem.* 72, 1166 (1968).

[5] K. Fueki and J. L. Magee, *Discussions Faraday Soc.* 36, 676 (1963).

[6] Visiting scientist from Western Illinois University, summer 1967.

[7] R. V. Fitzsimmons and E. J. Bair, *J. Chem. Phys.* 40, 451 (1964).

[8] Guest Scientist from Australian Atomic Energy Commission, Research Establishment, Sydney, Australia.

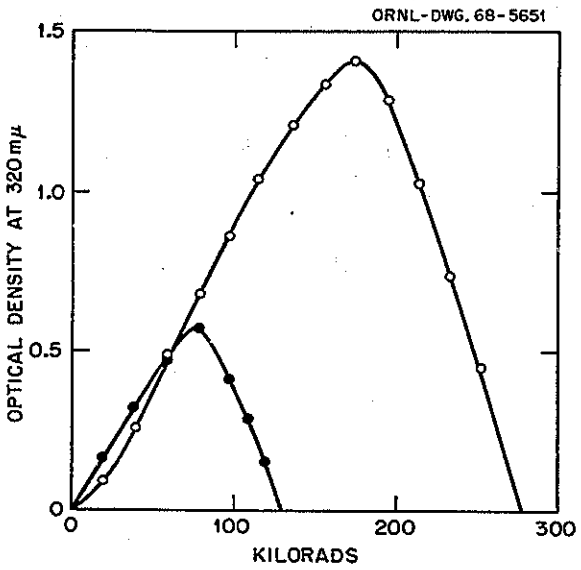

Fig. 4.1. Effect of Radiation Intensity on Ce(III) Oxidation in 4.0 *M* Sulfuric Acid Containing 0.026 *M* Ce(III). Radiation intensities: ●, 1.98 krad/min; ○, 19.5 krad/min.

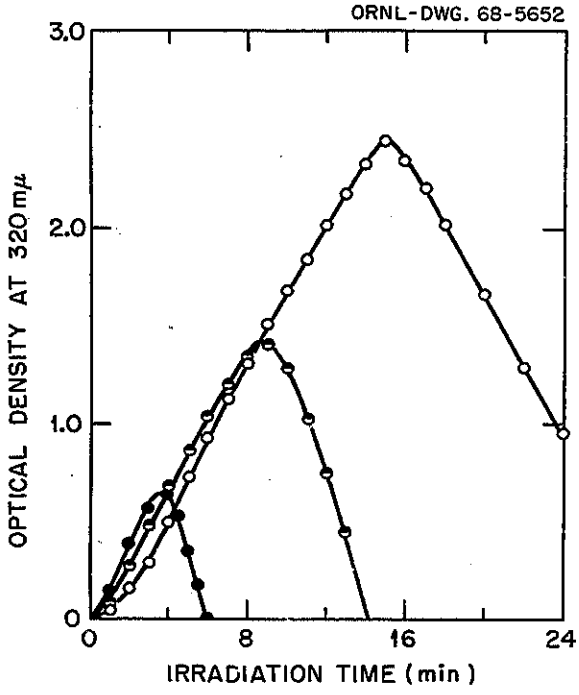

Fig. 4.2. Effect of Sulfuric Acid Concentration on Ce(III) Oxidation for Solutions Containing 0.026 *M* Ce(III). Sulfuric acid concentrations: ●, 2.0 *M*; ⊖, 4.0 *M*; ○, 6.0 *M*.

concentration, as shown in Fig. 4.2. The cause of the maximum followed by the sharp drop to zero is the increasing oxygen concentration with increase in dose. This was demonstrated by sparging the solution with helium during irradiation to inhibit formation of high concentrations of oxygen; then the Ce(IV) concentration increased and approached a limiting value asymptotically.

Figure 4.3 shows a rather complicated effect of initial Ce(IV) concentration on Ce(III) oxidation. At low initial Ce(IV) concentrations, the concentration of Ce(IV) decreases initially to a minimum, then increases to a maximum, and then decreases to zero. The maximum increase in Ce(IV) concentration which can be obtained decreases with increase in initial Ce(IV) until Ce(III) oxidation is no longer apparent. After 3 min of irradiation for the solution with highest initial Ce(IV) concentration, Ce(IV) reduction is linear with dose and $G(Ce^{III}) = 1.37$, which is close to $G(Ce^{III}) = 1.53$ for Ce(IV) reduction in air-saturated 4.0 *M* sulfuric acid containing 0.026 *M* Ce(IV).

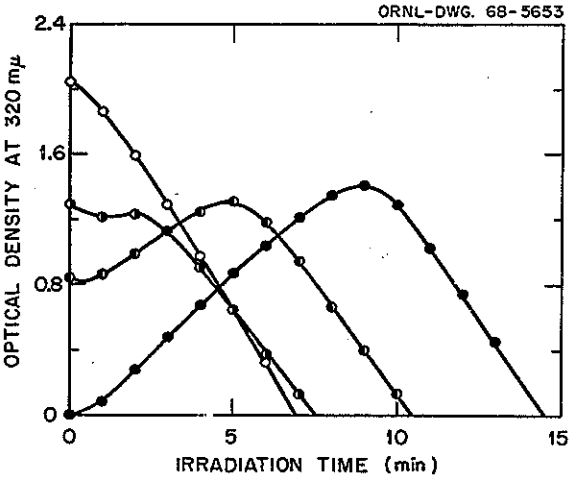

Fig. 4.3. Effect of Initial Ce(IV) Concentration on Ce(III) Oxidation in 4.0 *M* Sulfuric Acid Containing 0.026 *M* Ce(III). Initial Ce(IV) concentration indicated by initial optical density at 320 mμ due to Ce(IV).

These effects of radiation intensity, sulfuric acid concentration, and initial Ce(IV) concentration together with the observation that low initial concentrations of O_2, H_2O_2, and $H_2S_2O_8$ increase the initial rate of Ce(III) oxidation enabled us to establish the reaction mechanism for overall Ce(III) oxidation. The reaction of Ce(IV) with H_2O_2 and H atom is slow enough to enable reaction of H atom with H_2O_2,

$$H + H_2O_2 \longrightarrow H_2O + OH \,, \qquad (6)$$

to compete effectively with reactions (1) and (4). Furthermore, persulfuric acid and Caro's acid are additional products of irradiation which do not react with Ce(IV)[9] but which can react with H atom,

$$H + H_2S_2O_8 \longrightarrow H_2SO_4 + HSO_4 \,, \qquad (7)$$

$$H + H_2SO_5 \longrightarrow H_2SO_4 + OH \,, \qquad (8a)$$

$$H + H_2SO_5 \longrightarrow H_2O + HSO_4 \,, \qquad (8b)$$

to yield HSO_4 or OH radical, which can oxidize Ce(III). This mechanism requires that $G(Ce^{IV}) \leq 2G_{H_2}$, which is consistent with our observations.

The surprising observation that low initial concentrations of O_2 increase the initial rate of Ce(III) oxidation, while higher concentrations of O_2 cause reduction of Ce(IV), is attributed to the sequence of reactions (2), (-4), (6), and (5) with the following net reaction:

$$2H^+ + 2H + O_2 + 2Ce(III) \longrightarrow 2H_2O + 2Ce(IV) \,. \qquad (9)$$

The effect of low initial concentration of O_2 according to reaction (9) is oxidation of Ce(III) by H atoms with a concomitant decrease in O_2 concentration.

For the results shown in Figs. 4.1–4.3, solutions were irradiated in 2-cm cylindrical spectrophotometric cells of optically pure quartz. The concentrations of Ce(IV) were determined by the optical density of the solutions at 320 mμ using molar extinction coefficients of 6090, 6590, and 7070 for 2.0 *M*, 4.0 *M*, and 6.0 *M* sulfuric acid respectively.

[9] J. W. Boyle, *Radiation Res.* 17, 427 (1962).

REDUCTION OF CERIUM(IV) BY HYDROGEN PEROXIDE

H. A. Mahlman R. W. Matthews[10]
T. J. Sworski

The following reaction mechanism for reduction of Ce(IV) by H_2O_2 was indicated[11] in a study of the isotopic exchange reaction between Ce(IV) and Ce(III):

$$Ce(IV) + H_2O_2 \underset{k_{-1}}{\overset{k_1}{\rightleftharpoons}} Ce(III) + H^+ + HO_2 \,, \qquad (1)$$

$$Ce(IV) + HO_2 \xrightarrow{k_2} Ce(III) + H^+ + O_2 \,. \qquad (2)$$

This mechanism was confirmed[12] by a kinetic study using flow techniques, and the mean value for k_1k_2/k_{-1} of $1.28 \times 10^7\ M^{-1}\ sec^{-1}$ was reported for 0.4 *M* sulfuric acid.

The overall reduction of Ce(IV) by H_2O_2 is too fast in 0.4 *M* sulfuric acid to study by classical spectrophotometric techniques. However, during the course of our studies in the radiolysis of Ce(IV)-Ce(III) mixtures in 4.0 *M* sulfuric acid with a kilocurie ^{60}Co source, we observed postirradiation reduction of Ce(IV), presumably by H_2O_2. If this presumption be true, there would have to be a marked decrease in k_1k_2/k_{-1} with increase in sulfuric acid concentration. The dependence of k_1k_2/k_{-1} on sulfuric acid concentration has not been previously investigated. Prior kinetic studies[11,12] were in 0.4 *M* sulfuric acid.

The reduction of Ce(IV) by H_2O_2 was investigated both in sulfuric acid solutions from 2.0 *M* to 13.0 *M* and in ammonium acid sulfate solutions from 1.0 *M* to 5.0 *M*. The experimental procedures were identical to those previously employed[13] in our study of the reduction of Ce(IV) by HNO_2. Under our experimental conditions, an assumption that $k_{-1}[Ce(III)]/k_2\,[Ce(IV)] \gg 1$ appears to be valid, and the rate of Ce(IV) reduction is given by the equation

[10] Guest scientist from Australian Atomic Energy Commission, Research Establishment, Sydney, Australia.

[11] P. B. Sigler and B. J. Masters, *J. Am. Chem. Soc.* 79, 6353 (1957).

[12] G. Czapski, B. H. J. Bielski, and N. Sutin, *J. Phys. Chem.* 67, 201 (1963).

[13] T. J. Sworski and H. A. Mahlman, *Chem. Div. Ann. Progr. Rept. May 20, 1966*, ORNL-3994, pp. 44–46.

$$\frac{d[\mathrm{Ce(IV)}]}{dt} = -\frac{2k_1k_2[\mathrm{Ce(IV)}]^2\,[\mathrm{H_2O_2}]}{k_{-1}[\mathrm{Ce(III)}]}. \qquad (3)$$

Figure 4.4 shows the dependence of k_1k_2/k_{-1} on sulfuric acid and ammonium acid sulfate concentrations for experiments in which aqueous H_2O_2 solutions were mixed with sulfuric acid or ammonium acid sulfate solutions containing Ce(IV). The rate of Ce(IV) reduction adhered well to Eq. (3) except for 12.0 *M* and 13.0 *M* sulfuric acid solutions, in which k_1k_2/k_{-1} values were not independent of either Ce(IV) or Ce(III) concentration and were suspect. That the true values for k_1k_2/k_{-1} in 12.0 *M* and 13.0 *M* sulfuric acid are larger was established by reversing the experimental procedure. Cerium(IV) solutions were mixed with sulfuric acid solutions containing H_2O_2. The rate of Ce(IV) reduction decreased drastically with increasing age of the H_2O_2 solutions for 13.0 *M* sulfuric acid but not for 8.0 *M* sulfuric acid. The rate of reaction of H_2O_2 with sulfuric acid to form Caro's acid is reported[14] to be markedly dependent on sulfuric acid concentration and is significant under our experimental conditions in 12.0 *M* and 13.0 *M* sulfuric acid.

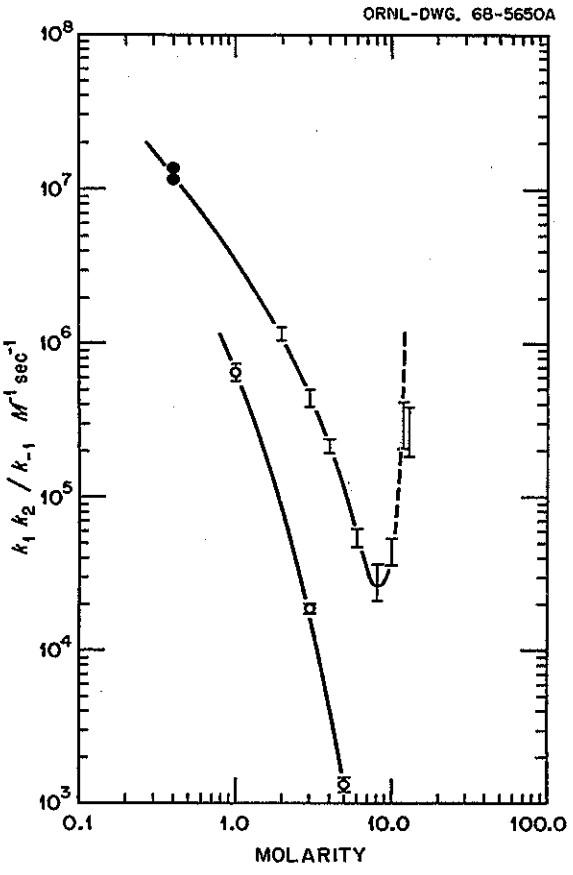

Fig. 4.4. Rate of Reduction of Cerium(IV) by Hydrogen Peroxide as a Function of Sulfuric Acid or Ammonium Acid Sulfate Concentration: I Sulfuric Acid Solutions; Φ Ammonium Acid Sulfate Solutions; ● Data of Czapski, Bielski, and Sutin.[12]

The striking minimum in the variation of k_1k_2/k_{-1} with sulfuric acid concentration reveals the explanation for the dependence of k_1k_2/k_{-1} on both sulfuric acid and ammonium acid sulfate concentration. The only quantity in sulfuric acid solutions which varies similarly is the concentration of SO_4^{2-}. The concentration of SO_4^{2-} is approximately equal to $0.3[H_2SO_4]$ from 1.0 *M* to 6.0 *M* sulfuric acid, reaches a maximum between 6.0 *M* and 8.0 *M* sulfuric acid, and then decreases for sulfuric acid concentrations greater than 8.0 *M*.[15] The concentration of SO_4^{2-} is approximately equal to $0.4[NH_4HSO_4]$ from 1.0 *M* to 5.0 *M* ammonium acid sulfate.[15]

Cerium(IV) in sulfuric acid solutions exists as a mixture Ce^{4+}, $CeSO_4^{2+}$, $Ce(SO_4)_2$, and $Ce(SO_4)_3^{2-}$ species with the following equilibrium constants:

$$K_1 = [CeSO_4^{2+}]/[Ce^{4+}][SO_4^{2-}],$$
$$K_2 = [Ce(SO_4)_2]/[CeSO_4^{2+}][SO_4^{2-}],$$
$$K_3 = [Ce(SO_4)_3^{2-}]/[Ce(SO_4)_2][SO_4^{2-}].$$

The dependence of Ce^{4+} concentration on SO_4^{2-} concentration is given by

$$[Ce^{4+}] = \frac{[\mathrm{Ce(IV)}]}{1 + K_1[SO_4^{2-}] + K_1K_2[SO_4^{2-}]^2 + K_1K_2K_3[SO_4^{2-}]^3}. \qquad (4)$$

If only Ce^{4+} could oxidize H_2O_2 according to reaction (1), then Eq. (4) shows that k_1k_2/k_{-1} would become inversely proportional to the cube

[14] J. M. Monger and O. Redlich, *J. Phys. Chem.* 60, 797 (1956).

[15] T. F. Young, L. F. Maranville, and H. M. Smith, *The Structure of Electrolytic Solutions*, p. 35, Wiley, New York, 1959.

of the SO_4^{2-} concentration as a limit at high SO_4^{2-} concentrations. Figure 4.4 shows that k_1k_2/k_{-1} is inversely proportional to the cube of the SO_4^{2-} concentration, at least to a first approximation. However, we cannot rule out the possibility that HO_2 does not reduce all Ce(IV) species and that k_1k_2/k_{-1} could be inversely proportional to higher powers of the SO_4^{2-} concentration at high SO_4^{2-} concentrations.

ALPHA-PARTICLE RECOIL TRACKS IN MICA

R. V. Gentry[16] J. W. Boyle

In 1967 Huang and Walker[17] evaporated a solution of ^{228}Th on muscovite mica and found that stable latent images of recoil tracks were produced by decay of the thorium. The latent images could be developed by chemical etching so as to be visible with a phase-contrast microscope. The induced pits they observed were identical in appearance to naturally occurring pits etched in thorium- and uranium-bearing micas. They failed to observe such tracks, however, in a sample of mica held next to a uranium foil. From their study they concluded that etchable latent images were not caused by the alpha particles but were caused by the heavy recoil nuclei accompanying alpha decay. In their case the thorium decay chain produced a significant number of multiple recoils (five in going from ^{228}Th to ^{208}Pb) during the time of the experiment, and they were unable to decide whether a single alpha recoil will produce an etchable latent image or whether several successive recoils are necessary.

Our collaboration was solicited to determine if a single recoil will produce an etchable image. A relatively short-lived alpha emitter which decays to a long-lived daughter is required, and several transuranium isotopes are well suited for this. A sample of americium in 0.5 *N* HNO_3 was obtained from J. R. Stokely at the Transuranium Research Laboratory. The sample had a specific alpha activity of 7.1×10^3 dis sec^{-1} μg^{-1}. Ninety-five percent of the alpha activity came from ^{243}Am ($T_{1/2}$ = 7950 years) and 5% from ^{241}Am ($T_{1/2}$ = 458 years), but either isotope is suitable for this experiment. Americium-243 decays via ^{239}Np (beta emitter) to ^{239}Pu, which has a half-life of 2.4×10^4 years. Americium-241 decays to ^{237}Np, which has a half-life of 2.2×10^6 years.

In the first experiment several samples were prepared by placing a small drop of americium solution on a piece of annealed phlogopite mica and evaporating to dryness. The samples were alpha counted so as to know the number of events taking place. After 30 to 270 min the samples were rinsed and etched in 48% HF at room temperature for 45 to 85 sec. Pits were observed with a phase-contrast microscope with the expected density in the areas covered by the evaporated drops and were absent in the rest of the sample.

In a second experiment a piece of mica was pressed against a "hot" sample and then etched as before. Identical tracks with expected densities were observed in the adjacent piece of mica.

It was concluded, therefore, that etchable latent images are produced in phlogopite by a single alpha recoil nucleus if the mica is within range of the recoil nucleus.

ENERGY TRANSFER IN THE RADIOLYSIS OF ORGANIC COMPOUNDS

A. Russell Jones

When a pure organic substance of low molecular weight is irradiated with high-energy radiations, any selective (nonstatistical) alteration of the chemical bonding must be due to selective localization of electronic energy within a molecular length, since it is unlikely that the high degree of vibrational energy localization necessary for bond breakage is a result of the accumulation of vibrational energy. Such a localization might be the result of (1) some sort of "condensation" of electronic energy at the point of chemical change, (2) random absorption of the electronic energy within a molecule, followed by specific inter- or intramolecular energy transfer to the point of chemical change, (3) random production of positive ions followed by the capture of the free electrons at the site of chemical change.

To gain information about the mechanism of the localization of electronic energy, a detailed study of the radiation decomposition of the homologous

[16] Columbia Union College, Institute of Planetary Sciences, Takoma Park, Md.

[17] W. H. Huang and R. M. Walker, *Science* 155, 1103 (1967).

series of aliphatic acids is being carried out, taking advantage of improvements in analytical methods that have been made since the earlier studies.[18] The results indicate that the only carbon-to-carbon bond breakage which occurs in the parent molecules is that which separates the carboxyl group from the aliphatic chain. The alkyl radical then undergoes decomposition during stabilization. This specificity of chemical action is apparently unaffected by the presence of iodine,[19] suggesting that neither free radicals nor negative ion formation is the cause of the specificity. The efficiency required of intra- or intermolecular energy transfer is quite high, since the decarboxylation yield only decreases from 5.0 to 3.5 for the first eight members of the series. In view of the very great increase in chain length and the great decrease in volume proportion of carboxyl between formic and caprylic acids, it appears that localization of the absorbed energy as the result of some sort of "condensation" of electronic energy at the point of chemical change offers a simpler explanation of the results.

RADIATION AND HOT-ATOM CHEMISTRY OF INORGANIC CRYSTALLINE SOLIDS

Infrared Measurements of ClO_4^- Production in ^{60}Co Gamma-Ray-Irradiated $KClO_3$

L. C. Brown G. E. Boyd

Infrared absorption measurements were employed to estimate the concentration of perchlorate ion formed in the crystal lattice of $KClO_3$ at 25° by energetic ionizing radiations. In addition, chemical determinations were made of the amount of ClO_4^- appearing in aqueous solution on dissolving the irradiated salt. A comparison (Table 4.1) of the concentrations in the crystal with those in aqueous solutions of the salt showed that, within experimental error, all the perchlorate ion found in solution was present originally within the irradiated solid. Virtually no perchlorate appeared to be produced by the hydrolysis of species such as Cl_2O_6 postulated heretofore by others as present in irradiated $KClO_3$ and responsible for the observation of ClO_4^- ion in aqueous solutions. The radiolytic yield of perchlorate was surprisingly large (cf. Table 4.2) and, for large doses, was found to increase less rapidly than linearly with the dose. The production of chlorite ion in $KClO_3$(c) also was observed (Fig. 4.5, curve *B*). Comparisons will be made of the concentration of ClO_2^- in the crystal and in aqueous solutions of the salt to determine if there are other precusors in the solid of the chlorite observed in solution. Investigations of the radiolytic production and yield of ozonide ion, O_3^-, are in progress.

[18] W. L. Whitehead, C. Goodman, and I. A. Breger, *J. Chim. Phys.* 48, 184 (1951).

[19] R. H. Johnsen, *J. Phys. Chem.* 63, 2041 (1959).

Table 4.1. Comparison of $KClO_4$ Content of ^{60}Co Gamma-Ray-Irradiated $KClO_3$ as Measured by Infrared Analysis of Solid and by Chemical Analysis of Aqueous Solution

Sample	Dose (ev per mole of $KClO_3$)	Mole % $KClO_4$ in Crystal (Infrared)	Mole % $KClO_4$ in Aqueous Solution of Crystal (Chemical)
	$\times 10^{23}$		
1	3.22	0.48 ± 0.05	0.55 ± 0.01
2[a]	4.37	0.57 ± 0.06	0.70 ± 0.02
3	4.42	0.65 ± 0.06	0.69 ± 0.01
4	14.0	1.96 ± 0.20	1.89 ± 0.06

[a] Sample irradiated at reduced pressure (<0.1 torr).

Table 4.2. Yields of Chlorine-Containing Species Produced by ^{60}Co Gamma Irradiation of Crystalline $KClO_3$

Sample	Dose (ev per mole of $KClO_3$)	$G(Cl^-)$	$G(ClO^-)$[a]	$G(ClO_2^-)$	$G(ClO_4^-)$[b]
	$\times 10^{23}$				
2[c]	4.37	1.55 ± 0.05	0.32 ± 0.01	2.08 ± 0.03	0.98 ± 0.03
3	4.42	1.65 ± 0.05	0.32 ± 0.01	2.05 ± 0.03	0.96 ± 0.02
Average	4.4	1.60 ± 0.07	0.32 ± 0.02	2.06 ± 0.04	0.97 ± 0.04
Literature[d]	$\leq$1.2	1.64 ± 0.09	0.27 ± 0.04	2.07 ± 0.07	1.13 ± 0.06

[a]These data presented as $G(ClO^-)$ may contain a slight contribution from $G(ClO_2)$. Due to the strong ClO_2(g) odor of the irradiated samples, and to the close agreement between these values and Burchill *et al.*[d] values, it is felt that the great majority of the ClO_2 escaped from the finely divided samples before dissolution for analysis.

[b]Calculated from analysis of aqueous solutions.

[c]See footnote *a*, Table 4.1.

[d]C. E. Burchill, P. F. Patrick, and K. J. McCallum, *J. Phys. Chem.* 71, 4560 (1967).

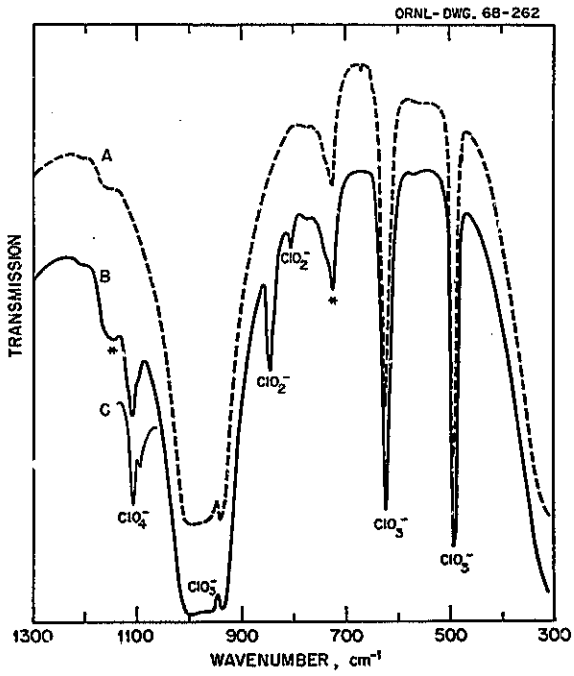

Fig. 4.5. Infrared Spectra of (*A*) Unirradiated $KClO_3$; (*B*) ^{60}Co Gamma-Ray-Irradiated $KClO_3$; and (*C*) A Typical $KClO_4$-$KClO_3$ Freeze-Dried Standard. The asterisks indicate the positions of Nujol absorbancies.

5. Organic Chemistry

PI-ROUTE SOLVOLYSES OF Δ^3-CYCLOPENTENYLETHYL TOSYLATES LABELED WITH ^{14}C OR DEUTERIUM

Vernon F. Raaen Charles E. Harding[1]
Clair J. Collins

Last year we published a mechanistic analysis of pi-route and sigma-route solvolyses of variously labeled cyclopentenylethyl and norbornyl esters,[2] in which we pointed out the advantages of labeling certain specific positions in the two different reactants. We have now prepared Δ^3-cyclopentenylethyl tosylates labeled with ^{14}C in the 1-ethyl position (1) and in the bridgehead position of the cyclopentene ring (2). The fractions of original radioactivity found in certain of the positions of the product, 2-*exo*-norbornyl acetate, are shown in structures I (from 1) and II (from 2):

ORNL-DWG. 68-5168

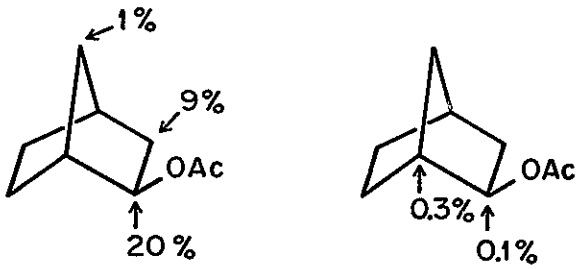

I II

The results are incompatible if we assume the two reactants proceed directly to norbornyl carbonium ions which undergo the usual[2] rearrangements. If, however, the cyclopentenyl group undergoes 1,2 shift between the α and β carbons of the ethyl moiety before formation of the norbornyl carbonium ion, the results become understandable. Such a prior rearrangement would cause considerable scrambling of the label in 1 but would not affect the label in 2. The small amount of ^{14}C in the 1 and 2 positions from 2 [structure II] thus becomes a measure[2] of 3,2 shift in the norbornyl carbonium ion.

THE PREPARATION AND HYDROLYSIS OF 5-*exo*-PHENYL-5-HYDROXY-2-*endo*-NORBORNYL-2-*d* TOSYLATE

Benjamin S. Benjaminov[3] Ben M. Benjamin
Clair J. Collins

5-*exo*-Phenyl-5-hydroxy-2-*endo*-norborneol-2-*d*, mp 103°, was prepared from lithium aluminum deuteride reduction of 5-*exo*-phenyl-5-hydroxynorbornanone. The tosylate ester, mp 130°, was obtained from the latter diol by treating it in pyridine solution with *p*-toluenesulfonyl chloride. Hydrolysis of the tosylate under previously described[4] conditions gave three compounds in the following yields: 5-*exo*-phenyl-5-hydroxy-2-*exo*-norborneol-2-*d*, 52.4%; 5-*endo*-phenyl-5-hydroxy-2-*exo*-norborneol-1-*d*, 16%; and 2-phenyl-2-nortricyclenol-5-*d*, 3%. The reaction scheme is shown in Chart I. Wagner-Meerwein shift was observed but hydride or deuteride shift was not.

[1]ORAU Predoctoral Fellow from the University of Tennessee, Knoxville.

[2]C. J. Collins and M. H. Lietzke, *J. Am. Chem. Soc.* 89, 6565–72 (1967).

[3]ORAU Research Participant June–September 1967 from Rose Polytechnic Institute, Terre Haute, Ind.

[4]C. J. Collins and B. M. Benjamin, *J. Am. Chem. Soc.* 89, 1652 (1967).

ORNL-DWG. 68-5178

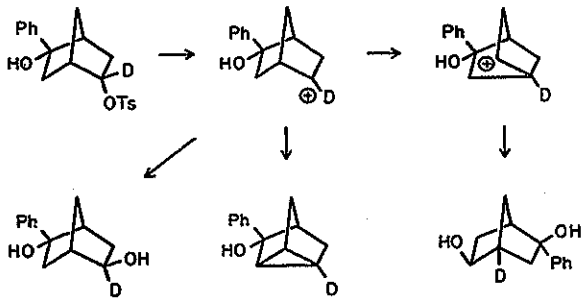

CHART I

DEAMINATION OF 3-*exo*- AND 3-*endo*-PHENYL-3-HYDROXY-2-*endo*-NORBORNYLAMINES

Michael Eckert[5] Clair J. Collins

In a continuing study[6] the title compounds 1 and 2 (Chart II) were subjected to deamination with $NaNO_2$ in acetic acid–sodium acetate solution, and the yields of the products were determined by vapor-phase chromatography.

ORNL-DWG. 68-4264

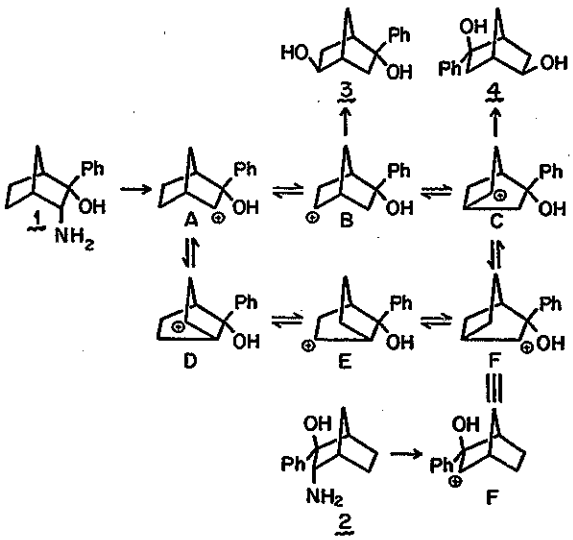

CHART II

The yields of diols 3 and 4 (see Chart II) were carefully examined in order to establish whether the amines 1 and 2 produce them in the same or in different ratios. This question is important to the nature of the Wagner-Meerwein pair (B⇌C) of cations, because if B and C are, in fact, combined as a single nonclassical ion, then we would presume the ratio 3:4 from either reactant should be the same. If, however, B and C are classical, open, unbridged ions, then providing the diols 3 and 4 are formed by the short routes (see Chart II), we might expect relatively more 3 from reactant 1 than from reactant 2. Preliminary results indicate the ratio 3:4 from 1 is about 1.5:1, whereas from 2 the ratio is more than 4:1. The yields of other products in the deamination of 2 indicate that 2 proceeds to 3 and 4 primarily through the long route (F→E→D→A→B→C). The results show "memory effects" which can be ascribed either to (1) the classical character of the intermediate carbonium ions or (2) the effect of the counter ion, which should be in different positions depending upon the nature of the reactant.

PHOTODIMERIZATION OF ISOPHORONE

V. F. Raaen

Isophorone (I), when irradiated with ultraviolet light, yields a large number of complex condensation products; gas-liquid chromatography shows that at least 11 components are present in the fraction of boiling point 160 to 170°/2mm. Alumina-column adsorption chromatography permitted the isolation of a third solid photodimer (II), melting point 114°. Two other photodimers, one a stereoisomer of II, melting point 215°, and III, whose melting point is 185°, were isolated previously from similar fractions of the irradiation mixture.

ORNL-DWG. 68-6668

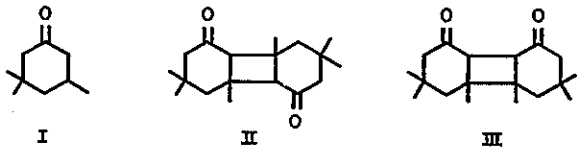

I II III

[5]ORAU Predoctoral Fellow from the University of Tennessee, Knoxville.

[6]M. Eckert, B. M. Benjamin, and C. J. Collins, *Chem. Div. Ann. Progr. Rept. May 20, 1967*, ORNL-4164, p. 48.

Both were described in earlier reports.[7,8] Cell parameters and space groups for the three carbonyl compounds are described by C. K. Johnson and A. Vos ("Crystal Structure of Two Stereoisomeric Photodimers of Isophorene," this report). Two of the dimers (melting points 215 and 185°) were reduced to the corresponding carbinols, which melt at 230 to 232° and 198 to 201° respectively. No further investigation is proposed.

NUCLEAR MAGNETIC RESONANCE SPECTRA OF ALLYL COMPOUNDS. ROTATIONAL ISOMERISM IN ALLYL ETHERS, ALLYL CHLORIDE, AND ALLYL BROMIDE

Ben M. Benjamin Amos P. Kennedy[9]

In continuation of our studies of rotational isomerism[10] we investigated the temperature dependence of the nmr spectra of several allyl ethers. As a test of the accuracy of our results and techniques in comparison with data already in the literature,[11,12] we decided to obtain similar information for allyl chloride. Although the results at room temperature were identical with the published data, the temperature dependence was somewhat surprising; we therefore decided to investigate allyl bromide also.

Experimental procedure was the same as described previously.[10] Probe temperature was determined from the separation of the methyl and hydroxyl resonances of methyl alcohol for low temperatures and from the separation of the methylene and hydroxyl resonances of ethylene glycol for high temperatures.

Reduction of the temperature-dependent data to a set of coupling constants and conformational free-energy differences was accomplished as follows: Consider an equilibrium between the three conformations of an allylic molecule which may exist in solution.

ORNL-DWG. 68-6667

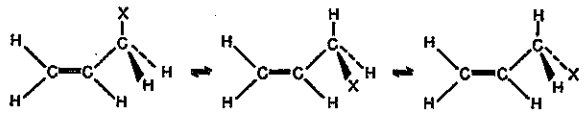

a b b′

Except for the fact that they are mirror images, **b** and **b′** are the same and have one *gauche* and one *trans*[13] coupling constant between the hydrogens on C-1 and C-2. Only *gauche* coupling is exhibited by **a**. In the dynamic state when rotation is rapid, the magnitude of the observed coupling will be an average of the contributions from **a** and **b**, and it will depend on the relative populations of the two forms. It can be shown that

$$J_{obs} = \frac{J_t + J_g(1 + e^{-\Delta F/RT})}{2 + e^{-\Delta F/RT}}, \qquad (1)$$

where J_{obs}, J_t, and J_g are the observed, *trans*, and *gauche* coupling constants respectively. At the high-temperature extreme when rotation is most rapid

$$J_\infty = \frac{2J_g + J_t}{3}. \qquad (2)$$

A subroutine was written for Eq. (1), and the program ORGLS[14] was used to obtain a least-squares fit for the $J_{1,4}$ values for allyl chloride determined at 15 different temperatures and allyl bromide determined at 11 different temperatures. The best values for allyl chloride were found to be $J_t = 31.08$, $J_g = -6.97$, and $\Delta F = 125$ cal.[15] Bothner-By[12] calculated $J_t = 13.4$, $J_g = 2.4$, and $\Delta F = 100$ cal. The calculated values for allyl

[7] V. F. Raaen, B. M. Benjamin, and C. J. Collins, *Chem. Div. Ann. Progr. Rept. June 20, 1963*, ORNL-3488, p. 59.

[8] V. F. Raaen and C. J. Collins, *Chem. Div. Ann. Progr. Rept. June 20, 1965*, ORNL-3832, p. 73.

[9] ORAU Research Participant June–September 1967 from Grambling College, Grambling, La.

[10] *Chem. Div. Ann. Progr. Rept. May 20, 1967*, ORNL-4164.

[11] A. A. Bothner-By, C. Naar-Colin, and H. Gunther, *J. Am. Chem. Soc.* 84, 2748 (1962).

[12] A. A. Bothner-By, S. Costellano, S. J. Ebersole, and H. Gunther, *J. Am. Chem. Soc.* 88, 2465 (1966).

[13] H. Conroy, p. 265 in *Advances in Organic Chemistry: Methods and Results*, Vol. II, Interscience, New York, 1960.

[14] William R. Busing and Henri A. Levy, ORNL-TM-271 (1962).

[15] E. L. Eliel, p. 236 in *Stereochemistry of Carbon Compounds*, McGraw-Hill, New York, 1962.

bromide using our data gave $J_t = 22.01$, $J_g = -1.73$, and $\Delta F = 278$ cal. It should be noted that theoretical[16] values for J_t and J_g have been predicted to be 8 to 9 Hz and 2 to 3 Hz, respectively, and the available experimental data for rigid compounds are in good agreement. Using Bothner-By's data we were unable to regenerate his parameters. Because of these inconsistencies it is thought that the analysis of the data is based on an incorrect model, and further work based on this possibility is planned.

The coupling constant $J_{1,4}$ in allyl ethers does not change over a wide temperature range even when one of the substituents on oxygen is bulky. This observation is in contrast to that reported earlier for allyl methyl ether,[12] which is least likely to show a conformational preference. It is therefore demonstrated that for the allyl ethers investigated, Eq. (1) reduces to the high-temperature expression Eq. (2), and rotation is not hindered at the experimentally accessible temperatures.

AN ISOTOPE EFFECT ON A SPIN-SPIN COUPLING CONSTANT

Ben M. Benjamin

Numerous deuterium isotope effects on the rates of reactions have been studied. Much of the work has been reviewed by Melander.[17] These effects are interpreted as being a consequence of differences in zero-point energy of the isotopic substituent. Raaen and Collins[18] discussed some deuterium isotope effects arising from steric factors. Mislow[19] has observed secondary isotope effects in the racemization of deuterium-substituted bridged biphenyls and ascribed the results to conformational changes arising from nonbonded repulsions of the isotopes in systems where highly crowded transition states would be required. An earlier suggestion indicated that small secondary isotope effects may arise from differences in steric requirements of protium and deuterium.[20]

It is known[21] that substitution of deuterium for hydrogen causes an upfield shift of 1 to 2 Hz in the nmr spectrum of neighboring hydrogens. The isotopic shift is thought to result from differences in vibrational amplitudes of H and D atoms. A simple calculation was done to determine the change of the value of the zero-point bending vibrations of CH_2 and CHD groups, and it was suggested that such small variations may lead to the observation of differences in spin-spin interactions. This report is an account of what is believed to be the first observation of a deuterium isotope effect on a hydrogen spin-spin coupling constant.

3-*endo*-Phenyl-2-*endo*-norbornanol (I) and its *exo*-5, *anti*-7 dideuterated counterpart (II) have been prepared and characterized.[22] The nmr signal for the *exo*-2 hydrogen of I (4.55 ppm in pyridine solution) is a quartet. It is coupled with the *exo*-3 hydrogen, 9.8 Hz, and the 1-bridgehead hydrogen, 4.3 Hz. The width at half height of each component of the quartet is 2.1 Hz, and no additional fine structure is discernible.[23] On the other hand, the components of the quartet for the

ORNL-DWG. 68-6666

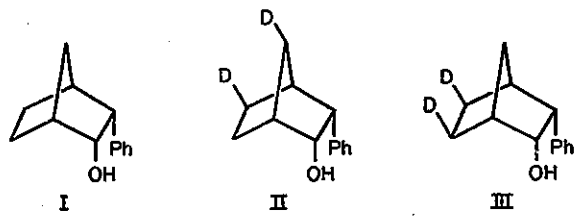

I II III

[16] M. Karplus, *J. Chem. Phys.* 30, 11 (1959).

[17] Lars Melander, *Isotope Effects on Reaction Rates*, Ronald Press, New York, 1960.

[18] V. F. Raaen and C. J. Collins, *Pure Appl. Chem.* 8, 347 (1964); V. F. Raaen, T. K. Dunham, D. D. Thompson, and C. J. Collins, *J. Am. Chem. Soc.* 85, 3497 (1963).

[19] K. Mislow, E. Simon, and H. B. Hopps, *Tetrahedron Letters*, 1011 (1962); K. Mislow, R. Graeve, A. J. Gordon, and C. H. Wahl, Jr., *J. Am. Chem. Soc.* 85, 1199 (1963); K. Mislow, R. Graeve, A. J. Gordon, and G. H. Wahl, *J. Am. Chem. Soc.* 86, 1733 (1964).

[20] L. S. Bartell, *J. Am. Chem. Soc.* 83, 3567 (1961).

[21] H. S. Gutowsky, *J. Chem. Phys.* 31, 1683 (1959).

[22] B. M. Benjamin and C. J. Collins, *J. Am. Chem. Soc.* 88, 1556 (1966).

[23] Similar results for both isotopic species were observed when dissolved in benzene, chloroform, and carbon tetrachloride. The effect was most pronounced in pyridine solution, however. Spectra were recorded on a Varian A-60 nmr spectrometer. The probe temperature was approximately 36°; TMS was employed as internal standard, $\delta = 0$ ppm. The spectrometer was calibrated at 500 Hz sweep width using the separation of the TMS-chloroform signals at 436 Hz and at 50 Hz sweep width using the separation of the outer components of the acetaldehyde quartet as 8.55 Hz. Resolution was 0.25 Hz.

exo-2 hydrogen of II have a width of 2.6 Hz at half height, and they are clearly resolved into doublets of 1.1-Hz separation (Fig. 5.1). The small splitting is ascribed to coupling with the *exo*-6 hydrogen, which is confirmed by the sharper signal for the *exo*-2 hydrogen of III, 1.4 Hz.[24]

[24]III was synthesized by hydroboration of 2-phenylnorbornene-2-*exo*-5,*exo*-6-d_2 and oxidation of the carbinol to 3-*endo*-phenyl-norbornanone-*exo*-5,*exo*-6-d_2, which was reduced with lithium aluminum hydride.

ORNL-DWG. 68-5644

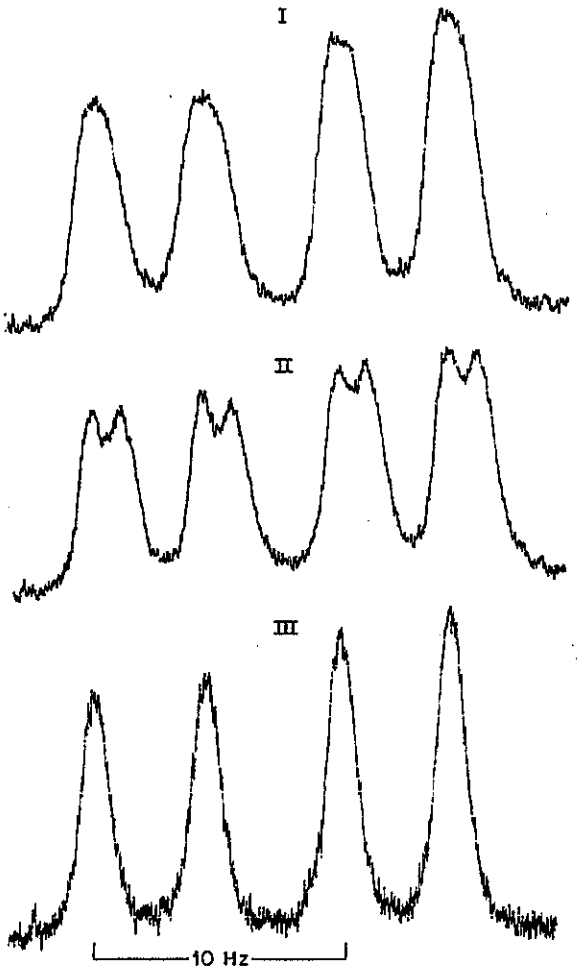

Fig. 5.1. The 60-MHz Signals for the *exo*-2 Hydrogen of 3-*endo*-Phenyl-2-*endo*-norbornanol (I), 3-*endo*-Phenyl-2-*endo*-norbornanol-5-*exo*-7-*anti*-d_2 (II), and 3-*endo*-Phenyl-2-*endo*-norbornanol-5-*exo*-6-*exo*-d_2 (III).

Long-range coupling of 1 to 2 Hz of this type was first observed by Anet,[25] and numerous examples have been recorded since. It has been pointed out that long-range coupling through four bonds may be observed in molecules having favorable geometry, that is, when the atoms are arranged in a planar W form, and the magnitude of the coupling has been predicted theoretically.[26] In models of molecules I and II the arrangement of the *exo*-H-2, C-2, C-1, C-6, *exo*-H-6 system appears to be nearly planar, and it is not immediately obvious why spin-spin coupling is larger in the deuterated species II than in the completely protonated molecule I. In order to facilitate interpretation of the observation, complete structures of I and II were determined in the crystalline state.[27]

Crystals of the two isotopic species were found to be completely isomorphous. However, in each case, the unit cells consisted of equal numbers of molecules of two different spatial arrangements (Fig. 5.2). Bond angles and intranuclear dis-

[25]F. A. L. Anet, *Can. J. Chem.* 39, 789 (1961).

[26]M. Karplus, *J. Chem. Physics* 33, 1842 (1960).

[27]The crystal structures were determined using neutron diffraction by Carroll K. Johnson, Chemistry Division, ORNL. A preliminary report was given at the Winter Meeting of the American Crystallographic Association, Atlanta, Ga., January 1967, p. 46. A complete account of the work will appear in a future publication.

ORNL-DWG. 68-6972

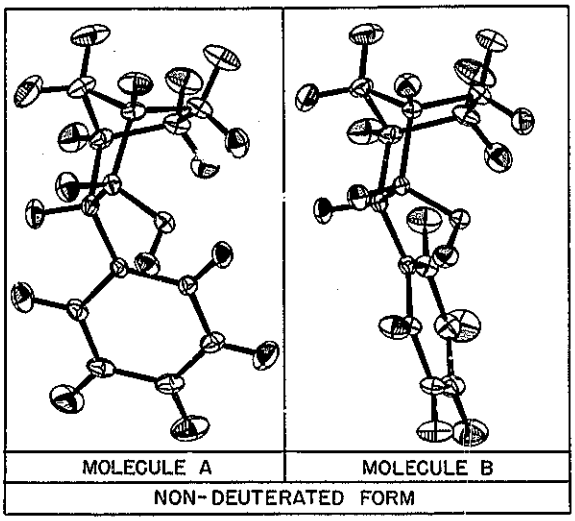

Fig. 5.2. The Steric Forms of 3-*endo*-Phenyl-2-*endo*-norbornanol.

tances in the two steric forms are not identical. The plane of the phenyl ring of isomer *A* bisects the norbornyl moiety so that one ortho hydrogen lies close to and in between the *endo*-5 and *endo*-6 hydrogens. The shapes and angles of the W are shown in Fig. 5.3. Looking at the W edgewise through the plane described by C-2, C-1, C-6 (Fig. 5.3*b*), it is seen that *exo*-2-H lies closer to the plane than *exo*-6-H. The distance between the centers of the *exo*-5-H and the 7-H *syn* to it is 2.568 A.

In contrast, the plane of the phenyl ring of steric isomer *B* is tangent to the norbornyl structure. It is bent out somewhat, and the entire framework is twisted. The resultant distortion affects the bond angles and lengths so that now the *exo*-6-H is closer to the C-2, C-1, C-6 plane (Fig. 5.3*d*), and the *exo*-5-H is also measurably further away from the 7-H *syn* to it, 2.731 A, a difference of 0.2 A in this distance for the two steric forms.

It has been suggested[28] that the smaller amplitude of vibration of deuterium compared with that of hydrogen is reflected in a smaller van der Waals radius and that consequently the distance of minimum approach of deuterium nuclei can be smaller than that for hydrogen. In recognition of the smaller steric requirement of deuterium, it seems plausible that in an arrangement where a pair of deuterium substituents are disposed in a *syn* relationship such as exists in II, they can be forced closer together than a pair of hydrogens similarly disposed. Since two conformations of I or II exist in the crystalline state, differing in the distances between *exo*-5-H and 7-H, it is reasonable to assume that the same conformations are preferred in solution. Although no differences were detected in the crystal structures of I and II within experimental error, this does not preclude the presence of small differences of conformational preferences in solution. Because deuterium atoms of II can permit the closer approach of positions 5 and 7, the *A* conformation must be the lower-energy form of the deuterium-containing molecule II in solution, and the *B* conformation must, therefore, be preferred for the hydrogen-containing molecule I. This is equivalent to proposing that the stereochemical form *A* provides the best arrangement for a spin-coupling mechanism.

Other similar molecules are being investigated to determine if there also changes occur in coupling constants when deuterium is substituted for hydrogen.

[28] A. R. Ubbelohde, *Trans. Faraday Soc.* 32, 525 (1936).

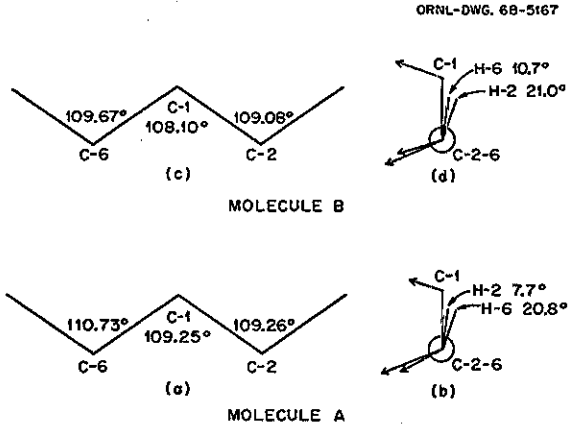

Fig. 5.3. The Angles Around C-2, C-1, C-6 of 3-*endo*-Phenyl-2-*endo*-norbornanol.

POLYMER STUDIES

C. E. Higgins W. H. Baldwin

Equilibria in the System: Poly(Hydroxypropyl Acrylate-co-Tetraethylene Glycol Dimethacrylate), Water, and Electrolyte

Cylinders of the copolymer (19 parts by weight of hydroxypropyl acrylate to 1 of tetraethylene glycol dimethacrylate) were prepared by the photochemical initiation method reported previously.[29] After the polymers had been washed with water they were equilibrated with 0.5 *M* sodium chloride. They showed 70% rejection of NaCl and a slight (15%) shrinkage. Equilibration with a mixture of 0.5 *M* NaCl and 0.02 *M* NaOH was accompanied by marked swelling (500%), slight salt rejection (20%), and intake of all the sodium hydroxide from the solution. Since the concentration of sodium hydroxide may well be

[29] W. H. Baldwin and C. E. Higgins, *Chem. Div. Ann. Progr. Rept. May 20, 1967*, ORNL-4164, p. 56.

reduced by saponification of ester groups, the mechanism of exchange in the presence of sodium hydroxide is being studied further.

Copolymers of 4-Vinylpyridine

Linear poly(4-vinylpyridine) is soluble in dilute mineral acid solutions and behaves as a polyelectrolyte. Poly(4-vinylpyridine) has a very low solubility (about 2 mg/liter) in distilled water. For other studies in this laboratory it is desirable to obtain a nonelectrolyte, poly(vinylpyridine), that has a higher affinity for water. Copolymers of 4-vinylpyridine with hydroxypropyl acrylate and with *N*-vinyl-2-pyrrolidone were selected for further study after it was observed that mixtures of homopolymers of these compounds were compatible in solution and in cast films.

Polymerization of mixtures of monomers using azobisisobutyronitrile indicates a preference of 4-vinylpyridine to polymerize with itself. However, by starting with a mixture of 4-vinylpyridine and *N*-vinyl-2-pyrrolidone (1:9 mole ratio) a copolymer of nearly 1:1 composition was obtained. The solubility (300 mg/liter) was significantly higher than the 7:3 copolymer (solubility in water 10 mg/liter). A copolymer consisting of 2 moles of 4-vinylpyridine to 1 mole of hydroxypropyl acrylate was no more soluble than homopolymer from 4-vinylpyridine.

VOLATILE METAL-ORGANIC COMPOUNDS

W. H. Baldwin

Volatile metal compounds are useful for the purification of metallic elements and for the preparation of other compounds. Wardlaw and Bradley[30] observed an interesting phenomenon among alkoxide derivatives. Maximum volatility and minimum association were found for more highly branched and higher-molecular-weight alkoxides rather than for the first members of the homologous series (methoxide or ethoxide). The most volatile such compound of zirconium is the tetra-*t*-butoxide and for thorium the triethylcarbinol derivative. This behavior has been explained on the basis of shielding the metal ion with the hydrocarbon radicals, thereby reducing intermolecular association of metal and oxygen atoms.

The somewhat more complex aluminoalkoxides studied by Meerwein and Bersin[31] in 1929, such as $Mg[Al(O\text{-}i\text{-}Pr)_4]_2$, were volatile and soluble in hydrocarbons. Later Albers *et al.*[32] prepared the analog with U(IV), obtaining the tetrakisaluminoisopropoxide, boiling at 143°C under 1 mm Hg pressure.

Using a modification of this method[32] we have prepared the erbium compound, $Er[Al(O\text{-}i\text{-}Pr)_4]_3$, melting at 108 to 110°C and distilling at 175°C under 1 mm Hg pressure. A degree of purification was obtained here, since the starting $ErCl_3$ was yellow, probably from contamination with iron, while the product was pink, the color of many erbium compounds.

[30] W. Wardlaw and D. C. Bradley, *Endeavour*, July 1955, p. 140.

[31] H. Meerwein and Th. Bersin, *Ann. Chem.* 476, 113 (1929).

[32] H. Albers, M. Deutsch, W. Krastinet, and H. von Osten, *Chem. Ber.* 85, 267 (1952).

6. Chemistry of Aqueous Systems

A TWO-STRUCTURE MODEL FOR ELECTROLYTIC SOLUTIONS

M. H. Lietzke R. W. Stoughton
R. M. Fuoss[1]

At low concentrations, properties of electrolytic solutions are those theoretically predicted for a model system in which the effects of all other ions on a reference ion can be treated as those of a continuous space charge, the familiar ion atmosphere proposed by Debye and Hückel. At high concentrations, on the other hand, the effects of near neighbors on a reference ion become far more significant than those of more distant ions; interionic electrostatic energies no longer are small compared with kT, and thereby the necessary condition for the existence of a smoothed charge density disappears. Clearly, then, a different model must be chosen as the basis of theory. The upper limit of the concentration scale corresponds to the randomized[2] fused salt; as solvent molecules are added to make concentrated solutions, average interionic distances will vary as the cube root of concentration. This naturally suggests a cell model for the higher concentrations. As the solution is diluted, we know that the $c^{1/3}$ behavior must give way to $c^{1/2}$ properties. There is, of course, no critical concentration at which a solution suddenly stops acting like a diluted and randomized crystal lattice and rearranges its ions to the distribution characteristic of the ion atmosphere. Rather, a smooth transition from one model to the other must occur. A stochastic description can be formulated[3] as

$$P(c) = P(0)\, f(c) + P(\infty)[1 - f(c)] , \qquad (1)$$

where P is the value of a given property of the solution at concentration c, $P(0)$ is the Debye-Hückel description of that property, $P(\infty)$ is the cell model description, and $f(c)$ satisfies the conditions

$$f(0) = 1 , \quad f(\infty) = 0 . \qquad (2)$$

(Here the symbols 0 and ∞ imply solute-solvent concentration ratios of 0:1 and 1:0, of course.) In effect, we propose to treat the solution as a mixture of two structures, the contribution of each being weighted by a partition function $f(c)$, much as the sum of contributions from two significant structures[4] has been used to describe the properties of liquids.

Quasi-lattice models have, of course, been considered for electrolytic solutions before, beginning with Ghosh[5] and Bjerrum;[6] these lead to $c^{1/3}$ laws. The high-concentration model described by $P(\infty)$, however, is not a lattice model but a cell model. The former would imply that solute particles are bound to equilibrium positions. No such restriction is made in a cell model; a solute particle may be anywhere in its cell, and empty cells matched by cells containing two ions (ion pairs) are not excluded. More recently,[7,8] attention has been called again to the persistent appearance of $c^{1/3}$ in the dependence on concentration of properties

[1]Yale University, New Haven, Conn.

[2]C. A. Angell, *J. Phys. Chem.* **70**, 3988 (1966); C. A. Angell, E. J. Sare, and R. D. Bressel, *J. Phys. Chem.* **71**, 2759 (1967).

[3]R. M. Fuoss and L. Onsager, *Proc. Natl. Acad. Sci. U.S.* **47**, 818 (1961).

[4]J. Walter and H. Eyring, *J. Chem. Phys.* **9**, 393 (1941); H. Eyring, T. Ree, and N. Hirai, *Proc. Natl. Acad. Sci. U.S.* **44**, 683 (1958).

[5]J. C. Ghosh, *J. Chem. Soc.* **113**, 449, 707 (1918).

[6]N. Bjerrum, *Z. Elektrochem.* **24**, 321 (1918); N. Bjerrum, *Z. Anorg. Chem.* **109**, 275 (1920).

[7]H. S. Frank and P. T. Thompson, pp. 113–34 in *The Structure of Electrolytic Solutions*, ed. by W. J. Hamer, Wiley, New York, 1959.

[8]E. Glueckauf, Part 7 (pp. 97–112) in *The Structure of Electrolytic Solutions*, ed. by W. J. Hamer, Wiley, New York, 1959.

such as logarithm of activity coefficient, equivalent conductance, and diffusion coefficients. But these formulations all face the obstacle of dilute solutions; experimentally, limiting properties go as the square root and not as the cube root of concentration. An expression of the form (1) obviously will by its construction give limiting square-root laws and then go over into a cube-root description at higher concentrations.

The explicit form of the transition function $f(c)$ is not important for a test of the idea of representing electrolytic solutions effectively as mixtures of two structures. Since we prefer a rather sharp transition we use the convenient exponential

$$f(c) = e^{-a\phi} , \quad (3)$$

where a is a constant, ϕ is the volume fraction of solute

$$\phi = Vc/1000 \quad (4)$$

computed on the basis of the molar volume V of the dry salt, and c is concentration in moles per liter. (Concentrations must be expressed in these units for our present purpose; the significant variable is distance between ions.) As a typical electrolytic property, we consider activity coefficients. Then for $P(0)$, we have a Debye-Hückel expression, while for $P(\infty)$, we choose a simple power series whose leading term is cube root of concentration. Thus,

$$\ln y = -e^{-a\phi}\mathring{A}I^{1/2}/(1 + 1.5I^{1/2}) + (B'I^{1/3} + C'I)(1 - e^{-a\phi}) , \quad (5)$$

which, for convenience in calculation, can be rearranged to

$$\ln y = -[\mathring{A}I^{1/2}/(1 + 1.5I^{1/2}) + B'I^{1/3} + C'I]e^{-a\phi} + B'I^{1/3} + C'I . \quad (6)$$

Here $\mathring{A}$ is the Debye-Hückel coefficient, I is the ionic strength computed on a molarity basis, B' and C' are for the moment to be considered as empirical constants, and y is the activity coefficient on a molar basis.

Conventionally, activity coefficients at concentrations above the range of high dilutions have been reproduced by equations of the form

$$\ln y = -\mathring{A}I^{1/2}/(1 + 1.5I^{1/2}) + BI + CI^2 + \ldots , \quad (7)$$

where B, C, etc., are empirical constants devoid of physical significance. Here we have arbitrarily set the Debye-Hückel denominator parameter to 1.5. Such equations have been applied to data up to quite high concentrations, despite the implications of the retention of the term in $I^{1/2}$; this term, of course, has its origin in the continuous space charge of the Debye-Hückel model and must lose all physical significance when the concentration is so high that the linearized Poisson-Boltzmann equation is no longer valid.

In order to test the relative effectiveness of Eqs. (6) and (7) in expressing the activity coefficients of electrolytes, data from the literature have been used. Values in the concentration range 0.1 to 2.0 m were taken from Robinson and Stokes,[9] while data in the range 0.001 to 0.1 m were taken from Landolt-Börnstein.[10] Since the activity coefficient values in Robinson and Stokes are presented on a molal basis and had to be converted to molar values, the choice of electrolytes studied was dictated somewhat by the availability of density data on the aqueous solutions.

Results and Discussion

The various electrolytes studied are listed in Fig. 6.1. The variances of fit were about the same on the average whether Eq. (6) or (7) was used. It is difficult to evaluate this observation since it has been quite common to smooth activity coefficient data with an extended Debye-Hückel equation [e.g., like (7)]. The significant point, however, is that whereas the B coefficients for Eq. (7) scatter widely, some being positive and some negative, the B' coefficients for Eq. (6) all cluster in a narrow region about −0.6 for the 1-1 electrolytes and about −1.15 for the 1-2 and 2-1 electrolytes; this result suggests that the coefficient B' has a physical meaning correlated with valence type.

Accordingly, by using a cell model, an expression was derived for B' in terms of the cationic charge z_1 and number of cations per molecule ν_1, the corresponding z_2 and ν_2 for the anion, and a cell constant A:

[9] R. A. Robinson and R. H. Stokes, *Electrolyte Solutions*, Academic, New York, 1955.

[10] *Landolt-Börnstein Tabellen*, Eq. III-c 2139-2162, Julius Springer, Berlin, 1936.

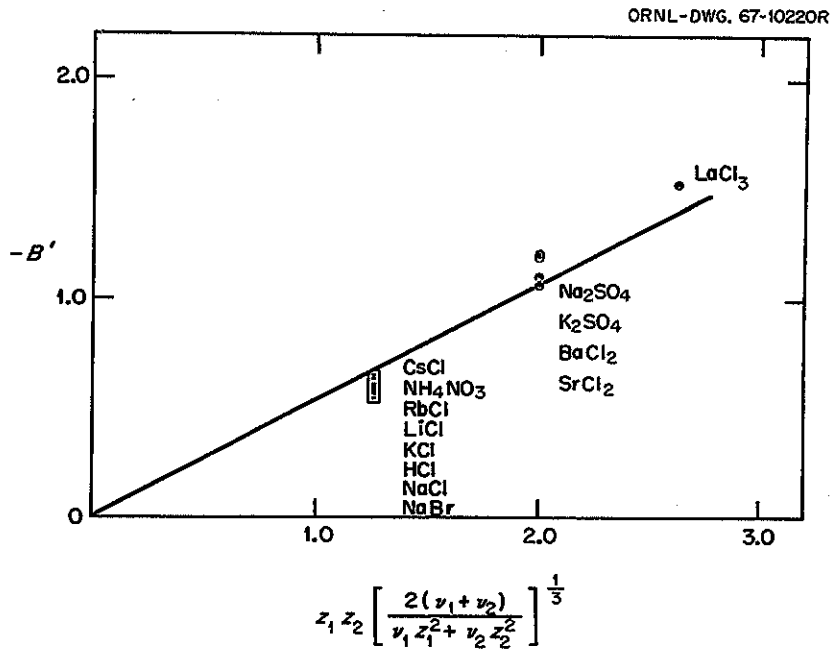

Fig. 6.1. Correlation of $-B'$ (Eq. 6) with Valence Type. z is the ionic charge and ν the number of ions per molecule.

$$-B' \cong 0.606 A z_1 z_2 \left[\frac{2(\nu_1+\nu_2)}{(\nu_1 z_1^2+\nu_2 z_2^2)}\right]^{1/3} . \quad (8)$$

Figure 6.1 is a plot of $-B'$ against the function of charges and numbers of ions given in Eq. (8). As seen in Fig. 6.1, the points fall roughly on a straight line going through the origin as required by expression (8).

Activity coefficients were calculated using the values of B' from the straight line in Fig. 6.1 for each valence type (i.e., assuming A was the same for all electrolytes). These values of B' were –0.66 for 1-1, –1.07 for 1-2 and 2-1, and –1.40 for 3-1 electrolytes. In each case the values of C' and of a were allowed to vary to give the best fit by the method of least squares. The average maximum deviations between the observed and calculated values in this region were 1.8% for the 1-1 electrolytes, 2.5% for the 1-2 and 2-1 electrolytes, and 8.3% for the $LaCl_3$. The slope of the line in Fig. 6.1 gives a value of about 0.88 for A compared with a Madelung constant of 1.75 for the NaCl crystal. This "discrepancy" is a consequence of the lack of longer-range structure due to thermal motion and diffusion. Glueckauf,[8] using a somewhat different treatment in obtaining values of B' and different concentration ranges, obtained values a little closer to the Madelung constants of crystals.

We computed for each salt studied the concentration $c_{0.5}$ at which the partition function is equal to 0.5. This represents the concentration at which the Debye-Hückel model and the cell model contribute equally to the logarithm of the activity coefficient. As expected, the higher the charge type, the lower the value of the concentration at which the cell model becomes important.

Since the values of $c_{0.5}$ and hence of a appear to correlate with valence type, the values of a obtained were plotted against the product of the valence of the cation and anion $z_1 z_2$; the plot was roughly linear. Values of $a \times 10^{-3}$ taken from this line were 3.3 for 1-1, 6.6 for 1-2 and 2-1, and 10.0 for 3-1 electrolytes. These values of $a \times 10^{-3}$ along with those of B' from Fig. 6.1 were used to fit all the activity coefficient data by the method of least squares (with C' in each case now being the

sole adjustable parameter). With only this one adjustable parameter, the variance of fit was within about 50% of that obtained using Eq. (6) with three adjustable parameters (a, B', and C') in the cases of LiCl, NaCl, KCl, RbCl, HCl, NaBr, and K_2SO_4; in the other six cases the variances of fit for the single parameter were three to seven times those for the three-parameter fit. This result suggests that a and B' are coefficients with direct physical origin, in the same sense that the coefficient $\mathcal{A}$ is derivable from a model and fundamental principles. Granting this premise, Eq. (1) is verified as a valid description of the properties of electrolytic solutions over the entire concentration range.

ELECTROMOTIVE FORCE MEASUREMENTS IN HCl-NaCl, HCl-KCl, HCl-RbCl, AND HCl-CsCl MIXTURES

M. H. Lietzke R. W. Stoughton
H. A. O'Brien, Jr.[11]

In a previous paper[12] it has been shown that the logarithm of the activity coefficient of HCl in various HCl–alkali metal chloride mixtures could be represented as shown in Eq. (1), while the corresponding expression for the logarithm of the salt in the acid-salt mixtures could be represented as shown in Eq. (2):

$$\ln \gamma_2 = -\mathcal{A}\rho^{1/2}\sqrt{I}/(1 + 1.5\sqrt{I}) + 2I[B_{22} + (B_{23} - B_{22})X_3] + 3I^2[C_{222} + 2(C_{223} - C_{222})X_3] , \quad (1)$$

$$\ln \gamma_3 = -\mathcal{A}\rho^{1/2}\sqrt{I}/(1 + 1.5\sqrt{I}) + 2I[B_{33} + (B_{23} - B_{33})X_2] + 3I^2[C_{333} + 2(C_{233} - C_{333})X_2 + (C_{333} + C_{223} - 2C_{233})X_2^2] . \quad (2)$$

In these equations the subscript 2 refers to the acid, while the subscript 3 refers to the salt, $\mathcal{A}$ is the Debye-Hückel limiting slope, ρ is the density of the solution, I is the ionic strength of the solution, X_q is the ionic strength fraction of the indicated component in the mixture, and the B_{ij} and the C_{ijk} are interaction coefficients (considering both pair-wise and three-way interaction between ions).

Emf measurements have now been completed on mixtures of HCl with NaCl, KCl, RbCl, and CsCl using cells of the type

$$\text{Pt-H}_2(p{=}1)|\text{HCl}(m_2), \text{MCl}(m_3)|\text{AgCl, Ag.}$$

In all cases the measurements were carried out in the temperature range 25 to 175° in solutions of total ionic strength 0.5 and 1.0 in which the ratio of HCl to MCl was varied. The activity coefficient $\gamma_\pm$ of HCl at each temperature and set of concentrations in the mixtures was evaluated by using the Nernst equation and previous values[13] of the standard potential $E°$ of the Ag-AgCl electrode:

$$E = E° - \frac{RT}{F}\ln [m_2(m_2 + m_3)] - \frac{2RT}{F}\ln \gamma_\pm . \quad (3)$$

In this equation m_2 and m_3 are the molalities of HCl and the appropriate salt, respectively, T is the absolute temperature, R is the gas constant, and F the faraday. The resulting values of the activity coefficient of HCl in each system were fitted by the method of least squares using Eq. (1) to obtain estimates of the interaction coefficients. In carrying out this calculation the temperature dependence of the interaction coefficients was chosen to be consistent with the assumption that ΔC_p for the cell reaction was constant; that is,

$$B_{ij} = \frac{b'_{ij}}{T} + b''_{ij} + b'''_{ij}\ln T .$$

Figure 6.2 shows how the log γ_{HCl} varies in mixtures containing 0.5 ionic strength fraction of salt at total ionic strengths of 0.5 and 1.0 at 25, 125, and 175°. As can be seen the log γ_{HCl} values at $I = 0.5$ are all lower (more negative) than the corresponding values at $I = 1.0$ at 25° and all higher (more positive) at 175°. The crossover points vary from mixture to mixture but seem to be in the vicinity of 100 to 125°. The greatest difference between the values at $I = 0.5$ and 1.0 at the extremes of temperature occurs with the HCl-RbCl mixtures.

Figure 6.3 shows how the log γ_{salt} varies with total ionic strength and fraction of acid at 25° for the various mixtures. In all cases the log γ values

[11] Isotopes Division.

[12] M. H. Lietzke, H. B. Hupf, and R. W. Stoughton, *J. Phys. Chem.* 69, 2395 (1965).

[13] M. H. Lietzke and R. W. Stoughton, *J. Phys. Chem.* 68, 3043 (1964).

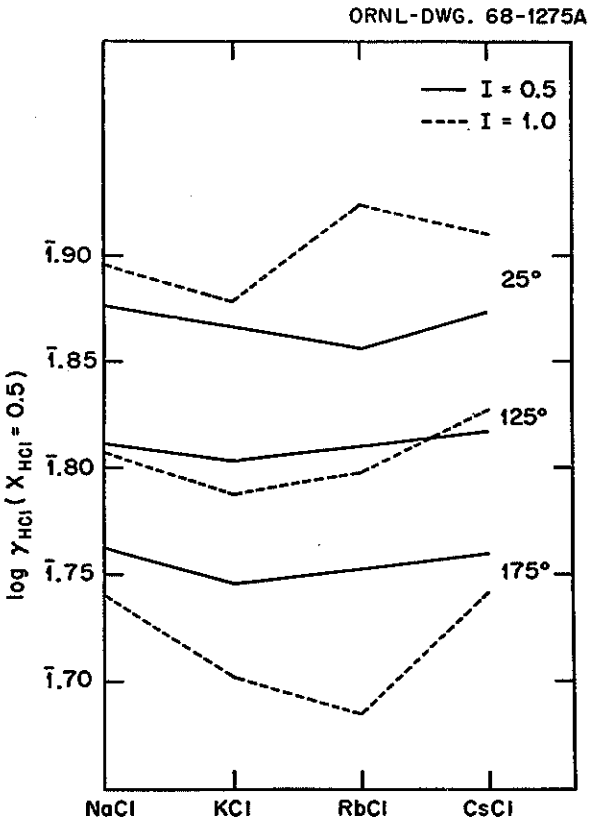

Fig. 6.2. Variation of log γ_{HCl} in HCl-NaCl, HCl-KCl, HCl-RbCl, and HCl-CsCl Mixtures Containing 0.5 Ionic Strength Fraction of Salt.

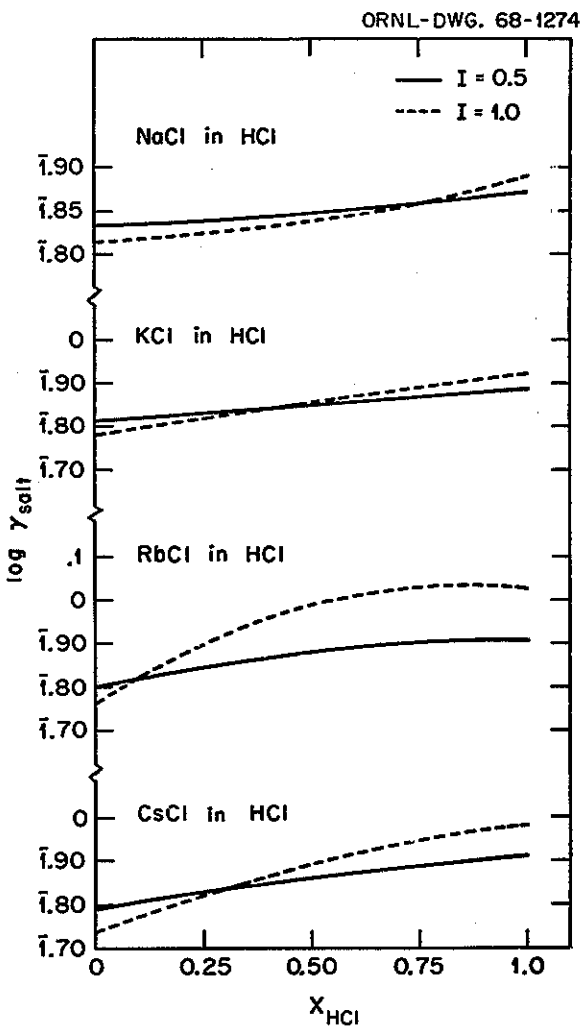

Fig. 6.3. Plots of log γ_{salt} vs Ionic Strength Fraction of HCl at 25° for HCl-NaCl, HCl-KCl, HCl-RbCl, and HCl-CsCl Mixtures.

are lower at $I = 1.0$ in the pure salt solutions and then cross the $I = 0.5$ curve. In the case of the HCl-NaCl mixtures, both curves are concave upward. In the HCl-KCl system the plots are linear: in other words both the HCl and the KCl obey Harned's rule in the HCl-KCl mixtures at 25°. In the HCl-RbCl and HCl-CsCl mixtures the log γ_{salt} vs X_{HCl} plots are concave downward. Note that in the HCl-RbCl mixtures the activity coefficient of the RbCl becomes greater than unity at high fractions of acid in solutions of total ionic strength 1.0.

The detailed results of this study will be reported in the open literature.

ELECTROMOTIVE FORCE MEASUREMENTS IN HCl-$MgCl_2$, HCl-$CaCl_2$, HCl-$SrCl_2$, AND HCl-$BaCl_2$ MIXTURES

M. H. Lietzke R. W. Stoughton
H. A. O'Brien, Jr.[14]

Emf measurements have been completed on mixtures of HCl with $MgCl_2$, $CaCl_2$, $SrCl_2$, and $BaCl_2$

[14]Isotopes Division.

using cells of the type

$$\text{Pt-H}_2(p{=}1)|\text{HCl}(m_2),\ \text{MCl}_2(m_3)|\text{AgCl, Ag.}$$

The measurements were carried out in the temperature range 25 to 60° (except for the HCl-$BaCl_2$ mixtures, where the range was 25 to 200°) in solutions of total ionic strength 0.5 and 1.0 in which the ratio of HCl to MCl_2 was varied. Activity coefficients of each component in each mixture were evaluated as described in the previous section, except that the temperature dependence of the interaction coefficients was chosen to be consistent with the assumption that ΔC_p for the cell reaction was zero; for example,

$$B_{ij} = \frac{b'_{ij}}{T} + b''_{ij}.$$

This assumption was made because the restricted temperature range of the measurements did not permit the evaluation of as many parameters as in the case of the HCl–alkali chloride mixtures, where the temperature range was 25 to 175°.

Figure 6.4 shows how the log γ_{HCl} varies in mixtures containing 0.5 ionic strength fraction of salt at total ionic strengths of 0.5 and 1.0 at 25 and 60°. As can be seen the log γ_{HCl} values at $I = 0.5$ are all lower (more negative) than the corresponding values at $I = 1.0$ at both 25 and 60°. Since the HCl-$BaCl_2$ mixtures were studied to 175°, it is of interest to examine the behavior of the log γ_{HCl} values in the corresponding mixtures at higher temperatures. As can be seen in Fig. 6.4, the values at both $I = 0.5$ and 1.0 are the same at 90°, while at 125° and above the value of log γ_{HCl} at $I = 0.5$ is now higher (less negative) than the value at $I = 1.0$. The same behavior would probably be exhibited in the other mixtures if the measurements were extended to temperatures higher than 60°. Note that the activity coefficient of HCl varies little from mixture to mixture.

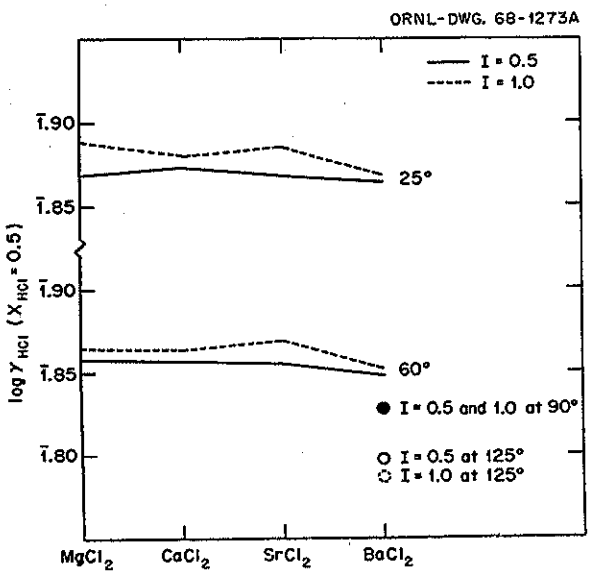

Fig. 6.4. Variation of log γ_{HCl} in HCl-$MgCl_2$, HCl-$CaCl_2$, HCl-$SrCl_2$, and HCl-$BaCl_2$ Mixtures Containing 0.5 Ionic Strength Fraction of Salt.

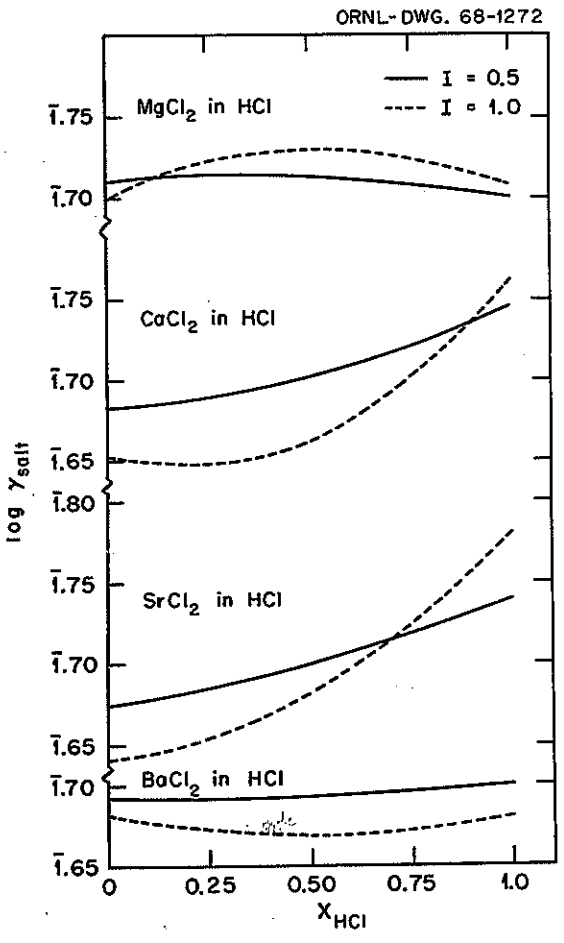

Fig. 6.5. Plots of log γ_{salt} vs Ionic Strength Fraction of HCl at 25° for HCl-$MgCl_2$, HCl-$CaCl_2$, HCl-$SrCl_2$, and HCl-$BaCl_2$.

Figure 6.5 shows how the log γ_{salt} values vary with total ionic strength and fraction of acid at 25° for the various mixtures. In all cases the log γ_{salt} values are lower at $I = 1.0$ in the pure salt solutions. In the case of $MgCl_2$, $CaCl_2$, and $SrCl_2$ the log γ_{salt} plots at $I = 1.0$ cross the plots at $I = 0.5$, and the log γ_{salt} values at zero concentration of salt ($X_2 = 1$) are higher at $I = 1.0$ than at $I = 0.5$. In the case of the HCl-$BaCl_2$ mixtures there is no such crossover. The activity coefficient curves are concave downward in the HCl-$MgCl_2$ mixtures and concave upward in the remaining systems.

A detailed description of these systems will be published in the open literature.

ELECTROMOTIVE FORCE MEASUREMENTS IN HCl-$AlCl_3$, HCl-$LaCl_3$, AND HCl-$GdCl_3$ MIXTURES

M. H. Lietzke R. W. Stoughton
H. A. O'Brien, Jr.[14]

Emf measurements have been completed on mixtures of HCl with $AlCl_3$, $LaCl_3$, and $GdCl_3$ using cells of the type

$$Pt\text{-}H_2(p{=}1)|HCl(m_2),\ MCl_3(m_3)|AgCl,\ Ag.$$

The measurements were carried out in the temperature range 25 to 175° (except for the HCl-$AlCl_3$ mixtures, where the range was 25 to 60°) in solutions of total ionic strength 0.5 and 1.0 in which the ratio of HCl to MCl_3 was varied. Activity coefficients of each component in each mixture were evaluated as described in the previous sections.

Figure 6.6 shows how the log γ_{HCl} varies in HCl-$AlCl_3$, HCl-$LaCl_3$, and HCl-$GdCl_3$ mixtures containing 0.5 ionic strength fraction of salt at total ionic strengths of 0.5 and 1.0 at 25 and 60°. At 25° the log γ_{HCl} values are all more negative at $I = 0.5$ than the corresponding values at $I = 1.0$, while at 90° they are more positive. The crossover point is at about 60°. In the other studies we found that the corresponding crossover temperatures are between 100 and 125° for mixtures of HCl with the alkali metal chlorides and about 90° for mixtures of HCl with the alkaline earth chlorides. Hence the higher the valence type of the salt the lower is the crossover temperature.

Figure 6.7 shows how the log γ_{salt} varies with total ionic strength and fraction of acid at 25° for

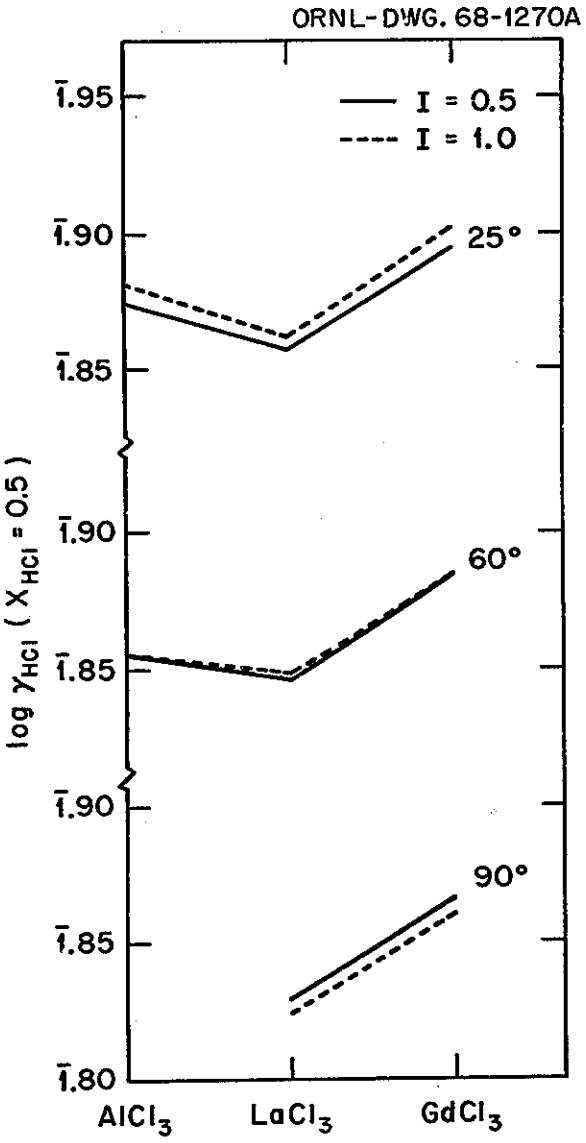

Fig. 6.6. Variation of log γ_{HCl} in HCl-$AlCl_3$, HCl-$LaCl_3$, and HCl-$GdCl_3$ Mixtures Containing 0.5 Ionic Strength Fraction of Salt.

the three mixtures. In all cases the log γ values are lower at $I = 1.0$ in the pure salt solutions. In the HCl-$AlCl_3$ and HCl-$GdCl_3$ systems the log γ_{salt} plots at $I = 1.0$ cross the plots at $I = 0.5$; both sets of curves are concave upward. There is no crossover in the log γ_{salt} plots for the HCl-$LaCl_3$ mixtures, and the curves are concave downward. The

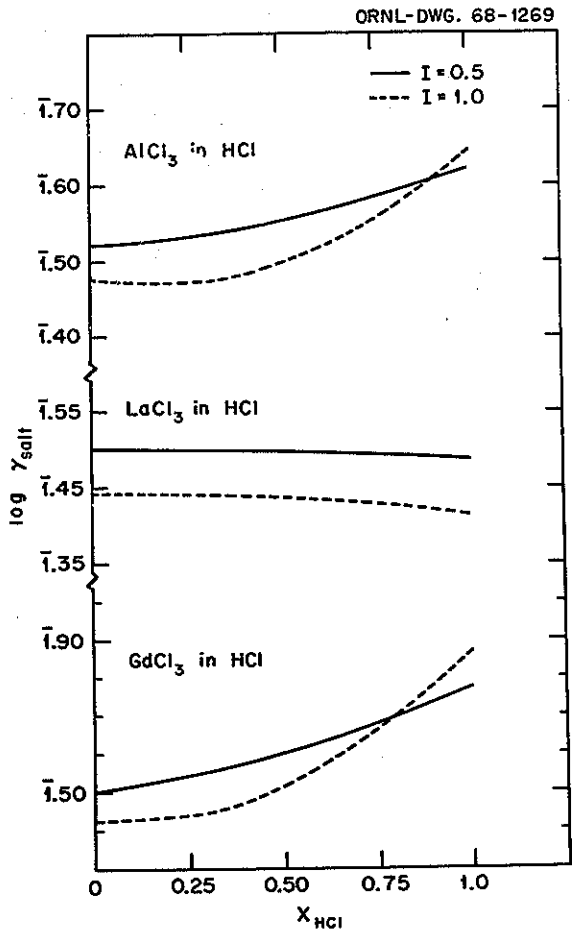

Fig. 6.7. Plots of log γ_{salt} vs Ionic Strength Fraction of HCl at 25° for HCl-$AlCl_3$, HCl-$LaCl_3$, and HCl-$GdCl_3$ Mixtures.

activity coefficient behavior of the $AlCl_3$ thus more closely resembles that of $GdCl_3$ than that of $LaCl_3$ in the corresponding HCl-salt mixtures. This behavior is not qualitatively unexpected since Al(III) is the least basic and La(III) the most basic of the three metal ions.

A detailed description of these systems will be published in the open literature.

FREE ENERGIES OF ELECTROLYTE MIXTURES

R. M. Rush
J. S. Johnson
Y. C. Wu[15]
G. Scatchard[16]
R. A. Robinson[17]

The importance of variations of free energies from ideality in chemical equilibria and kinetics is well appreciated. Information concerning these variations is of interest not only for its implications concerning the basic nature of solutions but also for its fundamental importance in, for example, the study of complexing reactions, estimation of molecular weights by thermodynamic methods, and interpretation of reaction rate data. In addition, as heats of mixing become available, knowledge of the free energies of mixing permit the calculation of entropies of mixing.

Our program to investigate the free energies of multicomponent electrolyte solutions has developed along three main lines during the past year: (1) a reevaluation of the activity coefficients from literature isopiestic data in the system NaCl-KCl-H_2O, (2) measurement of the osmotic and activity coefficients for binary mixtures of NaCl, Na_2SO_4, $MgSO_4$, and $MgCl_2$ in water, and (3) measurements of the osmotic coefficients in mixed perchlorate solutions.

A Reevaluation of the Activity Coefficients in the System NaCl-KCl-H_2O

Osmotic coefficients for the system NaCl-KCl-H_2O were measured by the isopiestic method several years ago by Robinson.[18] In this paper the activity coefficients for the components were calculated by the McKay-Perring method.[19] It seemed desirable to reevaluate the activity coefficients in this system by the method of Scatchard,[20] which we use in the interpretation of our own results. The details of our use of the Scatchard method

[15]Present address: National Bureau of Standards, Washington, D.C.

[16]Consultant; Professor of Physical Chemistry, Emeritus, Massachusetts Institute of Technology, Cambridge, Mass.

[17]Consultant; Washington, D.C.

[18]R. A. Robinson, *J. Phys. Chem.* 65, 662 (1961).

[19]H. A. C. McKay and J. K. Perring, *Trans. Faraday Soc.* 49, 163 (1953).

[20]G. Scatchard, *J. Am. Chem. Soc.* 83, 2636 (1961).

have been described in a previous annual report[21] and in a recent publication.[22]

The equations for the activity coefficients derived from the data of Robinson[18] by the Scatchard method are as follows:

$$\log (\gamma_{\pm A}/\gamma^{\circ}_{\pm A}) = (-0.02741m + 0.006160m^2 - 0.002158m^3 + 0.0001993m^4)y_B + 0.000325m^2y_B^2 , \quad (1)$$

$$\log (\gamma_{\pm B}/\gamma^{\circ}_{\pm B}) = (0.01642m - 0.007459m^2 + 0.002158m^3 - 0.0001993m^4)y_A + 0.000325m^2y_A^2 , \quad (2)$$

where $\gamma_{\pm A}$ and $\gamma_{\pm B}$ are the activity coefficients of NaCl and KCl, respectively, in the mixture, $\gamma^{\circ}_{\pm A}$ and $\gamma^{\circ}_{\pm B}$ are the activity coefficients of the pure salt solutions, m is the concentration in moles per kilogram of water, and y is the ionic strength fraction.

The maximum difference between results by the two computational methods in the region 1 to 5 m was 0.0025 in $\log \gamma_{\pm}$, corresponding to a difference of 0.6% in $\gamma_{\pm}$; the average difference for values calculated at $m = 1$, 3, and 5 was 0.0007 in $\log \gamma_{\pm}$. These results indicate clearly that for this system the McKay-Perring and the Scatchard methods give essentially the same results. A report of this investigation has been published.[23]

Osmotic and Activity Coefficients of Binary Mixtures of NaCl, Na_2SO_4, $MgSO_4$, and $MgCl_2$ in Water at 25°C[24]

The ORNL Water Research Program has been engaged in measurements of free energies of multicomponent aqueous solutions containing ions frequently found in natural waters. A variety of techniques have been used, including emf measurements with cation-sensitive electrodes. We have diverted part of our effort to this study. This also afforded an opportunity to check results obtained with a cation-sensitive glass electrode with those obtained by the isopiestic method.

Isopiestic measurements were made on the six binary mixtures of NaCl, Na_2SO_4, $MgSO_4$, and $MgCl_2$ in water at 25°C. The concentration range covered was $I = 1$ to 6 (I is the ionic strength on the molality scale); where solubilities permitted the study was extended to higher concentrations. The isopiestic procedure and equipment have been described previously.[25] In addition, emf measurements were made on NaCl-$MgSO_4$ mixtures with a cation-sensitive glass electrode and a silver–silver chloride electrode without junction. The emf procedure and equipment were essentially those described by Lanier.[26]

A partial summary of the results obtained is given in Figs. 6.8 and 6.9. In these figures the osmotic coefficient ϕ is given as a function of the ionic strength fraction y at $I = 3$. The solid lines represent calculated values using the Scatchard equation with coefficients derived from the experimental data by the method of least squares. This same equation permits the estimation of osmotic coefficients from data on the limiting single-electrolyte solutions without involving data on the mixtures. Such estimates are shown as dashed lines in the figures. (These dashed curves are straight lines only if both salts are of the same charge type.) The maximum deviation of the estimated from the observed values of ϕ at this concentration is 4%.

For two of the mixtures included in our study, NaCl-Na_2SO_4 and NaCl-$MgCl_2$, Lanier[26] has reported values of $\log \gamma_{\pm}$ for NaCl measured with a cation-sensitive glass electrode. The maximum difference between values of $\log \gamma_{\pm}$ for NaCl measured with the glass electrode and values calculated from the isopiestic results is 0.03 for NaCl-Na_2SO_4 and 0.01 for NaCl-$MgCl_2$, both at $I = 6$. These differences correspond to 3 and 1 mv, respectively, and are considerably smaller at lower concentrations. For NaCl-$MgSO_4$ mixtures there is a max-

[21] R. M. Rush and J. S. Johnson, *Chem. Div. Ann. Progr. Rept. May 20, 1967*, ORNL-4164, p. 64.

[22] R. M. Rush and J. S. Johnson, *J. Phys. Chem.* 72, 767 (1968).

[23] R. M. Rush and R. A. Robinson, *J. Tenn. Acad. Sci.* 43, 22 (1968).

[24] Research jointly sponsored by the Office of Saline Water, U.S. Department of the Interior, and U.S. Atomic Energy Commission under contract with Union Carbide Corporation.

[25] R. M. Rush and J. S. Johnson, *J. Chem. Eng. Data* 11, 590 (1966).

[26] R. D. Lanier, *J. Phys. Chem.* 69, 2697, 3992 (1965).

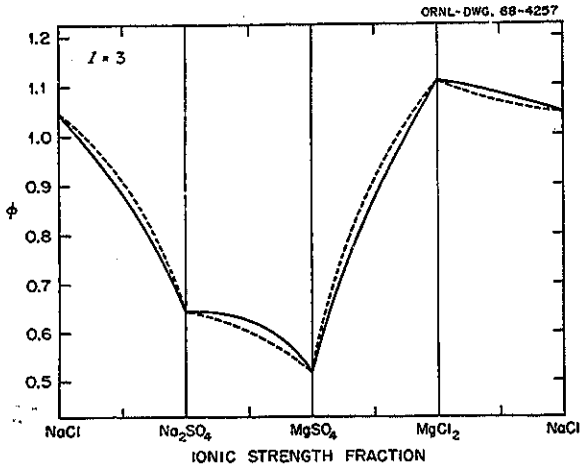

Fig. 6.8. Osmotic Coefficients for Mixtures; NaCl-Na_2SO_4, Na_2SO_4-$MgSO_4$, $MgSO_4$-$MgCl_2$, and $MgCl_2$-NaCl. Solid lines calculated from isopiestic results; dashed lines estimated from two-component data.

imum difference of 0.02 in log $\gamma_{\pm}$ for NaCl at $I = 6$ between our isopiestic results and both our emf measurements and unpublished emf measurements of Lanier. It thus appears that there is satisfactory agreement between the glass electrode results and those obtained by the isopiestic method, although the maximum differences are somewhat beyond experimental precision.

For NaCl-Na_2SO_4 mixtures, there are independent measurements of the activity coefficients of both components by emf measurements. These results are shown in Fig. 6.10. As before, the solid lines are values calculated from the isopiestic results with the Scatchard equations, and the dashed lines are estimates from the limiting single-electrolyte data. The data of Lanier are those referred to above. The results of Butler for the activity coefficients of NaCl were obtained with a sodium amalgam vs silver–silver chloride electrode system;[27]

[27] J. N. Butler, P. T. Hsu, and J. C. Synnott, *J. Phys. Chem.* 71, 910 (1967).

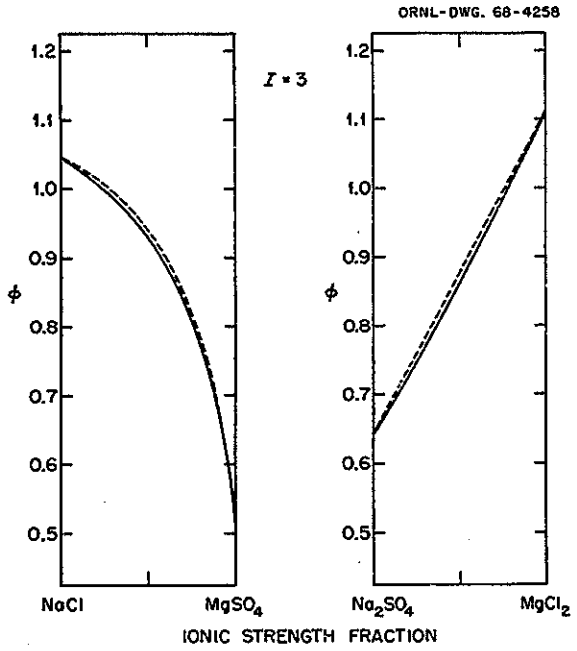

Fig. 6.9. Osmotic Coefficients for Mixtures; NaCl-$MgSO_4$ and Na_2SO_4-$MgCl_2$. Solid lines calculated from isopiestic results; dashed lines estimated from two-component data.

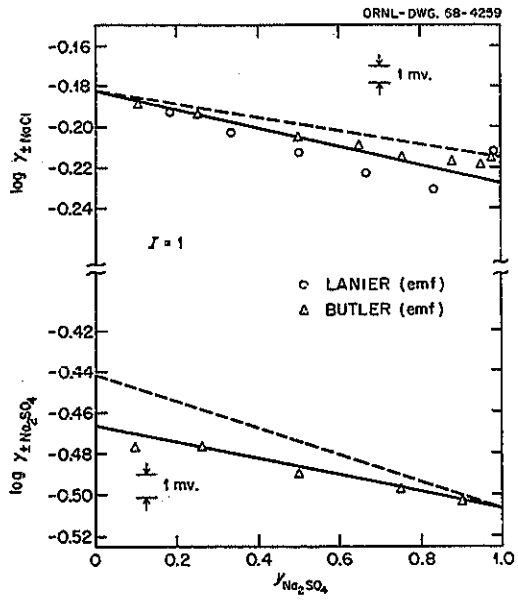

Fig. 6.10. Activity Coefficients in NaCl-Na_2SO_4 Mixtures. Solid lines calculated from isopiestic results; dashed lines estimated from two-component data. Experimental points obtained from Lanier, ref. 26, and Butler, refs. 27 and 28.

for the activity coefficients of Na_2SO_4 a lead amalgam–lead sulfate vs sodium-sensitive glass electrode system was used.[28] For these mixtures we thus have a satisfactory independent check on the activity coefficients of both components.

The excess free energy of mixing can also be calculated using the Scatchard equations and the coefficients obtained from the isopiestic results. The mixtures in our study consisted of the four pairs with common ions and the two pairs without common ions possible with the four solutes NaCl, Na_2SO_4, $MgSO_4$, and $MgCl_2$. It is thus possible to evaluate for the free energies of mixing the cross-square rule proposed by Young[29] for the heats of mixing of 1-1 electrolyte pairs. This rule states that for the heats of mixing of equal amounts of 1-1 electrolytes in solution, the sum of the heats for the mixtures with common ions is equal to the sum of the heats of the mixtures without common ions. This rule was also observed by Wood to be valid for mixtures of 2-1 electrolytes.[30]

The results of such calculations for the excess free energies of mixing at $I = 2$ are shown in Fig. 6.11. They indicate that the cross-square relationship is valid for the free energies of mixing for these electrolytes. As far as we know, there has been no published verification of this rule for the free energies of mixing. Our study is also unique in that it involves mixtures of electrolytes of different valence types.

ORNL-DWG. 68-4798

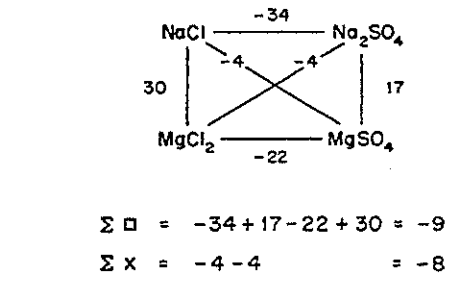

Fig. 6.11. Free Energy Relationships in Binary Mixtures of NaCl, Na_2SO_4, $MgSO_4$, and $MgCl_2$ in Water. Values calculated from isopiestic results.

Osmotic Coefficients of Mixed Perchlorate Solutions

The study of 1-1 perchlorate mixtures reported in the previous annual report[21] has been completed and a paper published describing the results.[22] Work is in progress on $HClO_4$-$UO_2(ClO_4)_2$ mixtures and will be extended to include $NaClO_4$-$UO_2(ClO_4)_2$, $HClO_4$-$Ba(ClO_4)_2$, and $NaClO_4$-$Ba(ClO_4)_2$ mixtures. These perchlorate salts of divalent cations were selected because the osmotic coefficients of $UO_2(ClO_4)_2$ are very high in concentrated solutions, and those of $Ba(ClO_4)_2$ are low, in comparison with other members of this valence type.

[28] J. N. Butler, Tyco Laboratories, personal communication, 1968.

[29] T. F. Young, Y. C. Wu, and A. A. Krawetz, *Discussions Faraday Soc.* 24, 37, 77, 80 (1957).

[30] R. H. Wood and H. L. Anderson, *J. Phys. Chem.* 70, 992 (1966).

PHYSICAL CHEMISTRY OF POLYELECTROLYTE SYSTEMS

Aqueous Electrolyte Solutions: The Thermodynamics of Mixed Chloride-Nitrate Systems

J. Padova

Activity coefficients of potassium chloride in aqueous mixtures of potassium nitrate were estimated from measurements at 25°C in the ionic strength interval 0.2 to 3.0 *m* with a cell consisting of a cation-sensitive glass electrode vs silver–silver chloride electrode. The measuring circuit, which has been described,[31] consists of a vibrating reed electrometer in conjunction with a Leeds and Northrup K-3 potentiometer for the emf determinations. The only change made was the use of a silver–silver chloride reference electrode prepared from optical silver chloride crystals.[32] This electrode was stable over long periods even when subjected to frequent changes from one dilute chloride solution to another.

Activity coefficients derived from the cell measurements were in good agreement with those calculated from gravimetric isopiestic measurements

[31] R. D. Lanier, *J. Phys. Chem.* 69(11), 3992 (1965).

[32] J. Greyson, *J. Electrochem. Soc.* 109, 745 (1962).

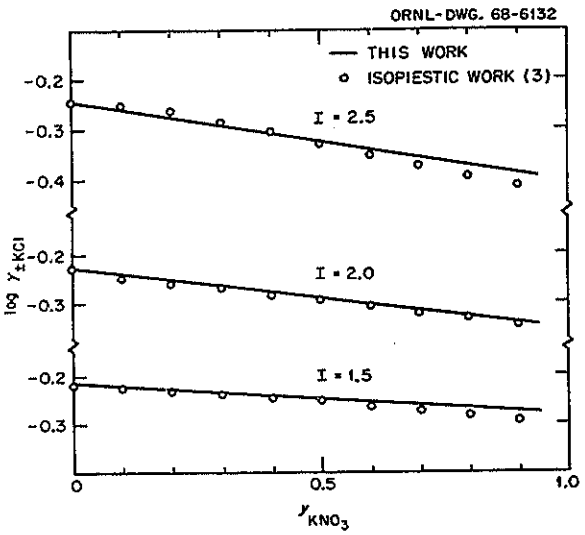

Fig. 6.12. Activity Coefficients of KCl in KCl-KNO_3 Aqueous Mixtures.

carried out on the same system[33] (see Fig. 6.12). Harned's rule[34] applied within experimental error to the activity coefficients of KCl, whereas two parameters were needed to represent the activity coefficients of KNO_3. The method of Rush and Johnson[35] based on the procedure suggested by Scatchard[36] was applied to the analysis of the osmotic coefficients for the KCl-KNO_3 mixtures. The equation for Φ of a three-component mixture is[35]

$$\Phi = 1 + \frac{I}{\nu_A m_A + \nu_B m_B}\left[\alpha_A + (\alpha_A - \alpha_B)y_B + \beta_{AB}^{(o)} y_B(1 - y_B) + \beta_{AB}^{(1)} y_B(1 - y_B)(1 - 2y_B)\right], \quad (1)$$

where α_j is determined from two-component data, y_j is the ionic strength fraction, and $\beta_{jk}^{(I)}$ are functions of I, the ionic strength, determined by the least-squares fitting of expression (1) to the experimental osmotic coefficient of the three-component solution. The agreement between values calculated by the above method and experimental values for the osmotic coefficients was not satisfactory; only about 80% of the data were within ±0.005 (see Fig. 6.13). The standard deviation of the fit to Eq. (1) was 0.0048, compared with 0.0005 for NaCl-KCl mixtures.[37]

Similar computations were applied to the systems LiCl-$LiNO_3$ (standard deviation = 0.005)[38] and NaCl-$NaNO_3$ (standard deviation = 0.005).[39] The applicability of the Scatchard method for the estimation of activity coefficients in mixtures of alkali-metal chlorides with nitrate seems to be less successful than for mixtures of alkali-metal chlorides. A different approach is being elaborated.

Thermodynamics of the Sodium Polystyrenesulfonate–Sodium Chloride System

J. Padova

Studies of the interactions between polyelectrolytes and simple electrolytes in aqueous solution may be useful in understanding and explaining the various properties of ion exchange reactions.[40] Polystyrenesulfonate, which forms the "backbone" of strong-acid-type cation exchangers, has been chosen for this study.

The effect of the molecular weight of the polystyrenesulfonate on colligative properties was investigated with the gravimetric isopiestic method. Problems met with in the analytical determination of the equivalent weight of the polymer were overcome, and a reliable method utilizing lightly cross-linked strong-acid cation exchangers was elaborated and checked by flame photometry measurements. Preliminary experiments indicated a significant dependence of the osmotic coefficient, ϕ, on the molecular weight, $\bar{M}_w$, of the polyelectrolyte; ϕ increased with concentration and with molecular weight (Fig. 6.14) in agreement with observations

[33] S. Amdur, J. Padova, and A. Schwarz, to be published; preliminary communication, *Israel J. Chem.* 5(4a), 23 (1967).

[34] H. S. Harned and B. B. Owen, *The Physical Chemistry of Electrolyte Solutions*, chap. 14, ACS Monograph Ser., 3d ed., Reinhold, New York, 1958.

[35] R. M. Rush and J. S. Johnson, *J. Phys. Chem.* 72, 767 (1968).

[36] G. Scatchard, *J. Am. Chem. Soc.* 83, 2636 (1961).

[37] R. M. Rush, private communication.

[38] R. A. Robinson and C. K. Lim, *Trans. Faraday Soc.* 49, 1144 (1953).

[39] A. N. Kirgintsev and A. V. Lukyanov, *Russian J. Phys. Chem. (English Transl.)* 38, 867 (1964).

[40] G. E. Boyd, S. Lindenbaum, and G. E. Myers, *J. Phys. Chem.* 65, 577 (1961).

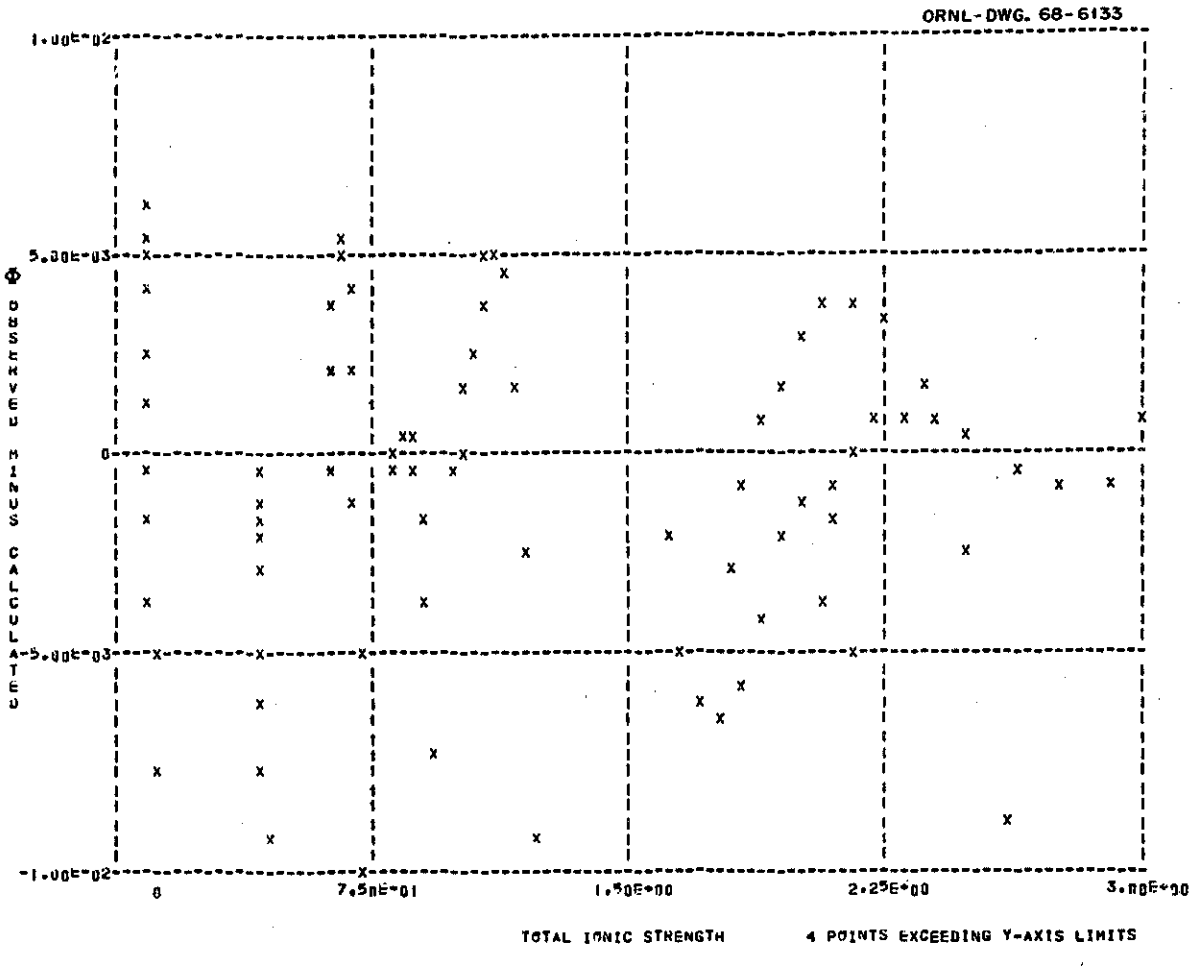

Fig. 6.13. Test of Fit of Experimental Values for Osmotic Coefficients for $KCl-KNO_3$ Aqueous Mixtures to Calculated Values.

by Bonner.[41] The molecular weight dependence had not been noticed before[42] because most of the measurements were carried out either at low concentrations or with only one molecular weight. The concentration effect has been noticed before,[41,43,44] and the molecular weight dependence may be confirmed by comparing the data obtained for different molecular weights by different investigators.[43,44]

The extrapolation of the data to infinite dilution gives a value of $\phi = 0.3$ as compared with Marinsky's value[43] of 0.22 for a sodium polystyrenesulfonate of molecular weight ca. 500,000. Earlier measurements of the osmotic coefficients of the sodium salt of a lightly cross-linked polystyrenesulfonate extrapolate to 0.4.[45]

[41] O. D. Bonner and J. R. Overton, *J. Phys. Chem.* 67, 1035 (1963).

[42] J. A. Marinsky, *Ion Exchange*, chap. 9, Marcel Dekker, New York, 1966.

[43] P. Chu and J. A. Marinsky, *J. Phys. Chem.* 71, 4352 (1967).

[44] N. Ise and T. Okubo, *J. Phys. Chem.* 72(4), 1361 (1968).

[45] G. E. Boyd and B. A. Soldano, *Z. Elektrochem.* 57, 162 (1953).

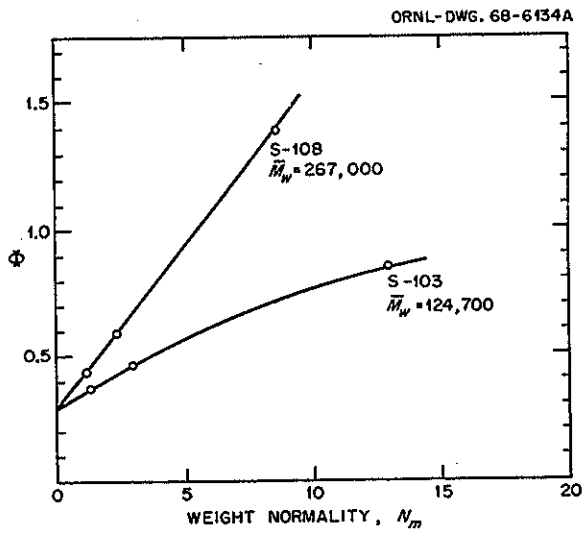

Fig. 6.14. Concentration Dependence of Osmotic Coefficients for Linear Sodium Polystyrenesulfonates in Aqueous Solutions at 25° (Szwarc Polymers).

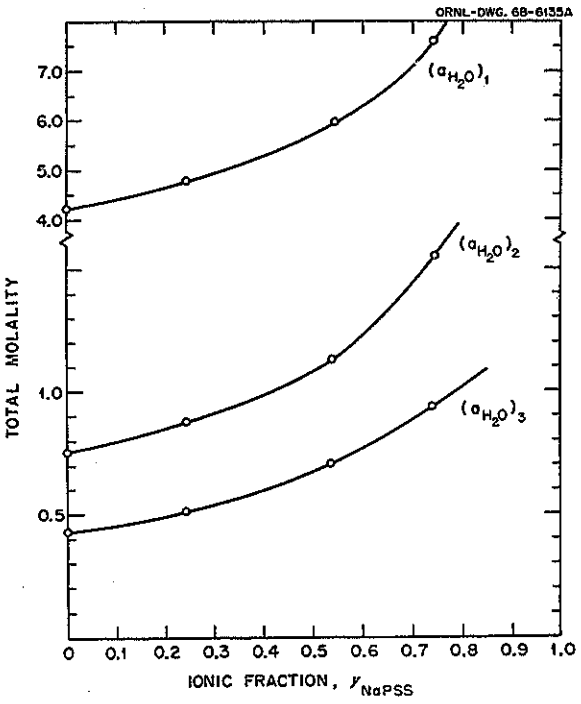

Fig. 6.15. Isopiestic Molalities of Sodium Polystyrenesulfonate (S-108)–Sodium Chloride–Water Mixtures at 25° at Various Water Activities, $(a_{H_2O})_1 < (a_{H_2O})_2 < (a_{H_2O})_3$.

Isopiestic vapor pressure comparisons are being conducted with the system sodium polystyrenesulfonate–sodium chloride at various ratios of salt to polyelectrolyte. The higher molecular weight polymer ($\bar{M}_w$ = 267,000) was chosen to minimize "end effects" on the osmotic coefficient. The data obtained thus far indicate that the polymer-salt mixture behaves like an ordinary mixture of simple electrolytes (Fig. 6.15).

A glass electrode vs silver–silver chloride electrode cell will be used to measure the activity coefficients of sodium chloride in the system. These measurements together with measurements of the osmotic coefficient obtained by the isopiestic method should give an unambiguous definition of what is meant by the "polyelectrolyte activity coefficient." The so-called additivity rule,[46] whereby the osmotic pressure π of a mixture of a polyelectrolyte and an electrolyte is assumed to be given by

$$\pi = \pi_p + \pi_s ,$$

where π_p represents the osmotic pressure of the salt-free polyelectrolyte solution and π_s the osmotic pressure of the polyelectrolyte-free salt solution, will be checked. It has been implied[47] that "additivity" does not hold for accurate measurements.

[46] A. Katchalsky and Z. Alexandrowicz, *J. Polymer Sci.* A1, 2093 (1963).

The Free Energy of a Polyelectrolyte at Infinite Dilution

J. Padova

The thermodynamic treatment of a fluid in an electrostatic field has been shown[48–50] to apply to the calculation of various properties of solutions of electrolytes. The gain in the free energy of the

[47] A. Katchalsky, Z. Alexandrowicz, and O. Kedem, in *Chemical Physics of Ionic Solutions*, ed. by B. E. Conway and R. G. Barradas, Wiley, New York, 1966.

[48] J. Padova, *J. Chem. Phys.* 39, 1552 (1963).

[49] J. Padova, *Electrochim. Acta* 12, 1227 (1967).

[50] J. Padova, *J. Phys. Chem.* 72, 796 (1968).

fluid due to the electrostatic field is given by the expression

$$\Delta G = (1/4\pi) \iint \overline{E}\, d\overline{D}\, dv \ , \qquad (1)$$

where $\overline{E}$ and $\overline{D}$ are the electric field and electric displacement vectors and dv is the elementary volume.

For an isotropic fluid, expression (1) may be written

$$\Delta G = (1/8\pi) \iint E_d\, d(E^2)\, dv \ , \qquad (2)$$

where E_d is the differential dielectric constant of the solvent. This expression may be used in the calculation of the free energy of a polyelectrolyte at infinite dilution and takes into account the dependence of the dielectric constant of the fluid on the electrostatic field due to the polyelectrolyte. Two models were considered:

1. the spherical model corresponding to the coiled microion, which is only slightly dissociated by definition;
2. the cylindrical model corresponding to the linear polyelectrolyte that may be more or less dissociated.

The electric field dependence of the differential dielectric constant E_d is given by Grahame's expression[51]

$$E_d = n^2 + (E_0 - n^2)/(1 + bE^2) \ ,$$

where n and E_0 are the refractive index and static dielectric constant of the solvent, respectively, b is a constant equal to 1.1×10^{-8} (esu)$^{-2}$, and E is the electrostatic field strength. The relation between E and r is obtained[48] through the relation

$$E_d = dD/dE \ ,$$

where

$$D = n^2E + [(E_0 - n^2)/b^{1/2}] \tan^{-1} (b^{1/2}E) \ , \qquad (3)$$

which for a spherical model gives

$$n^2E + [(E_0 - n^2)/b^{1/2}] \tan^{-1} (b^{1/2}E) = \alpha Ne/r^2 = e/\rho^2 \ , \qquad (4)$$

and for a cylindrical model gives

$$n^2E + [(E_0 - n^2)/b^{1/2}] \tan^{-1} (b^{1/2}E) = \alpha e/\lambda r = e/\rho \ . \qquad (5)$$

The integration of expression (2) is carried out numerically using relations (4) and (5) as a function of the "reduced radius" ρ. In the first case

$$\rho = r/\sqrt{\alpha N} \ ,$$

where α is the fraction dissociated, N the polymerization number of the polyelectrolyte, and r the distance from the spherical charge center. In the second case

$$\rho = \lambda r/\alpha \ ,$$

where α is the dissociation fraction, λ is the distance between two consecutive charges, and r is the distance from the central axis of the cylinder.

From the graph of E_d vs ρ (Fig. 6.16) we may learn as a function of the defined parameter the regions wherein dielectric saturation occurs causing volume exclusion and, from Fig. 6.17, the free energy in the reference state for a desired model of polyelectrolyte.

The electrostriction caused by the polyelectrolyte will be calculated according to an earlier method,[48]

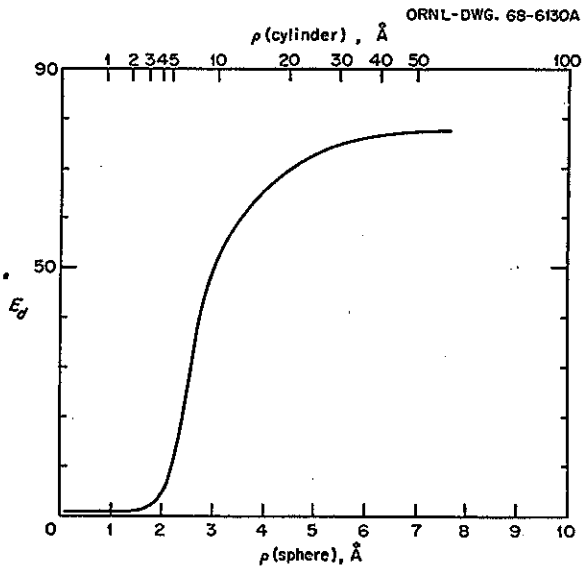

Fig. 6.16. The Differential Dielectric Constant E_d vs the Reduced Radius ρ.

[51] D. C. Grahame, *J. Chem. Phys.* **21**, 1054 (1953).

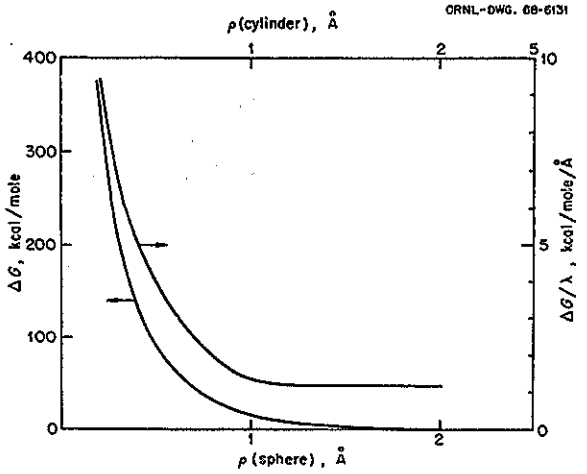

Fig. 6.17. The Electrostatic Part of the Increase in Free Energy ΔG vs the Reduced Radius ρ.

and the dimension of a specific polyelectrolyte will be determined by the relation between electrostriction and apparent molal volume.

The interactions between a dielectric saturated polyion and small electrolyte will be investigated as a function of the concentration of both components.

Thermodynamic Quantities in the Exchange of Zinc with Sodium Ions in Variously Cross-Linked Polystyrenesulfonate Cation Exchangers at 25°

G. E. Boyd F. Vaslow
S. Lindenbaum

Standard free energy, $\Delta G°$, and enthalpy, $\Delta H°$, changes for the reaction of zinc ion in dilute aqueous solutions with sodium ion in cross-linked polystyrenesulfonic acid type cation exchangers were estimated from equilibrium ionic distribution and heat of exchange measurements at 25°. The selective uptake of Zn^{2+} ion was accompanied by the absorption of heat and by an increase in the standard entropy, $\Delta S°$. A maximum in $\Delta G°$ with increasing exchanger cross-linking was observed with the exchanger containing approximately 8% divinylbenzene, in contrast to $\Delta H°$ and $\Delta S°$, which increased progressively with cross-linking. The difference in the entropies of hydration of zinc and sodium ions appeared to be a major factor in determining $\Delta S°$, which in turn governed the selective uptake of the former ion. [Abstract of published paper: *J. Phys. Chem.* **71**, 2214 (1967).]

Thermodynamic Properties at 25° of Aqueous Solutions of *p*-Ethylbenzenesulfonic Acid and Its Alkali Metal Salts. Comparisons with Cross-Linked Polystyrenesulfonate Type Cation Exchangers

G. E. Boyd A. Schwarz[52]
F. Vaslow J. W. Chase[53]

Molal osmotic and mean molal activity coefficients, ϕ and γ, and apparent molal heat contents, ϕ_L, of aqueous solutions of *p*-ethylbenzenesulfonic acid (*p*-EBSA) and its alkali metal salts were determined at 25° for a wide range of concentrations. The strength of the acid was inferred to be less than that of HNO_3, and evidence was obtained for ion-pair formation with the cesium salt. The concentration dependence of ϕ_L was unusual in that values above the Debye-Hückel limiting slope were observed with all but cesium *p*-EBS. Calculations of solvent relative partial molal entropies, $S_1 - S_1^\circ$, indicated that the *p*-ethylbenzenesulfonate anion possessed "water structure forming" properties. Free energies of dilution, ΔG_D (computed from ϕ and γ for the alkali metal salts and free acid), and the differences between these were compared with the standard free energy changes, $\Delta G°_{ex}$, for ion exchange reactions between the alkali metal cations and hydrogen ion in cross-linked polystyrenesulfonic acid type cation exchangers. Differences in ϕ_L were also compared with standard heats of cation exchange, $\Delta H°_{ex}$. The concordance between the various thermodynamic quantities indicated that the analogy between concentrated electrolyte mixtures and cation exchangers was valid. [Abstract of published paper: *J. Phys. Chem.* **71**, 3879 (1967).]

[52]Deceased; formerly of the Soreq Nuclear Research Center, Yavne, Israel.

[53]Present address: Eastman Kodak Co., Rochester, N.Y.

The Binding of Quaternary Ammonium Ions by Polystyrenesulfonic Acid Type Cation Exchangers

G. E. Boyd Q. V. Larson

A thermodynamic study was made of the binding of quaternary *n*-alkylammonium ions by cross-linked polystyrenesulfonic acid type cation exchangers. Calorimetric measurements of the exchange reactions with sodium ion at 25° showed that the enthalpy and entropy changes were negative for the preferential binding of tetramethyl- and tetraethylammonium ions by lightly cross-linked sodium-form exchanger, but, with tetra-*n*-propyl- and tetra-*n*-butylammonium ions, heat was absorbed and the entropy increased markedly. The increase in the preferential uptake with the size of the tetra-*n*-alkylammonium ion therefore was determined by the entropy increase in the exchange reaction (i.e., hydrophobic bonding). The selective uptake of Me_4N^+ ion decreased with increasing exchanger cross-linking, and with nominal 8% DVB exchanger the Na^+ ion was preferred for all compositions. The heat of exchange became progressively less negative, and with the most highly cross-linked preparation heat was absorbed when Me_4N^+ replaced the Na^+ ion, but the entropy change remained constant. The decrease in the binding of Me_4N^+ ion with increased cross-linking was attributed to the increase in enthalpy of the molecular network of the ion exchanger when it expanded to accommodate the large organic cation. A comparison of the enthalpy with the free energy of swelling showed that the entropy also increased, which is contradictory to the hypothesis that ion exchangers are rubber-like gels. The more highly cross-linked polystyrenesulfonate exchangers behaved as if they were in a glasslike state (i.e., a rubber below its gel point). [Abstract of published paper: *J. Am. Chem. Soc.* 89, 6038 (1967).]

Thermal Effects in Ion Exchange Reactions: Heats of Ion Exchange

G. E. Boyd

Heat may be evolved or absorbed in a variety of reactions exhibited by ion exchangers: in the interchange of ions with those in aqueous or nonaqueous media, in the solvation of solvent-free exchangers, in swelling and deswelling, and in acid-base neutralization. Thermal effects accompanying reactions involving ions find practical application in analytical and preparative ion exchange chromatography. Quantitative values for heats of ion exchange are essential to an understanding of the separations principles governing many areas of application and research, as, for example, in the saline water problem, in chemical process waste treatment and water pollution, in the transport of ions in living cells and in soils, and in numerous separations in the chemical and pharmaceutical industries.

Heats of ion exchange are small, and sensitive calorimetric methods are needed for their measurement. With synthetic organic ion exchangers the heat effects are dependent: (1) on the electronic and molecular structure of the exchanging ion and on its charge in solution; (2) on the nature of the ionogenic group of the exchanger and on the cross-linking of the latter. Moreover, the heat of exchange itself may be temperature dependent.

A concise summary of the findings from calorimetric studies at ORNL is presented. (Abstract of paper published in *Analytical Calorimetry*, Plenum, New York, 1968.)

Heat Capacity Changes in Ion Exchange Reactions: The Exchange of Tetra-*n*-butylammonium with Sodium Ion in Cross-Linked Polystyrenesulfonate

G. E. Boyd Q. V. Larson
Siegfried Lindenbaum

Calorimetric measurements of the temperature dependence of the standard enthalpy of ion exchange, ΔH°, were performed for the reaction in dilute aqueous solution of tetra-*n*-butylammonium with sodium ion in lightly cross-linked sulfonated polystyrene type cation exchanger. Between 15 and 35°C the value of ΔH° *decreased* from 2.39 to 1.38 kcal per equivalent, corresponding to an average standard heat capacity change of $\Delta C_p^\circ = -53 \pm 9$ cal per equivalent per degree. The sign and magnitude of ΔC_p° are consistent with the hypothesis that large, singly charged organic cations such as the tetra-*n*-alkylammonium ions in aqueous solution produce an extensive ordering of the water structure in their vicinity. The prediction of ΔC_p° values for the exchange reactions in dilute solutions of singly charged cations (and anions) with one another is discussed. [Abstract of published paper: *J. Phys. Chem.* 72, 2651 (1968).]

Osmotic Coefficients of Aqueous Solutions of Tri-*n*-alkylsulfonium Halides at 25°

Siegfried Lindenbaum

Osmotic coefficients measured by the gravimetric isopiestic vapor pressure equilibration method are reported for trimethyl- and tri-*n*-butylsulfonium chloride and bromide and for trimethyl-, tri-*n*-propyl-, and tri-*n*-butylsulfonium iodide. These results are compared with previously reported data on tetraalkylammonium salts. The osmotic coefficients for the sulfonium salts are in general lower than those for the corresponding ammonium salt; however, the relative order and the shape of the osmotic coefficient vs concentration curves are remarkably similar. This comparison confirms the suggestion that the solution properties of these cations are largely dominated by the nature and length of the hydrocarbon substituents on the central sulfur or nitrogen atom. The suggestions previously put forward to account for the behavior of the quaternary ammonium salts, that is, water structure promotion, water structure enforced ion pairing, and micelle formation, are examined and compared in the light of the free energy behavior of the aqueous sulfonium salt solutions. [Abstract of published paper: *J. Phys. Chem.* **72**, 212 (1968).]

The Heat of Fusion of Tetra-*n*-alkylammonium Fluoride – Clathrate Hydrate

Siegfried Lindenbaum

Solutions of tetra-*n*-butylammonium fluoride have many unusual properties. They have extremely high values for the activity coefficients and heats of dilution. Clathrate hydrates readily crystallize from solutions of tetra-*n*-butylammonium fluoride, whose structure has been compared with that of aqueous solutions containing structure-promoting ions such as tetraalkylammonium ions.[54] It was of interest, therefore, to measure the heat of fusion of this hydrate. Since the hydrate melt is stable at room temperature, it was possible to measure the heat of solution of the crystalline hydrate and the hydrate melt and thus obtain the heat of fusion by difference.

A solution of tetrabutylammonium fluoride was prepared by neutralizing a solution of Bu_4NOH with HF. Purity was established by analyzing for Bu_4N^+ by the precipitation and weighing of the tetraphenylboride. The composition was adjusted to $Bu_4NF\cdot 41H_2O$, and this solution was used for the x-ray scattering experiments described elsewhere in this report.[55] Clathrate hydrate crystals of composition $Bu_4NF\cdot 30.22H_2O$ were crystallized from this solution. The heat of solution of the crystalline hydrate ΔH_s° is 40,765 ± 15 cal/mole, and the heat of solution of the melt ΔH_s° is –6,357 ± 2 cal/mole, to give a heat of fusion of 47,122 cal per mole of $Bu_4NF\cdot 30.22H_2O$, or 1559 cal per mole of H_2O, at 25°C. This result is close to the value for the heat of fusion of ice at 25°C, 1638 cal/mole.

The Heat of Dilution of Tetra-*n*-butylammonium Chloride

Siegfried Lindenbaum

Apparent and partial molal volume studies of tetra-*n*-alkylammonium halides in aqueous solution[56] have revealed that, for some of these salts, these quantities when plotted against the molality show a minimum at about 1.6 *m*. This is approximately the composition of the clathrate hydrate formed by the tetra-*n*-butylammonium halides, $(n\text{-}C_4H_9)_4NX\cdot 32.8H_2O$. It has been suggested in view of the minimum in the partial molal volume curves[56] that there may be a relationship between the structure of the solid hydrate and the aqueous solution. It was expected that in the vicinity of this concentration other physical properties also might be expected to show a marked change.[57] Previous measurements of the heats of dilution[58] of tetra-*n*-alkylammonium chloride were not sufficiently detailed or accurate to determine whether an inflection occurred in the vicinity of the clathrate composition in a plot of the apparent molal heat content, ϕ_L, vs concentration. It was the purpose of this work to measure ϕ_L very accu-

[54] H. S. Frank and W-Y Wen, *Discussions Faraday Soc.* 24, 133 (1957).

[55] A. H. Narten, "X-Ray Diffraction Studies of Liquids," this report.

[56] W. Y. Wen and S. Saito, *J. Phys. Chem.* 68, 2639 (1964).

[57] W. Y. Wen, private communications.

[58] S. Lindenbaum, *J. Phys. Chem.* 70, 814 (1966).

rately at small intervals (every 0.2 m) of concentration from 0.0 to 2.6 m. The calorimeter was essentially similar to that described previously[58] with some minor modifications to improve accuracy and sensitivity. Heats of dilution were reproducible to 0.2% or 3 cal/mole, whichever is larger. The data (Table 6.1) were accurately represented by the following cubic equation obtained by the method of least squares using the data from 0.5 to 2.6 m:

$$\phi_L = -192.106 + 2374.9m + 425.472m^2 - 153.385\,m^3 \; ; \quad (1)$$

standard deviation of fit, $\sigma = 10.2$. No inflections or other anomalies are discernible in the region of interest.

Table 6.1. Apparent Molal Heat Content of Tetra-*n*-butylammonium Chloride Solutions at 25°

m	ϕ_L (cal/mole)	m	ϕ_L (cal/mole)
0.10006	201	1.3651	3444
	202		3454
0.20111	395	1.5064	3835
	389		3832
			3837
0.2982	614	1.7070	4340
	614		4344
0.4007	854	1.8071	4585
	854		4599
0.5049	1102	1.9825	4995
	1110		5000
0.6964	1607	2.0466	5124
	1611		5123
			5139
0.9011	2175	2.2906	5628
	2172		5617
1.0251	2512	2.4788	5968
	2512		5970
1.2556	3171	2.6436	6232
	3165		6240

SALT-INDUCED STRUCTURE TRANSITIONS IN AQUEOUS SOLUTION

F. Vaslow

Measurements of the apparent molal volumes of the alkali halides have continued with the primary purpose of investigating the nature of abrupt changes in the slope of the apparent molal volume ϕ_v vs root concentration $\sqrt{c}$ curves found for some of the salts. The emphasis has been on obtaining extremely precise $\Delta\phi_v/\Delta\sqrt{c}$ curves rather than integral values, with the measurements of density being made to 0.2 ppm for all concentrations and measurements of increments of stock solution being made to about 10 ppm. The statistics of the final curves indicate that these values are realistic estimates of the average errors of measurement. Results obtained for the $\Delta\phi_v/\Delta\sqrt{c}$ curve of LiCl using the precise techniques confirm the existence of an abrupt slope transition suggested in the original paper,[59] and the new results have been published.[60]

The apparent molal volumes of LiBr and LiI are being studied, again with emphasis on precise $\Delta\phi_v/\Delta\sqrt{c}$ curves. For LiBr two runs in excellent agreement suggest that within the resolution of these experiments there may be a discontinuity in the $\Delta\phi_v/\Delta\sqrt{c}$ curve at $\sqrt{c} = 1.14$; around this point $\Delta\phi_v/\Delta\sqrt{c}$ drops abruptly from about 1.165 to 1.130.

Two runs with LiI gave results qualitatively similar to the LiBr curves except that the apparent discontinuity seemed to be much larger, and its position was different in the two runs ($\sqrt{c} = 1.12$ and 0.97).

If these curves are in fact discontinuous, they may represent behavior similar to λ-point transitions in crystals or in liquid helium. Such transitions are highly sensitive to impurities or other conditions, and variations in the transition point are not unreasonable. Different batches of LiI were used for the two runs, each containing small amounts of free iodine and alkali which are probably not the same in the two batches, so that differences might occur in a sensitive system.

The LiI results can be compared with the earlier results[61] for CaI_2 and SrI_2. While the points avail-

[59] F. Vaslow, *J. Phys. Chem.* **70**, 2286 (1966).

[60] F. Vaslow, *J. Phys. Chem.* **71**, 4585 (1967).

[61] A. Heydweiller, *Ann. Physik* [4] **30**, 873 (1909).

able are too few for detailed analyses, these curves show a precipitous drop in slope over a short concentration range generally similar to the effect in lithium salts but apparently much larger.

The existence of discontinuities in the properties of aqueous solutions has not been previously established, and such behavior could be considered highly unusual. While the results obtained here are consistent among themselves and with earlier work, they are nevertheless based on a very high precision of measurement, and only a few points of each curve determine the nature of the transition. Consequently, detailed study is necessary before it is clear that these very interesting results are not due to artifact or error.

HYPERFILTRATION WITH DYNAMICALLY FORMED MEMBRANES[62]

J. N. Baird[63]
W. H. Baldwin
J. Csurny
Neva Harrison
C. E. Higgins
J. S. Johnson
K. A. Kraus[64]
D. C. Michelson
J. W. Meyers[65]
J. J. Perona[66]
H. O. Phillips
S. B. Sachs[67]
H. C. Savage[65]
R. Shea[68]
A. J. Shor[65]
Warren Sisson[66]
Wm. T. Smith, Jr.[69]
G. Westmoreland

The separations process work of the Water Research Program continued to emphasize studies of hyperfiltration (reverse osmosis). Attention remained concentrated on salt-filtering properties of membranes dynamically formed on porous bodies from materials added to feed solutions. These salt-filtering films were exploited for basic studies of transport through membranes under pressure as driving force and were investigated for possible practical application in desalination and pollution control. Typical examples of studies under way during the year follow.

Concentration Dependence of Salt Rejection by an Ion Exchange Membrane

Preliminary attempts to correlate salt rejections by hydrous Zr(IV) oxide anion exchange membranes with ion-exclusion (Donnan) theory have been discussed.[70] Although experimental results were qualitatively in accord with predictions, quantitative differences were considerably outside experimental error. The importance of these studies in establishing a description of transport through ion exchange membranes led us to obtain more extensive experimental data (Fig. 6.18) and to try various assumptions concerning activity coefficients in the membrane phase in calculation of the distribution coefficient,

$$D^* = m^*/m \qquad (1)$$

[where m indicates concentration, the units being moles per kilogram of water for both the membrane (*) and aqueous phases], for comparison with rejection by the membrane.

For a test of theory, the effect of buildup of salt concentration at the membrane-feed interface on salt rejection,

$$R = 1 - m_\omega/m_\alpha , \qquad (2)$$

where subscript ω indicates the effluent or product solution and α the solution at the high-pressure membrane-feed solution interface, must be eliminated. Values of R were estimated from the observed rejections,

$$R_{obs} = 1 - m_\omega/m_f , \qquad (3)$$

where f indicates feed concentration, by an extrapolation to infinite feed circulation velocity, described in last year's report[70] and elsewhere.[71]

To obtain values of R which can be compared in a simple manner with values of D^* computed from ion-exclusion theory, it is further necessary that the flux through the membrane be sufficient to realize the limiting rejection R_∞. The pressures necessary for essential attainment of R_∞ were identified experimentally.

---

[62] Sponsored by the Office of Saline Water, U.S. Department of the Interior.

[63] General Engineering and Construction Division.

[64] Director's Division.

[65] Reactor Chemistry Division.

[66] Chemical Technology Division.

[67] Visiting Scientist from the Weizmann Institute, Israel.

[68] Co-op student from the University of Tennessee.

[69] Department of Chemistry, University of Tennessee.

[70] *Chem. Div. Ann. Progr. Rept. May 20, 1967*, ORNL-4164, p. 70.

[71] A. J. Shor, K. A. Kraus, J. S. Johnson, Jr., and W. T. Smith, Jr., *Ind. Eng. Chem. Fundamentals* 7, 44 (1967).

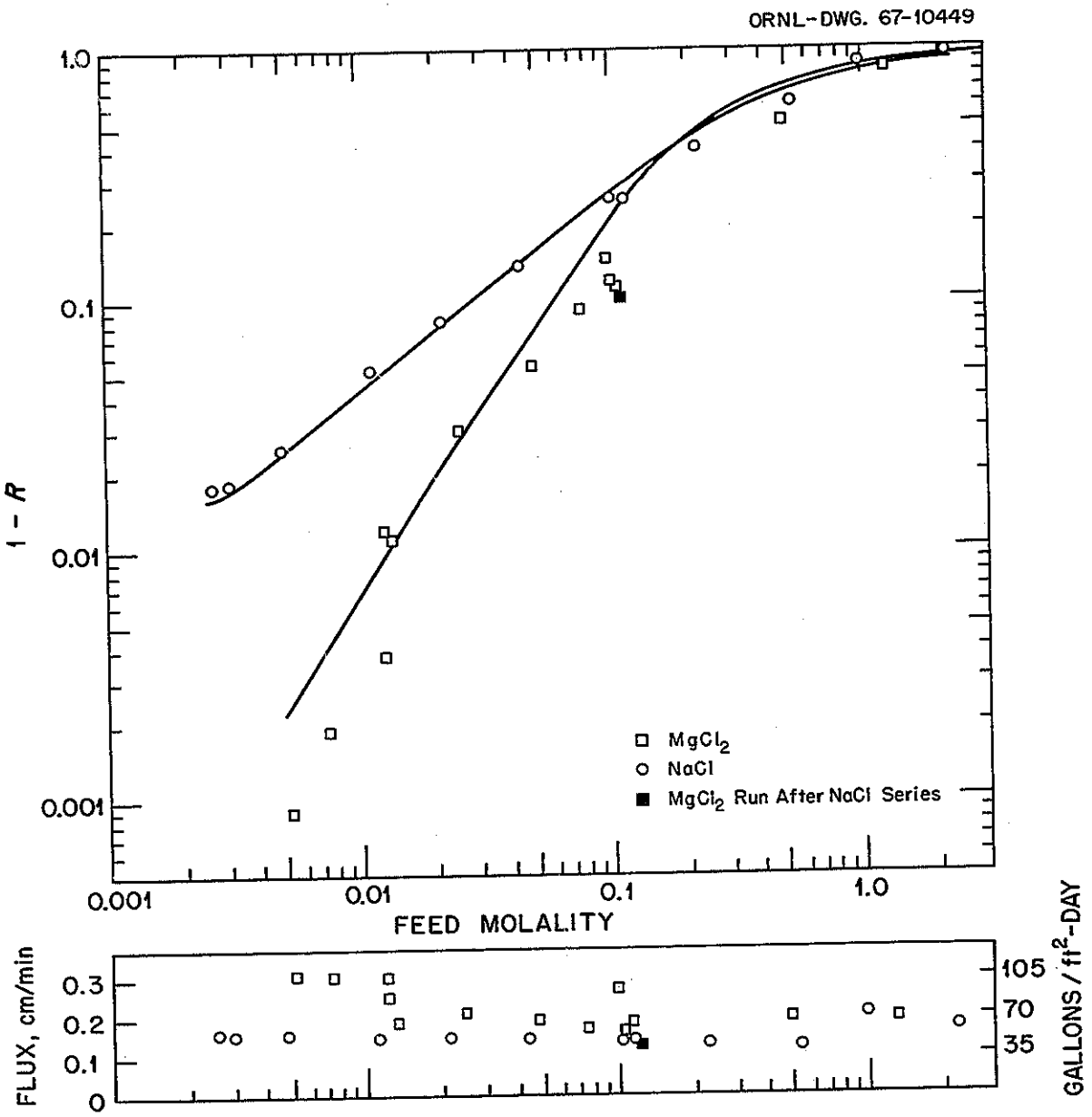

Fig. 6.18. Effect of Feed Concentration on the Rejection of a Hydrous Zr(IV) Oxide Membrane. Points, values extrapolated to infinite circulation velocity; curves, values calculated from ion exclusion model. Capacity $C^* = 0.45$ moles/kg H_2O. Porous carbon tube (4 A). Pressure, 800 psig.

The relation[72] between R_∞ and D^* is

$$R_\infty = 1 - \beta D_\alpha^* , \qquad (4)$$

where β is a coefficient describing coupling between solute and solvent flux. For neutral, low-water-content cellulose acetate membranes, whose transport properties have been extensively studied, $\beta = 0$ is a good first approximation, and one of our objectives was to find if β is different for the high-water-content ion exchange membrane used in this study.

If $R_\infty < 1$, β must by Eq. (4) be other than zero. Since our results show (Fig. 6.18) that R_∞ approaches zero at high feed concentration, unity appears to be the best approximation for β, and we shall assume $\beta = 1$.

If the same standard state is selected for both membrane and a two-component solution phase, the equation describing the equilibrium distribution for an electrolyte $MA_{\nu-1}$, A being a monovalent counterion (that ion having charge sign opposite to that of the fixed charge on the ion exchanger) is

$$\begin{aligned} m_M m_A^{(\nu-1)} \gamma_\pm^\nu &= (\nu-1)^{(\nu-1)} m^\nu \gamma_\pm^\nu \\ &= m_M^* m_A^{*(\nu-1)} \gamma_\pm^{*\nu} \\ &= m^*[C^* + (\nu-1)m^*]^{(\nu-1)} \gamma_\pm^{*\nu} , \end{aligned} \qquad (5)$$

C^* being ion exchange capacity in moles per kilogram of water in the ion exchange phase and $\gamma_\pm$ being the activity coefficient of $MA_{\nu-1}$. The coion molality m_M^* is the molality, m^*, of the "invading" electrolyte. The equation for the distribution coefficient follows from (5):

$$D^* \left[\frac{C^*}{(\nu-1)m} + D^* \right]^{\nu-1} \Gamma^\nu - 1 = 0 , \qquad (6)$$

where $\Gamma = \gamma_\pm^* / \gamma_\pm$. If Γ can be estimated, we can compute D^* as a function of solute concentration and valence type for a membrane of capacity C^* and compare computed values with salt rejection.

Independent measurement of C^* is difficult for dynamically formed membranes. The test of theory is therefore to see if, for reasonable assumptions concerning Γ, a single value of capacity will fit all results. We reported last year that neither assuming $\Gamma = 1$ nor taking into account only the known solution phase activity coefficient variations gave an adequate fit to our preliminary data; this was confirmed with our present results. It appears that activity coefficients in the membrane phase must be considered.

A reasonable assumption is that $\gamma_\pm^*$ has the same value at a given ionic strength as $\gamma_\pm$; the ionic strength in the membrane is taken to be

$$I^* = Sm^* + C^* , \qquad (7)$$

S being the factor relating ionic strength and molality, 1 for NaCl and 3 for $MgCl_2$. The capacity and counterions are considered to be a 1,1 electrolyte in Eq. (7).

With this assumption concerning Γ, we have selected by least-squares procedure a value of C^* giving the best fit to the NaCl rejection; using this value of C^* (0.45 equivalent per kilogram of water) rejections were computed for $MgCl_2$. Figure 6.18 gives the comparison between experimental and computed rejections. The fit is good for NaCl and reasonable for $MgCl_2$, especially in view of analytical difficulties with the dilute effluents at low $MgCl_2$ concentrations.

To summarize, rejections for NaCl over about a 1000-fold feed concentration range and from 98 to <10% rejection and for $MgCl_2$ over a 200-fold concentration range and rejections from >99% to ~15% can be correlated by ion-exclusion theory with a single adjustable parameter, the capacity. Self-consistency argues that the assumption of complete coupling of solvent and solute flow is basically correct.

Additives

The range of substances from which membranes (particularly in the ion exchange class) can be formed dynamically is large. There are many feeds, however, even though having the low concentrations for which ion exchange membranes may be useful, for which we have as yet no membrane of clear practical utility. In particular, natural brackish waters usually contain polyvalent ions of both charge signs; rejection properties of ion exchange membranes are frequently adversely affected by multivalent counterions. The search for additives which form membranes of superior properties continues to be of central importance.

[72] J. S. Johnson, L. Dresner, and K. A. Kraus, chap. VIII in *Principles of Desalination*, ed. by K. S. Spiegler, Academic, 1966.

In the past year we have attempted to delineate the areas of usefulness of our previously studied membranes in the presence of polyvalent counterions by tests similar to those reported[70] for hydrous Zr(IV) oxide. We have continued investigation of membranes formed with salts of weak polyelectrolytes, which may be converted to neutral membranes by changing the pH; among others, poly(vinyl pyridine) and polyimines have received attention. Recent results have indicated that the irreproducibility of neutral membrane properties may be somewhat alleviated and the low permeabilities associated with the neutral form may be increased by use of high feed circulation velocities during formation, a procedure that presumably gives a more homogeneous and thinner film. Various other additives have also been investigated, for example, polyglutamic acid, a synthetic polypeptide, and graphitic oxide.

We have also improved rejections by forming membranes and polyelectrolyte additives having higher charge density. Figure 6.19 summarizes some results with polyacrylate membranes; at neutral pH values, R_{obs} for 0.05 *M* NaCl scatters around 70%, compared with 30 to 40% obtained with poly(vinylbenzyltrimethylammonium chloride) or poly(styrenesulfonate), for example. Such an increase is not surprising, although it is encouraging that the effect of the increase in charge density of the organic matrix on capacity is apparently not nullified by an increase in water content of the membrane. What was unexpected was that in an experiment covering several weeks, much higher rejections were attained. Soon after initial preparation, the membrane rejected 72% of solute from 0.05 *M* NaCl (140 gal day^{-1} ft^{-2} at 1500 psig) and 41% from 0.025 *M* $MgCl_2$ (15 gal day^{-1} ft^{-2}); the aged membrane rejected 95% from 0.05 *M* NaCl (9 gal day^{-1} ft^{-2}) and 92% from 0.025 *M* $MgCl_2$ (3 gal day^{-1} ft^{-2}). The reason for these high rejections, particularly with $MgCl_2$, which has a polyvalent counterion, is not yet definitely established.

Another surprising aspect is the high negative rejection of HCl (effluent more concentrated than feed) from acid solutions (Fig. 6.19). Negative rejections of acid from mixed acid-salt solutions have been previously observed, but not to this extent.

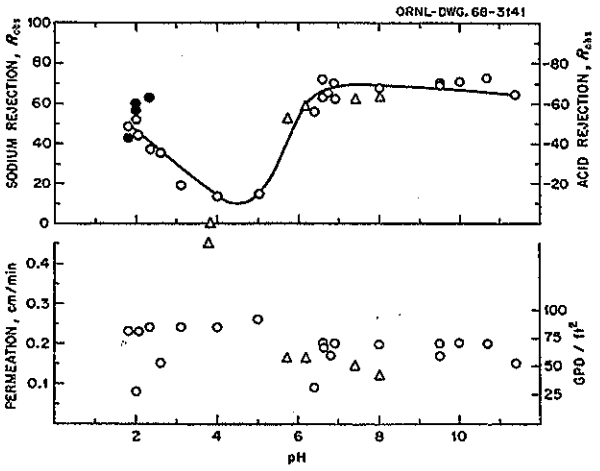

Fig. 6.19. Hyperfiltration with a Dynamically Formed Polyacrylate Membrane.

Porous Supports

Practical success of dynamically formed membranes requires finding suitable cheap porous supports. To be useful, the support must be strong enough, when in a configuration favorable for hyperfiltration, to support the required pressures. It must have pores small and homogeneous enough to allow the additive to form a rejecting film; at the same time, pressure drop of the product stream after passage through the membrane should not be excessive.

Coarsely porous bodies pretreated with filter aids (fine particulate or fibrous dispersions) would appear to offer great promise of meeting these criteria. By utilizing supports having pores of 5 μ and up, sources of usable materials are extended into the ordinary commercial filter range. Pretreatment with filter aid gives a fine-grained support on which to form the membrane, backed by a large-pored structure to transmit the treated water. Perhaps most important, however, this configuration should be easily backwashed, to restore production rate should it drop to undesirably low values because of fouling or other causes. Loss of permeability is sometimes a major problem in hyperfiltration, both with the usual cast membranes and with dynamically formed membranes.

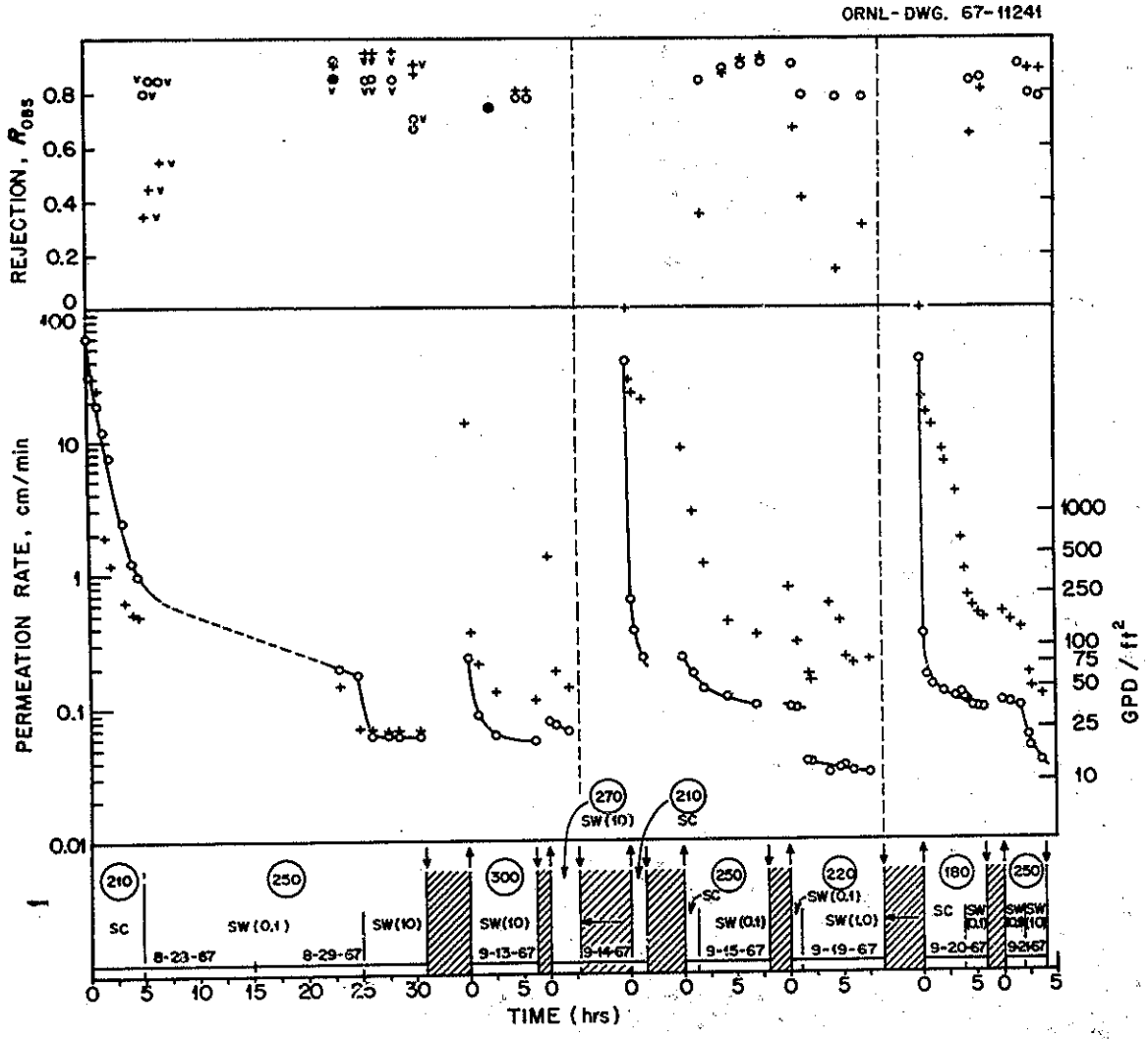

+ Purolator, PS-11, >30μ median pore diameter; circ. rate ~1.2 m sec^{-1}
o Stainless steel, *ca.* 5μ median pore diameter; circ. rate ~2.1 m sec^{-1}

SW(0.1) Sulfite waste solution (0.1% solids by weight)
SC Supercel; 100 ppm; median particle size, ~8μ

(250) Pressure, 250 psig
↑ Startup; ↓ Shutdown; ← Backwash
v Rejection estimated visually; others, spectrophotometrically (281 mμ)

Fig. 6.20. Hyperfiltration of Sulfite Wash Liquors with Porous Tubes Pretreated with Supercel. Effect of backwashing. ~32°C.

The results of many tests during the past year confirm the promise of this concept. An example is presented in Fig. 6.20. The feed was a sulfite wash liquor, and the membrane was formed from its constituents, without any extraneous additives,[73] on supports pretreated with a diatomite filter aid. The pore sizes of both tubes were too large for formation of a membrane with this feed without the pretreatment.[73] With a 5-μ stainless steel support, the membrane rejected in most cases 80% or more of the colored matter; performance of the large-pored experimental Purolator filter was more erratic. Backwashing successfully removed the membrane and restored permeability.

Restoration of permeability is further demonstrated in a series of membrane formations and removals in a study of mixed poly(vinylpyrrolidone)-poly(vinylpyridine) membranes formed on stainless steel tubes pretreated with a ~4-μ perlite filter aid (Fig. 6.21).[74] The permeabilities after backwashing ("initial") were generally about a hundred times those with formed membranes ("final").

[73]J. J. Perona, F. H. Butt, S. M. Fleming, S. T. Mayr, R. A. Spitz, M. K. Brown, H. D. Cochran, K. A. Kraus, and J. S. Johnson, *Environ. Sci. Technol.* 1, 991 (1967).

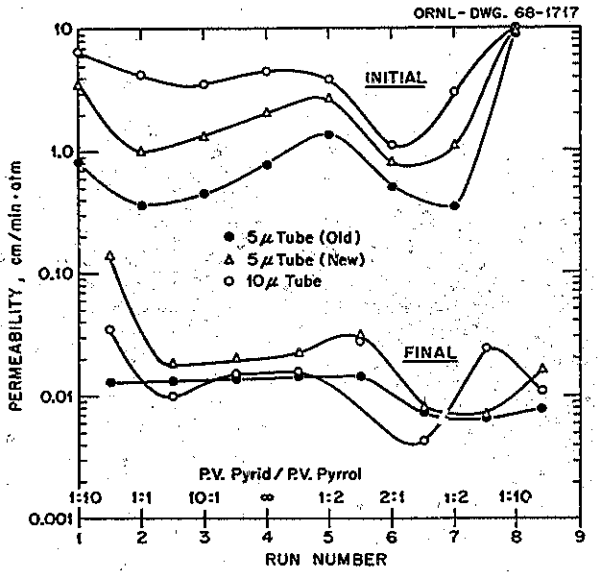

Fig. 6.21. Restoration of Permeability in Mixed Poly-(vinylpyrrolidone)-Poly(vinylpyridine) Membranes. "Initial" refers to freshly backwashed porous support, "final" to porous support with formed membrane.

Possible Practical Applications Other than Desalination

We reported last year that dynamically formed membranes might be useful in processing liquors generated in the washing of wood pulp in the sulfite process. As well as extending our studies in this area, we have looked briefly at the use of dynamically formed membranes for the preparation or concentration of sols for the sol-gel process in the manufacture of nuclear fuel, for processing of reactor cooling water, for beneficiation of lake water, and for sewage treatment. Figure 6.22 summarizes results of treatment of effluent from a primary sewage treatment. The membrane was formed from feed constituents on a ~0.9-μ ceramic tube, and the experiment was conducted in a titanium loop equipped with a 100-gpm circulation pump. Feed was concentrated to less than a fifth of its original volume; the term "volume reduction fraction" in the ordinate of Fig. 6.22 refers to the ratio of loop volume to volume of feed introduced into the loop. In most cases, rejections based on chemical oxygen demand were in excess of 80%. Transmission rates were near 50 gal day^{-1} ft^{-2} and seemed to be maintained at that value, presumably because of the high circulation velocities used (pump speed was controlled by the frequency of the power supply). The sharp rise in permeability at the end of experiment probably indicates a tube failure.

ACTIVITY COEFFICIENTS OF SALTS IN AQUEOUS SOLUTIONS OF PYRIDINE AND PYRIDINIUM SALTS[75]

W. H. Baldwin K. A. Kraus
H. E. Hellwege[76] R. J. Raridon

Studies of activity coefficients of salts in water-organic systems, measured by various methods, are continuing to provide insight into the mechanism of

[74]These experiments were performed by a team of the MIT School of Chemical Engineering Practice, Roy D. Talus, Robert E. Rosenberger, and James T. Murphy; S. M. Fleming, director, and H. D. Cochran, assistant director, of the Oak Ridge Station also participated in the work.

[75]Research jointly sponsored by the Office of Saline Water, U.S. Department of the Interior, and by the U.S. Atomic Energy Commission under contract with the Union Carbide Corporation.

[76]Summer research participant, 1967, from Rollins College, Winter Park, Fla.

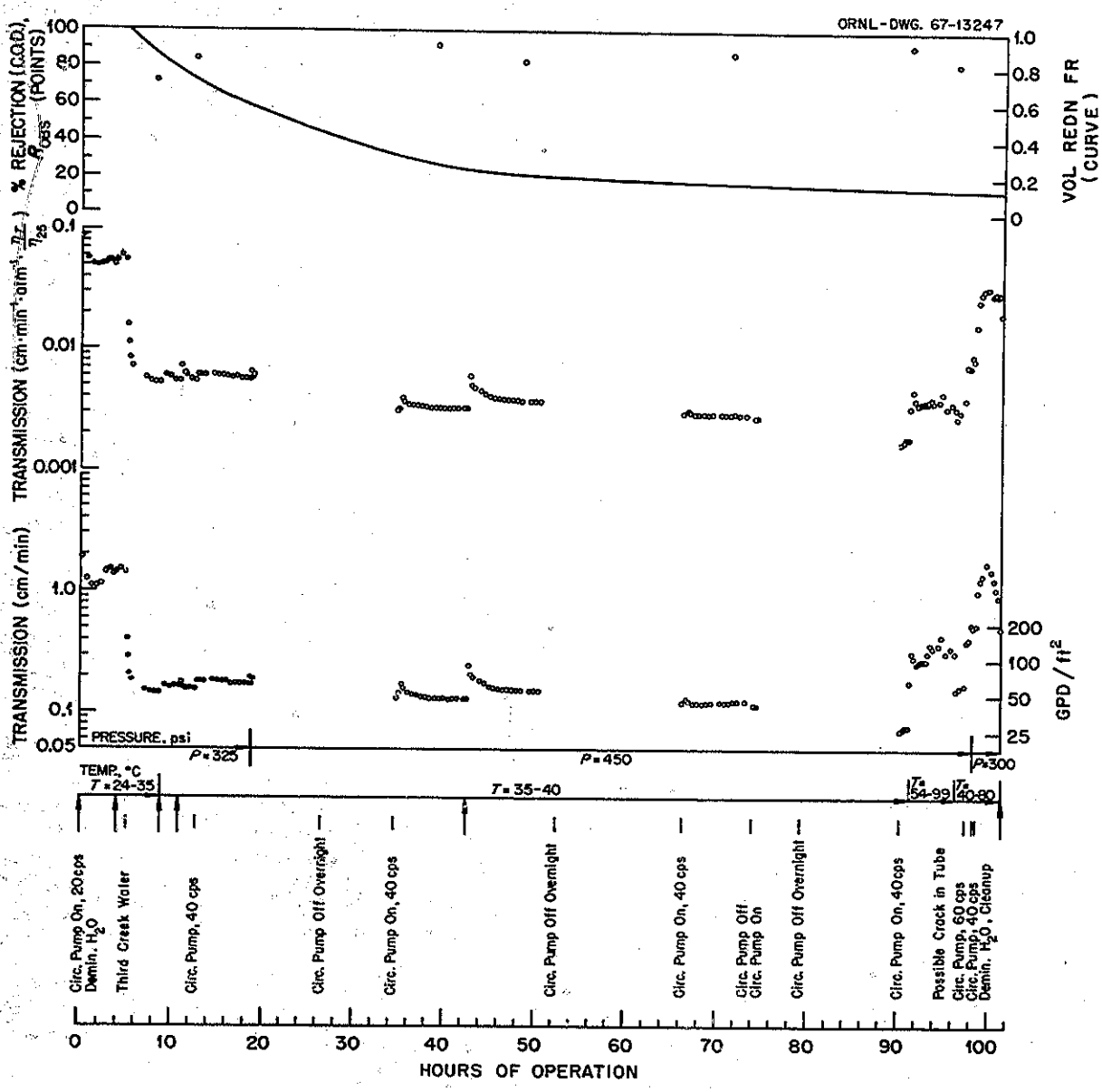

Fig. 6.22. Hyperfiltration by Membranes Dynamically Formed from Feed Constituents on a Porous Tube. Feed, discharge from Third Creek disposal pond in Knoxville; C.O.D. *ca.* 500; tube, porcelain (03 Selas).

salt rejection by hyperfiltration membranes in addition to expanding the knowledge of properties of solutions. The present study involves the activity coefficient relationships in the pyridine-water system, which is of particular interest since the system is an adequate model for hyperfiltration membranes made with pyridine-containing polymers and because, through neutralization by acid addition, it may be a model for charged membranes and ion exchangers.

A relationship[77] between solution properties and membrane properties is given in the following equations:

$$1 - R_\infty = \beta D^* , \tag{1}$$

where for a neutral membrane

$$D^* = \frac{1}{\Gamma^*} = \frac{\gamma_\pm}{\gamma_\pm^*} \tag{2}$$

and for an anion exchange membrane and salt MX_b

$$D^* = \left[\frac{1}{(C^*/bm) + D^*}\right]^b \left[\frac{1}{\Gamma^*}\right]^{b+1} ; \tag{3}$$

R_∞ is the limiting salt rejection of a membrane, D^* is an equilibrium distribution coefficient, and β is the coupling coefficient between salt and water, which is presumed to have a value between 0 and 1; C^* is the ion exchange capacity of a membrane, and when it is small, Eq. (3) reduces to Eq. (2). The starred quantities are defined in terms of amounts per kilogram of water, a useful relationship for discussing membranes, rather than per kilogram of total phase. The quantity Γ^* measures the relative selectivity of the medium for salt and water. For membranes it is desirable to have Γ^* as large as possible. Hopefully, by choosing the proper system, activity coefficients of salts in solutions can be used to estimate the possible salt-rejecting characteristics of a membrane.

Activity coefficients of NaCl, K_2SO_4, and Cs_2SO_4 were calculated from solubility measurements in pyridine-water mixtures. In some cases the pyridine was partially or completely neutralized with acid. In a recent paper[78] the activity coefficients

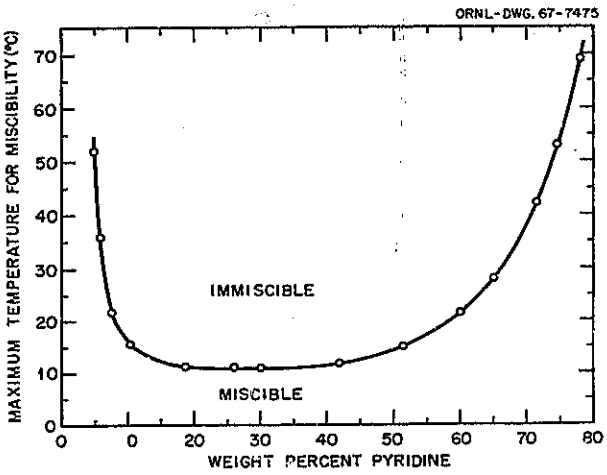

Fig. 6.23. Effect of Temperature on the Miscibility of Pyridine-Water Mixtures Saturated with NaCl.

of NaCl in saturated pyridine-water mixtures at 5 and 25° were presented. The reason for measuring solubilities at the two temperatures is shown in Fig. 6.23. There is a miscibility gap at 25° in the NaCl-saturated system, but this disappears below about 11°. It was of interest to see whether the presence of a miscibility gap would influence the activity coefficients of the salt measured in the miscible region. An activity coefficient ratio is calculated from solubility data as follows:

$$\Gamma = \frac{\gamma_{\pm(o)}}{\gamma_\pm} = \frac{\text{activity coefficient in mixed solvent}}{\text{activity coefficient in pure water}} = \frac{\Gamma^*}{f_w} , \tag{4}$$

where f_w is weight fraction of water and where the subscript (o) refers to an organic-water mixture. For pyridine-water mixtures

$$\Gamma_{NaCl} = m_{NaCl}/m_{NaCl(o)} , \tag{5}$$

$$\Gamma_{K_2SO_4} = m_{K_2SO_4}/m_{K_2SO_4(o)} . \tag{6}$$

In Fig. 6.24, Γ^* is plotted as a function of the pyridine content. The ratios at the two temperatures are essentially identical, showing that one can use data obtained in partially miscible systems for comparison with data from completely miscible

[77] K. A. Kraus, A. J. Shor, and J. S. Johnson, *Desalination* 2, 243 (1967).

[78] R. J. Raridon, W. H. Baldwin, and K. A. Kraus, *J. Phys. Chem.* 72, 925 (1968).

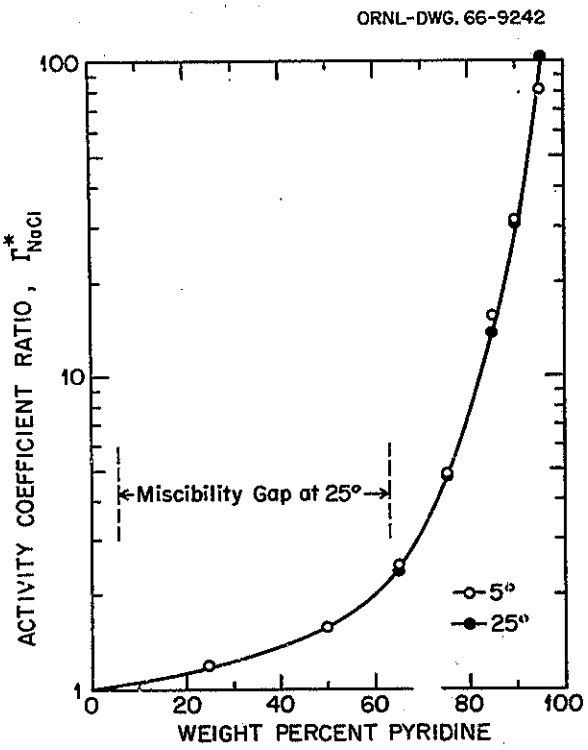

Fig. 6.24. Activity Coefficient Ratios of NaCl in Pyridine-Water Mixtures at 5 and 25°C.

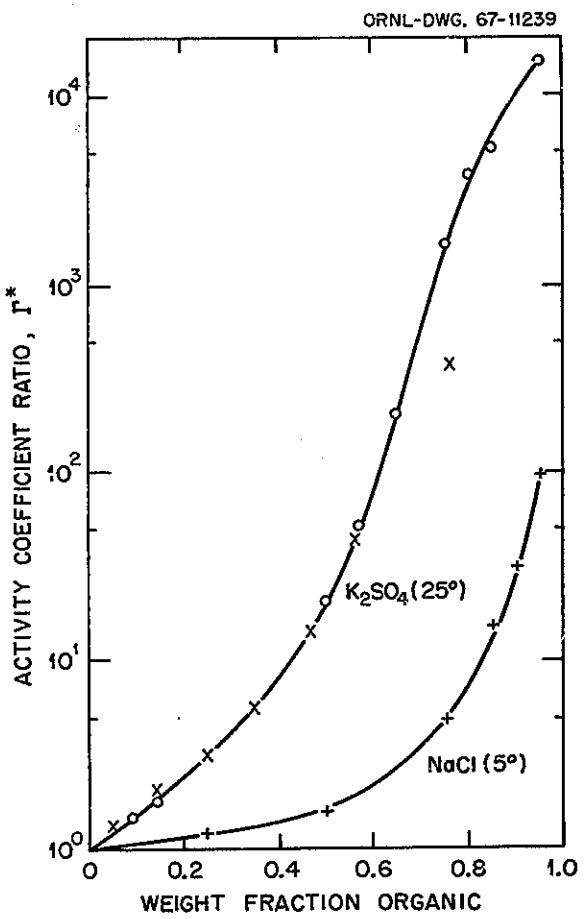

Fig. 6.25. Activity Coefficients of K_2SO_4 and NaCl in Pyridine-Water Mixtures. [X, Fox and Gauge, *J. Chem. Soc.* 97, 377(1910).]

systems. These results could also be used to predict the minimum salt rejection for a pyridine-based membrane as a function of water content. The predicted values compared favorably with experimental results for cast membranes with polyvinylpyridine (PVP) grafted onto cellulose and with dynamic membranes using PVP.

Figure 6.25 gives a comparison of Γ^* values for K_2SO_4 and NaCl in pyridine-water mixtures. The values for K_2SO_4 are much higher, especially at low water fraction. For Cs_2SO_4 there is a miscibility gap at 25°, so that measurements could only be made for solutions containing at least 78% pyridine. The Γ^* values for Cs_2SO_4 over this limited range are 2 to 10 times higher than for K_2SO_4. However, some experimental difficulties were encountered with K_2SO_4 at low water fraction, so that the Γ^* values for Cs_2SO_4 in this range were used for predicting membrane properties. One would predict from these data that K_2SO_4 or Cs_2SO_4 would be rejected better than NaCl by a pyridine-containing membrane. It has been observed experimentally that under certain conditions sulfate is indeed better rejected than chloride by a dynamic PVP hyperfiltration membrane.

For comparison with charged membranes, activity coefficient ratios for K_2SO_4 were calculated from solubility measurements in pyridine–water–sulfuric acid mixtures as follows:

$$\Gamma_{K_2SO_4} = \frac{m_{K_2SO_4}}{m_{K_2SO_4(o)}} \left[1 + \frac{m_{H_2SO_4(o)}}{m_{K_2SO_4(o)}} \right]^{-1/3} \quad . \quad (7)$$

All concentrations are for saturated solutions except the acid concentration in the neutralized sys-

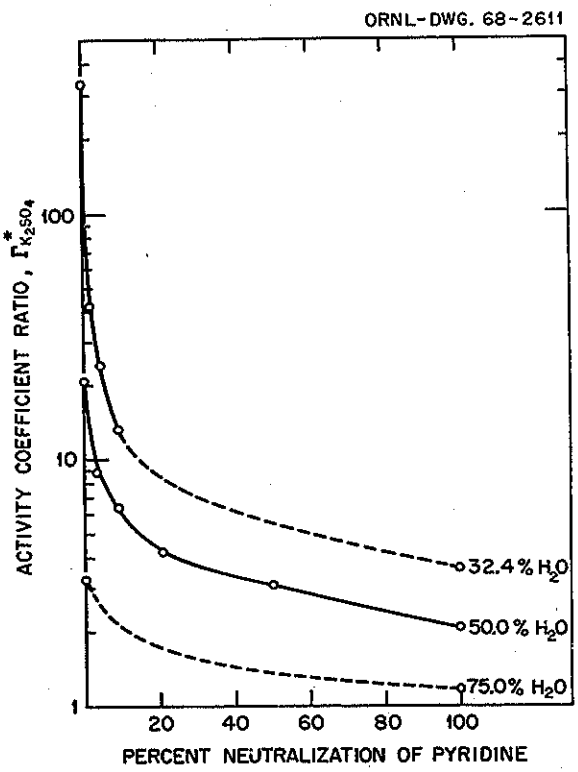

Fig. 6.26. Activity Coefficient Ratios of K_2SO_4 in Pyridine-H_2O-H_2SO_4 Systems at 25°.

tems. In Fig. 6.26, Γ^* is plotted as a function of percent neutralization at three different water contents. The water content is calculated from the weight of water in the system including pyridinium salt but not K_2SO_4. There is a sharp decrease in Γ^* with increased neutralization, particularly at low water content.

An attempt has been made to account for the variation of Γ^* with water fraction and percent neutralization by using an extended Debye-Hückel expression which included two or three additional terms as follows:

$$\log \gamma_{\pm} = -\frac{S\sqrt{I}}{1 + A\sqrt{I}} + BI + CI^2 + DI^3 , \qquad (8)$$

$$\log \frac{\Gamma_1}{\Gamma_2} = \frac{S(\sqrt{I_2} - \sqrt{I_1})}{(1 + A\sqrt{I_1})(1 + A\sqrt{I_2})} + B(I_1 - I_2) + C(I_1^2 - I_2^2) + D(I_1^3 - I_2^3) , \qquad (9)$$

$$S = 0.509 z_i z_j (\epsilon_1/\epsilon_{13})^{3/2} , \qquad (10)$$

$$A = a'(\epsilon_1/\epsilon_{13})^{1/2} , \qquad (11)$$

where ϵ_1 and ϵ_{13} are the dielectric constants of pure water and the water-organic mixture respectively. When the pyridine is partially neutralized, the solution becomes conducting, and dielectric constant measurements cannot be made. The assumption is made that ϵ_{13} is determined by the ratio of pyridine and water present, regardless of the percent neutralization of the pyridine. The value in pyridine-water alone is Γ_1, and Γ_2 is the value to be calculated in the system containing pyridinium salt. The solid lines in Fig. 6.27 are the calculated Γ_2 values for 50 and 100% neutralization. The parameter a' was taken as 1.5. The B and C parameters used were those calculated from data for Na_2SO_4 in water.[79] It was felt that these

[79] M. H. Lietzke and R. W. Stoughton, *Proc. Natl. Acad. Sci.* 59, 39 (1968).

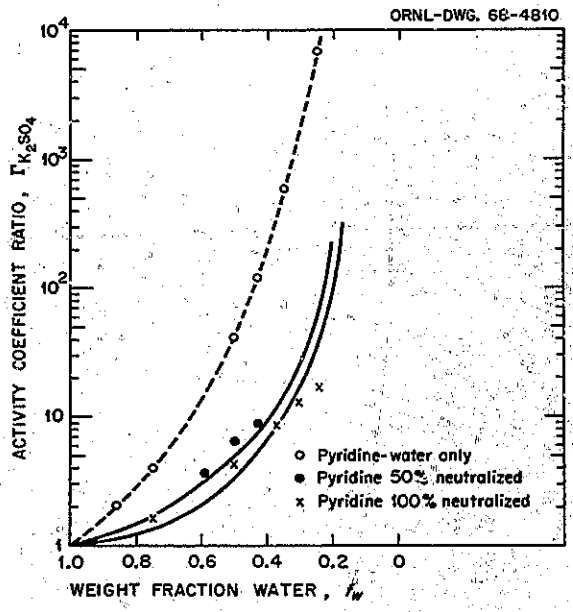

Fig. 6.27. Activity Coefficients of K_2SO_4 in the Pyridine-Water-H_2SO_4 System. [Solid lines calculated from parameters for Na_2SO_4, Lietzke and Stoughton, *Proc. Natl. Acad. Sci. U.S.* 59, 39(1968).]

parameters would be more applicable than those for K_2SO_4 since the activity coefficients of the two salts, which are essentially identical up to the solubility limit of K_2SO_4, are known to much higher concentrations for Na_2SO_4, and the interest here is in the high concentration region. Considering the several assumptions made, the calculated curves agree surprisingly well with the experimental values. Further experimental measurements are planned.

Similar data for the activity coefficient ratios of NaCl in pyridine-water-HCl mixtures are shown in Fig. 6.28. The Γ_{NaCl} values are computed from the relationship

$$\Gamma_{NaCl} = \frac{m_{NaCl}}{m_{NaCl(o)}} \left[1 + \frac{m_{HCl(o)}}{m_{NaCl(o)}} \right]^{-1/2} . \quad (12)$$

In this system there is very little change in Γ as a function of degree of neutralization. Here also the calculated curves closely approximate the experimental results although the parameters used are again calculated from data in water alone.[80]

The activity coefficients of the salts in pyridine-water alone can be correlated with the dielectric constant of the medium as illustrated in Fig. 6.29. Similar plots have been used[81] to compare activity coefficients at infinite dilution of salt in different water-organic systems. The plots for NaCl were roughly linear but with different slopes for different water-organic mixtures. Apparently similar linear variations hold at saturation. The slope is presumed to be inversely proportional to the radius of the ions. The A parameter in the Debye-Hückel equation is also assumed to be related to the size of the ions. For a three-parameter fit, allowing A, B, and C all to vary, one would calculate $A = 1.15$ for K_2SO_4 in water, while Lietzke and Stoughton[80] calculated $A = 1.31$ for NaCl. Thus the ratio of A parameters is at least qualitatively the same as the inverse ratio of slopes, indicating that one could roughly approximate the activity coefficients of one salt in a water-organic mixture if the activity coefficients of another salt were known for the same mixture. As was seen in the case of the neutralized pyridine systems, one could approximate the activity coefficient ratios in the pyridine–water–pyridinium-salt mixtures from knowledge of the activity coefficients of the salt in water alone.

[80] M. H. Lietzke and R. W. Stoughton, ORNL-CF-61-7-38.

[81] R. D. Lanier, *J. Phys. Chem.* 69, 2697 (1965).

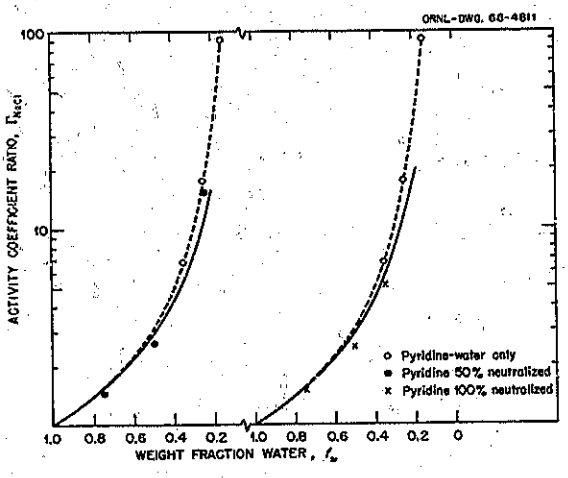

Fig. 6.28. Activity Coefficients of NaCl in the Pyridine-Water-HCl System. (Solid lines calculated from parameters for NaCl, Lietzke and Stoughton, ORNL CF-61-7-38.)

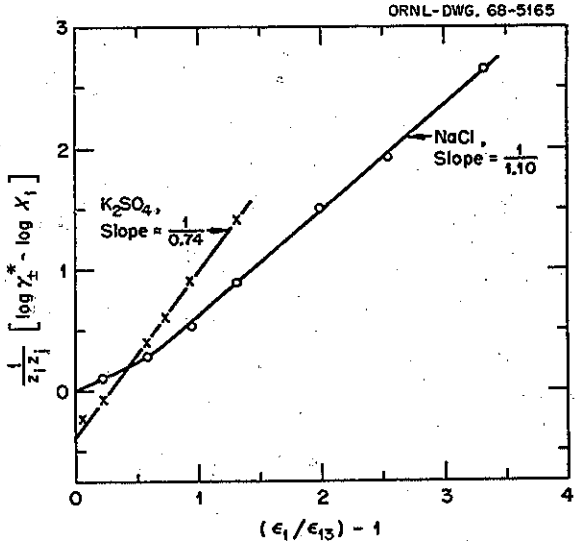

Fig. 6.29. Correlation of Activity Coefficients of NaCl and K_2SO_4 in Pyridine-Water Mixtures with Dielectric Constant of Medium.

ELECTROLYSIS OF FLOWING STREAMS WITH SCREEN ELECTRODES[82]

F. Nelson P. M. Lantz K. A. Kraus

In continuation of studies on electrolysis of flowing streams, properties of screen electrodes were investigated. In studies reported in the last annual report[83] it was shown that the capillary tube model could be used to explain aspects of the electrochemical behavior of porous electrodes. If porous electrodes are considered a labyrinth of capillary tubes, the limiting (i.e., diffusion-controlled) currents observed in flowing streams can be expressed as sums of the limiting currents of individual capillaries of the porous electrodes. The relationship given by Blaedel *et al.*[84,85] for a tubular electrode, which is based on the convective diffusion equations derived by Levich,[86] was used:

$$i_{lim} = 5.31 \times 10^2 \, nc\mathcal{D}^{2/3} l^{2/3} V_f^{1/3} . \qquad (1)$$

In Eq. (1), i_{lim} is the current (amp), n is the number of electrons involved in the redox reaction, c is the concentration of electroactive species (moles/liter), $\mathcal{D}$ is the diffusion coefficient (cm^2/sec), V_f is the volume flow rate (cm^3/sec), and l is the length (cm) of the electrode. We have now tested this "capillary model" with platinum screen electrodes under a large range of flow conditions. The screen electrodes were prepared by cementing platinum screens in glass tubing, *ca.* 5 mm inside diameter (area = 0.205 cm^2). The screens were mounted at right angles to the axis of the tubes; they projected sufficiently beyond the outer wall so that electrical contact could be made with clip leads. Both a fine mesh (*A*) and a coarse mesh (*B*) screen were used. Screen *A* had 1090 mesh openings per square centimeter, and screen *B* had 331 mesh openings per square centimeter. Wire diameters were 0.006 and 0.024 cm respectively; screen thicknesses are twice the wire diameters.

A typical current-voltage curve obtained with one of the electrodes (screen *A*) is shown in Fig. 6.30.

[82]Research jointly sponsored by the Office of Saline Water, U.S. Department of the Interior, and by the U.S. Atomic Energy Commission under contract with the Union Carbide Corporation.

[83]K. A. Kraus *et al.*, *Chem. Div. Ann. Progr. Rept. May 20, 1967*, ORNL-4164, p. 86.

[84]W. J. Blaedel, C. L. Olson, and L. R. Sharma, *Anal. Chem.* 35, 2100 (1963).

[85]W. J. Blaedel and L. N. Klatt, *Anal. Chem.* 38, 879 (1966).

[86]V. G. Levich, *Physicochemical Hydrodynamics*, translation by Scripta Technica, Inc., Prentice-Hall, Englewood Cliffs, N.J., 1962.

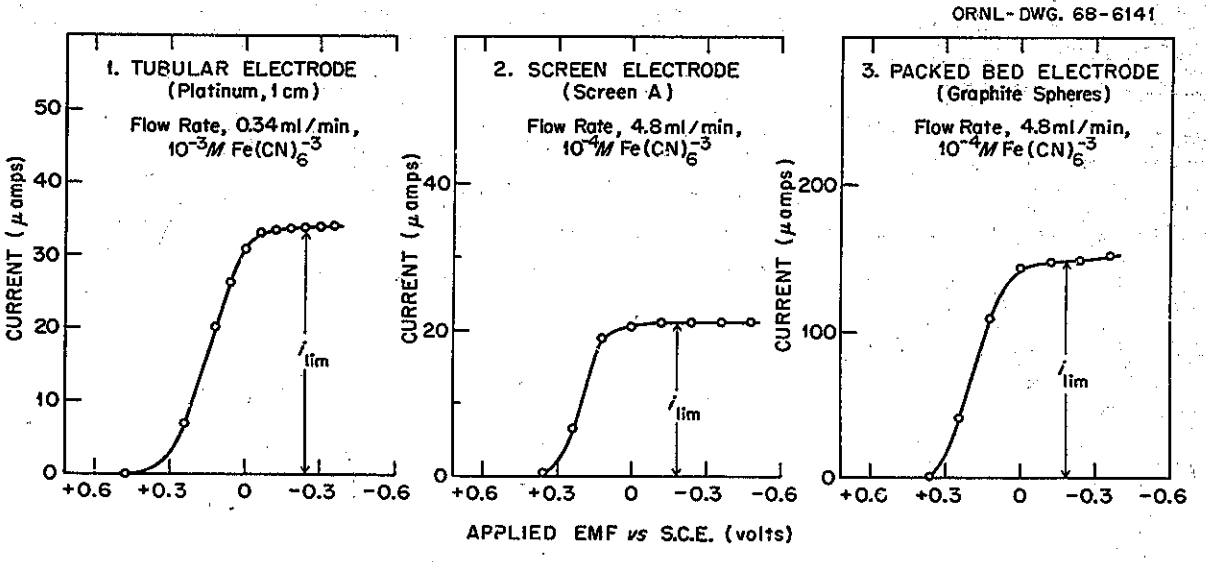

Fig. 6.30. Current-Voltage Curves for Screen, Tubular, and Packed-Bed Electrodes.

The experiment was carried out at a flow rate of 4.8 ml/min (23.4 cm/min) with 1×10^{-4} *M* $Fe(CN)_6^{3-}$ in 2*M* KCl as supporting electrolyte. A well-defined limiting current plateau is observed in the potential region beyond the redox potential of the $Fe(CN)_6^{3-}$-$Fe(CN)_6^{4-}$ couple (*ca.* 0.25 v vs saturated calomel electrode). The current-voltage curve is similar to those observed earlier with tubular and packed-bed electrodes; these are shown in Fig. 6.30 for comparison.

The effect of $Fe(CN)_6^{3-}$ concentration on limiting current is shown in Fig. 6.31 for typical flow experiments with screen *A*. Flow rate was constant at 3.82 ml/min (18.6 cm/min). In the $Fe(CN)_6^{3-}$ concentration range 5×10^{-5} to 1×10^{-3} *M*, the limiting current, i_{lim}, varies linearly with *M* $Fe(CN)_6^{3-}$, and the quotient i_{lim}/M $Fe(CN)_6^{3-}$ is essentially constant. Deviations from the mean are only about ±2%; this precision compares favorably with the reproducibility observed in conventional polarography with a dropping mercury electrode.

The effect of flow rate on limiting current with screen electrodes is shown in Fig. 6.32 as a log-log plot of i_{lim}/c vs flow rate, V_f. The results were obtained with *ca.* 10^{-3} to 10^{-5} *M* $Fe(CN)_6^{3-}$ in 2 *M* KCl. Except at very low and very high flow rates, the function is essentially linear, with slope

$$\frac{d \log (i_{lim}/c)}{d \log V_f} = \frac{1}{3}$$

as expected from Eq. (1).

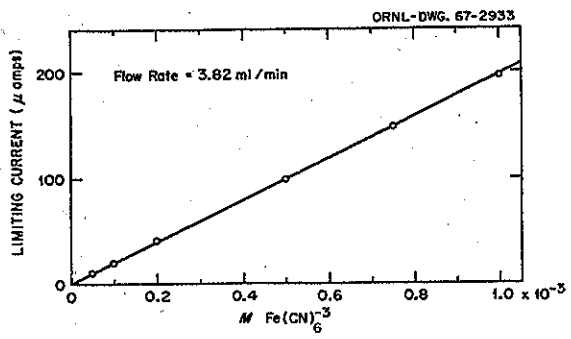

Fig. 6.31. Variation of Limiting Current with *M* $Fe(CN)_6^{3-}$. Screen electrode: screen A, area 0.205 cm^2; electrolyte: 2 *M* KCl.

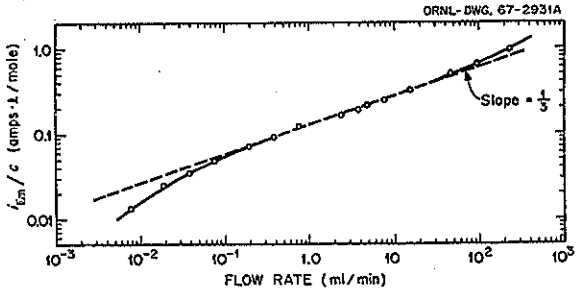

Fig. 6.32. Variation of Limiting Current with Flow Rate. Screen electrode A, area 0.205 cm^2. Solution 10^{-4} to 10^{-3} *M* $Fe(CN)_6^{3-}$ in 2 *M* KCl.

As shown earlier with porous carbon electrodes, the limiting currents in screen electrodes are in good agreement with limiting currents computed by a capillary tube model, assuming each screen opening represents an individual capillary with length, *l*, equal to the thickness of the screen. Limiting currents computed with Eq. (1) for both screen electrodes agreed within about 10% with the corresponding experimental values of limiting currents in the regions where log-log plots of i_{lim}/c vs V_f have slope $\frac{1}{3}$.

DIFFUSION STUDIES[87]

H. O. Phillips
A. E. Marcinkowsky[88]
K. A. Kraus
S. B. Sachs[89]
Y. C. Wu[90]

As part of the study of aqueous electrolyte solutions, a more detailed evaluation of the reliability of the porous frit method was carried out. Self-diffusion coefficients of Na^+ ($\mathcal{D}_{Na}$) in NaCl solutions from 0.05 to 5 *M* were determined and found to be in satisfactory agreement with the data of Mills.[91]

---

[87]Research jointly sponsored by the Office of Saline Water, U.S. Department of the Interior, and by the U.S. Atomic Energy Commission under contract with the Union Carbide Corporation.

[88]Present address: Technical Center, Union Carbide Corporation, South Charleston, W.Va.

[89]Visiting Scientist from the Weizmann Institute, Israel.

[90]Present address: U.S. Department of Commerce, National Bureau of Standards, Washington, D.C.

[91]R. Mills, *J. Am. Chem. Soc.* 77, 6116 (1955).

Preliminary measurements were carried out with 0.1 and 1 *M* NaCl solutions in the temperature range 15 to 85°C. The temperature coefficient was in reasonable agreement with that expected from the limiting ionic conductances. It thus appears that room-temperature calibration of the frits is satisfactory for evaluation of the temperature variation of self-diffusion coefficients.

Self-diffusion coefficients $\mathbb{D}_{Na}$ were determined in a number of sodium salt solutions, including mono-, di-, and trisodium phosphate. As a good first approximation $\mathbb{D}_{Na}$ varied as expected from the viscosities of the solutions.

In the water-organic studies, determination of $\mathbb{D}_{Na}$ at 25°C in polyethylene glycol–water systems was essentially completed. The measurements were carried out at constant 0.1 *M* NaCl concentration; the maximum polyethylene glycol (PEG) concentration was *ca.* 30% where the viscosity (η) of the solution was almost 1000 centipoises. The self-diffusion coefficients were relatively insensitive to viscosity; at the highest concentration studied, $\mathbb{D}_{Na}$ was 0.39×10^{-5} cm^2/sec, compared with 1.28×10^{-5} cm^2/sec in 0.1 *M* NaCl. The observed $D\eta$ product in the PEG-H_2O system rises rapidly with η while it is relatively independent of η in such low-molecular-weight viscous organic-water systems as those of glycerol[92] and glucose[93] (Fig. 6.33). The values of $\mathbb{D}_{Na}$, however, could

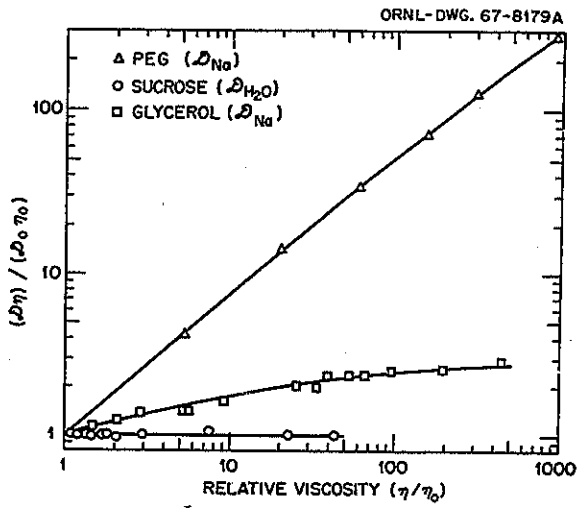

Fig. 6.33. Relative Diffusion Coefficient–Viscosity Products for Some Organic-Water Mixtures.

reasonably be correlated with the fractional water contents f_v of the solutions. As we have also found for other systems, a plot of log $\mathbb{D}_{Na}$ vs log f_v is essentially linear. In the PEG-H_2O system the slope is *ca.* 3.3.

In an extensive study of diffusion in glycerol triacetate–water mixtures (containing 1.4 *M* $NaClO_4$), $\mathbb{D}_{Na}$ was found to vary qualitatively as expected from the viscosities of the solutions. The $D\eta$ products, however, had a shallow maximum near $f_v = 0.4$.

[92] A. E. Marcinkowsky, H. O. Phillips, and K. A. Kraus, *J. Phys. Chem.* 72, 1201 (1968).

[93] R. R. Irami and A. W. Adamson, *J. Phys. Chem.* 62, 1517 (1958).

7. Electrochemical Kinetics and Its Application to Corrosion

STUDIES ON THE INORGANIC INHIBITORS OF CORROSION

G. H. Cartledge

In continuation of the study of the mechanism by which certain XO_4^{n-} ions inhibit the corrosion of iron, the function of the molybdate ion has been investigated in further detail. The first part of this study was described previously.[1] It was shown that anodic passivation is facilitated by a noncathodic effect of this ion also, but activation on open circuit disclosed the existence of two or three distinct steps, the number being determined by the concentration of Fe(II) ions in the electrolyte.

The initial film formed at the lowest polarizing potentials was shown to contain Fe(II) and MoO_4^{2-} ions. At a certain quite definite potential this film begins to be oxidized, and incipient passivation occurs. Full passivation requires further oxidation at more noble potentials, however, and the presence of two steps suggested intermediate formation on the electrode of an Fe(II)-Fe(III)-MoO_4^{2-} component analogous to magnetite. The existence of such mixed complexes was established by spectrophotometric measurements on molybdate solutions containing the respective iron ions singly or in mixture, and solids of corresponding composition were isolated. Electron diffraction patterns of stripped films prepared at several potentials confirmed the change of structure with applied potential.

The presence of Fe(II) ions in the electrolyte was found to accelerate anodic passivation by deposition of the oxidation product on the electrode. When polarization was carried to potentials noble to +200 mv (S.C.E.) a "superpassive" state was produced. This was indicated by the appearance of the third halt or inflection in the potential-time curve on open circuit. The value, E_h, of this halt depends upon the concentration of the solution with respect to Fe(II), H^+, and MoO_4^{2-}. Figure 7.1 illustrates the influence of the Fe(II) concentration for a particular pH and molybdate concentration. Figure 7.2 shows the changes in the composition of the film believed to be occurring in the different regions of potential.

The superpassive state is considered to arise when the film has been fully oxidized to Fe(III) components to a sufficient depth, after which the noble polarizing potential removes additional electrons from the film, producing trapped positive holes, represented in Fig. 7.2 as Fe^{x+}. These are postulated to be reduced stepwise by reaction with Fe(II) ions, either from the solution (rapidly) or by diffusion from the metal (slowly), thus accounting for the considerable differences observed in the activation curves.[2]

The passivation of iron in molybdate solutions is seen to be complicated by chemical participation of the anions in a manner not exhibited by TcO_4^-, MnO_4^-, and CrO_4^{2-}. Additional details are presented in a manuscript already submitted for publication in *Corrosion*.

[1] G. H. Cartledge, *Chem. Div. Ann. Progr. Rept. May 20, 1967*, ORNL-4164, p. 92.

[2] For a similar observation in borate solutions, see M. Nagayama and M. Cohen, *J. Electrochem. Soc.* 109, 781 (1962); 110, 670 (1963).

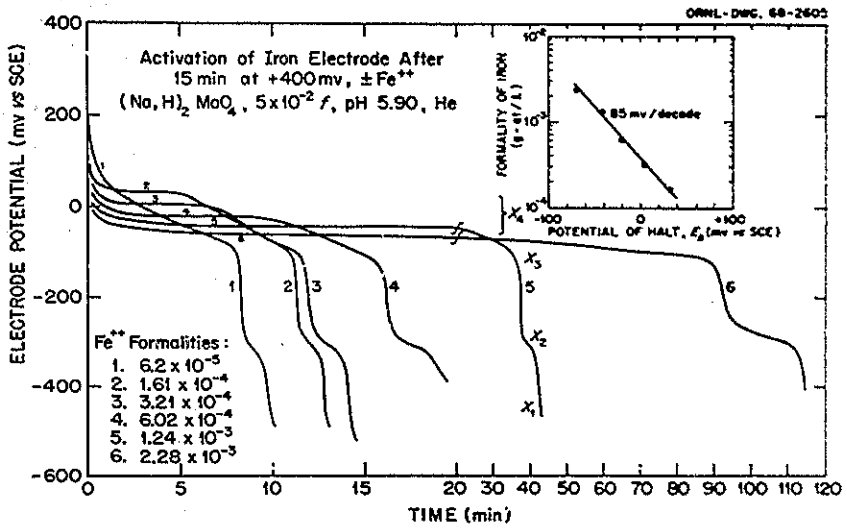

Fig. 7.1. Effect of Fe(II) Ions in Producing a "Superpassive" Halt and (Insert) Its Variation with Concentration in 5×10^{-2} f Molybdate at pH 5.90.

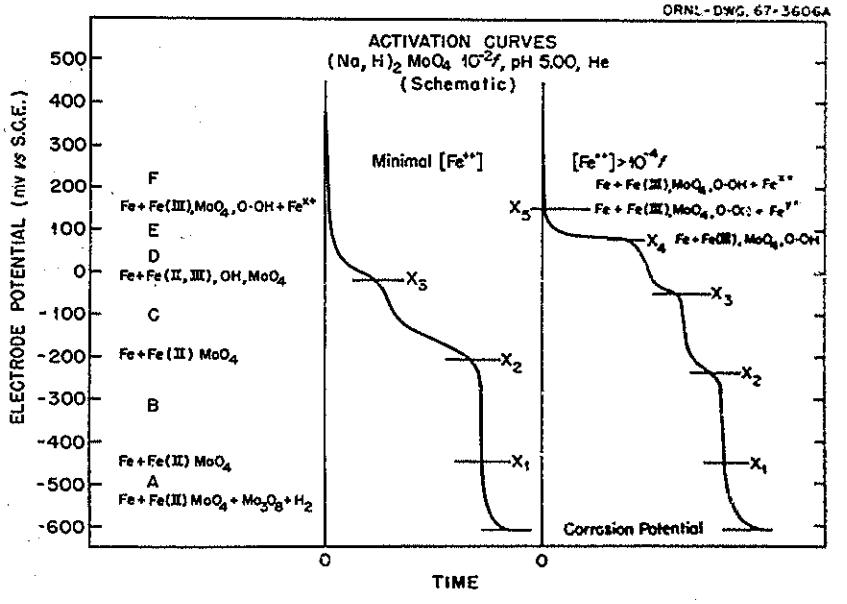

Fig. 7.2. Schematic Interpretation of the Active-Passive Transitions in Terms of Components on the Surface of an Electrode.

A GENERALIZED INTERPRETATION OF THE PASSIVE STATE

G. H. Cartledge

For metals that are not inherently resistant to water or oxygen, the chief characteristics of the passive state are the relatively noble potential, the electronic conductance of the film, and its very low solubility. The assumption of trapped positive holes, made to account for the superpassive state in the molybdate system, has been extended to the passive state of iron in the absence of inhibiting anions. For this purpose, use was made of the concept of the ionic potential and its influence on such properties as the solubility and acid-base character of oxides.[3] In the papers of ref. 3 it was shown that the function $\phi_i \equiv z/r$ (ionic charge over crystal radius) serves to differentiate the ways in which oxides behave toward water. Cations having $\sqrt{\phi_i} < 2.2$ give oxides with base-forming character; for those with $\sqrt{\phi_i} > 3.2$ the oxide is acid-forming, whereas intermediate values lead to very insoluble and inert oxides. As applied to the passive state, this means that injection of a sufficient (but not too large) concentration of positive holes raises the average ionic potential of the iron ions in the film into the region in which the oxide becomes much less soluble than the known and stable oxides of iron. The noble potential, the electronic conductance, and the enhanced solubility are thus accounted for by one and the same condition. On this basis, the onset of activation occurs when the concentration of positive holes has been diminished sufficiently by reaction with Fe(II) ions or by externally applied cathodic polarization. The Flade potential, in the absence of inhibitors, or the potential X_4 of the initial preactivation process in Fig. 7.2 may then be assumed to indicate when this condition has been reached. These characteristic potentials are thus determined kinetically by the concentrations of any species that participate in the pertinent electrode processes.

This interpretation of passivity has been incorporated into a manuscript on the molybdate system which was presented orally at the Cleveland meeting of the National Association of Corrosion Engineers (March 18–21, 1968) and submitted for publication.

[3] G. H. Cartledge, *J. Am. Chem. Soc.* **50**, 2855, 2863 (1928).

ELECTROCHEMICAL BEHAVIOR OF TITANIUM

E. J. Kelly

The subject of this report is the oxidation of Ti(III) ions in solution to Ti(IV) at the passive titanium electrode, and the role of this reaction in studies on the passive state of titanium.

Steady-state current-potential curves for titanium in H_2-saturated 1 *N* H_2SO_4 are shown in Fig. 7.3. Titanium undergoes active-state dissolution in this medium at the corrosion potential, E_c. As the electrode potential is made increasingly positive (noble), the anodic current passes through a maximum at the "critical potential," E_p, and then diminishes sharply as the metal is

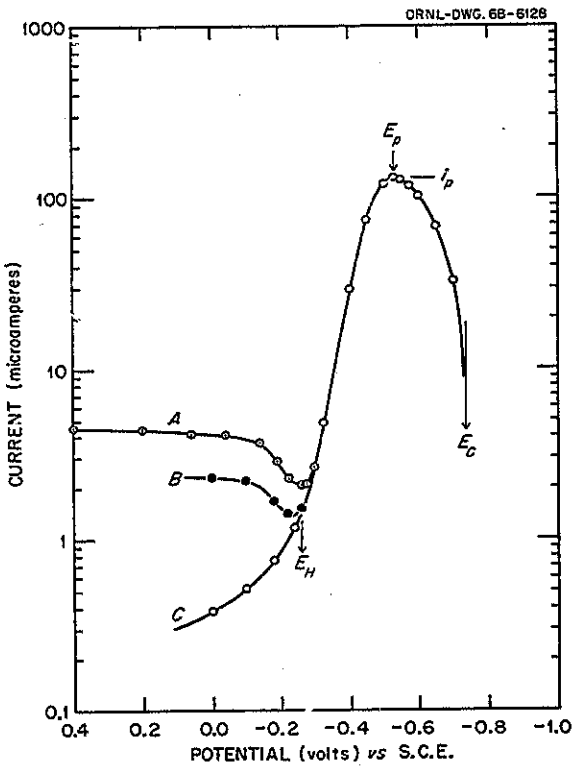

Fig. 7.3. Steady-State Current-Potential Curves for Titanium (Area = 3.0 cm^2) in H_2-Saturated 1 *N* H_2SO_4 at 30°C.

transformed from the active to the passive state. Along curve A, which has been regarded as characteristic of titanium,[4,5] the current passes through a minimum in the vicinity of the reversible hydrogen electrode potential, E_H, and then rises into a region where the rate of oxidation is virtually independent of potential. The independence of the current in the passive state might suggest that the mechanism of titanium oxidation in this region is similar to that of iron, which also exhibits a potential-independent anodic current in the passive potential region. However, numerous experiments with both commercially pure (99.5%) and zone-refined (99.97%) titanium showed that, although exceptionally reproducible current-potential data were obtained in the potential region between E_c and approximately -0.3 v vs S.C.E., significant variations appeared in the polarization curves at more positive potentials, as illustrated by curves A and B.

It has been established that in the active and active-passive transition regions (i.e., in the potential region where curves A, B, and C coincide) titanium is oxidized to Ti(III) ion in solution.[2] In the passive state the substrate metal is oxidized to form the passive oxide film (TiO_2). The possibility existed that, in addition to oxidation of the substrate metal, Ti(III) ions which accumulate in the solution phase during active-state dissolution of titanium are oxidized at the passive surface at such a rate that the current corresponding to this reaction could account for the variation in curves such as A and B. To test this hypothesis, the polarization curve was retraced, starting at E_c; at each potential setting more positive than -0.4 v vs S.C.E., the solution was replaced with Ti(III)-free solution. The result is shown by curve C of Fig. 7.3.

With the electrode in a steady state at 0.0 v vs S.C.E., a solution of known concentration of Ti(III) ions in H_2-saturated 1 N H_2SO_4 was added in increments to the 200 ml of Ti(III)-free solution in the test cell. Upon completion of the additions, the current had increased to the value given by curve B. The remainder of curve B was then obtained by polarization in the negative potential direction. If i_0 represents the current corresponding to zero concentration of Ti(III) ions and i is the observed current, then a plot of log $(i - i_0)$ vs log $[v/(v_0 + v)]$, where v_0 is the volume of Ti(III)-free solution in the cell and v is the volume of standard Ti(III) solution added, should result in a straight line, the slope of which is equal to the order with respect to Ti(III) of the oxidation reaction of Ti(III) to Ti(IV). The results of the Ti(III) addition experiment are shown in Fig. 7.4. The order with respect to Ti(III) is 0.975 ± 0.026; that is, the oxidation reaction is first order in Ti(III).

The results described above show that only curve C corresponds to the oxidation of substrate metal to the passive TiO_2 film and that the rate of this process is not independent of potential as in the case of iron. Curves A and B result from the oxidation of Ti(III) ions in solution. The independence of this reaction with potential at the more positive potentials possibly result from the fact that the reaction rate may depend only on the oxide-solution interfacial potential difference, $\Delta\phi_s$. If $d\Delta\phi_{ox}/dE$ is virtually equal to

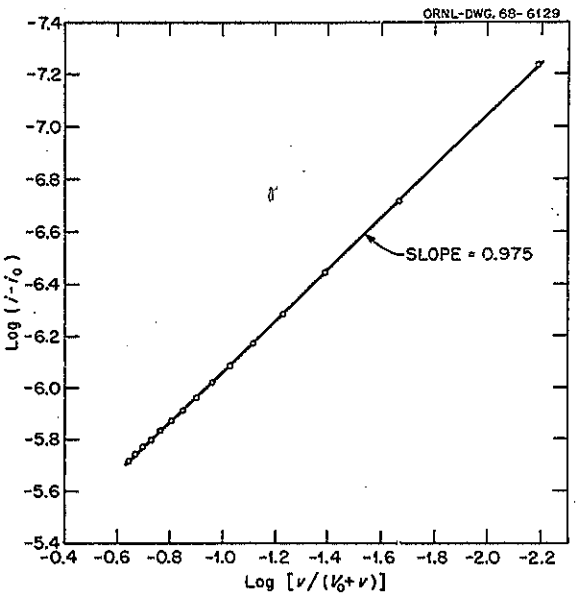

Fig. 7.4. Oxidation of Ti(III) Ions in Solution to Ti(IV) at the Passive Titanium Electrode; Determination of Order with Respect to Ti(III). $v_0 = 200$ ml, $i_0 = 3.77 \times 10^{-7}$ amp. Final Ti(III) concentration *ca.* 7×10^{-4} *M*. Electrode potential = 0.0 v. vs S.C.E.

[4] M. Stern and H. Wissenberg, *J. Electrochem. Soc.* 106, 756 (1959).

[5] E. J. Kelly, *Chem. Div. Ann. Progr. Rept. May 20, 1967*, ORNL-4164, p. 90.

unity, where $\Delta\phi_{ox}$ is the potential drop across the oxide film and E is the electrode potential, then since

$$d\Delta\phi_s/dE = 1 - d\Delta\phi_{ox}/dE ,$$

$\Delta\phi_s$ remains essentially independent of E.

KINETICS OF INITIATION OF CREVICE CORROSION[6]

F. A. Posey

Further progress was made during the report period on development of theoretical models for the early stages of initiation of crevice corrosion, with special reference to the case of titanium. In addition to considering the reduction of dissolved molecular oxygen and the accumulation of hydrogen ions in a crevice due to diffusion and reaction, the effect of migration of reactants and products on the initiation process has now been included. Consequently it is possible to estimate both the distributions of hydrogen ions and dissolved oxygen in a crevice and the distribution of potential in the aqueous phase as a function of various kinetic and geometric parameters.

In the early stages of the initiation of crevice corrosion of titanium, the net current density at any point (x, cm) in the crevice and time (t, sec) is given to a first approximation by

$$\frac{j(x, t)}{j_0} = 1 - \frac{C_O(x, t)}{C_O^0}, \qquad (1)$$

where $j(x, t)$ is the difference in the current densities of anodic and cathodic processes (amp/cm^2), j_0 is the corrosion rate (amp/cm^2), which is assumed to be constant, $C_O(x, t)$ is dissolved oxygen concentration (moles/cm^3), and C_O^0 is the initial oxygen concentration (moles/cm^3). In the case of titanium the anodic process consists of the formation of a TiO_2 passive layer, with simultaneous production of hydrogen ions according to the appropriate stoichiometry, while the cathodic process is reduction of molecular oxygen to form hydroxide ions, which can neutralize hydrogen ions formed as one of the products of the anodic process. We do not consider here an added complication due to the autocatalytic nature of the anodic process on passive titanium in confined areas at sufficiently high acidity.[7] In crevices of the proper dimensions, diffusion of O_2 from the external solution into the crevice is insufficient to maintain the supply of cathodic reactant. With time, hydrogen ions accumulate, and chloride ions (or other anions) are transported into the crevice to preserve electroneutrality, the net anodic current density becomes appreciable, and a significant potential drop develops in the solution phase. If the acid concentration and potential drop are large enough, it is then possible for the system to transform to the mode of active corrosion (not treated here), in which the metal corrodes with hydrogen evolution in the absence of a protective oxide layer.

The rate of accumulation of hydrogen ions in the crevice is given approximately by

$$\frac{\partial C_H(x, t)}{\partial t} = D_H \left\{ \frac{\partial^2 C_H(x, t)}{\partial x^2} + \frac{\partial}{\partial x}\left[C_H(x, t) \frac{\partial \Phi(x, t)}{\partial x} \right] \right\} + \frac{j(x, t)}{F\delta}, \qquad (2)$$

where $C_H(x, t)$ and D_H are the concentration (moles/cm^3) and diffusion coefficient (cm^2/sec) of hydrogen ions, F is Faraday's constant (coulombs/equivalent), δ is crevice thickness (cm), and $j(x, t)$ is defined by Eq. (1). The dimensionless potential variable $\Phi(x, t)$ is equal to $\phi_s(x, t)\, F/RT$, where RT/F is the thermal volt equivalent (v) and $\phi_s(x, t)$ is the Galvani or inner potential of the solution phase (v). The rate of accumulation of oxygen in the crevice is described by

$$\frac{\partial C_O(x, t)}{\partial t} = D_O \frac{\partial^2 C_O(x, t)}{\partial x^2} \frac{j_0}{nF\delta} \cdot \frac{C_O(x, t)}{C_O^0}, \qquad (3)$$

where D_O is the diffusion coefficient of oxygen (cm^2/sec) and where n is the number of electrons involved in the reduction reaction. The rate of accumulation of chloride ions is given by

[6]Research jointly sponsored by the Office of Saline Water, U.S. Department of the Interior, and by the U.S. Atomic Energy Commission under contract with the Union Carbide Corporation.

[7]F. A. Posey and S. S. Misra, *Chem. Div. Ann. Progr. Rept. May 20, 1967*, ORNL-4164, p. 83.

$$\frac{\partial C_{Cl}(x,\,t)}{\partial t} = D_{Cl}\left\{\frac{\partial^2 C_{Cl}(x,\,t)}{\partial x^2} - \frac{\partial}{\partial x}\left[C_{Cl}(x,\,t)\,\frac{\partial \Phi(x,\,t)}{\partial x}\right]\right\}, \quad (4)$$

where $C_{Cl}(x,\,t)$ and D_{Cl} are the concentration (moles/cm^3) and diffusion coefficient (cm^2/sec) of the chloride ion. Equations (2), (3), and (4) must be solved simultaneously with the electroneutrality restriction, $C_H(x,\,t) = C_{Cl}(x,\,t) = C_{HCl}(x,\,t)$, and the following initial and boundary conditions:

$$\begin{aligned} &C_H(x,\,0) = C_H(0,\,t) = C^0_{HCl}\,,\\ &C_{Cl}(x,\,0) = C_{Cl}(0,\,t) = C^0_{HCl}\,,\\ &C_O(x,\,0) = C_O(0,\,t) = C^0_O\,,\\ &\left.\frac{\partial C_H(x,\,t)}{\partial x}\right|_{x=l} = \left.\frac{\partial C_{Cl}(x,\,t)}{\partial x}\right|_{x=l}\\ &\qquad = \left.\frac{\partial C_O(x,\,t)}{\partial x}\right|_{x=l} = 0\,. \end{aligned} \quad (5)$$

In boundary conditions (5) the length of the crevice is denoted by l (cm), and concentrations of hydrogen ions, chloride ions, and oxygen are maintained constant at their initial values ($C^0_H = C^0_{Cl} = C^0_{HCl}$ and C^0_O) at the mouth of the crevice.

The general solutions of Eqs. (2), (3), and (4) with the boundary conditions (5) give the transient behavior of the system in terms of relations involving Jacobian theta functions. The behavior of these general solutions is somewhat difficult to visualize without resort to numerical methods, and the distributions of concentration and potential attained in the ultimate steady state are of more direct interest. Equations (6) and (7) give the steady-state distributions of HCl and O_2 in the crevice as a function of the various parameters. The parameter P in Eqs. (6) and (7) is given by $j_0/(\delta n F D_O C^0_O)$; the quantity $1/(P)^{1/2}$ is a measure of the depth of penetration of oxygen into the crevice in the steady state:

$$\frac{C_{HCl}(x)}{C^0_{HCl}} = 1 + \frac{j_0}{2\delta F D_H C^0_{HCl}}\,x\left(l - \frac{x}{2}\right) - \frac{nD_O C^0_O}{2D_H C^0_{HCl}}\left\{1 - \frac{\cosh[\sqrt{P}(l-x)]}{\cosh(\sqrt{P}l)}\right\}, \quad (6)$$

$$\frac{C_O(x)}{C^0_O} = \frac{\cosh[\sqrt{P}(l-x)]}{\cosh(\sqrt{P}l)}. \quad (7)$$

The distribution of potential in the aqueous phase inside the crevice is given by

$$\Phi(x) - \Phi(0) = \ln\,[C_{HCl}(x)/C^0_{HCl}]\,, \quad (8)$$

where the ratio $C_{HCl}(x)/C^0_{HCl}$ is given explicitly by Eq. (6). In a manner common to other problems of this type, the potential drop in the crevice is composed additively of two components. One of these is an Ohmic potential drop, the magnitude of which may be obtained by multiplying Eq. (8) by the ratio $2D_H/(D_H + D_{Cl})$. The other component is a junction potential due to differences in mobilities of hydrogen and chloride ions; this component may be calculated by multiplying Eq. (8) by the ratio $(D_{Cl} - D_H)/(D_H + D_{Cl})$.

The importance of the present derivation lies principally in the use of Eq. (8) to estimate the potential drop developed in a crevice. It follows from Eq. (8) that the difference in interfacial potential difference $[\Delta\Phi(x)]$ between the mouth and the base of a crevice is given by

$$\Delta\phi(0) - \Delta\phi(l) = \frac{RT}{F}\ln\left\{1 + \frac{j_0 l^2}{4\delta F D_H C^0_{HCl}} - \frac{nD_O C^0_O}{2D_H C^0_{HCl}}\,[1 - \mathrm{sech}(\sqrt{P}l)]\right\}. \quad (9)$$

The interfacial potential difference at the base of the crevice is polarized negatively by the passage through the solution phase of anodic current due to the corrosion reaction. If the potential is low enough and if the hydrogen ion concentration attains a sufficiently high value, then active corrosion of the metal can commence.

The relations presented above may be used to estimate the ultimate acid concentration and potential drop developed in a crevice. Table 7.1 contains results of such a calculation, using Eqs. (6) and (9), which was based on certain assumed values of parameters thought to be typical of the titanium system. Values of corrosion rate (j_0) as a function of temperature were estimated from available experimental data. Estimates of the diffusion coefficient of the hydrogen ion were obtained from values of

Table 7.1. Estimates of Acid Concentration and Potential Drop Developed in a Titanium Crevice as a Function of Temperature[a]

T (°C)	j_0 (amp/cm^2)	D_H (cm^2/sec)	$C_{HCl}(l)$ (M)	$\Delta\phi(0) - \Delta\phi(l)$ (v)
25	2×10^{-8}	9.3×10^{-5}	5.57×10^{-2}	0.221
50	4×10^{-8}	1.35×10^{-4}	7.68×10^{-2}	0.244
100	2×10^{-7}	2.1×10^{-4}	2.47×10^{-1}	0.325
150	7×10^{-7}	2.7×10^{-4}	6.72×10^{-1}	0.405
200	2×10^{-6}	3.5×10^{-4}	1.48×10^{0}	0.485

[a]Assumed values of parameters: $\delta = 10^{-5}$ cm; $l = 1$ cm; $C^0_{HCl} = 10^{-5}$ M.

limiting equivalent conductance[8] with use of the Nernst-Einstein relation between ionic mobility and diffusion coefficient. Crevice thickness was assumed to be approximately equal to the mean surface roughness of polished metal surfaces.[9] Other measurements on the influence of hydrogen ion concentration on polarization curves of titanium and numerous observations on crevice specimens in autoclave and loop experiments show that the hydrogen ion concentration is of the order of magnitude of 1 M and the potential drop in the crevice is of the order of magnitude of 0.4 to 0.5 v before severe crevice attack in the active mode of corrosion can be initiated. The results of Table 7.1 show that temperatures of approximately 150°C and above are required to fulfill these conditions for crevices of the assumed dimensions. This conclusion is in good agreement with accumulated experience in corrosion testing of titanium crevice specimens.[10] The increase of corrosion rate with temperature determines principally whether or not sufficient acidity and potential drop can be developed in a crevice to allow initiation of active corrosion of pure titanium.

[8]A. S. Quist and W. L. Marshall, *J. Phys. Chem.* 69, 2984 (1965).

[9]*Tool Engineers Handbook*, p. 1330, American Society of Tool Engineers, McGraw-Hill, New York, 1949.

[10]J. C. Griess, Jr., "Crevice Corrosion of Titanium in Aqueous Salt Solutions," submitted to *Corrosion*.

EFFECT OF HYDROGEN ION CONCENTRATION ON THE CORROSION RATE OF PASSIVE TITANIUM[11]

D. V. Subrahmanyam[12] F. A. Posey

A kinetic model for the buildup of acid in a confined area during the initiation of crevice corrosion of titanium was reported previously.[13] There it was assumed that the corrosion rate of titanium in the passive region is essentially independent of hydrogen ion concentration except at high acidities, where corrosion rate was assumed to vary directly with hydrogen ion concentration. The model was able to account for the existence of experimentally observed induction periods for the initiation of severe crevice corrosion. The assumptions rested on fragmentary data in the literature and on various observations made in high-temperature loop and autoclave experiments.[14] We have studied in more detail the effect of hydrogen ion concentration on the corrosion of passive titanium in 1 M NaCl at temperatures below 100°C.

[11]Research jointly sponsored by the Office of Saline Water, U.S. Department of the Interior, and by the U.S. Atomic Energy Commission under contract with the Union Carbide Corporation.

[12]Visiting scientific staff member from India.

[13]F. A. Posey and S. S. Misra, *Chem. Div. Ann. Progr. Rept. May 20, 1967*, ORNL-4164, p. 83.

[14]J. C. Griess, Jr., "Crevice Corrosion of Titanium in Aqueous Salt Solutions," submitted to *Corrosion*.

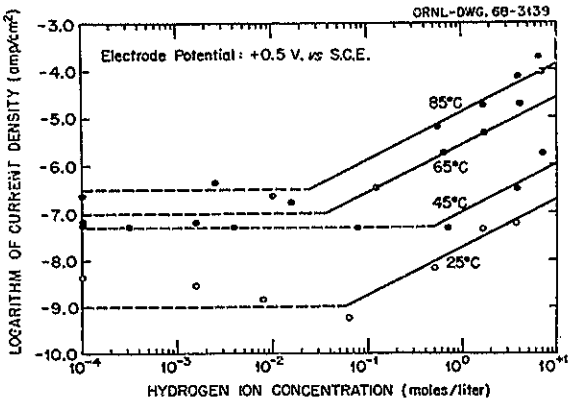

Fig. 7.5. Influence of Hydrogen Ion Concentration and Temperature on the Passive Corrosion Rate of Zone-Refined Titanium in 1 *M* NaCl.

Figure 7.5 shows experimental data on the corrosion rate of passive zone-refined titanium, held potentiostatically at an electrode potential of +0.5 v vs S.C.E., as a function of hydrogen ion concentration and temperature (10^{-6} amp/cm^2 equals approximately 0.34 mil/year for Ti). In spite of considerable scatter of the data, expectations were confirmed that the corrosion rate is practically independent of acidity up to about 0.1 *M* HCl, beyond which the rate increases in a manner proportional to the hydrogen ion concentration. Lines of unit slope were drawn through the data at high acidity in Fig. 7.5. Measurements of this type present difficulties because of problems of reproducibility and of the time required to establish steady states. A minimum of 24 hr was allowed for the attainment of a steady state for each point in Fig. 7.5. As noted above, the corrosion rate begins to depend directly on hydrogen ion concentration at about 0.1 *M* HCl. In a confined area, this is the acidity which would have to be attained in order for the corrosion reaction to become autocatalytic. Our data show no clearly defined variation of this transition region with temperature. Such data are in qualitative agreement with observations made previously in high-temperature autoclave experiments that solutions contained in highly corroded crevice regions attain acidities as high as 1 *M* HCl.[14]

ANALYSIS FOR THE CHLORIDE ION IN SALINE SOLUTIONS[15]

R. E. Meyer P. M. Lantz
F. A. Posey

A rapid chronopotentiometric method for the analysis of chloride ion in aqueous solution was described in a previous report.[16] This method is based on measurement of the transition time, τ, required to deplete the boundary layer of chloride ion when AgCl is formed on a metallic silver substrate by application of a sufficiently large anodic current. It was found possible to improve markedly the determination of the transition time by use of a derivative technique. Figure 7.6 illustrates a typical chronopotentiogram along with its time derivative. Formerly the transition time was determined by measuring the interval between the onset of polarization and the point of inflection on the rapid rise of potential that accompanies depletion of the boundary layer.

[15]Research jointly sponsored by the Office of Saline Water, U.S. Department of the Interior, and by the U.S. Atomic Energy Commission under contract with the Union Carbide Corporation.

[16]R. E. Meyer, F. A. Posey, P. M. Lantz, A. S. Lyle, and K. A. Kraus, *Chem. Div. Ann. Progr. Rept. May 20, 1967*, ORNL-4164, p. 87.

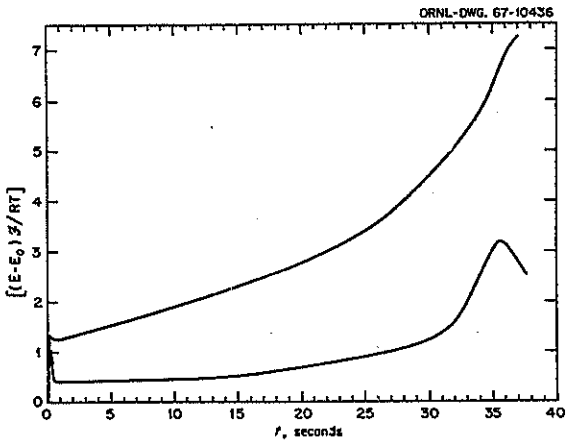

Fig. 7.6. Chronopotentiometric Wave and Its Derivative for Formation of AgCl on Ag. $C_0 = 4.86 \times 10^{-3}$ *M* NaCl, $i = 3.26 \times 10^{-4}$ amp/cm^2, transition time = 35.6 sec, 0.5 *M* Na_2SO_4.

Examination of the derivative curve shows that this point of inflection may be accurately determined by the location of the maximum of the peak.

The reproducibility of the electrode surface proved to be the most serious problem with respect to analytical accuracy. It was found that a considerable improvement could be made if a precisely timed cycle of operations was used. For this purpose automatic timer circuits were constructed which timed the anodic formation of the film, the subsequent reduction of the film, and the pause between cycles. In addition, we found that reproducibility could be improved by alternately forming and reducing a film of AgCl at the highest concentration of chloride ion likely to be encountered in the analysis.

Apparatus for the derivative and timer circuits was developed and built with the assistance of members of the Instrumentation and Controls Division.[17] This apparatus is illustrated schematically in Fig. 7.7. The derivative was supplied by a unit which made use of a Philbrick P65AU operational amplifier and a 20-μf differentiating capacitor. The output of the derivative unit and the potential of the silver electrode were both monitored with a dual-channel recorder.

Table 7.2 shows a series of determinations which were made under conditions designed to obtain maximum precision. The electrode was cali-

[17] We gratefully acknowledge the aid of L. H. Thacker in development of the derivative unit and H. G. Lingenfelter for help with the timer circuits.

ORNL-DWG. 67-10434

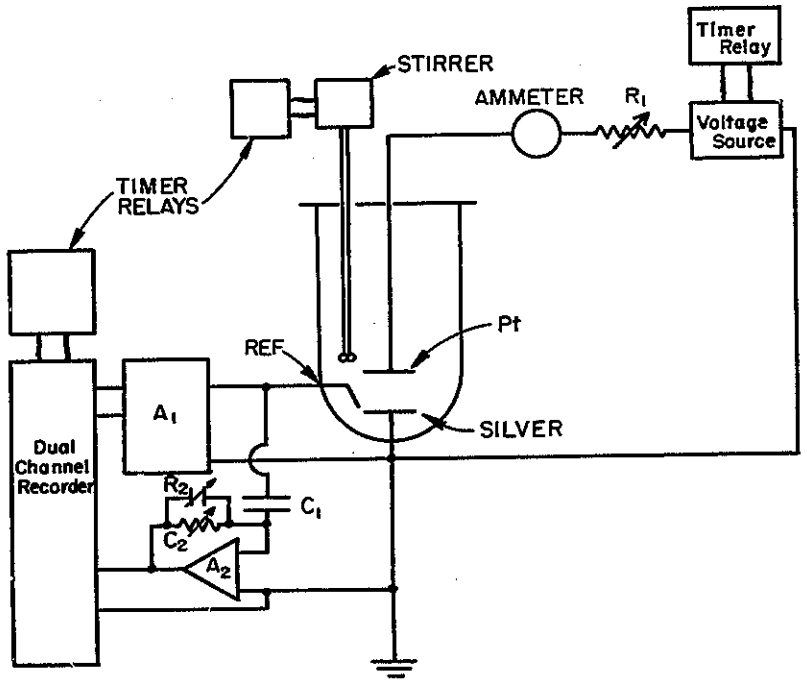

Fig. 7.7. Schematic Diagram of Apparatus for Recording Chronopotentiometric Waves and Their Derivatives. R_1, variable resistors for current control; C_1, differentiating capacitor; A_1, electrometer; A_2, operational amplifier; R_2 and C_2, resistor and capacitor used to control gain and response of derivative unit.

Table 7.2. Comparison of Chronopotentiometric and Chloridometric Methods for Chloride Analysis of Long Island Sound Water

Chloridometric (*M*)	Chronopotentiometric (*M*)	Percent Difference
0.2171	0.2123	−2.2
0.1094	0.1098	0.4
0.05537	0.05570	0.6
0.02749	0.02769	0.7
0.01388	0.01398	0.7
0.006961	0.06933	−0.4
0.001865	0.001866	0.05

brated with solutions of known concentration at transition times close to 5 sec. Unknowns were interspersed in the calibration runs using transition times of 5 sec with the same electrode surface. Unknowns were prepared by dilution with distilled water of a sample of Long Island Sound seawater as shown in Table 7.2. Analyses of the unknowns were checked with a Buchler-Cotlove chloridometer, an instrument which makes use of coulometric titration and is accurate to 1%. The agreement between the two methods of analysis is within the sum of the precision expected for the two methods.

The upper limit of concentration for practical analyses is about 0.5 *M*. Above this concentration, currents required are too large, and the electrode deteriorates rapidly. The lower limit for accurate analysis is about 0.005 *M*; below this concentration the derivative peak broadens, making it impossible to determine transition times accurately. (A manuscript describing this work in detail has been accepted for publication by the *Journal of Electroanalytical Chemistry.*)

DETERMINATION OF KINETIC CONSTANTS FROM CHRONOPOTENTIOGRAMS[18]

R. E. Meyer F. A. Posey

The standard kinetic expression for the current density of reactions of the type illustrated by anodic formation of AgCl on silver is given by the expression

$$i = i_0 \frac{C_i}{C_0} \exp\left[\alpha z(E - E_0)F/RT\right] - i_0 \exp\left[-(1-\alpha)z(E-E_0)F/RT\right] , \quad (1)$$

where i_0, the exchange current density, is

$$i_0 = nFk_a C_0 \exp\left[+\alpha z E_0 F/RT\right] = nFk_c \exp\left[-(1-\alpha)zE_0F/RT\right] . \quad (2)$$

In these equations, k_a and k_c are heterogeneous rate constants for the anodic and cathodic reactions respectively, C_i is the concentration of the diffusing ion at the interface, C_0 is the initial concentration throughout the solution, α is the transfer coefficient of the anodic reaction, and the rest of the terms have their usual significance. The equilibrium potential, E_0, is the potential that an Ag-AgCl electrode system attains at the concentration C_0, and at this potential $C_i = C_0$. Implicit in these equations is the assumption that the activity of AgCl remains constant during polarization.

The standard boundary conditions for chronopotentiometry are satisfied for this case, so that

$$C_i/C_0 = 1 - (t/\tau)^{1/2} , \quad (3)$$

where

$$\tau^{1/2} = \pi^{1/2} nFD^{1/2} C_0/2i , \quad (4)$$

D is the diffusion coefficient of the diffusing ion, and τ, the transition time, is the time at which C_i theoretically decreases to zero. On setting $\exp\left[z(E - E_0)F/RT\right] = \theta$, we have from Eqs. (1) and (3)

$$i/i_0 = (C_i/C_0)\theta^{\alpha} - \theta^{-(1-\alpha)} , \quad (5)$$

or

$$1 - (t/\tau)^{1/2} = (i/i_0)\theta^{-\alpha} + \theta^{-1} . \quad (6)$$

[18]Research jointly sponsored by the Office of Saline Water, U.S. Department of the Interior, and by the U.S. Atomic Energy Commission under contract with the Union Carbide Corporation.

If $(E - E_0)$ and τ are known, then the unknown parameters αz and i_0 may be obtained from chronopotentiometric waves by plotting the data according to the following equation, derived from Eq. (6):

$$\log [1 - (t/\tau)^{1/2} - \theta^{-1}] = \log (i/i_0) - \frac{\alpha z}{2.303} \frac{(E - E_0)F}{RT}. \quad (7)$$

The quantity on the left is plotted vs $(E - E_0)F/RT$, and the slope and intercept yield αz and i_0 respectively. This method of plotting chronopotentiometric data is particularly suitable for the analysis of quasi-reversible systems, like the Ag-AgCl system, where polarizing current densities required to achieve normal transition times are comparable in magnitude with the exchange current density.

Figure 7.8 shows a plot of data taken from a chronopotentiogram and plotted according to Eq. (7). Except for the initial section, the plot is linear, and the kinetic constants found are reasonable. Table 7.3 shows results taken for various experimental conditions. Because the formation of AgCl is not always a well-defined, reproducible process, variability in the kinetic constants is to be expected. Deviation of the initial section of the curve in Fig. 7.8 results from the fact that some overshoot is observed on the initial section of the chronopotentiograms.

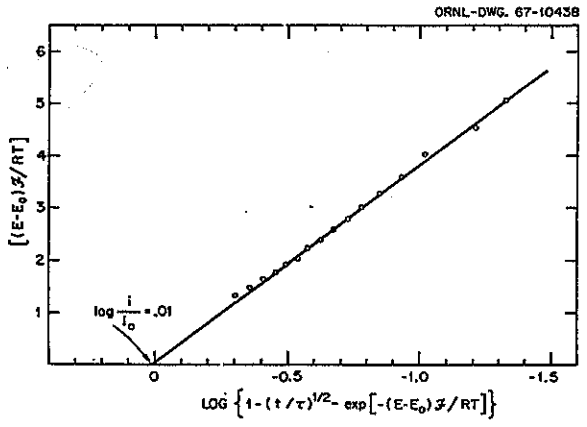

Fig. 7.8. Determination of Kinetic Constants from Chronopotentiometric Wave. $C_0 = 4.86 \times 10^{-3}$ *M* NaCl; $i = 3.26 \times 10^{-4}$ amp/cm^2; transition time = 35.6 sec; 0.5 *M* Na_2SO_4.

Table 7.3. Kinetic Constants Derived from Chronopotentiometric Waves

C_0(NaCl) (molarity)	i (amp/cm^2)	τ (sec)	α	i_0 (amp/cm^2)
$\times 10^{-3}$	$\times 10^{-4}$			$\times 10^{-4}$
4.9	2.56	56.7	0.63	3.32
4.9	4.42	20.6	0.52	4.07
4.9	6.63	9.7	0.56	6.19
4.9	8.85	5.8	0.56	5.92
4.86	3.26	35.6	0.61	3.17
9.93	8.40	19.75	0.79	6.10
49.5	33.5	29.7	0.71	22.8

INFLUENCE OF INERT ELECTROLYTES ON CHRONOPOTENTIOMETRIC CONSTANTS[19]

F. A. Posey R. E. Meyer

Measurements of transition times in chronopotentiometry are influenced by the presence of inert electrolytes. In studies on the Ag-AgCl system, a large number of measurements of the "chronopotentiometric constant" have allowed us to assess in some detail effects of ionic strength and of the presence of inert electrolytes on the determination of chloride ion concentration by this method. Longer transition times are observed as the relative concentration of inert electrolyte decreases, because the transference number of the reacting ion, Cl^- in this case, becomes appreciable compared with the transference numbers of the current-carrying ions.

Some insight into the influence of inert electrolyte on the chronopotentiometric constant may be obtained by solution of a special case of the transport equations which apply to the motion of ions in the chronopotentiometric situation. We have treated the case where three ions are present in the system: Na^+, Cl^-, and X^-, where X^- is an inert univalent anion. Assumed conditions correspond to anodic chronopotentiometry with

[19]Research jointly sponsored by the Office of Saline Water, U.S. Department of the Interior, and by the U.S. Atomic Energy Commission under contract with the Union Carbide Corporation.

the silver electrode of NaCl of initial concentration C_0 in the presence of added inert electrolyte, NaX, of concentration C_1. The appropriate system of transport equations can be solved explicitly only for the special case where all diffusion coefficients are equal, so that $D_{Na} = D_{Cl} = D_X = D$. Here we present only final results and do not consider details of concentration and potential profiles during the course of the chronopotentiometric transient.

The time required for the chloride ion concentration at the electrode surface to reach zero is the transition time (τ). Equation (1) gives the transition time as a function of the initial concentration of NaCl (C_0) and of inert electrolyte, NaX (C_1):

$$\tau^{1/2} = \frac{F(\pi D)^{1/2}}{j} \times \left[(C_0 + C_1) - \sqrt{C_1(C_0 + C_1)} \right]. \quad (1)$$

In Eq. (1), j is applied current density (amp/cm^2), and F is Faraday's constant (coulombs/equivalent). The chronopotentiometric constant is given by $\gamma = j\sqrt{\tau}/C_0$, and if one recalls that $\gamma_0 = F\sqrt{\pi D}$ is the value of this constant in the absence of inert electrolyte, then Eq. (2) is obtained for the relative value of the chronopotentiometric constant as a function of the ratio of inert electrolyte (NaX) to NaCl, C_1/C_0:

$$\frac{\gamma}{\gamma_0} = 1 + \frac{C_1}{C_0} - \sqrt{\frac{C_1}{C_0}\left(1 + \frac{C_1}{C_0}\right)}. \quad (2)$$

The behavior of this function is shown in Fig. 7.9.

The noteworthy feature of the result shown in Fig. 7.9 is that whereas the chronopotentiometric constant observed in nearly pure NaCl solutions is very sensitive to small amounts of inert electrolyte, the constant observed in excess of inert electrolyte is remarkably insensitive to the ratio C_1/C_0. For example, the chronopotentiometric

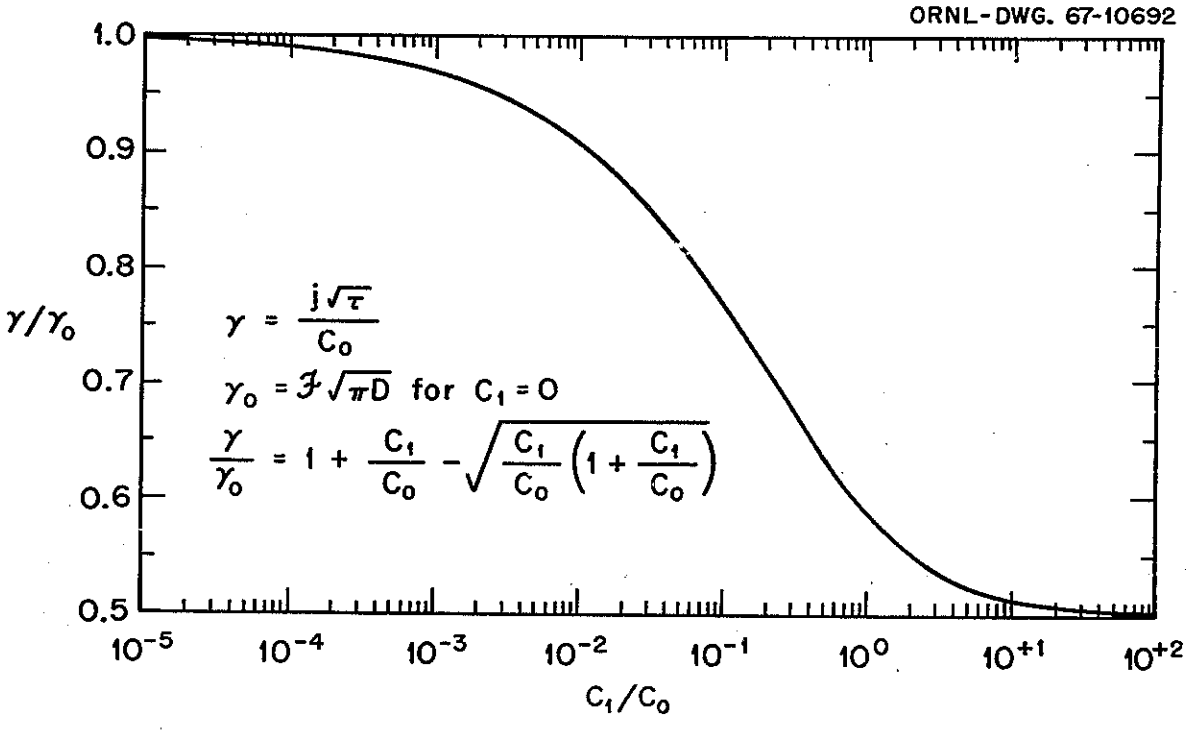

Fig. 7.9. Variation of Chronopotentiometric Constant with Concentration of Inert Electrolyte ($D_{Na} = D_{Cl} = D_X = D$).

constant for $C_1/C_0 = 10^{-3}$ is about 3% different from that in the absence of inert electrolyte. However, for $C_1 = C_0$ the constant differs from that for the limiting case of large excess of inert electrolyte by only about 17%. This result suggests the possibility of using intentional additions of inert electrolyte to suppress effects of low levels of inert salts on the chronopotentiometric constant. The effect of inert electrolyte on chronopotentiometric constants in other cases is not as amenable to complete analysis as the case treated here. However, the behavior is expected to be similar to that noted above.

CHRONOPOTENTIOMETRY IN FLOWING STREAMS[20]

R. E. Meyer P. M. Lantz
F. A. Posey

Chronopotentiometry shows promise for analyses in flowing streams because individual determinations of the transition time may be made in only a few seconds. However, the boundary conditions of the mathematics upon which chronopotentiometry is based require that the solution be quiescent during an individual determination. Two approaches are therefore possible in designing a system for analytical purposes. One is the obvious approach of temporarily stopping the flow and waiting for the solution to become quiescent. The other approach is to determine the transition time, if possible, while the solution is flowing and to investigate effects of various parameters such as flow rate upon the transition time. We are following the latter approach in systems in which fully developed laminar flow is present.

The experimental arrangement used in these studies is shown schematically in Fig. 7.10, where a rectangular electrode of length l and width w is located flush with one of the surfaces of the channel ($y = 0$). The width of the channel (d) was approximately eight times larger than the channel height (h) to ensure favorable hydrodynamic conditions and to avoid undesirable end effects. The midstream velocity is denoted by U_0. The polarizing electrode, not shown in Fig. 7.10, was located above the test electrode in the opposite channel wall ($y = h$) to ensure, as far as possible, uniform current density. In order to aid development of laminar flow, a diffuser was located at a distance L upstream from the test electrode. The entire experimental assembly was machined from Lucite into which electrodes of sheet material were cemented with epoxy.

Measurements of the transition time as a function of solution flow rate are shown in Fig. 7.11 for electrodes of various sizes and shapes. At low flow rates, transition times are the same as those observed in quiescent solution. As the flow rate is increased the transition time at first remains nearly the same but ultimately increases

ORNL-DWG. 68-3137

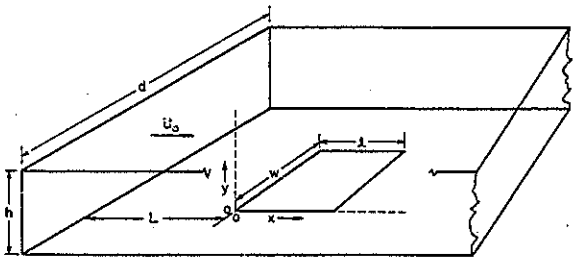

Fig. 7.10. Typical Experimental Configuration for Electroanalysis in Flowing Solution.

ORNL-DWG. 68-3138

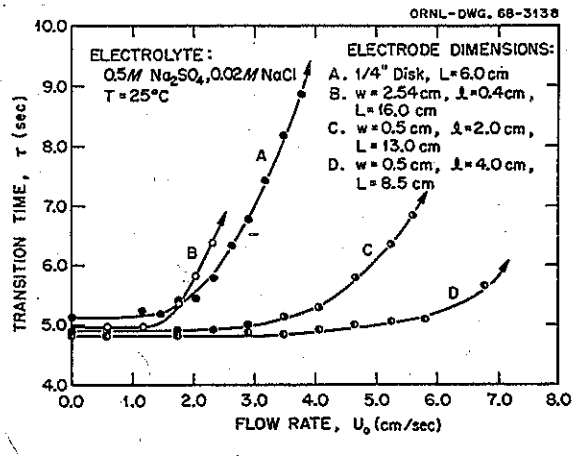

Fig. 7.11. Variation of Transition Time with Flow Rate for the Analysis of Chloride Ion with the Silver Electrode.

[20]Research jointly sponsored by the Office of Saline Water, U.S. Department of the Interior, and by the U.S. Atomic Energy Commission under contract with the Union Carbide Corporation.

due to partial replenishment of the boundary layer by the flow. On further increase of the solution velocity it becomes no longer possible to observe transition times. At midstream the solution is actually exchanged several times during the course of the measurement under ordinary circumstances. However, the transition time is sensitive to conditions only in the diffusion boundary layer (about 10^{-3} to 10^{-2} cm), and it will be recalled from hydrodynamic theory that solution velocity drops off to zero at the wall. In effect, therefore, during an individual measurement only slight exchange of solution occurs in the boundary layer. The fact that velocities are low at the boundaries of the cell has the undesirable effect that the response of the system to changes in concentration will be slower than one would expect considering the average velocity.

For analytical purposes it is essential to develop guidelines which relate observables to system parameters such as channel and electrode dimensions and flow rates. We have also developed mathematical descriptions of chronopotentiometry and voltammetry in flowing streams for several modes of operation. Further experimental work is in progress to test the validity and utility of these predictions.

8. Nonaqueous Systems at High Temperature

MOLTEN-SALT–METAL SOLUTIONS

EMF Measurements in Molten Rare-Earth Metal–Metal-Halide Solutions

Harry R. Bronstein

In continuation of an electrochemical study of metal-salt interactions[1-3] the following systems were investigated: Ce-$CeBr_3$, Pr-$PrBr_3$, and La-LaI_3.

Previous measurements employing a cell of the type

$$Ta|MCl_3,\ M^0(\text{dissolved})|KCl\left|\begin{matrix}\text{Vycor}\\ \text{glass}\end{matrix}\right|KCl|Cl_2,\ C$$

demonstrated a similar electrochemical behavior for Ce-$CeCl_3$, Pr-$PrCl_3$, and Nd-$NdCl_3$ solutions. In all three systems the presence of a lower-valent species formed on dissolving the metal in the trichloride according to

$$M + 2MCl_3 \longrightarrow 3MCl_2$$

explained the results. The data fitted a cell reaction $MCl_2 + \frac{1}{2}\ Cl_2 \rightleftharpoons MCl_3$, that is, an oxidation-reduction process at the electrode involving the transfer of one electron:

$$M^{2+} \longrightarrow M^{3+} + e^- \ .$$

This similarity was in marked contrast to the electrical conductance behavior, which varied from a sizable nonionic (i.e., electronic) contribution in the Ce-$CeCl_3$ solutions to a negligible one in the Nd-$NdCl_3$ solutions.[4] Current theories regarding the conduction mechanism of the electronic component of dilute solutions of metals in molten salts postulate a very small mean free path for the electron – a "hopping" of an electron between metal ions in different valence states.[5-9] The magnitude of the electronic (not metal-like) contribution to the overall conductivity by this mechanism reflects the "intrinsic jump frequency" – greatest for the electron in the Ce-$CeCl_3$ solution and negligible in the Nd-$NdCl_3$ solutions.

The emf results for the La-$LaCl_3$ and the La-$LaBr_3$ solutions at metal concentrations below approximately 3 mole % were similar to those for the above systems. Deviation from this behavior with increasing concentration was interpreted as possibly indicating the polymerization of the divalent cation, La^{2+}, to a trimer, $(La^{2+})_3$, which in its electrochemical behavior might be indistinguishable from a "solvated metal atom," $La(LaX_3)_2$.

The present results for the Ce-$CeBr_3$ and the Pr-$PrBr_3$ solutions are those anticipated in that the electrochemical behavior conforms to a one-electron transfer at the electrode, $M^{2+} \rightarrow M^{3+} + e^-$. This is shown by Fig. 8.1, a plot of the emf vs $\log_{10}(N_{PrBr_3}/N_{PrBr_2})$ for the cell

---

[1] H. R. Bronstein, *J. Electrochem. Soc.* 112, 1032 (1965).

[2] H. R. Bronstein, *Chem. Div. Ann. Progr. Rept. May 20, 1966*, ORNL-3994, p. 98.

[3] H. R. Bronstein, *Chem. Div. Ann. Progr. Rept. May 20, 1967*, ORNL-4164, p. 97.

[4] Cf. reviews by M. A. Bredig, "Mixtures of Metals with Molten Salts," in *Molten Salts* (ed. by Milton Blander), Interscience, New York, 1964; and by J. D. Corbett, "The Solutions of Metals in Their Molten Salts," in *Fused Salts* (ed. by B. R. Sundheim), McGraw-Hill, New York, 1964.

[5] M. A. Bredig, *J. Chem. Phys.* 37, 914 (1962).

[6] K. S. Pitzer, *J. Am. Chem. Soc.* 84, 2025 (1962).

[7] S. A. Rice, *Discussions Faraday Soc.* 32, 181 (1961).

[8] D. O. Raleigh, *J. Chem. Phys.* 38, 1677 (1953).

[9] K. Ichikawa and M. Shimoji, *Trans. Faraday Soc.* 62, 3543 (1966).

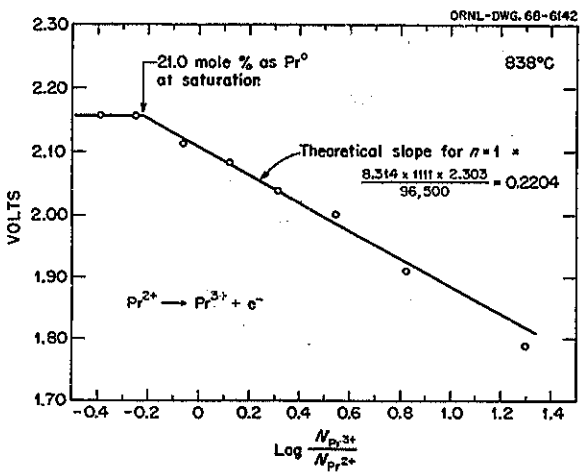

Fig. 8.1. E in Relation to $\log_{10} (N_{Pr^{3+}}/N_{Pr^{2+}})$, 838°C, for the cell

$$Ta|PrBr_3,\ x\ Pr^0(\text{dissolved})|KBr\left|\begin{matrix}\text{Vycor}\\ \text{glass}\end{matrix}\right|KCl|Cl_2, C.$$

$$Ta|PrBr_3,\ PrBr_{(3-n)}|KBr\left|\begin{matrix}\text{Vycor}\\ \text{glass}\end{matrix}\right|KCl|Cl_2,\ C\ .$$

Again, as in the La-$LaCl_3$ and La-$LaBr_3$ solutions, at metal concentrations to 4 mole %, the La-LaI_3 solutions obey the one-electron process. However, with increasing concentration of metal, polymerization of the divalent cation, La^{2+}, to a trimer $(La^{2+})_3$ apparently occurs, and the electrode process seems to be $(La^{2+})_3 \rightarrow 3La^{3+} + 3e^-$. This apparent polymerization of lanthanum is somewhat reminiscent of that of bismuth metal in its molten halide solutions.[4]

The solubility limits determined by the emf technique are in very good agreement with values obtained by other methods (see last two columns of Table 8.1). The large discrepancy in the solubility of La in LaI_3 as determined by the emf technique (25 mole % La^0) and as obtained from phase equilibria (33 mole % La^0) is as yet unexplained.

At saturation the solutions are in equilibrium with essentially pure (liquid or solid) metal. In

Table 8.1. EMF, Junction Potentials, and Solubilities in Some Molten Rare-Earth Metal–Metal-Halide Systems

System	Temperature (°C)	Measured EMF (v) at Saturation (Metal Phase Present)[a]	Estimated EMF (v) from Literature E^0 Values for MX_3, $\gamma_{MX_3} = 1$	Liquid Junction Potential (v)		Solubility (mole % metal)	
				Estimated	Experimental E_j	Emf Method	Electrical Conductance and Phase Equilibrium
La-$LaCl_3$	895	2.350	2.944	0.594		8.5	9.0
La-$LaBr_3$	812	2.370 (2.116)[a]	2.560	0.444		14.0	14.5
La-LaI_3	845	2.170 (1.411)	1.920	0.509		25.0	33.0
Ce-$CeCl_3$	855	2.350	2.924	0.574	0.600	8.6	9.0
Ce-$CeBr_3$	804	2.310 (2.056)	2.502	0.446		13.0	13.5
Pr-$PrCl_3$	855	2.400	2.903	0.503		16.4	17.8
Pr-$PrBr_3$	838	2.158 (1.904)	2.465	0.560		21.0	20
Nd-$NdCl_3$	800	2.150[b]			0.570	25.0	26.0

[a] Potentials measured vs the (Vycor|KCl|Cl_2, C) reference electrode. Values in parentheses are converted to the proper anion electrode.

[b] At saturation, phase in equilibrium with solution is solid $NdCl_2$.

these cases, with the exception of the Nd-$NdCl_3$ system, where solid $NdCl_2$ is present, the measured cell potentials can be compared with approximate cell potentials as calculated from estimated values of the standard free energies of formation of the trihalides.[10] Unity is assumed for the activity coefficient of the trihalide. Also, by using the E^0 values for KBr and KI, the measured potentials obtained with the Vycor|KCl|Cl_2, C reference electrode may be converted to the potential which would pertain to KBr|Br_2, C or KI|I_2, C electrodes.

Columns 3 and 4 of Table 8.1 show discrepancies of several hundred millivolts between experimental and estimated emf values. These rather sizable differences are attributed to surprisingly large liquid junction potentials existing at the boundary between the molten rare-earth solutions and the bridging KCl melt. To explain the differences otherwise would require the absurd activity coefficient of 10^6 for the various trihalides.[11]

For a direct experimental demonstration of the occurrence of a liquid junction potential of the magnitude estimated, the following cells were examined:

$$(+),\ C,\ Cl_2|NdCl_3\left|\begin{matrix}\text{quartz}\\ \text{frit}\end{matrix}\right|KCl\left|\begin{matrix}\text{Vycor}\\ \text{glass}\end{matrix}\right|KCl|Cl_2,\ C,\ (-) \quad (A)$$

$$(+),\ C,\ Cl_2|CeCl_3\left|\begin{matrix}\text{quartz}\\ \text{frit}\end{matrix}\right|KCl\left|\begin{matrix}\text{Vycor}\\ \text{glass}\end{matrix}\right|KCl|Cl_2,\ C,\ (-) \quad (B)$$

Cell *A*, at 800°C, gave 0.570 v and cell *B*, at 850°C, 0.600 v, that is, liquid junction potentials of the order of magnitude estimated. If 0.600 v from cell *B* is added to the observed potential at saturation for the Ce-$CeCl_3$ system, the agreement of the resulting value, 2.950 v, with the estimated value, 2.924 v, is remarkable considering the assumption of $\gamma = 1$ made for the $CeCl_3$.

[10] W. J. Hamer, M. S. Malmberg, and B. Rubin, *J. Electrochem. Soc.* 103, 8 (1956) and 112, 750 (1965).

[11] A similar disagreement by 0.7 v, observed by S. Senderoff and G. W. Mellors [*J. Electrochem. Soc.* 105, 224 (1958)] for the cell

$$Mo|Ce_{(sat'd)},\ CeCl_3||CeCl_3|Cl_2,\ C$$

must be interpreted as having resulted from an unsuspected reaction of the melt with the ceramic container and asbestos diaphragm [H. R. Bronstein, A. S. Dworkin, and M. A. Bredig, *J. Phys. Chem.* 64, 1344 (1960) and 66, 44 (1962)]. Such an extreme junction potential would be impossible for the rather similar liquids of this cell.

It has been demonstrated previously that the potential of the reference electrode system including its junction with the metal–metal-halide solution does not change within the time necessary to complete the experiment or with variation of the concentration of the solution studied.[1] Therefore, the measured dependence of the emf on concentration is not affected by the magnitude of the liquid junction potential.

The Solubility of Thorium Metal in Molten Lithium Fluoride–Thorium Tetrafluoride Mixtures

H. R. Bronstein M. A. Bredig

A knowledge of the free energy of formation of ThF_4 in various molten mixtures of LiF-ThF_4 would be of value to the MSRB reprocessing study. An emf study of a cell of the type

$$Th^0|xThF_4,\ (1-x)\,LiF|H_2,\ HF,\ Pt$$

is the most obvious method for determining this quantity. The cell container must of necessity be nickel because of the presence of HF in the H_2, HF, Pt electrode.

However, a study by C. J. Barton and H. H. Stone[12] has cast some doubt about the feasibility of such measurements in a nickel container. A thorium rod suspended in a molten mixture of the LiF-ThF_4 (73 and 27 mole % respectively), contained in a nickel crucible, disappeared after 16 hr at 600°C. Black magnetic material removed from the cooled melt analyzed 45% Ni and 30% Th, while nonmagnetic material contained 22% Ni and 49.5% Th. An explanation was based on the possibility that a subfluoride of thorium forms, for example, according to

$$3ThF_4 + Th^0 \longrightarrow 4ThF_3\ ,$$

and that the ThF_3, when it diffuses to the nickel wall, disproportionates because of the formation of the Th-Ni intermetallic compound. However, the speculative nature of this explanation was emphasized as very little is known about the existence of a ThF_3.[13]

[12] C. J. Barton and H. H. Stone, ORNL-TM-2036 (November 1967).

[13] J. C. Warf, *J. Am. Chem. Soc.* 74, 1864 (1952).

If such a reaction with the nickel container actually occurs, severe complications would arise in an attempt to measure the free energy of formation of ThF_4 in the above cell. Before abandoning this much-preferred cell arrangement, a reinvestigation of the reaction of Th^0 with the $LiF\text{-}ThF_4$ melt was deemed desirable.

A carefully dehydrated mixture of $LiF\text{-}ThF_4$ (73 and 27 mole % respectively) was melted in a thorium crucible and held in the molten state under an atmosphere of dry argon at 620°C. The melt was occasionally stirred with a thorium stirrer. After a heating period of 16 hr, a sample of the molten liquid was withdrawn in a tantalum cup. The apparatus utilized for this experiment has been previously described[14] and illustrated.[15]

The analysis of the sample indicated that approximately 2.0 mole % thorium metal had apparently dissolved in the melt. However, the errors involved in the determination of the total fluorine, thorium, and lithium contents were such that the value of the above solubility of thorium in the melt is very much in doubt. A different technique was therefore used in subsequent tests.

A $\frac{1}{8}$-in. nickel rod was suspended in the melt for a period of 5 hr at 620°C. At the termination of the experiment the solidified melt was removed from the thorium crucible. A blackish layer of material was found at the bottom of the melt. Apparently segregation had occurred upon slow cooling. This black material reacted with hydrochloric acid.

A volumetric determination of the gas evolved from a weighed sample of this material on treatment with acid yielded a value of 12% by weight as thorium metal, assuming the total gas was hydrogen. Spectrographic analysis showed the presence of only very minor quantities of other metals as impurities. Of some significance is the absence of detectable quantities of nickel, possibly attributable to the very small surface ratio of nickel rod to thorium crucible. X-ray examination of the blackish material showed lines mainly of the compounds existing in the original melt composition,[16] that is, principally $3LiF\cdot ThF_4$ and a small amount of $Li_7Th_6F_{31}$. Two additional, very weak lines were also noted probably from the black material which microscopic examination showed to be finely dispersed throughout.

To increase the surface ratio of nickel to thorium, a nickel crucible was employed to contain the melt. The melt was occasionally stirred by means of the thorium metal stirrer. Samples were taken at temperature. These samples were treated with acid, and the volume of gas collected, assumed to be hydrogen, was found to correspond to a thorium metal solubility of 0.1 mole %. Again, nickel was not detected analytically. From the bottom of the melt, after cooling, blackish specks were separated from the bulk of the melt. These were treated with sulfuric acid, and the gas evolved was collected and analyzed mass spectrographically. The gas showed the presence of hydrogen and the absence of gases derived from carbides, phosphides, or sulfides.

Our results place an upper limit of 0.1 mole % on the solubility of thorium metal in molten Li_3ThF_7. At this time we have no explanation for the apparent discrepancy between our results and those of Barton and Stone,[12] except possibly the absence of gas stirring in our experiments.

(Note added in proof: Without change in the low solubility value we have now verified the findings of Barton and Stone by gas stirring of the melt. Details will be reported separately.)

Metal–Metal-Fluoride Miscibility

A. S. Dworkin M. A. Bredig

We had suggested[17] that some of the rare-earth metal–metal-difluoride systems (Eu, Sm, and Yb) might exhibit complete miscibility similar to that found for the alkaline-earth fluoride systems, the metals having similar heats of vaporization. We have measured the SmF_2-Sm and YbF_2-Yb systems with our cooling curve apparatus, holding the mixtures in tantalum capsules. The results in Fig. 8.2 do indeed show that the miscibility of the YbF_2-Yb system is between that of CaF_2-Ca and that of BaF_2-Ba. These findings represent the first observation of complete miscibility, in the liquid state, of a rare-earth metal with one of its halides.

[14] H. R. Bronstein, A. S. Dworkin, and M. A. Bredig, *J. Phys. Chem.* 66, 44 (1962).

[15] A. S. Dworkin, H. R. Bronstein, and M. A. Bredig, *Discussions Faraday Soc.* 32, 188 (1962).

[16] R. E. Thoma (ed.), *Phase Diagrams of Nuclear Reactor Materials*, ORNL-2548, p. 72 (1959).

[17] A. S. Dworkin and M. A. Bredig, *Chem. Div. Ann. Progr. Rept May 20, 1967*, ORNL-4164, pp. 95–100.

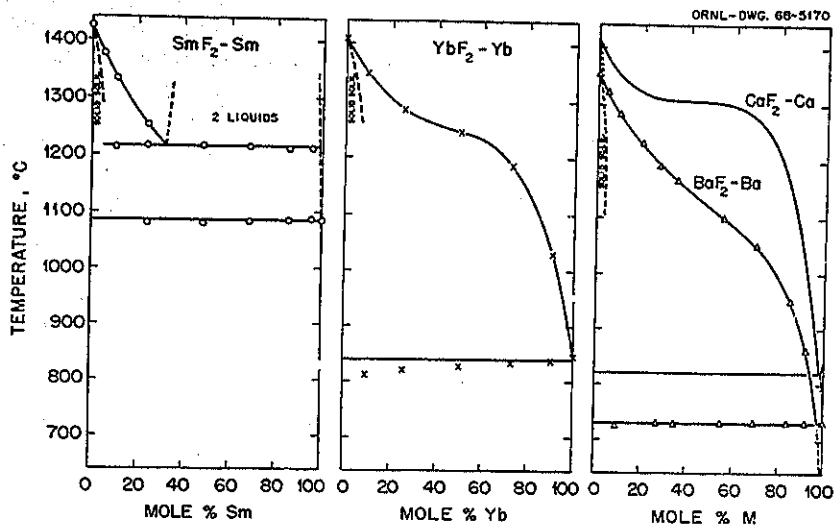

Fig. 8.2. Equilibrium Phase Diagrams of Metal Fluoride–Metal Systems, MF_2-M (M = Sm, Yb, Ca or Ba).

It is the only example among these systems, thus far, of the absence of a miscibility gap at any temperature and is likely to be joined by only one other rare-earth metal-salt system, EuF_2-Eu. There is a large monotectic solubility of Sm in SmF_2 (32 mole %), but from that concentration to almost 100% Sm a large miscibility gap exists. We would predict that the EuF_2-Eu system is very similar to CaF_2-Ca and that, if TmF_2 is stable, the solubility of Tm metal in liquid TmF_2 is much less than that of Sm in SmF_2, as the heat of vaporization of Tm exceeds that of Sm by 13 kcal/mole.

The dotted solid solution lines in Fig. 8.2 were estimated on the basis of a two-particle effect ($Yb \rightarrow Yb^{2+} + 2e^-$) on the melting points of the difluorides and of an estimated entropy of fusion for these salts of 4 eu/mole. This figure is based on our assumption that the rare-earth difluorides, having the fluorite type of structure, are similar to the alkaline-earth fluorides in that they have a diffuse transition in the solid and a low entropy of fusion.

Our values for the melting points of the Yb and Sm metals are somewhat higher than those found in the literature. We believe this is due to a small amount of oxygen in the metals we used, which raises the melting point. The melting points of YbF_2 and SmF_2, 1407 and 1425°C, respectively, agree quite well with those in the literature.

We have also attempted to measure the solubility of Nd in NdF_3, and as in the CeF_3-Ce and LaF_3-La systems we find little or no solubility.

HIGH-TEMPERATURE THERMOCHEMISTRY

Heat Contents of $NaBF_4$, $NaBF_4$-NaF (92-8 Mole %), and LiF-BeF_2-ThF_4 (72-16-12 Mole %)

A. S. Dworkin M. A. Bredig

The heat contents of a proposed MSBR coolant, $NaBF_4$-NaF (92-8 mole %), and a possible single-region MSBR fuel salt mixture, LiF-BeF_2-ThF_4 (72-16-12 mole %), were measured using a copper block drop calorimeter. Each mixture was contained in a sealed platinum capsule, which in turn was sealed into an Inconel capsule especially designed for our heat content apparatus.

The following equations were obtained for the heat content, $H_t - H_{25°C}$, of the $NaBF_4$-NaF eutectic in calories per gram:

$$H_t - H_{25} = -5.90 + 2.30 \times 10^{-1} t + 2.90 \times 10^{-4} t^2,\ 25\text{–}243°C;\ \pm 0.5\%$$

$$\Delta H_{trans} = 14.5 \pm 0.3\ cal/g,\ 243°C$$

$$H_t - H_{25} = 0.39 + 3.37 \times 10^{-1} t,\ 243\text{–}381°C;\ \pm 0.2\%$$

$$\Delta H_{fusion} = 31.0 \pm 0.3\ cal/g,\ 381°C$$

$$H_t - H_{25} = 22.1 + 3.60 \times 10^{-1} t,\ 381\text{–}600°C;\ \pm 0.1\%$$

The specific heat of the liquid is then the derivative of the last equation or 0.360 cal g^{-1} $°C^{-1}$ with an estimated error of less than 2%.

The heat content of pure $NaBF_4$ was calculated from the above data by subtracting the contribution of the NaF assuming no heat of mixing. Kelley's measurements of the high-temperature heat content of NaF[18] were used in the calculations. The following equations were derived for the heat content, $H_T - H_{298°K}$, of $NaBF_4$ in calories per mole:

$$H_T - H_{298} = -4.965 \times 10^3 + 6.716T + 3.336 \times 10^{-2} T^2,\ 298\text{–}516°K;\ \pm 0.5\%$$

$$\Delta H_{trans} = 1630 \pm 30\ cal\ mole^{-1},\ 516°K;\quad \Delta S_{trans} = 3.15\ eu/mole$$

$$H_T - H_{298} = -10.196 \times 10^3 + 37.22T,\ 516\text{–}679°K;\ \pm 0.2\%$$

$$\Delta H_{fusion} = 3090 \pm 60\ cal/mole,\ 679°K;\quad \Delta S_{fusion} = 4.55\ eu/mole$$

$$H_T - H_{298} = -8.514 \times 10^3 + 39.29T,\ 679\text{–}900°K;\ \pm 0.1\%$$

Figure 8.3 represents the derived results for the heat content of $NaBF_4$.

The following equations represent the data tor LiF-BeF_2-ThF_4 (72-16-12 mole %) in calories per gram:

$$H_t - H_{25} = -5.28 + 2.07 \times 10^{-1} t + 6.33 \times 10^{-5} t^2,\ 25\text{–}445°C;\ \pm 0.5\%$$

[18] K. K. Kelley, *U. S. Bur. Mines Bull.* 584, 171 (1960).

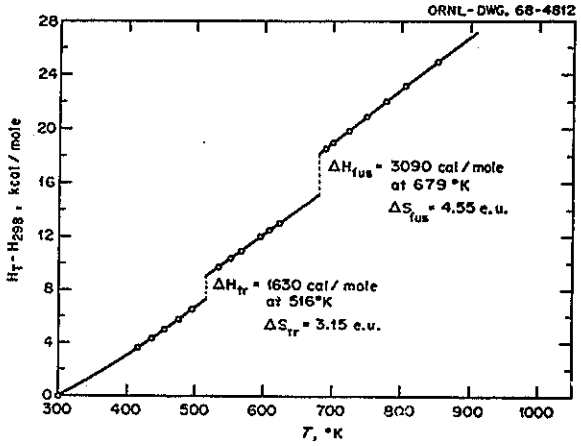

Fig. 8.3. Heat Content, $H_T - H_{298}$, of $NaBF_4$.

$$H_t - H_{25} = 11.34 + 3.237 \times 10^{-1} t,\ 500\text{–}750°C;\ \pm 0.1\%$$

There is no isothermal heat of fusion for the mixture. According to the phase diagram, the mixture partially melts isothermally at about 445°C, after which the melting continues to 500°C, at which temperature it is completely liquid. No experimental points were obtained in the temperature interval 445 to 500°C.

Using the above data together with suitable literature data, the specific heats of various possible fuel salt mixtures have been estimated to about 4% for molten-salt reactor engineering purposes.

Nonideality of Mixing in Potassium Fluoroborate–Sodium (or Potassium) Fluoride Systems[19]

M. A. Bredig

Experimental phase diagram data available from work in the Reactor Chemistry Division[20] were examined for deviations from ideality of mixing.

[19] For more details see *MSR Program Semiann. Progr. Rept. Feb. 29, 1968*, ORNL-4254.

[20] C. J. Barton *et al.*, *MSR Program Semiann. Progr. Rept. Aug. 31, 1967*, ORNL-4191, pp. 158–59, Figs. 13.1 to 13.4.

Liquidus curves for KF and NaF, in the binary system KF-KBF_4 and the reciprocal salt system NaF-KBF_4, respectively, were slightly revised in accordance with an appropriate application of the known enthalpies of fusion, ΔH_m, of NaF and KF. It became apparent that the KF-KBF_4 system deviates little from ideality, whereas the reciprocal salt mixtures NaF-KBF_4, containing cations and anions of widely differing sizes, show large positive deviations from ideality. The latter were estimated semiquantitatively in terms of the partial molar excess free energy of NaF, $\bar{G}^E_{NaF}$, by means of the equation

$$\bar{G}^E_{NaF} = RT \ln \gamma_{NaF} = \Delta H_m [(T/T_m) - 1] + \Delta C_p (T_m - T) - T \Delta C_p \ln (T_m/T) - RT \ln N^2_{NaF} ,$$

with $\Delta C_p = 1.0$ cal deg^{-1} mole^{-1}. The excess chemical potential of NaF is not simply proportional to $a_{KBF_4} = (1 - N_{NaF})^2$, the ideal "Temkin" activity of KBF_4. The shape of the NaF liquidus and the high value (12,000 cal/mole) of $\bar{G}^E_{NaF}$ below $a_{KBF_4} = 0.1$ suggest strongly that replacement of NaF by LiF together with that of $CsBF_4$ for KBF_4 would lead to separation into two molten salt phases.

Heat Content of Lanthanide Bromides and Iodides

A. S. Dworkin M. A. Bredig

High-temperature heat content measurements have been made for eight rare-earth bromides and iodides. Together with the measurements for six rare-earth chlorides reported last year,[21] this work puts the high-temperature thermochemistry of members of this important group of halides on an experimental basis for the first time.

Table 8.2 gives the coefficients of the equation for the temperature dependence of the enthalpy for the eight bromides and iodides. Table 8.3 lists the enthalpy and entropy of fusion (and transition when applicable) of these eight together with others measured previously.[22,23] The structure type at room temperature and the entropy at 1300°K relative to that at room temperature are also listed. This high temperature (at which much of the entropy data is extrapolated) is chosen so as to permit a comparison of the entropy of all these halides in the liquid state.

For most of the halides (chlorides, bromides, and iodides) of $Y(OH)_3$, $PuBr_3$, and BiI_3 structures, $\Delta S_m + \Delta S_{tr}$ is about 12 ± 1 eu/mole. The slight differences among them are likely due to various ion size effects. However, the YCl_3-type compounds (YCl_3, $DyCl_3$, $HoCl_3$, and $ErCl_3$) have a significantly lower ΔS_m (~7.5 eu/mole) and $S_{1300°K} - S_{298}$ (~46.5 eu/mole) The crystal structure of the heavy rare-earth bromides has not been reported as yet, but on the basis of our results for $GdBr_3$ and $HoBr_3$ we would predict that they also have the YCl_3 structure. One might expect the entropy of all the rare-earth halides in the liquid to be very similar. However, this is not the case for the YCl_3-type compounds, indicating that they have either a higher degree of order in the liquid or a higher entropy in the solid below room temperature where no C_p data are as yet available.

Although a transition has been reported for GdI_3,[24] the small heats of transition for GdI_3 and TbI_3 and T_{tr} for TbI_3 were measured in this work for the first time.

Diffuse Transitions in Compounds of the Fluorite and Antifluorite Type

A. S. Dworkin M. A. Bredig

In previous reports[25,26] we have shown that simple substances of the type AB_2, such as CaF_2, $SrCl_2$, and K_2S, which possess either the fluorite or the antifluorite type of crystal structure have abnormally low entropies of fusion. On the basis

[21] A. S. Dworkin and M. A. Bredig, *Chem. Div. Ann. Progr. Rept. May 20, 1967*, ORNL-4164, pp. 95–100.

[22] A. S. Dworkin and M. A. Bredig, *J. Phys. Chem.* 67, 697 (1963).

[23] *Ibid.*, p. 2499.

[24] J. E. Mee and J. D. Corbett, *Inorg. Chem.* 4, 88 (1965).

[25] A. S. Dworkin and M. A. Bredig, ORNL-3832, p. 111 (1965).

[26] A. S. Dworkin and M. A. Bredig, *J. Chem. Eng. Data* 8, 416 (1963).

Table 8.2. Coefficients for Enthalpy Equations

$H_T - H_{298}$ (cal/mole) $= a + bT + cT^2 + dT^{-1}$

Compound	a	b	c	d	Average Percent Error	Temperature Range (°K)
	$\times 10^3$		$\times 10^{-5}$	$\times 10^4$		
$CeBr_3$	−7.003	22.640	2.929	0.682	0.14	298–1005
	−5.558	36.493			0.02	1005–1100
$NdBr_3$	−7.097	22.432	3.297	3.448	0.18	298–955
	−7.128	37.027			0.04	955–1100
$GdBr_3$	−7.105	23.208	1.258	2.204	0.19	298–1058
	−7.271	33.331			0.02	1058–1200
$HoBr_3$	−7.228	23.438	1.528	3.108	0.40	298–1192
	−6.186	34.448			0.05	1192–1300
LaI_3	−7.353	23.222	2.368	6.529	0.27	298–1051
	−5.015	36.273			0.02	1051–1200
NdI_3	−6.904	21.715	4.279	1.478	0.10	298–847
	−5.860	28.057			0.04	847–1060
	−5.668	37.224			0.01	1060–1200
GdI_3	−7.657	24.288	0.900	10.002	0.27	298–1013
	−12.925	30.638			0.04	1013–1204
	−7.986	37.250			0.02	1204–1300
TbI_3	−7.658	23.902	1.878	10.865	0.34	298–1080
	−11.313	29.717			0.01	1080–1228
	−7.244	37.585			0.01	1228–1300

of our heat content measurements, we have attributed this to the occurrence of a diffuse transition, that is, one spread out over a considerable range of temperatures, with an entropy change, in the solid state, of the same order of magnitude as that of fusion. The transition is ascribed to the gradual disordering of the B ions, that is, their distribution over two types of lattice positions, or a gradual "melting" of the B ion sublattice. We postulate that this interesting and important phenomenon is not limited to the three substances we have studied thus far but is a general characteristic of the lattice dynamics of crystals of the fluorite and antifluorite type, with significant consequences for physical properties such as self-diffusion and electrical or thermal conductivity. We have described our measurements on K_2S and discussed pertinent literature data from this point of view in a recent paper.[27]

Pretransition Behavior of Solid Potassium and Thallium Sulfate

A. S. Dworkin M. A. Bredig

We have derived improved equations for our previously reported[28] high-temperature heat content measurements of K_2SO_4 and Tl_2SO_4 through the use of a computer program[29] to calculate high-temperature thermodynamic functions. The program sets $\Delta H = 0$ and fixes C_p at 298°K by means of an input parameter. For K_2SO_4 the meas-

[27] A. S. Dworkin and M. A. Bredig, *J. Phys. Chem.* 72, 1277 (1968).

[28] A. S. Dworkin and M. A. Bredig, *Chem. Div. Ann. Progr. Rept. May 20, 1966*, ORNL-3994, p. 95.

[29] T. G. Godfrey and J. M. Leitnaker, ORNL-TM-1599 (1966).

Table 8.3. Enthalpy and Entropy of Fusion and Transition of Lanthanide Bromides and Iodides

Compound	T_m (°K)	ΔH_m (kcal/mole)	ΔS_m (eu/mole)	T_{trans} (°K)	ΔH_{trans} (kcal/mole)	ΔS_{trans} (eu/mole)	$\Delta S_m + \Delta S_{tr}$ (eu/mole)	$S_{1300°K} - S_{298°K}$ (eu/mole)	Structure Type at 25°C
$LaBr_3$	1061	13.0	12.3				12.3		$Y(OH)_3$ (hexagonal)
$CeBr_3$	1005	12.4	12.4				12.4	53.4	$Y(OH)_3$
$PrBr_3$	966	11.3	11.7				11.7		$Y(OH)_3$
$NdBr_3$	955	10.9	11.4				11.4	53.1	$PuBr_3$ (orthorhombic)
$GdBr_3$	1058	9.1	8.6				8.6	46.7	?
$HoBr_3$	1192	12.0	10.0				10.0	48.1	?
LaI_3	1051	13.4	12.7				12.7	52.9	$PuBr_3$
CeI_3	1033	12.4	12.0				12.0		$PuBr_3$
PrI_3	1011	12.7	12.6				12.6		$PuBr_3$
NdI_3	1060	9.9	9.4	847	3.3	3.9	13.3	54.5	$PuBr_3$
GdI_3	1203	12.9	10.7	1013	0.14	0.14	10.8	49.5	BiI_3 (hexagonal)
TbI_3	1228	13.7	11.2	1080	0.33	0.30	11.5	50.6	BiI_3

ured value[30] of $C_p = 31.1$ cal deg^{-1} mole^{-1} at 298°K was used, and for Tl_2SO_4 a C_p of 35 cal deg^{-1} mole^{-1} obtained by extrapolation of our high-temperature heat content data was used. The program also enables one to incorporate necessary terms beyond the quadratic used previously.[28]

The new equations for $H_T - H_{298}$ (cal/mole) are as follows:

Tl_2SO_4

Orthorhombic: $H_T - H_{298} = -2921 + 9.724T + 2.834 + 10^{-2}T^2 - 7.447 \times 10^5/T$, 298 – 774°K; ±0.4%

Transition: $\Delta H_{tr} = 160 \pm 60$ cal/mole, 774°K

K_2SO_4

Orthorhombic: $H_T - H_{298} = -11732 + 33.95T - 5.35 \times 10^{-4}T^2 + 8.49 \times 10^{-6}T^3 + 4.27 \times 10^5/T$, 298 – 857; ±0.5%

Transition: $\Delta H_{tr} = 2020 \pm 80$ cal/mole

The equations for the high-temperature hexagonal forms and the liquid Tl_2SO_4 remain the same as before.

The addition of a cubic term to the standard Kelley heat content equation improved the fit of the data for K_2SO_4 and resulted in a heat capacity curve with an inflection at about 600°K. This is in essential agreement with previously discussed pretransition behavior[28] and with adiabatic heat capacity measurements reported[31] since the completion of our experiments. The additional term neither improved the fit nor changed the C_p curve for Tl_2SO_4 and therefore was not used in that case.

The significant differences in transition behavior of potassium and thallium sulfates are discussed in detail in a paper now in preparation.

[30] G. E. Moore and K. K. Kelley, *J. Am. Chem. Soc.* 64, 2949 (1942).

[31] N. E. Shmidt, *Russ. J. Inorg. Chem. English Transl.* 12, 929 (1967).

HIGH-TEMPERATURE CRYSTAL CHEMISTRY

High-Temperature Crystal Structures of Some $M(RX_4)$ Compounds

M. A. Bredig

Sodium tetrafluoroborate, $NaBF_4$, proposed as a coolant for the Molten-Salt Breeder Reactor, undergoes a solid-state transition at 243°C.[32] By analogy with $NaClO_4$, which at room temperature has the same orthorhombic (pseudotetragonal) $CaSO_4$ type of structure as $NaBF_4$, S. Cantor estimated the technically important volume change as 18%.[33] On the other hand, one finds very different volume changes for a similar transition into an alleged cubic, rock salt type of structure of α-$CaSO_4$ at 1200°, which had strangely been assigned two highly differing lattice constants. An original $a_0 = 7.8$ A[34] was recently "corrected" to 6.8 A,[35] apparently just to bring $CaSO_4$ with its smaller cation in line with α-$SrSO_4$ (7.1 A) and α-$BaSO_4$ (7.2 A). The value 7.8 A corresponds to an enormous volume expansion of 57%, strangely unnoted by the original investigator,[34] while $a_0 = 6.8$ A yields an expansion of less than 2%, also improbable. On examination I found the original x-ray data[34] to deviate from $a_0 = 6.8$ A by an average of +14%, as compared with ±3% for $a_0 = 7.8$ A. Even the smaller error seemed unacceptable as merely experimental, since those for $SrSO_4$ and $BaSO_4$, in the same study, were much smaller.

A search for a different structure, better fitting the experimental data and at the same time accounting rationally for the presence of the smaller Ca^{2+} ion, led to the hexagonal α-ZnS (wurtzite) type of structure, with $a_0 = 4.98 \pm 0.02$ A, $c_0 = 7.67 \pm 0.03$ A, and fourfold (tetrahedral) rather than sixfold (octahedral) coordination. Figure 8.4, bottom section, demonstrates the far better fit of the new structure.

The substitution of an optically anisotropic (hexagonal) structure for the cubic (isotropic) one

[32] A. S. Dworkin and M. A. Bredig, preceding paper, this report.

[33] S. Cantor, MSR-68-46 (3-36-68).

[34] O. W. Flörke, *Naturwissenschaften* 39, 478 (1952).

[35] Ralph W. G. Wyckoff, *Crystal Structures*, 2d ed., fol. 3, p. 56, Interscience, 1965.

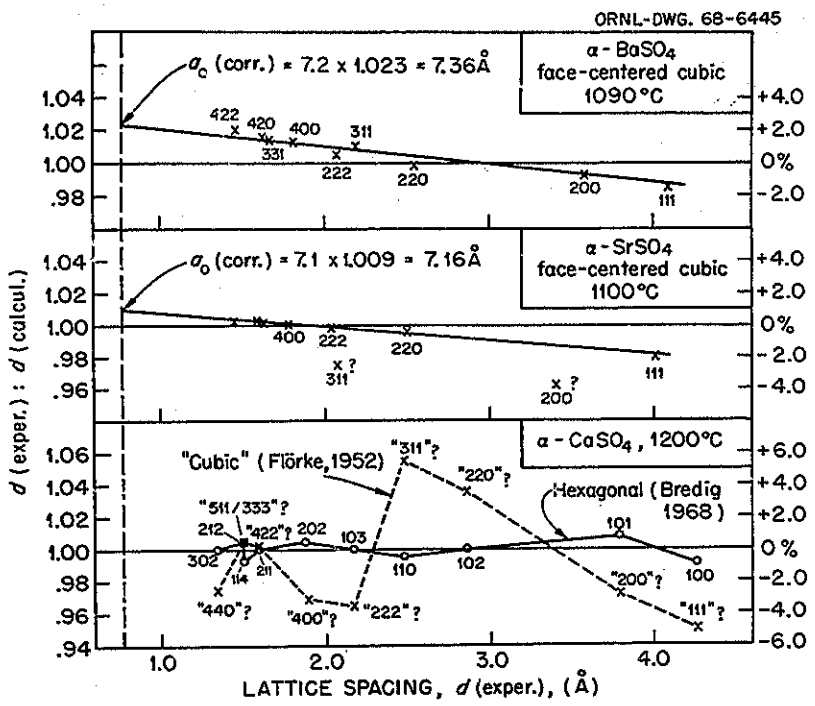

Fig. 8.4. New Interpretation of High-Temperature X-Ray Diffraction Patterns of Alkaline Earth Sulfates.

puts the x-ray data in agreement with the results of a careful optical study,[36] also neglected by the earlier authors, in which α-$CaSO_4$, in contrast to α-$SrSO_4$ and α-$BaSO_4$, was found to exhibit considerable double refringence.

For cubic α-$SrSO_4$ and α-$BaSO_4$, Fig. 8.4 shows a definite trend of the deviations with diffraction angle (θ). Revised lattice parameters obtained by extrapolation to $\theta = 90°$, or $d = (\lambda/2) \sin \theta = 0.77$ A, where the effect of a presumed distortion of the sample vanishes, are 7.16 ± 0.03 A for $SrSO_4$ and 7.36 ± 0.02 A for $BaSO_4$. They correspond to large expansions, 18%, over the volumes of the orthorhombic forms at room temperature, in fair agreement with 15% for isostructural $KClO_4$,[35] with which the volume expansion of only 8% derived from the original $a_0 = 7.2$ for $BaSO_4$ was in distinct disagreement.

The newly established volume expansion of 9% (replacing 57 and 2%, above) for hexagonal α-$CaSO_4$ is not likely to affect the validity of Cantor's estimate of 18% for $NaBF_4$, based as it was upon the assumed di-isomorphism (orthorhombic/cubic) with $NaClO_4$ rather than $CaSO_4$.[33] It is reasonable that at elevated temperature $NaBF_4$ behaves like the other 1:1 electrolyte, $NaClO_4$, rather than the 2:2 electrolyte, $CaSO_4$, even though all three have the same structure at room temperature.

Both the hexagonal α-form of $CaSO_4$ and the cubic one of $NaBF_4$ require further investigation, especially the consideration of more precisely measured intensities, preferably with single crystals rather than powders. It is furthermore necessary in this way to exclude the nickel arsenide type of structure, also of hexagonal symmetry, but with sixfold rather than fourfold coordination of the ions. Either of these structures would appear to be novel for compounds of the type $M(RX_4)$.

[36] W. Grahmann, *Z. Anorg. Chem.* 81, 257 (1913).

9. Chemical Physics

EFFECTS OF TEMPERATURE ON THE NEAR-INFRARED ABSORPTION SPECTRA OF MOLECULES IN THE CONDENSED STATES

W. C. Waggener A. J. Weinberger
R. W. Stoughton

A first stage has been reached in our study of the liquid state by near-infrared spectroscopy over a wide range of temperature. Satisfactory spectra have been obtained for H_2O and D_2O from −20 to 250°C and for CO_2, *n*-hexane, cyclohexane, NH_3, and HF from below their melting points to above their critical points. Selected bands in the CO_2 spectrum were fitted satisfactorily to Lorentz distribution functions, and the dependence of intensity on density was that required by the Lorentz theory for broadening, as expected for a nonassociated molecule. This year we have developed computer programs to calculate and plot our data and have found a curve-fitting program adequate for the job of resolving complex, overlapping spectra such as those of highly associated liquids, of which water is an example.

We have remeasured the H_2O spectrum (0.60 to 1.34 μ) at 17 temperatures in the range 0 to 250°C. Starting with the 250° spectrum, we succeeded in resolving the familiar 0.96-μ and 1.15-μ bands into four and five components (mixed Gauss-Lorentz distribution functions) respectively. The components were introduced in accord with the relative positions and intensities of the centers of appropriate vibrational-rotational bands in the gas. Two components of the intense 1.4-μ band which contribute to the background were added, and the variance of fit obtained from 0.86 to 1.34 μ was 0.030×10^{-3} liter mole^{-1} cm^{-1} (range of ϵ was 0 to 25×10^{-3}). The 250° values of the component band parameters were then used as trial parameters in fitting the spectrum at the next lower temperature.

By this procedure we are fitting our 11-band vibrational model to the H_2O spectrum at each of the 17 temperatures including 0°C, and at present are beginning to analyze the component band parameters as a function of temperature. The changes in the parameters with temperature are generally monotonic; however, the occurrence of qualitative differences in this dependence indicates a high degree of specificity.

We are measuring the spectrum of liquid H_2S in the 0.6- to 1.9-μ region using a 2.54-cm Inconel cell, and we now have data at seven temperatures from the melting point (−83°C) to within a degree of the critical point (100°C). We have found that the prominent, nearly isolated band at 1.6 μ ($\Delta\nu_{1/2} = 95$ cm^{-1} at 22°C), though appearing simple and symmetric, cannot be fitted with one or even several mixed Gauss-Lorentz distribution functions. This composite band is of especial interest because it undoubtedly arises from the same group of vibrational transitions which produce the 1.15-μ band in the spectrum of liquid H_2O. We anticipate now that a comparable number of components contribute, and the effect of temperature upon the component parameters should help differentiate the role of the H bond in affecting the 1.15-μ band of H_2O.

Anhydrous Hydrogen Fluoride

We have extended our examination of the extremely broad, strongly asymmetric band in the region of the second harmonic of the H-F vibrational frequency down to and below the freezing point (–83°C) by shortening the sample cell from 0.254 to 0.0825 cm. The data taken with the two cell lengths, when plotted, revealed inconsistencies of several percent which were traced to elongation of the shorter cell as a function of pressure. The problem is currently under study; however, it is clear that the very slight movement in the threaded window assemblies seriously limits our window design in very short cells.

Our initial analysis of the HF band at higher temperatures indicated that it is a monomer-polymer composite, consisting of the rotation-vibration spectrum of monomeric HF (viz., free end groups), centered near 1.3 μ and overlapped, more or less, on the high-wavelength side by a highly temperature- and density-sensitive structureless band. We believe this band arises from the coupling of a continuous distribution of vibrational and librational transitions of polymeric species with the ν ($2 \leftarrow 0$) transition. The polymer component dominates the composite band over the entire temperature range of the liquid state, although the monomer component is clearly evident from the critical point to 60°C. The half bandwidth at the critical point (825 cm^{-1} at 188°C) increases steeply with decreasing temperature, reaching a maximum (1115 cm^{-1}) near 60°. Below 60°, with the monomer spectrum disappearing, the half bandwidth decreases to 1050 cm^{-1} and 1020 cm^{-1} for the liquid and solid, respectively, at the freezing point (–83°C). Here again, the band has become structured, possessing at least two resolvable components which are clearly visible in the spectrum of both the solid and the liquid. The intensity of the higher-frequency component predominates in the liquid spectrum (ν_{max} = 6625 cm^{-1}), while the lower-frequency component dominates the spectrum of the solid (ν_{max} = 6250 cm^{-1}).

We have extended the demonstrated operational range of our equipment from –100 to –185° by using liquid nitrogen, directly introduced into the sample cell cooler channel, instead of nitrogen-cooled helium. Also, we have operated a cell successfully in the range from 2200 to 5500 psia by strengthening parts of the cell window assembly and by using a wider-range pressure transducer.

INTRAMOLECULAR ENERGY TRANSFER IN ACTINIDE β-DIKETONES. EXCHANGE OF LANTHANIDE AND ACTINIDE IONS IN A CONVENIENT METHOD OF SCANNING ACTINIDE COMPLEXES FOR APPLICATION TO LIQUID LASERS

L. J. Nugent, R. D. Baybarz, J. R. Tarrant, G. K. Werner, J. L. Purnett, O. L. Keller, Jr.

See p. 40.

CHARGE-TRANSFER SPECTRA OF LANTHANIDE AND ACTINIDE TRIHALIDES IN SOLUTION

J. L. Burnett, R. D. Baybarz, L. J. Nugent

See p. 40.

SELF-ACTIVATED THERMOLUMINESCENCE IN SEVERAL LANTHANIDE- AND ACTINIDE-DOPED THORIUM DIOXIDE CRYSTALS

C. B. Finch, G. K. Werner, L. J. Nugent, M. M. Abraham

See p. 41.

CALORIMETRY

Attempt to Prepare Anhydrous $H_3Re_3Cl_{12}$

R. H. Busey

It has become increasingly apparent in recent years that many transition elements form a number of interesting compounds containing two or more metal atoms in which there are strong bonds between the metal atoms themselves. This behavior is particularly pronounced in compounds of Nb, Ta, Mo, W, and Re. Rhenium trichloride, Re_3Cl_9, is an example of such a metal atom cluster compound. The structure[1] consists of Re_3Cl_9 clusters in which the three rhenium atoms form an equilateral triangle with three bridging Cl atoms in the plane of the triangle and with six terminal Cl atoms bonded to the rhenium atoms, three above and three below the Re_3 plane. The Re_3Cl_9 molecules are very stable, persisting in the vapor at 600°C.[2] This basic Re_3Cl_9 unit readily adds three Cl^- ions to give the anion $Re_3Cl_{12}^{3-}$ found in salts of the type $Cs_3Re_3Cl_{12}$.[3] The three additional Cl atoms in $Re_3Cl_{12}^{3-}$ form additional terminal Cl atoms in the plane of the Re_3 and the three bridging Cl atoms. This ion persists when the salt is dissolved in dilute hydrochloric acid.

Preparation of anhydrous $H_3Re_3Cl_{12}$, the acid of the salt $Cs_3Re_3Cl_{12}$, would not only be of intrinsic interest, but the compound could prove valuable as a starting material for other inorganic preparations.

An attempt to prepare $H_3Re_3Cl_{12}$ was made by contacting a sample of $Re_3Cl_9(c)$ with anhydrous liquid hydrogen chloride. Rhenium trichloride is readily soluble in a variety of solvents, and it was hoped that the compound would dissolve by reaction with the HCl to give a solution of $H_3Re_3Cl_{12}$ in HCl(*l*). Approximately 15 ml of HCl(*l*) contained in a storage bulb over P_2O_5 at CO_2 temperatures was distilled onto a 0.203-g sample of Re_3Cl_9 at liquid-nitrogen temperature. The liquid nitrogen around the sample was replaced by a CO_2 trap, which caused the solid HCl to melt. No evidence of dissolution was observed. No evidence of solution was observed when the HCl(*l*) and sample were agitated by temporarily removing the CO_2 trap, which caused bumping or boiling. After about 2 hr the HCl(*l*) was distilled off the sample.

There was no visible change in the sample. The sample weight after the HCl(*l*) treatment was 0.202 g, confirming that little or no reaction had occurred. If a compound like $H_3Re_3Cl_{12}$ exists, other methods for its preparation must be sought.

Enthalpy of Hydrolysis of Rhenium Trichloride. Enthalpy and Free Energy of Formation of Rhenium Sesquioxide

R. H. Busey E. D. Sprague[4]
R. B. Bevan, Jr.

The thermodynamic properties of $ReCl_3(c)$ are well established.[5] The trichloride is readily hydrolyzed to hydrated Re_2O_3 in alkaline solution in the absence of oxygen.[6] The sesquioxide is rapidly oxidized to perrhenate by oxygen and reduces water with hydrogen evolution at 100°C.[6] The enthalpy of formation of Re_2O_3 may be determined from the enthalpy of hydrolysis of $ReCl_3$, provided the oxide is kinetically stable in alkaline

[1] F. A. Cotton and J. T. Mague, *Inorg. Chem.* 3, 1402 (1964).

[2] K. Rinke and H. Schafer, *Angew. Chem.* 4, 148 (1965).

[3] J. A. Bertrand, F. A. Cotton, and W. A. Dollase, *Inorg. Chem.* 2, 1166 (1963); W. T. Robinson, J. E. Fergusson, and B. R. Penford, *Proc. Chem. Soc.*, 1963, p. 116.

[4] Temporary employee, summer 1967.

[5] (*a*) J. P. King and J. W. Cobble, *J. Am. Chem. Soc.* 82, 2111 (1960); (*b*) R. B. Bevan, Jr., R. A. Gilbert, and R. H. Busey, *J. Phys. Chem.* 70, 147 (1966).

[6] W. Geilmann and F. W. Wrigge, *Z. Anorg. Allgem. Chem.* 214, 239 (1933).

solution for a period of time sufficient to carry out the observation.

It has been found possible to determine this enthalpy utilizing a solution calorimeter previously described.[7] The calorimeter has been modified to give a more rapid response by incorporating a thermistor and a specially constructed 450-ml Dewar with a very thin inner wall (~0.2 mm). The performance of the calorimeter was tested by measurements on tris(hydroxymethyl)aminomethane (THAM).[8]

The anhydrous $ReCl_3$ used was the same material employed and described previously.[5b] Its purity was rechecked by a Mohr volumetric chloride determination and was 100.04%. All handling of the $ReCl_3$ was done in a vacuum-type dry box filled with argon and dried with P_2O_5. The NaOH solutions used in the calorimeter were boiled and purged with argon or nitrogen to remove dissolved oxygen. To ensure the absence of oxygen within the calorimeter, a weighed amount (50 to 100 mg) of $ReCl_3$ was added to the calorimetric solution just before final closure of the calorimeter.

The calorimetric results for the hydrolysis reaction,

$$ReCl_3(c) + 3OH^- = \frac{1}{2} Re_2O_3(c) + \frac{3}{2} H_2O + 3Cl^- , \quad (1)$$

are presented in Table 9.1. The hydrated sesquioxide is precipitated, but since the composition is unknown, all thermodynamic data given in this paper refer to Re_2O_3 ignoring its hydration water, as is customary. The average oxidation state of the rhenium following a hydrolysis run was determined by oxidation of the rhenium in the calorimetric solution to ReO_4^- by adding excess standardized 0.2 *N* NaClO and determining the excess iodometrically with standardized 0.1 *N* $Na_2S_2O_3$. The average result was 3.12 ± 0.02 for the average oxidation state. Two determinations made directly on samples of $ReCl_3(c)$ also gave 3.12 ± 0.02. The agreement is interpreted to mean that no significant change in oxidation state occurred when the trichloride was hydrolyzed. In all the above determinations the ClO^- was in twofold excess of the stoichiometric amount required to oxidize Re(III) to ReO_4^-. This might not have been sufficient[9] and may account for the apparent high original average oxidation state.

[7](*a*) R. H. Busey, K. H. Gayer, R. A. Gilbert, and R. B. Bevan, Jr., *J. Phys. Chem.* 70, 2609 (1966); (*b*) R. H. Busey, H. H. Dearman, and R. B. Bevan, Jr., *J. Phys. Chem.* 66, 82 (1962).

[8]S. R. Gunn, *J. Phys. Chem.* 69, 2902 (1965); R. J. Irving and I. Wadso, *Acta Chem. Scand.* 18, 195 (1964).

[9]King and Cobble, ref. 5*a*, in their calorimetric determination of the enthalpy of oxidation of $ReCl_3(c)$ to ReO_4^- used three- to sevenfold excess ClO^- with no inconsistencies reported.

Table 9.1. Enthalpy of Hydrolysis of $ReCl_3(c)$ by NaOH Solution at 25°C

Run No.	$[OH^-]$ (*N*)	$ReCl_3(c)$ (g)	$-\Delta H_1$ (kcal per mole of $ReCl_3$)
4	0.151	0.5498	54.54
5	0.146	0.5225	54.24
6	0.146	0.3266	54.45
7	0.145	0.3406	54.40
8	0.0512	0.2967	54.37
11	0.290	0.3176	54.91[a]
12	0.295	0.3248	54.17
13	0.0992	0.3198	54.23
14	0.0978	0.3269	54.63
15	0.102	0.3017	54.34
			$\Delta H_1^\circ = -54.29 \pm 0.12$

[a]Rejected by Chauvenet's criterion.

The enthalpies of dilution of NaOH and NaCl required for correcting the observed ΔH_1 results to infinite dilution were taken from Harned and Owen.[10] The relative partial molal enthalpy of water is negligible. The corrected enthalpy is $\Delta H_1^\circ = -54.29 \pm 0.12$ kcal per mole of $ReCl_3$. This datum combined with ΔH_f° [$ReCl_3$(c)] = −63.0 kcal/mole[5a] and the enthalpies of formation of OH^-, Cl^-, and H_2O taken from Latimer[11] gives for the enthalpy of formation of hydrated rhenium sesquioxide ΔH_f° (Re_2O_3) = −119.2 kcal/mole at 25°C.

The entropy of Re_2O_3 is estimated to be 32 ± 2 cal deg^{-1} $mole^{-1}$ by comparison with the known entropies of other sesquioxides. This gives −59 ± 2 cal deg^{-1} $mole^{-1}$ for the entropy of formation of Re_2O_3 from its elements. The free energy of formation at 25°C then is $\Delta F_f^\circ(Re_2O_3) = \Delta H_f^\circ - T\,\Delta S_f^\circ = -101.6 \pm 0.6$ kcal/mole.

The electrode potentials of the half reactions

$$2Re + 6OH^- = Re_2O_3 + 3H_2O + 6e^-$$

and

$$Re_2O_3 + 2OH^- + 3H_2O = 2ReO_2{\cdot}2H_2O + 2e^-$$

are computed to be 0.333 ± 0.004 and 1.25 ± 0.01 v respectively.[12] Rhenium sesquioxide is thus thermodynamically unstable with respect to disproportionation into Re metal and $ReO_2{\cdot}2H_2O$ and with respect to being oxidized by water to $ReO_2{\cdot}2H_2O$. The apparent stability observed in this research must be a kinetic stability.

The potential diagram of rhenium in basic solution including the data of this research and thermal data given by King and Cobble[13] is given in Fig. 9.1.

ORNL-DWG. 68-5177

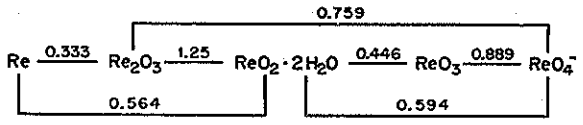

Fig. 9.1. Redox Scheme of Rhenium in Basic Solution. Potentials in volts.

MICROWAVE AND RADIO-FREQUENCY SPECTROSCOPY

Paramagnetic Resonance Study of Gamma-Irradiated Single Crystals of Formic Acid

Robert W. Holmberg

A study of the electron spin resonance spectra of the formyl radical, HĊO, and other radicals produced upon irradiation of single crystals of formic acid with ^{60}Co gamma rays has been undertaken. When a crystal of HCOOH was irradiated at 77°K and observed without warming at this temperature, a complicated central spectrum of many partially resolved lines near $g = 2$ was seen. Lines characteristic of the formyl radical were seen only very weakly. After annealing in dry ice (195°K) for about 1 hr, irreversible changes in the spectrum occurred. (All observations reported here were made after recooling the sample to 77°K.) The central spectrum had simplified, and the lines from formyl were now intense. Both spectra were anisotropic. Figure 9.2 shows the spectrum obtained with the applied magnetic field oriented along one of the crystal axes. Lines labeled *H* are hyperfine lines from ^1H in HĊO, while those labeled *C* appear because of the small amount of ^{13}C present in natural abundance. Two other ^{13}C lines are lost in the central part of the spectrum. The spectrometer gain was increased a factor of 50 in the neighborhood of the ^{13}C lines to show them with appreciable intensity.

Detailed measurements of the positions of both the H and ^{13}C lines of the formyl radical were made with the magnetic field oriented parallel to the basal planes of the orthorhombic formic acid crystal.[14] From these measurements, the g tensor

[10] H. S. Harned and B. B. Owen, *The Physical Chemistry of Electrolytic Solutions*, 2d ed., Reinhold, New York, 1950.

[11] W. M. Latimer, *Oxidation Potentials*, 2d ed., Prentice-Hall, New York, 1952.

[12] Auxiliary data from refs. 7a and 11.

[13] J. P. King and J. W. Cobble, *J. Am. Chem. Soc.* 79, 1559 (1957).

[14] F. Holtzberg, B. Post, and I. Fankuchen, *Acta Cryst.* 6, 127 (1953).

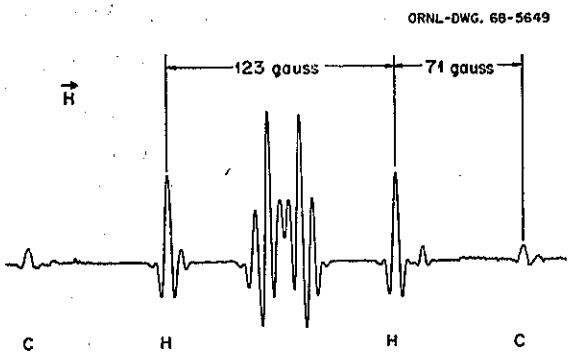

Fig. 9.2. The Electron Spin Resonance Spectrum (Second Derivative) of a Gamma-Irradiated Formic Acid Single Crystal. The magnetic field was parallel to a crystallographic axis.

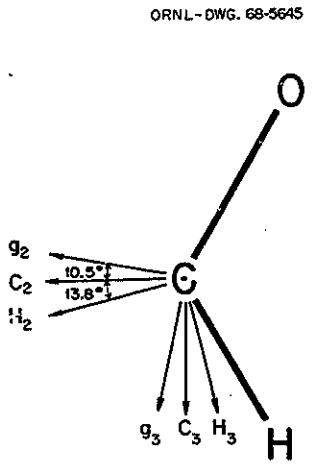

Fig. 9.3. An Approximate Association of Principal Directions of the Tensors for the Formyl Radical with Its Structure. g refers to the g tensor, C to ^{13}C hyperfine tensor, and H to ^{1}H hyperfine tensor.

and hyperfine tensors for both H and ^{13}C have been deduced. The principal values of these tensors are: $g_1 = 2.0032$, $g_2 = 2.0018$, $g_3 = 1.9944$; $H_1 = 120$, $H_2 = 123$, $H_3 = 135$ gauss; $C_1 = 122$, $C_2 = 156$, $C_3 = 114$ gauss.

An attempt was made to relate the principal directions of the tensors to atomic positions of formic acid[14] without success. Movement of the formyl radical evidently occurs when it is formed. A detailed analysis of the relationship between the tensors and the structure of the formyl radical has not been completed, but some general observations can be made and are discussed with reference to Fig. 9.3.

Spectroscopic studies of the radical in the gas phase[15] show that it is bent with an H–C–O angle of 119.5°. It is likely that this structure is not greatly changed when trapped in the formic acid lattice. Although the principal axis systems of the tensors are differently oriented, the principal directions g_1, C_1, and H_1 are the same to within about 5°. It is assumed that this direction is perpendicular to the plane of the HCO molecule. (Figure 9.3 is an approximation in that it ignores these small deviations from colinearity and the consequent nonplanarity of the other tensor elements.) The largest ^{13}C interaction, C_2, has been taken to be in the direction of the bisector of the HCO angle. This is expected for an unpaired electron in a σ s-p hybrid orbital on the carbon. This association of principal elements with structure seems very reasonable when the g and C tensors are compared with those of a similar radical, CO_2^-. This radical is symmetric, with parallel g and C tensors. The following principal values have been reported:[16] $g_1 = 2.0032$, $g_2 = 2.0016$, $g_3 = 1.9973$; $C_1 = 134.6$, $C_2 = 177.3$, $C_3 = 131.7$ gauss. The orientations of these values are the same as those shown for the C tensor of Fig. 9.3.

Annealing studies of formic acid irradiated at 77°K reveal a number of paramagnetic species whose chemical relationship is not understood. The complicated central spectrum seen before annealing is probably due to a mixture of radicals. The more simple central spectrum after about 1 hr of annealing at 195°K has not been analyzed in detail, but the pattern of lines shown in Fig. 9.2 for one orientation suggests a hyperfine interaction from three protons, two of which are alike. Such a spectrum might arise from the radical $\dot{C}(OH)_2$. With further annealing at dry ice temperature, this central spectrum slowly decays

[15] D. A. Ramsay, p. 1 in *Advan. Spectry.*, vol. I, Interscience, New York, 1959.

[16] S. A. Marshall, A. R. Reinberg, R. A. Serway, and J. A. Hodges, *Mol. Phys.* 8, 225 (1964).

and almost completely disappears after 4 or 5 hr. The formyl radical, whose parameters have been discussed above, reaches a maximum concentration in about 1 hr and then slowly decays. A second, non-symmetry-related, formyl radical grows in at a slower rate and then, too, decays. The weak lines near the H hyperfine lines of Fig. 9.2 are due to this formyl species. Both the H and ^{13}C hyperfine lines from this second formyl radical have been seen. Detailed measurements of the line positions have not been made, so a comparison of the tensors of the two radicals is not yet possible. Weaker lines with H hyperfine spacings characteristic of formyl radical, but different from the two main formyl radical spectra, have also been seen on annealing.

Paramagnetic Resonance Study of Aliphatic Nitroanion Radicals in Photolyzed Solutions

Henry Zeldes Ralph Livingston

Aliphatic nitroanion radicals have been generated by photolysis of two kinds of solutions at room temperature. They were studied by electron paramagnetic resonance during photolysis as the solutions flowed through an irradiation cell in the microwave cavity. Judging from the change in signal strength as the liquid flow rate was varied, the nitroanion radical lifetimes are an appreciable fraction of a second in the solutions studied.

Strong aliphatic nitroanion radical spectra were found during photolysis of many basic aqueous solutions containing nitrite ion and an aliphatic compound. The radicals are ones which result from replacing a hydrogen atom attached to a carbon atom of the compound by NO_2^-. A reasonable mechanism is that the radical R· is produced from the aliphatic compound RH by reaction with an excited nitrite ion and that R· then combines with NO_2^-, which was present in high concentration, to form $RNO_2\cdot^-$:

$$NO_2^- + RH \xrightarrow{h\nu} R\cdot + HNO_2\cdot^- , \qquad (1)$$

$$R\cdot + NO_2^- \longrightarrow RNO_2\cdot^- . \qquad (2)$$

Nitroanion radicals which were produced this way and whose spectra were analyzed in detail are $HOCH_2NO_2\cdot^-$, $^-O_2CNO_2\cdot^-$, $^-O_2CCH_2NO_2\cdot^-$, $^-O_2CCH_2CH_2NO_2\cdot^-$, $^-O_2CCH(NO_2\cdot^-)CH_3$, $CH_3COCH_2NO_2\cdot^-$, $CH_3CH_2COCH_2NO_2\cdot^-$, $H_2NCOCH_2NO_2\cdot^-$, $CH_3CH(NH_2)NO_2\cdot^-$, and $(CH_3)_2NCH_2NO_2\cdot^-$. Aqueous solutions containing nitrite ion did not give nitroanion radicals in the absence of base except for those containing formate ion and acetone. In these cases the spectra were very weak compared with those obtained after adding base.

In an acetone-rich solution containing nitrite ion, but no base, another kind of radical was produced. This solution was found to be unstable. The parameters for this radical are reasonable for the iminoxy radical $CH_3COCH=\dot{N}O$. This radical may have been produced from the oximinoketone $CH_3COCH=NOH$, which was present before photolysis as a result of the nitrosation of acetone. Photolysis of NO_2^- may then have led to the abstraction of a hydrogen atom to give the observed radical.

A methyl alcohol solution containing nitrite ion and some water but no base also gave a different kind of radical, which has been tentatively identified as $(HOCH_2)_2\dot{N}O$. The parameters were found to be typical of dialkyl nitroxide radicals. The proposed radical may have been formed by a mechanism given by Hoffmann, Hodgson, and Jura:[17]

$$R\cdot + RNO_2\cdot^- \longrightarrow RN=O + RO^- , \qquad (3)$$

$$R\cdot + RN=O \longrightarrow R_2\dot{N}O , \qquad (4)$$

where in this case R· is $\dot{C}H_2OH$. Again it is assumed that R· is produced from RH by photolysis of NO_2^- and that R· and NO_2^- combine to form $RNO_2\cdot^-$. Without base and with not too much NO_2^- present, reactions (3) and (4) are assumed to become important.

Aliphatic nitroanion radicals were also produced by photolysis of aqueous solutions containing aliphatic nitro compounds. Only solutions containing nitromethane and nitroethane were investigated in detail. Strong spectra were obtained, but only after base was added to the solutions. The nitromethane[18] and nitroethane[19] anion radicals

---

[17] A. K. Hoffmann, W. G. Hodgson, and W. H. Jura, *J. Am. Chem. Soc.* 83, 4671 (1961).

[18] W. E. Griffiths, G. F. Longster, J. Myatt, and P. F. Todd, *J. Chem. Soc.* (B), 533 (1967).

[19] L. H. Piette, P. Ludwig, and R. N. Adams, *J. Am. Chem. Soc.* 84, 4212 (1962).

had been prepared previously in aqueous solutions by electrolysis and studied by electron paramagnetic resonance. Our parameters for $CH_3CH_2NO_2^-$ agreed with those reported[19] earlier. We found small resolved splittings for the CH_3 protons which were not resolved in the earlier work. Our coupling values for the N nucleus of $CH_3NO_2^-$ in two solutions, one mostly water and the other mostly ethyl alcohol, were almost the same. However, they were larger than the values reported[18] previously in aqueous 10% methyl alcohol and aqueous 10% isopropyl alcohol.

It is possible that hydrogen abstraction is the important process leading to nitroanion radicals for our solutions containing nitromethane and nitroethane. Not much base was needed to form the radicals, and its function may have been to neutralize the conjugate acid RNO_2H to form $RNO_2\cdot^-$.

With the exception of $^-O_2CNO_2\cdot^-$, the hyperfine couplings for the nitro group N are in the neighborhood of 25 gauss, which is typical for aliphatic nitroanions.[19] The value for $^-O_2CNO_2\cdot^-$ is 14.38 gauss, and this value is like that of an aromatic nitroanion in aqueous solution. The low value for $^-O_2CNO_2\cdot^-$ indicates that the nitro group π-electron system is strongly coupled to the π-electron system of the rest of the molecule and that the molecule is planar. The coupling value for ^{13}C present in natural abundance was measured for this radical and found to be small (3.74 gauss). This too is reasonable for an unpaired electron occupying a π-orbital of the planar molecule. Further details of this work will be published elsewhere.[20]

Paramagnetic Resonance Study of Free Radicals Formed in Amides and an Imide

Ralph Livingston Henry Zeldes

Paramagnetic resonance spectra of free radicals formed by abstracting hydrogen from simple and *N*-methyl-substituted formamides and acetamides and from succinimide have been studied. The hydrogen abstraction was brought about by ultraviolet irradiation of a solution of the amide or imide containing either hydrogen peroxide or acetone. The ·OH radical is formed upon photolysis of hydrogen peroxide which then abstracts hydrogen, while photolysis of acetone gives an excited molecule which is then capable of abstracting hydrogen. In the latter case the hydroxyisopropyl radical, $(CH_3)_2\dot{C}OH$, is formed from the acetone, and its spectrum is usually observed.

The hydrogen bonded to carbon is abstracted from formamide giving $\dot{C}ONH_2$. Other workers[21] observed an almost identical spectrum for this radical after preparing it by the rapid-mixing technique, but they interpreted the spectrum as arising from HCONH, since, among other things, the values for the hyperfine couplings of the two hydrogens were strikingly different. We felt that the inequivalence of the coupling values was reasonable for $\dot{C}ONH_2$, which would be a sigma radical. Other sigma radicals have shown similar inequivalences. An experiment with deuterium was carried out in order to remove the ambiguity as to which hydrogen was abstracted from formamide. A solution of 12% formamide and 12% acetone in D_2O was photolyzed. Through exchange, essentially all of the formamide was converted to $HCOND_2$, while the hydrogen of the acetone did not exchange. The overall photolytic process was

$$CH_3COCH_3 + HCOND_2 \longrightarrow (CH_3)_2\dot{C}OH + \dot{C}OND_2 \cdot$$

Spectra for both product radicals were observed, and it was clear that the radical from formamide contained deuterium and no hydrogen. Moreover, the hydroxyisopropyl radical contained a hydrogen rather than deuterium in the hydroxyl position, further showing that H had been abstracted. Finding H rather than D in $(CH_3)_2\dot{C}OH$ had further significance, since this radical was present in D_2O solution, and it is known that the hydroxyl hydrogen will exchange. This radical is estimated to have a lifetime of about 10^{-3} sec, which means that the exchange must proceed at a rate slow compared with this time. This is a novel method of obtaining information on an exchange process of this type. The process is much too slow to produce dynamic exchange phenomena, which may sometimes be observed in paramagnetic resonance spectra.

A methyl hydrogen was abstracted from *N*,*N*-dimethylformamide to give $HCON(CH_3)(\dot{C}H_2)$.

[20] H. Zeldes and R. Livingston, *J. Am. Chem. Soc.*, in press (July 1968).

[21] P. Smith and P. B. Wood, *Can. J. Chem.* 44, 3085 (1966).

Two radicals were observed in about equal amounts. These were rotational isomers and illustrated a lack of free rotation about the nitrogen bond to the carbon of the CO group. On the other hand, *N*-methylformamide gave only a single radical, $HCONH(\dot{C}H_2)$. Rotational isomers were not observed, presumably because the parent molecule from which the radical was made was present essentially all in one isomeric form. A methyl hydrogen was abstracted from acetamide to give $\dot{C}H_2CONH_2$, while the hydrogen abstracted from *N*-methylacetamide appeared to be from the *N*-methyl group. A mixture of radicals was obtained from *N*,*N*-dimethylacetamide, which could not be analyzed in detail, but the radicals were probably rotational isomers, similar to the situation found for *N*,*N*-dimethylformamide. The hydrogen abstracted from succinimide was from a CH_2 group.

Relaxation times were measured for the spectrum from $\dot{C}H_2CONH_2$, and the thermal relaxation time and spin-spin relaxation time were found to be equal. This suggested why spectra reported for radicals made by the rapid-mixing technique typically consist of lines much broader than those formed photolytically. The rapid-mixing method usually involves a redox system with a paramagnetic ion. The presence of this ion shortens the relaxation times.

Accurate hyperfine couplings and *g* values were measured for most of the observed radicals. Greater detail has been published elsewhere.[22]

NEUTRON AND X-RAY CRYSTALLOGRAPHY

An Aid to the Analysis of Interionic and Intermolecular Forces in Crystals

W. R. Busing

In molecular or ionic crystals, in contrast to covalent or metallic crystals, forces of intramolecular or intraionic origin may to a good approximation be regarded as intrinsic properties of the molecules or ions, more or less independent of the environment. It should be possible to develop a model for the remaining forces, those of intermolecular or interionic origin, which contribute to the stability of the crystal. Experimental information useful for determining the parameters of such a model could include some or all of the following: (1) lattice parameters and atomic coordinates observed by diffraction techniques, (2) thermochemical information, (3) elastic constants obtained by ultrasonic measurements, (4) lattice frequencies from infrared or Raman spectroscopic studies, and (5) details of lattice dynamics observed by inelastic neutron scattering methods. The resulting model could then be used to calculate values for any or all of the above-listed properties. Specifically, it should be possible (1) to predict the lattice parameters and atomic coordinates of unknown crystal structures, (2) to calculate the relative stabilities of different modifications of the same substance, (3) to compute anisotropic temperature factors for comparison with the results from diffraction experiments, and (4) to calculate the joint distributions of the thermal motion of atoms in a crystal so that reliable corrections could be made to apparent bond distances. Information obtained from the study of crystals would also be applicable to work on noncrystalline materials such as the prediction of the configurations of polypeptides.[23-25]

The classic work in this field is that of Born and Mayer,[26] who interrelated the lattice constants, elastic constants, and thermochemical data for the alkali halides by means of a model of this kind. More recently Kitaigorodskii[27] and Williams[28] have determined the attractive and repulsive parameters of hydrocarbon molecules on the basis of experimental crystal structures. Pawley[29] has used the model thus obtained to calculate the lattice vibration dispersion functions, elastic constants, anisotropic temperature factors, and infrared and Raman lattice frequencies for naphthalene and anthracene. In another study

[22] R. Livingston and H. Zeldes, *J. Chem. Phys.* 47, 4173 (1967).

[23] P. DeSantis, E. Giglio, A. M. Liquori, and A. Ripamonti, *Nature* 206, 456 (1965).

[24] D. A. Brant and P. J. Flory, *J. Am. Chem. Soc.* 87, 2791 (1965).

[25] R. A. Scott and H. A. Scheraga, *J. Chem. Phys.* 45, 2091 (1966).

[26] M. Born and J. E. Mayer, *Z. Physik* 75, 1 (1932).

[27] A. I. Kitaigorodskii, *Tetrahedron* 14, 230 (1961); *J. Chim. Phys.* 63, 6 (1966).

[28] D. E. Williams, *J. Chem. Phys.* 45, 3770 (1966); *J. Chem. Phys.* 47, 4680 (1967).

[29] G. S. Pawley, *Phys. Status Solidi* 20, 347 (1967).

Baur[30] has shown that the orientations of water molecules in several ionic crystalline hydrates can be predicted by considering the hydrogen bond as due entirely to simple electrostatic forces.

As an aid to this kind of work, a general computer program has been prepared which can be used in two ways: (1) Given the experimental lattice parameters and atomic coordinates for a crystal structure, the program will adjust the coefficients in the expression for the energy, or (2) given the coefficients which define this aspect of the model, the program will adjust the parameters of a trial structure.

The basic form of the energy expression used by the program is

$$W = \frac{1}{2} \sum_i \sum_j \frac{Q_i Q_j}{r_{ij}} - \frac{D_i D_j}{r_{ij}^6} + A_i A_j \exp[-(B_i + B_j) r_{ij}] ,$$

in which i ranges over the atoms in one unit cell and j extends over all atoms not in the same rigid body as atom i. In the first term, which represents the Coulomb energy, Q_i is the effective charge of atom i, and r_{ij} is the distance between the centers of atoms i and j. The second term represents van der Waals attraction, and D_i is a coefficient related to the polarizability of atom i. The final term, which includes two parameters, A_i and B_i, for each atom, represents the repulsive energy of the model. In the evaluation of W the Coulomb energy is obtained by Ewald's method,[31] in which the series is separated into reciprocal-lattice and direct-lattice sums.

Polarizable atoms are introduced by considering each atom i as composed of a shell and a core with charges Q_{si} and Q_{ci}, respectively, and with centers displaced from each other by a distance d_i. The expression for W is then elaborated by extending the Coulomb-energy term to include shell-shell, shell-core, core-shell, and core-core interactions and by adding another term, $\sum_i P_i d_i^2$, in which P_i is a coefficient of resistance to polarization for atom i.

The parameters defining W are considered in two groups. The set to be designated q_k, which includes the parameters Q_i, D_i, A_i, B_i, and P_i, are called coefficients of the model. Another set, p_k, entering into W indirectly through the values r_{ij}, are called structural parameters and may include the lattice parameters and the translations and rotations of groups of atoms assumed to be rigid. The model will be in static equilibrium if the energy, W, is a minimum with respect to these structural parameters; that is, if $\partial W/\partial p_k = 0$ for all k. The program uses the method of least squares, minimizing $\sum_k (\partial W/\partial p_k)^2$ to approach this condition. The derivatives of the types $\partial W/\partial p_k$, $\partial^2 W/\partial p_k \partial p_l$, and $\partial^2 W/\partial p_k \partial q_l$, which are needed for the nonlinear least-squares refinement, are obtained numerically by incrementing the appropriate parameters and recalculating W.

The two ways of using the program correspond to (1) fixing the structural parameters at their experimental values and varying the coefficients of the model or (2) fixing the coefficients of the model and varying the structural parameters. Structural parameters which are not known experimentally, such as the components of displacement of the shell relative to the core of a polarizable atom, are always included among the p_k's and varied to minimize $\sum_k (\partial W/\partial p_k)^2$.

The structures of crystals of low symmetry tend to yield more information than those of high symmetry. Thus the structure of NaCl yields only the cubic lattice parameter and therefore can be used to determine only one coefficient in the expression for W. The structure of orthorhombic $BaCl_2$, on the other hand, provides nine observations: three lattice parameters and two coordinates for each of three nonequivalent atoms. (The third coordinate of each atom is fixed by symmetry.) For $BaCl_2$, therefore, it should be possible to establish up to nine parameters of the model.

Because it is not always possible to recognize intuitively which parameters are well determined, it has been found useful to use the method of principal-component analysis for the solution of the least-squares equations. The eigenvectors of the matrix of normal equations are computed, and these describe independent linear combinations of the variables. The corresponding eigenvalues provide measures of how well each linear combination is determined. If insufficient information is available, it is necessary to forego the adjustment of those linear combinations which are

[30] W. H. Baur, *Acta Cryst.* 19, 909 (1965).

[31] P. P. Ewald, *Ann. Physik* 64, 253 (1921).

poorly determined. For example, in the case of the A_i's, which play the roles of atomic radii in the repulsive energy, it often happens that their sums are well determined but their differences are not. The program adjusts only those linear combinations of parameters which are meaningful for the determination of W.

Usually the program will be used first to adjust the energy coefficients on the basis of the experimental structure. If the model has fewer parameters than the structure, it will generally not be possible to reduce the derivatives $\partial W/\partial p_k$ exactly to zero. For the resulting model the structural parameters can then be varied to minimize W. The calculated structure can then be compared with the observed one. Listed in Table 9.2 are the observed[32] parameters of $BaCl_2$ together with those calculated from a model which was established as described. The agreement is reasonably satisfactory.

For this structure the calculation of the energy W to three significant figures required 0.10 sec on the IBM 360/75. For each cycle of least-squares refinement, W was calculated as many as 164 times in the evaluation of the derivatives. Five cycles of refinement required about 90 sec of machine time.

[32] K. Sahl, *Beitr. Mineral. Petrog.* 9, 111 (1963).

Table 9.2. Comparison of the Observed and Calculated Parameters for $BaCl_2$

Parameter	Observed	Calculated	Difference
a	9.415	9.468	0.053
b	7.878	7.843	−0.035
c	4.731	4.733	0.002
Ba x	0.1180	0.1170	−0.0010
y	0.2504	0.2495	−0.0009
Cl(1) x	0.431	0.429	−0.002
y	0.356	0.354	−0.002
Cl(2) x	0.829	0.831	0.002
y	0.473	0.472	−0.001

Addition of Higher Cumulants to the Crystallographic Structure-Factor Equation

C. K. Johnson

A variety of mathematical models can be used to describe the time-averaged vibrational displacement of an atom in a crystal. The most popular model in current use is based on the probability density function, or frequency function (fr.f.), of the trivariate normal distribution, which is written as

$$\Phi(u^1, u^2, u^3) = \frac{|p_{ij}|^{1/2}}{(2\pi)^{3/2}} \times \exp\left[-\frac{1}{2}\sum_{i,j=1}^{3} p_{ij}(u^i - x^i)(u^j - x^j)\right], \quad (1)$$

where u^1, u^2, u^3 are the contravariant components of a three-dimensional random variable (displacement vector), x^1, x^2, x^3 are the parameters of the mean of the fr.f., and the matrix $||p_{ij}||$ with covariant components is the inverse of the dispersion (variance-covariance) matrix $||\sigma^{ij}||$ defined in Eq. (2) below. The determinant of $||p_{ij}||$ is denoted as $|p_{ij}|$.

The characteristic function (c.f.) or Fourier transform of the fr.f. defined in Eq. (1) is

$$\phi(t_1, t_2, t_3) = \exp(i\sum_{i=1}^{3} x^i t_i - \frac{1}{2}\sum_{i,j=1}^{3} \sigma^{ij} t_i t_j), \quad (2)$$

where i, if not used as an index, is $\sqrt{-1}$. If we make the change of variables $t_i = 2\pi h_i$ and $||\beta^{ij}|| = ||b^{ij}||/2\pi^2$ $(i, j = 1, 2, 3)$, then multiply $\phi(h_1, h_2, h_3)$ by the atomic scattering factor $f(h_1, h_2, h_3)$, and sum over the n atoms of the unit cell, we obtain

$$F(h_1, h_2, h_3) = \sum_{k=1}^{n} f_k(h_1, h_2, h_3) \times \exp(2\pi i \sum_{i=1}^{3} x_k^i h_i - \sum_{i,j=1}^{3} b_k^{ij} h_i h_j), \quad (3)$$

which is the usual formulation for the structure factor equation with Miller indices (h_1, h_2, h_3),

anisotropic temperature factor coefficients b^{ij} $(i, j = 1, 2, 3)$, and fractional positional parameters (x^1, x^2, x^3). In other words, a c.f., transformed by the change of variables $t_i = 2\pi h_i$ $(i = 1, 2, 3)$, is a structure factor equation for a unit point scatterer. The use of the trivariate normal fr.f. model is called the quadratic approximation because of the quadratic form which appears in Eq. (1). Although Eq. (3) is an adequate model for most investigations in structural crystallography, there are instances when a more elaborate model is justified, for example, in systems involving librations or anharmonic vibrations.

Let us expand the c.f. ψ of an arbitrary trivariate fr.f. Ψ in terms of cumulants as

$$\psi(t_1, t_2, t_3) = \exp\left(i \sum_{i=1}^{3} {}^1K^i t_i + \frac{i^2}{2!} \sum_{i,j=1}^{3} {}^2K^{ij} t_i t_j + \frac{i^3}{3!} \sum_{i,j,k=1}^{3} {}^3K^{ijk} t_i t_j t_k + \frac{i^4}{4!} \sum_{i,j,k,l=1}^{3} {}^4K^{ijkl} t_i t_j t_k t_l + \ldots\right) . \quad (4)$$

The terms ${}^1K$, ${}^2K$, ${}^3K$, and ${}^4K$ are by definition the first four cumulants or semi-invariants of the fr.f. Ψ; they are tensors of rank 1 through 4 consecutively. Each of the tensors is invariant to pairwise interchanges of its indices, so that there are 3, 6, 10, and 15 unique elements in the four successive tensors. The problem of accurately determining 19 or 34 parameters per atom in the general case instead of the usual 9 parameters is discouraging, but it is not impossible. The four tensors describe the mean $({}^1\mathbf{K} \equiv \mathbf{x})$, the dispersion $(||{}^2K|| \equiv ||\sigma||)$, the skewness, and the kurtosis (peakedness-flatness) of the corresponding fr.f.

The fr.f. Ψ whose c.f. is Eq. (4) can be approximated by the first four terms of the Edgeworth series expansion[33–35] based on Eq. (1). This expansion is an asymptotic expansion using the derivatives of a normal fr.f. and for the trivariate case is

$$\Psi(u^1, u^2, \mu^3) = \left[1 - \frac{1}{6} \sum_{i,j,k=1}^{3} {}^3K^{ijk} D_i D_j D_k + \left(\frac{1}{24} \sum_{i,j,k,l=1}^{3} {}^4K^{ijkl} D_i D_j D_k D_l + \frac{10}{720} \sum_{i,j,k,q,r,s=1}^{3} {}^3K^{ijk}\, {}^3K^{qrs} D_i D_j D_k D_q D_r D_s\right)\right] \times \Phi(u^1, u^2, u^3) , \quad (5)$$

where D_i is the covariant differential operator $\partial/\partial u^i$. The individual D operators are commutative since the space is Euclidean. For example, the operator $D_j D_l D_i D_k = D_i D_j D_k D_l = \partial^4 / \partial u^i \partial u^j \partial u^k \partial u^l$. The correction term in parentheses in Eq. (5) is omitted if ${}^4K$ is not determined. For purposes of numerical evaluation, Eq. (5) can be reformulated in terms of the cumulant tensors and tensors containing multivariate Hermite polynomials.[33]

The modes and antimodes of a fr.f. are the local maxima and minima of probability density. In a centrosymmetric fr.f. the mean and a mode (or antimode) coincide. For a noncentrosymmetric fr.f. they may differ. The third cumulant tensor ${}^3K$ (skewness tensor) can be used in combination with ${}^1K$ and ${}^2K$ to locate the major mode of the fr.f. Intuitively, it seems that the mode may be a better estimate of the equilibrium position of an atom than is the mean (center of gravity).

If the procedure used to derive Eq. (3) from Eq. (2) is applied to Eq. (4), the resulting structure factor equation can be considered the "Edgeworth series model." The form of the equation is similar to the generalized structure-factor formalism of Dawson.[35] This model is basically a statistical model, free of kinematic assumptions, as is the trivariate normal fr.f. model (3).

The structure-factor least-squares program OR XFLS was modified to incorporate the third cumulant tensor using Eqs. (6) to (8) given below. For a crystal with n atoms in the unit cell, the structure factor at $\mathbf{h} = (h_1, h_2, h_3)$ is

$$F(\mathbf{h}) = A(\mathbf{h}) + i\, B(\mathbf{h}) , \quad (6)$$

[33] J. M. Chambers, *Biometrika* 54, 367 (1967).

[34] H. Cramer, *Random Variables and Probability Distributions*, chap. 7, Cambridge University Press, Cambridge, 1962; M. G. Kendall and A. Stuart, *The Advanced Theory of Statistics*, vol. 1, chap. 6, Hafner, 1958.

[35] B. Dawson, *Proc. Roy. Soc. A* 298, 255 (1967).

where

$$A(\mathbf{h}) = \sum_{r=1}^{n} \beta_r(\mathbf{h})\{f_r'(\mathbf{h}) \cos[\alpha(\mathbf{h})] - f_r''(\mathbf{h}) \sin[\alpha(\mathbf{h})]\},$$

$$B(\mathbf{h}) = \sum_{r=1}^{n} \beta_r(\mathbf{h})\{f_r'(\mathbf{h}) \sin[\alpha(\mathbf{h})] + f_r''(\mathbf{h}) \cos[\alpha(\mathbf{h})]\}, \quad (7)$$

and

$$\alpha_r(\mathbf{h}) = 2\pi \sum_{i=1}^{3} x_r^i h_i - \sum_{i,j,k=1}^{3} c_r^{ijk} h_i h_j h_k,$$

$$\beta_r(\mathbf{h}) = \exp\left(-\sum_{i,j=1}^{3} b_r^{ij} h_i h_j\right). \quad (8)$$

The variable coefficients x^i, b^{ij}, and c^{ijk} are ${}^1K^i$, $(2\pi^2)\ {}^2K^{ij}$, and $(4\pi^3/3)\ {}^3K^{ijk}$ $(i, j, k = 1, 2, 3)$. The atomic scattering factor $f(\mathbf{h})$ is complex with real part $f'(\mathbf{h})$ and imaginary part $f''(\mathbf{h})$ to account for the effects of anomalous dispersion.

Preliminary results on the refinement of crystal structures with the new model have been very encouraging. With a full set of accurate three-dimensional data, the variables are sufficiently independent to produce a well-conditioned linearized problem which can be readily solved with the usual least-squares normal-equations method. On option, the program can also solve the observational equations directly using the singular-value-decomposition method of Golub,[36] a technique which is extremely useful for rank-deficient least-squares problems.

An interpretation of the third-rank skewness tensor c for the thermal motion of an atom can be derived from (5). The correction term being added to the symmetric trivariate normal fr.f. $\Phi(u^1, u^2, u^3)$ is the antisymmetric trivariate function

$$\chi(u^1, u^2, u^3) = -\frac{1}{8\pi^3} \sum_{i,j,k=1}^{3} c^{ijk} D_i D_j D_k \Phi(u^1, u^2, u^3). \quad (9)$$

The c tensor can be decomposed by group theory into a sum of tensors of increasing symmetry. The general procedure for a tensor of any rank is given by Sirotin.[37] For any site symmetry it is possible to find a set of orthonormal tensor bases which span the space (one to ten dimensions) of the skewness constants. These tensors define three-dimensional antisymmetric functions into which any skewness function $\chi(u^1, u^2, u^2)$ may be decomposed. These basic antisymmetric functions can be plotted in stereoscopic pairs to illustrate the geometric aspects of the skewness.

Segmented-Body Analysis of Thermal Motion

C. K. Johnson

Further progress has been made toward generalizing the segmented-body approach to thermal-motion analysis outlined in last year's annual report.[38] A segmented body is a network of coupled rigid bodies; the individual rigid bodies are called segments.

Suppose we have a segmented body with two segments S_A and S_B. The displacement of S_B as seen from S_A is attributed to motion in a "joint" J_2 coupling S_B to S_A. The displacement of S_A as seen from some stationary point, "ground," is attributed to motion in a joint J_1 coupling S_A to ground. Finally, the displacement of S_B as seen from ground is described as the addition of motions of joints J_1 and J_2. The motion in a joint is given in terms of three translations and three rotations relative to an origin and an orthonormal triplet of basis vectors. Each joint has its own origin and basis tripiet, which are chosen to minimize the number of parameters needed to describe the motion. For example, torsion about a chemical bond coupling two segments is described by placing the origin on one of the atoms of the bond and one axis of the basis triplet along the bond; thus only one parameter is needed to describe the torsion.

Schomaker and Trueblood's analysis of rigid body motion[39] can be used to describe the mean-square displacement of atom j due to the mean-

[36] G. H. Golub and P. Businger, Stanford University Technical Report No. CS73 (1967).

[37] Yu. I. Sirotin, *Soviet Phys.-Cryst. (English Transl.)* 5(2), 157–320 (1960; also see Yih-O Tu, *Acta Cryst.* A24, 273 (1968).

[38] C. K. Johnson, *Chem. Div. Ann. Progr. Rept. May 20, 1967*, ORNL-4164, p. 127.

[39] V. Schomaker and K. N. Trueblood, *Acta Cryst.* B24, 63 (1968).

square motion of joint k. We define the following 3×3 matrices:

U_j, the mean-square displacement matrix for atom j in the "global Cartesian system." The components of this matrix are the "observed" quantities derived from the anisotropic temperature-factor coefficients.

Q_k, a rotation matrix to transform displacement coordinates from the "local Cartesian system" of joint k to the global Cartesian system.

$R_{jk}(x_j, p_k, Q_k)$, the transformation matrix to transform rotational displacement coordinates from the local Cartesian system of joint k to linear displacement coordinates in the global system. This matrix is a function of the position x_j of atom j and of the origin p_k and the orientation Q_k of the local Cartesian system for joint k.

T_k, L_k, S_k, the mean-square translation, libration, and screw-coupling matrices of Schomaker and Trueblood. These matrices are all based on the local Cartesian system of joint k with origin at p_k. The components of these matrices are the variables to be determined.

In the one-segment–one-joint (rigid body) problem the matrix of observational equations for atom j is

$$[Q\ R_j] \begin{bmatrix} T & S^T \\ S & L \end{bmatrix} \begin{bmatrix} Q^T \\ R_j^T \end{bmatrix} = U_j , \qquad (1)$$

and the equation for the complete system of n atoms connected as a rigid body is

$$A_{(3n\times 6)}\, B_{(6\times 6)}\, A^T_{(6\times 3n)} = C_{(3n\times 3n)} . \qquad (2)$$

A partitioned matrix representation of Eq. (2) is shown in Fig. 9.4, from which the structure of

ORNL-DWG. 67-7432

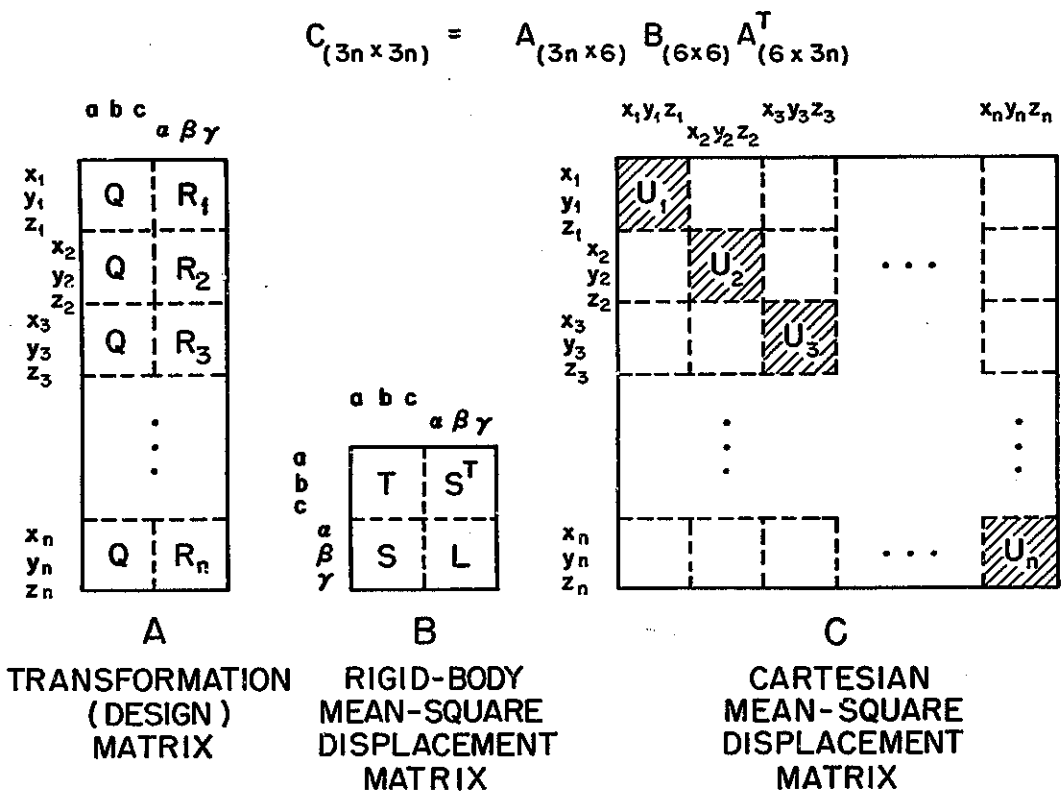

Fig. 9.4. Matrices Defining Mean-Square Displacements of an n-Atom Rigid Body.

ORNL-DWG. 67-7434

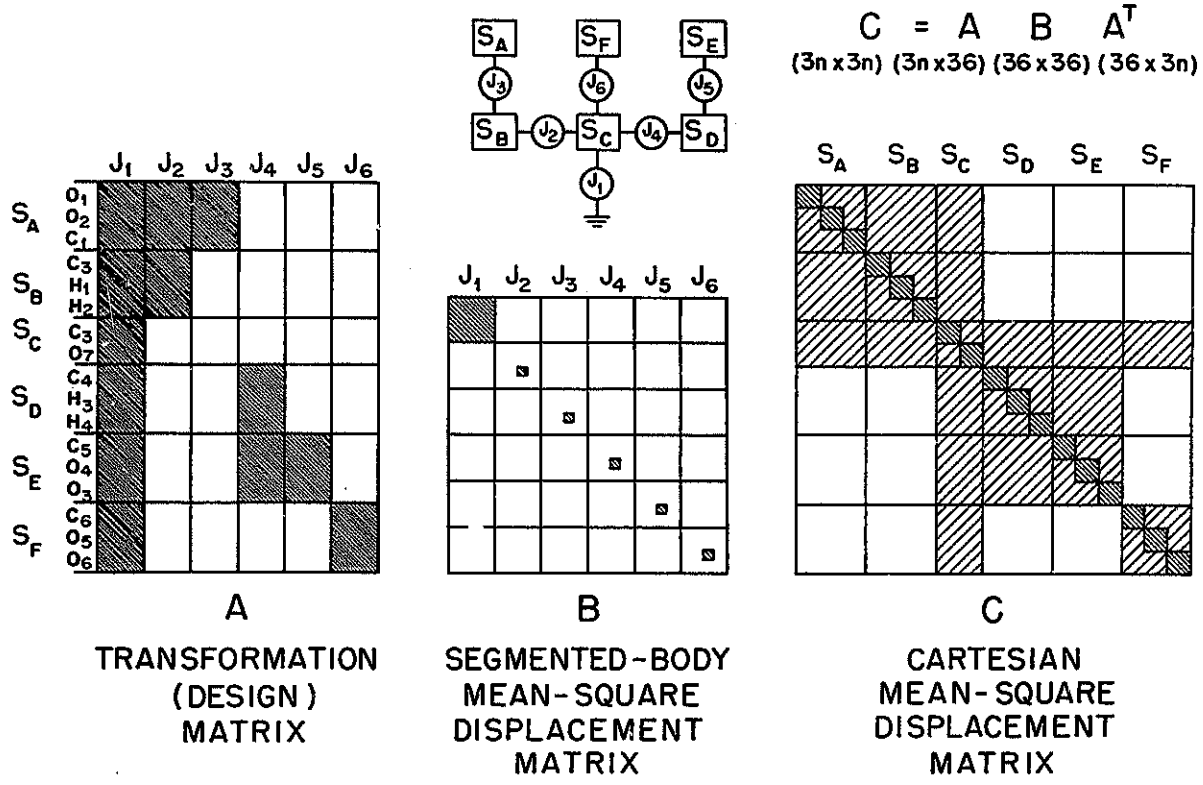

Fig. 9.5. Matrices for Segmented-Body Analysis of Citric Acid Using Six Riding Segments and Six Flexible Joints.

matrices **A**, **B**, and **C** may be related to matrices **Q**, **R**, **S**, **T**, **L**, and **U**. The off-diagonal submatrices of **C** are the interatom interaction mean-square amplitudes, which cannot be obtained from crystal structure data alone.

The basic equation for the segmented-body model is Eq. (2), except that the dimensions of the **A** and **B** matrices are changed. The new matrices for a specific example (citric acid) are shown in Fig. 9.5; this system is described as a segmented body with six segments and six joints. The 6×6 matrices along the block diagonal of **B** are identical to the rigid-body mean-square displacement matrix (**B** in Fig. 9.4). The off-diagonal blocks are cross terms, which in the "riding approximation" are defined to be zero. Each of the blocks along the diagonal in **B** represents a "joint" between two segments, or between a segment and "ground," and may represent either complete or restricted freedom of motion. For each joint, the origin and orthonormal basis triplet are chosen so that specific internal molecular motions are permitted.

The design matrix **A** shown in Fig. 9.5 is constructed by columnwise adjoining six transformation matrices (each having entries for all atoms) of the type shown in Fig. 9.4, one for each joint. The unshaded areas in **A** correspond to replacement of entries of zeros. The pattern of these zeros describes the sequence of riding of the segments and corresponds to the logic in the block diagram at the top center of Fig. 9.5, which is derived by mechanistic considerations of the citric acid molecule shown in Fig. 9.6. For ex-

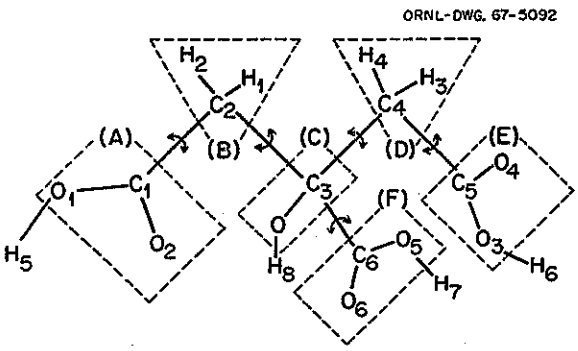

Fig. 9.6. Internal Torsional Motions of Citric Acid. Rigid segments A through F are enclosed by dashed lines.

ample, the motion of joint J_1 is carried to all segments; hence there are no unshaded areas in the J_1 column of **A**. The motion of joint J_2 is transmitted only to segments S_A and S_B, since in the riding approximation all other segments are unaffected by this motion. In the rows of the **A** matrix we see, for example, that segment S_A has the additive mean-square displacements resulting from the motion of joints J_1, J_2, and J_3.

The kinematic significance of "segment S_A riding on segment S_B" is that segment S_A has all the mean-square displacements resulting from the motion of segment S_B and, in addition, has an extra component of mean-square displacement uncorrelated with the motion of segment S_B. The additional motion is defined mathematically to be uncorrelated by the zeros in the off-diagonal blocks of matrix **B** in Fig. 9.5. If the actual inter-segment mean-square amplitudes of interaction should be known, they can be used to improve the model; however, such interaction terms cannot be determined directly from Bragg diffraction data alone. Further work is under way to add other data to the analysis, for example, observed spectroscopic vibrational frequencies for certain types of internal molecular vibrations.

A major numerical problem encountered in segmented-body analysis is an occasional dependent linear combination of variables. In this case, the resulting rank-deficient least-squares normal-equations matrix cannot be inverted with the usual matrix inversion procedures because the matrix is singular. The only solution is to identify the dependent linear combination and modify the model to eliminate the combination. On a trial and error basis this can be extremely time consuming and frustrating because of the complexity of the kinematic relationships. The statistical technique of regression on principal components[40] and the related technique of singular-value decomposition[41] provide practical solutions to the problem. These methods have been incorporated into the computer program for the segmented-body analysis. Both procedures are based on an eigenfunction decomposition and an elimination of the linear combinations (eigenvectors) corresponding to the zero, or very small, eigenvalues. Regression on principal components operates on the least-squares normal-equations matrix, while singular-value decomposition operates directly on the observational equations.

Sorting, Scaling, and Averaging Program for Crystal Diffraction Data

H. A. Levy R. D. Ellison

A set of diffraction data from a single crystal may include replicate and equivalent measurements and may involve measurements made by more than one technique, measurements on different samples, or measurements at different wavelengths. These data may be obtained in a random order. A frequently desired step in the evaluation of a crystal structure from such a data set is the reduction to an ordered set of values for non-equivalent reflections; this task may involve the determination of scaling factors to be applied to subsets of the data and the averaging of appropriately chosen scaled values. A computer program to accomplish this task is described here.

The program operates in two parts: Part 1 sorts the data according to a specified order of Miller indices (transformed if desired to identify equivalences) and subset identification, and averages over either a subset or the total set for a given reflection. Part 2 determines the scaling factors by a least-squares criterion. In the usual application, Part 1 for averaging over subsets is followed by Part 2 to evaluate scale factors, and finally by Part 1 to average the properly scaled values.

[40] W. F. Massy, *J. Am. Statist. Assoc.* **60**, 234 (1965).
[41] G. Golub, *Numerische Math.* **7**, 206 (1965).

The scale factor determination is carried out as suggested by Hamilton[42] by minimizing the quantity

$$\sum_i \sum_j [(Y_{ij} - S_j Z_i)/\sigma_{ij}]^2 ,$$

where Y_{ij} is the observed value of reflection i in subset j, σ_{ij} is its estimated standard error, the quantities S_j are the desired scale factors for subsets j, and Z_i are "best values" for the reflections i. The sum over i is for all measurements occurring in more than one subset. This nonlinear fitting, which determines values for S_j and Z_i, is carried out by means of a modification of the general FORTRAN least-squares program ORGLS.[43]

Further Refinement of the Crystal Structure of 6-Mercaptopurine Monohydrate

G. M. Brown

In last year's *Annual Report*[44] preliminary results from x-ray analysis of the crystal structure of the antileukemic drug 6-mercaptopurine were presented. It was discovered on publication of these results in abstract form[45] that another precise determination had been performed concurrently at the University of Washington by E. Sletten, J. Sletten, and L. H. Jensen.[46] Comparison of the two sets of results showed some discrepancies, slight but apparently significant. The remainder of the work on refinement of the 6-mercaptopurine structure at Oak Ridge has been carried out with especial care in an attempt to be sure that these discrepancies do not arise through the effects of faulty procedures in treating the data at any stage. However, the discrepancies remain about the same, emphasizing the familiar problem that attaining high accuracy in crystal-structure analysis is more difficult than attaining high precision in the fitting of a model to a set of experimental data.

Table 9.3. Unit-Cell Parameters of 6-Mercaptopurine

Standard errors corresponding to the least significant digits of the parameters are given in parentheses

	Sletten *et al.*	This Work
a	15.294(2) A	15.3314(4) A
b	7.732(1) A	7.7255(1) A
c	12.379(1) A	12.3397(2) A
β	101.64(1)°	101.526(2)°

Perhaps the most striking discrepancies between the Oak Ridge (OR) and University of Washington (UW) results are those between the two sets of unit-cell parameters, which remain even after redetermination of each set, including redetermination of the parameters of the UW crystal at OR. For each parameter (see Table 9.3) the difference between the two determinations is several times the corresponding standard error, the difference for the parameter c being especially marked. It seems likely that the differences in cell parameters arise from ~2% of unknown impurity now known to have been present in the UW sample of 6-mercaptopurine.

Refinement of the 6-mercaptopurine structure based on the OR intensity data was continued after correction of the data for absorption effects, a step which had been omitted in the preliminary work. Intensity data from θ-2θ scans below 30° 2θ were omitted in favor of the data from Ω scans which had been recorded in the same range; the data from the Ω scans are relatively free of errors in background resulting from absorption edge effects of the filter.

The OR data set showed very slight effects of extinction, the maximum effect for the most intense reflection being a reduction of intensity of only about 15% below the calculated intensity. Only about 20 of the 3792 reflections were affected by as much as 1%. The least-squares program used includes an extinction correction procedure,[47] which appeared to work quite satisfactorily. The

[42] W. H. Hamilton, *Acta Cryst.* 18, 129 (1965).

[43] W. R. Busing and H. A. Levy, *ORGLS, a General FORTRAN Least-Squares Program*, ORNL-TM-271 (June 1962).

[44] *Chem. Div. Ann. Progr. Rept. May 20, 1967*, ORNL-4164, p. 124.

[45] *Abstracts Am. Cryst. Assoc.*, Summer Meeting, Minneapolis, 1967, p. 26.

[46] E. Sletten, J. Sletten, and L. H. Jensen have kindly furnished a copy of the manuscript reporting their work.

[47] The second-order approximation of W. H. Zachariasen, *Trans. Am. Cryst. Assoc.* 1, 33 (1965). This procedure was coded into the least-squares program XFLS by H. Yakel of this laboratory.

data of the UW group do not show any extinction effects, probably because the crystal specimen used was smaller and because its crystalline domains were smaller (as indicated by quite broad peaks in θ-2θ scans).

For comparison with the results of the UW work, a least-squares refinement with the OR data was performed under conditions identical to those used by the UW group – same weighting scheme; same cutoff value of $(\sin\theta)/\lambda$, 0.714 A^{-1}; refinement on the structure-factor magnitudes F_0. The UW data and the OR data were also used in refinements in which the values F_0^2 were the observations, with a weighting scheme which gives relatively much more weight to the lower values of F_0^2. Comparison of these two pairs of results shows that the different weighting has little effect on the results and indicates that the OR and UW structures are significantly if only slightly different. Though differences in bond lengths involving the heavy atoms are rather small (maximum magnitude 0.007, mean 0.0032, rms 0.0036 A), a number of them amount to several times the corresponding standard deviations. The difference in purity of the OR and UW crystals is the probable cause of these small discrepancies, as well as of those in the cell parameters.

In further refinement procedures using the OR data, it was found that the effects on the derived molecular geometry of increasing the $(\sin\theta)/\lambda$ cutoff value from 0.714 to 0.857 A^{-1} and of using anisotropic instead of isotropic thermal parameters for the hydrogen atoms are trivial. There does appear to be some sensitivity to changes in the weighting.

Since attempts at refinement from x-ray data of anisotropic thermal parameters of hydrogen atoms have rarely been successful, the fact that anisotropic parameters were successfully refined in this case (when the full set of OR data were used) is of considerable interest. It is clear, however, that the thermal parameters of H(1) and H(7), on N(1) and N(7), respectively, cannot be interpreted in terms of thermal motion only: the probability ellipsoids[48] of H(1) and H(7) have odd shapes and orientations (see Fig. 9.7), which are probably related to deficiencies in the model as it describes the electron distribution in the molecule.

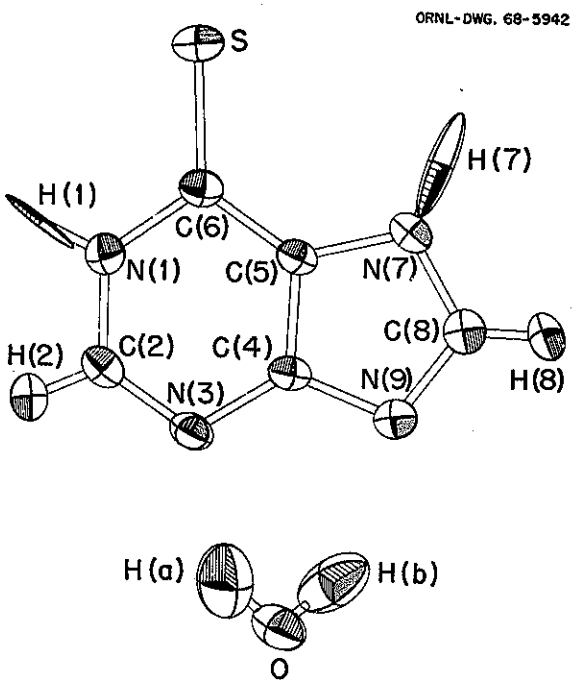

Fig. 9.7. The 50% Probability Ellipsoids of the 6-Mercaptopurine and Water Molecules in the Crystal Structure of 6-Mercaptopurine Monohydrate. For each molecule the view direction is perpendicular to the molecular plane.

An electron density difference map in the average plane of the nearly planar 6-mercaptopurine molecule was computed using the magnitudes $|F_0 - F_c|$, with F_c not including the hydrogen contributions and with signs of calculated structure factors including these contributions. There is some elongation in the peaks representing H(1) and H(7), but not so much as might be expected from Fig. 9.7. A striking feature of the map, which is quite similar to one prepared at UW, is that there is a low peak (0.15 to 0.40 electron/A^3, to be compared with peaks of 0.70 to 0.95 electron/A^3 for the hydrogen atoms) centered near the middle of each ring bond. Further analysis of difference maps is in progress, but it seems clear now that these peaks reflect real departures, caused by chemical bonding, from the spherical atoms assumed in the model.

The appearance in the difference map of these "bonding" peaks suggested that refinement be done including only data beyond the value of 0.5

[48] C. K. Johnson, *ORTEP: A Fortran Thermal-Ellipsoid Plot Program for Crystal Structure Illustrations*, ORNL-3794 (Revised), p. 70 (June 1965).

in (sin θ)/λ, in order to show, by comparison of results with those from the other refinements, any effects on the derived parameters from the fact that the model used does not take account of bonding effects on the electron distribution. Any departures in the actual structure from the spherical atomic electron distributions assumed in the model for the atoms at rest would chiefly affect only the low-angle terms omitted, according to the argument of Jeffrey and Cruickshank.[49] There are, in fact, slight but significant differences between the parameters from this refinement and those from one which includes the low-angle data. The parameters from this refinement are judged to describe most accurately the actual structure of 6-mercaptopurine. The calculated bond lengths and valence angles are shown in Table 9.4 with those of Sletten, Sletten, and Jensen for comparison.

Table 9.4. Bond Lengths and Angles in 6-Mercaptopurine Monohydrate

Standard errors are given in parentheses

Bond	Sletten *et al.*	This Work
Bond length, A		
N(1)–C(2)	1.350 (0.0020)	1.3578 (0.0013)
C(2)–N(3)	1.307 (0.0020)	1.3086 (0.0015)
N(3)–C(4)	1.364 (0.0016)	1.3607 (0.0012)
C(4)–C(5)	1.397 (0.0020)	1.3963 (0.0011)
C(5)–C(6)	1.396 (0.0020)	1.4051 (0.0013)
C(6)–N(1)	1.384 (0.0017)	1.3722 (0.0013)
C(6)–S	1.676 (0.0016)	1.6774 (0.0008)
C(5)–N(7)	1.370 (0.0017)	1.3729 (0.0013)
N(7)–C(8)	1.346 (0.0021)	1.3522 (0.0014)
C(8)–N(9)	1.326 (0.0019)	1.3326 (0.0014)
N(9)–C(4)	1.363 (0.0018)	1.3683 (0.0013)
N(1)–H(1)	0.85 (0.016)	0.881 (0.017)
C(2)–H(2)	0.95 (0.014)	0.956 (0.012)
N(7)–H(7)	0.86 (0.019)	0.874 (0.019)
C(8)–H(8)	0.96 (0.016)	0.954 (0.012)
O–H(A)	0.80 (0.023)	0.821 (0.020)
O–H(B)	0.83 (0.023)	0.836 (0.019)
Bond angle, deg		
C(6)–N(1)–C(2)	125.40 (0.12)	124.89 (0.09)
N(1)–C(2)–N(3)	125.05 (0.12)	124.99 (0.09)
C(2)–N(3)–C(4)	112.98 (0.12)	113.45 (0.08)
N(3)–C(4)–C(5)	124.24 (0.12)	123.96 (0.09)
C(4)–C(5)–C(6)	121.92 (0.11)	121.61 (0.08)
C(5)–C(6)–N(1)	110.38 (0.13)	111.07 (0.08)
C(5)–C(6)–S	127.01 (0.10)	126.62 (0.07)
N(1)–C(6)–S	122.61 (0.10)	122.30 (0.08)
C(6)–C(5)–N(7)	132.18 (0.13)	132.59 (0.08)
C(4)–C(5)–N(7)	105.88 (0.12)	105.79 (0.08)
C(5)–N(7)–C(8)	106.11 (0.12)	106.24 (0.08)
N(7)–C(8)–N(9)	113.59 (0.12)	113.46 (0.10)
C(8)–N(9)–C(4)	104.52 (0.12)	104.21 (0.08)
N(9)–C(4)–C(5)	109.90 (0.11)	110.29 (0.08)
N(9)–C(4)–N(3)	125.85 (0.12)	125.74 (0.08)
C(6)–N(1)–H(1)	119.5 (1.1)	119.76 (0.8)
H(8)–C(8)–N(9)	124.5 (1.1)	123.40 (0.8)
H(1)–N(1)–C(2)	115.1 (1.1)	115.31 (0.8)
N(1)–C(2)–H(2)	113.8 (1.0)	113.00 (0.8)
H(2)–C(2)–N(3)	121.1 (1.0)	121.95 (0.7)
C(5)–N(7)–H(7)	125.0 (1.2)	126.22 (0.9)
H(7)–N(7)–C(8)	128.9 (1.2)	127.48 (0.9)
N(7)–C(8)–H(8)	121.9 (1.1)	123.13 (0.8)
H(A)–O–H(B)	103.4 (2.2)	101.99 (1.4)

The Crystal Structure of Isoboldine Hydrobromide

G. M. Brown L. H. Hall[50]

A base $C_{19}H_{21}O_4N$ isolated from the Brazilian plant *Croton celtidifolius* by Dr. Rod Barnes[51] has been shown by x-ray analysis of its hydrobromide to be identical in structure and absolute configuration with the aporphine alkaloid isoboldine[52] (1), as had been suggested in part from a mass-spectroscopic analysis.[51]

ORNL-DWG. 68-6664

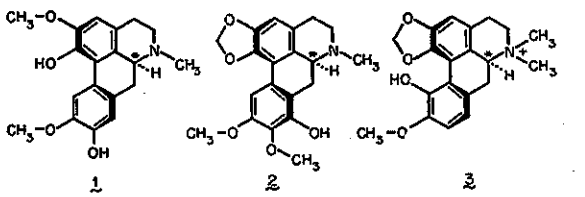

1 ISOBOLDINE 2 LEUCOXINE 3 N-METHYLBULBOCAPNINIUM CATION

The unit-cell parameters of the orthorhombic crystals (space group $P2_12_12_1$), which were de-

[49] G. A. Jeffrey and D. W. J. Cruickshank, *Quart. Rev. Chem. Soc. London* 7, 335 (1953).

[50] Department of Chemistry, Florida Atlantic University, Boca Raton; now at Department of Chemistry, Eastern Nazarene College, Quincy, Mass.

[51] Private communication.

[52] For references on isoboldine and other aporphine alkaloids, see the review by M. Shamma and W. A. Slusarchyk, *Chem. Rev.* 64, 59 (1964).

rived by the method of least squares[53] from measurements of 2θ, χ, and ϕ of 12 reflections using the Oak Ridge computer-controlled x-ray diffractometer,[53] are: $a = 7.543(1)$, $b = 21.402(2)$, $c = 11.503(1)$ A. There are four formula units $C_{19}H_{21}O_4N\cdot HBr$ per cell. A total of 2135 independent reflection intensity data were recorded with the θ-2θ scan technique and Cu $K\alpha$ radiation to the 2θ limit 159.4°. The raw data from the diffractometer were converted in the usual preliminary processing to a set of observed structure-factor squares F_0^2 and standard errors $\sigma(F_0^2)$. Absorption corrections were not made.

The solution for the structure was achieved in a straightforward manner by the classical heavy-atom method, and refinement proceeded smoothly. The anomalous dispersion property of bromine (tabulated value[54] of $\Delta f'' = 1.4$) was used to establish the absolute configuration by the method suggested by Hamilton and Ibers.[55,56] The values of the usual measures of goodness of fit,[57] $R(F)$, $R(F^2)$, $R(wF^2)$, and σ_1, are given in Table 9.5 for both of the two possible absolute configurations of the alkaloid cation. The ratio of the two values of $R(wF^2)$ is the Hamilton R-factor ratio $\mathcal{R}$. Comparison of the value of $\mathcal{R}$, 1.093, with the theoretical ratio $\mathcal{R}_{1,1909,0.005}$, 1.002 [from Hamilton's tables[56] for the probability level 0.005 and the appropriate dimension of the hypothesis and number of degrees of freedom (1 and 1909, respectively)], shows that the probability of incorrect choice of handedness is very much less than 0.5%. This independent determination of absolute configuration agrees with the assignment already made for isoboldine from measurements of optical rotation and optical rotatory dispersion.[52,58,59] The absolute configuration is the same as that found earlier in this laboratory for leucoxine[60] (2) and also the same as that in bulbocapnine methiodide (3), which has also been determined both by optical methods[52,58,59] and by x-ray analysis.[52,61]

The bond lengths in the isoboldine cation are given in Fig. 9.8, which shows the correct absolute configuration. Generally, as expected, the bond lengths are in quite close agreement with the corresponding bond lengths in leucoxine[60] (2).

An aspect of the structure of the aporphine alkaloids of considerable interest is the degree of twist about the central bond C(12)–C(13) of the biphenyl structure (rings *A* and *D*) embedded in the molecule. In isoboldine hydrobromide the twist is ~20°, to be compared with twists of ~14° in leucoxine hydrobromide and 30° in bulbocapnine methiodide. These differences can be understood readily in a qualitative way. There is relatively little interference in leucoxine between O(22) and the hydrogen atom on C(11); the twist is probably determined mostly by the attachment of the rings *B* and *C* to the biphenyl nucleus. In isoboldine, however, atom O(22) is closer to the hydrogen on C(11), not being pulled away from it by ring closure with C(17); the angle C(13)–C(14)–O(22) is 120.6° in isoboldine, 7.2° less than the angle in leucoxine. As a result, there is significantly more twist in isoboldine. The twist is greatest

[53] W. R. Busing, R. D. Ellison, H. A. Levy, S. P. King, and R. T. Roseberry, *The Oak Ridge Computer-Controlled X-Ray Diffractometer*, ORNL-4143 (January 1968).

[54] D. H. Templeton, p. 214 in *International Tables for the Determination of Crystal Structures*, vol. 3, Kynoch Press, Birmingham, England, 1962.

[55] J. A. Ibers and W. C. Hamilton, *Acta Cryst.* 17, 781 (1964).

[56] W. C. Hamilton, *Acta Cryst.* 18, 502 (1965).

[57] Definitions: $R(F)$ and $R(F^2)$ are defined by

$$\Sigma\left|\,|F^x_{obs}| - S^x|F^x_{cal}|\,\right| / \Sigma |F^x_{obs}| ,$$

with $x = 1$ and $x = 2$, respectively;

$$R(wF^2) \equiv [\Sigma w(F^2_{obs} - S^2F^2_{cal})^2/\Sigma wF^4_{obs}]^{1/2} ;$$

$$\sigma_1 \equiv [\Sigma w(F^2_{obs} - S^2F^2_{cal})^2/(n-p)]^{1/2} ,$$

where p is the number of parameters fitted to the n observations. The factor S is the factor scaling the values $|F_{cal}|$ to the values $|F_{obs}|$.

[58] C. Djerassi, K. Mislow, and M. Shamma, *Experientia* 18, 53 (1962).

[59] J. C. Craig and S. K. Roy, *Tetrahedron* 21, 395 (1965).

[60] G. M. Brown, *Chem. Div. Ann. Progr. Rept. May 20, 1966*, ORNL-3994, p. 114.

[61] T. Ashida, R. Pepinsky, and Y. Okaya, *Acta Cryst.* 16 (suppl.), A48 (1963).

Table 9.5. Measures of Goodness of Fit for the Two Possible Absolute Configurations of Isoboldine

Configuration	$R(F)$	$R(F^2)$	$R(wF^2)$	σ_1
Right	0.0676	0.1101	0.1458	2.695
Wrong	0.0751	0.1202	0.1594	2.945

ORNL-DWG. 67-12653

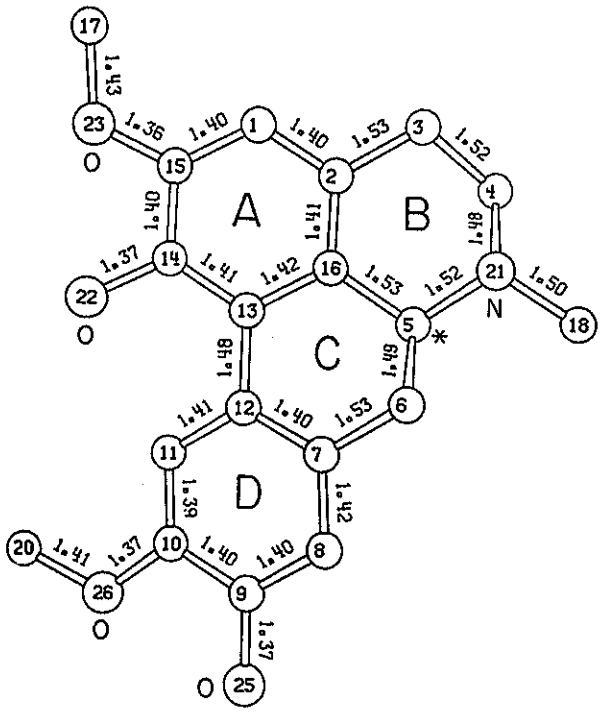

Fig. 9.8. Bond Lengths in the Isoboldine Cation in Crystalline Isoboldine Hydrobromide. The standard errors are all about 0.01 A. The correct absolute configuration is shown. The numbering of atoms (which omits 19 and 24) is consistent with the numbering used in an earlier study of leucoxine hydrobromide (see text). Atoms not labeled are carbon atoms; hydrogen atoms are not shown. The asterisk identifies the one asymmetric carbon atom.

in bulbocapnine methiodide because of the replacement of the H on C(11) by the larger OH group, even though the five-membered ring is present in this compound, as in leucoxine. It may eventually be possible and useful to correlate twist angles in the aporphine series with the optical rotatory dispersion properties. For this reason we intend to continue structure analysis in the series.

Although the hydrogen atoms themselves have not been located in this study, it seems clear that there are three kinds of hydrogen bonds, as shown in Table 9.6. The angles given in the table show

Table 9.6. Hydrogen Bonds in the Crystal Structure of Isoboldine Hydrobromide

Bond	Distance (A)	Angle	Degrees
N(21)—H ... Br^-	3.187	C(4)—N(21) ... Br^-	108.0
		C(5)—N(21) ... Br^-	108.2
		C(18)—N(21) ... Br^-	108.4
O(22)—H ... Br^-	3.197	C(14)—O(22) ... Br^-	138.7
O(25)—H ... Br^-	3.158	C(9)—O(25) ... Br^-	108.0

that the two hydrogen bonds N(21)—H ... Br^- and O(25)—H ... Br^- must be nearly linear but that the bond O(22)—H ... Br^- is rather angular.

A drawing of the isoboldine hydrobromide structure in the *a* axis projection is shown in Fig. 9.9.

The Molecular Structure of Glycolic Acid: Molecular Orientation and Thermal Motion

R. D. Ellison H. A. Levy

The crystal structure of glycolic acid as derived from neutron diffraction data was reported in a previous annual report.[62] We present here a supplementary discussion of the electron spin resonance (ESR) spectrum of gamma-irradiated glycolic acid[63] as related to the structure and considerations of the nature of the thermal motion of the glycolic acid molecules, including the effect on the bond-distance values.

The crystal structure[62] contains two crystallographically nonequivalent types of molecules, each of which occurs in a hydrogen-bonded chain parallel to the monoclinic **b** axis; these chains are cross-linked by somewhat longer, weaker hydrogen bonds into a loose three-dimensional network. The dimensions and local environment of the two molecular types are closely similar, but their orientations in the crystal lattice are distinctly different.

ESR Spectrum. — ESR spectra of gamma-irradiated crystalline glycolic acid, reported by Atherton and Whiffen,[63] were attributed to the glycolyl radical, O—$\dot{C}$(H)—COOH, formed by ionization of the neutral molecule and subsequent loss of a hydrogen

[62] R. D. Ellison and H. A. Levy, *Chem. Div. Ann. Progr. Rept. May 20, 1967*, ORNL-4164, p. 126.

[63] N. M. Atherton and D. H. Whiffen, *Mol. Phys.* 3, 1 (1960).

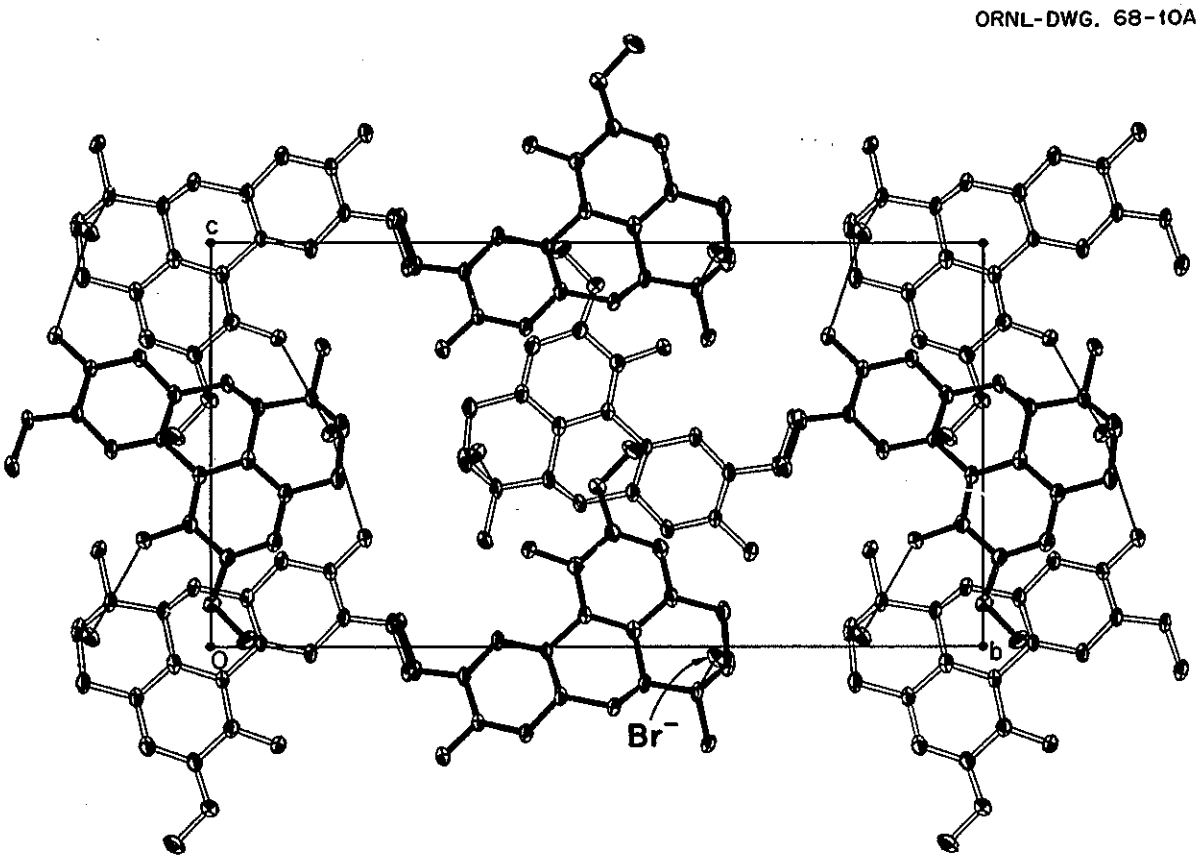

Fig. 9.9. The Structure of Isoboldine Hydrobromide in the *a* Axis Projection. The single lines indicate hydrogen bonds. The two hydrogen bonds N(21) – H . . . Br^- and O(22) – H . . . Br^- overlap in the projection.

atom. Although the monoclinic unit cell of glycolic acid was known to contain two crystallographically nonequivalent molecules, the spectra were interpreted in terms of a single orientation, and the authors therefore suggested that all molecules are parallel (or antiparallel) to each other and perpendicular to the crystal **c** axis. This conclusion was based largely on the observation that the ESR spectra are nearly symmetric with respect to twofold rotation about the **c** axis and about the mutual normal of **b** and **c**, thus displaying simulated orthorhombic symmetry superposed on actual monoclinic symmetry.

The observed crystal structure[62] does not confirm the suggestion of parallel or antiparallel molecules. The origin of the pseudo symmetry is, however, illustrated in Fig. 9.10, which shows a projection along **b** of the nonprimitive *B*-centered cell, in which **b** and **c** are common to the quoted monoclinic cell and the new **A** is **2a** + **c**; the length of *A* is 16.24 A, and the angle to **c** is 89.21°. It is clear that some pairs of molecules of the two types may be approximately interconverted by the operation of screw axes, and others by the operation of glide planes, which are parallel to the pseudo-orthorhombic directions. For example, the molecule designated in the figure (2, –0.37) is related approximately to molecule (1, –0.32) as though there were a twofold screw axis parallel to **c**. However, this operator does not convert molecule (1, –0.32) into (2′, –0.13); these latter are approximately related as though there were a glide plane parallel to the **b**-**c** plane.

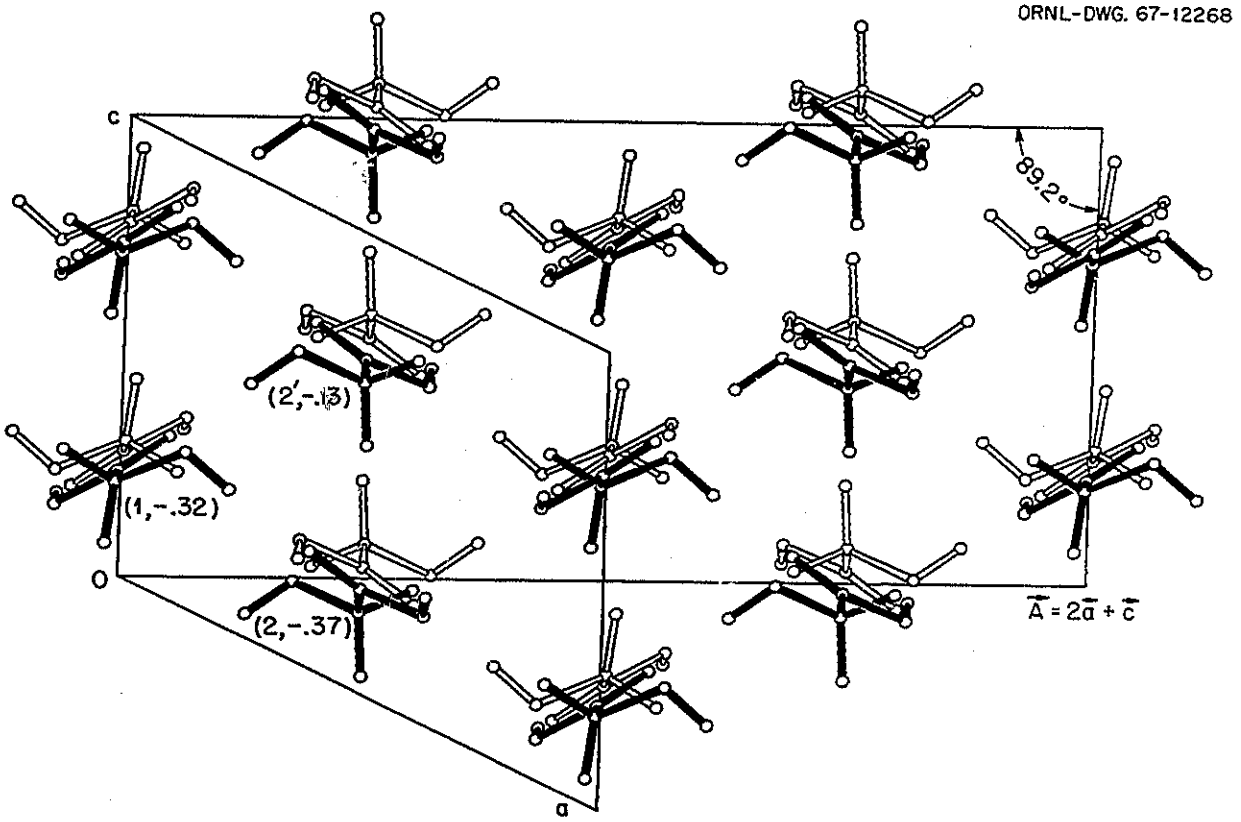

Fig. 9.10. The Crystal Structure of Glycolic Acid Viewed in b-Axis Projection. Both the primative monoclinic cell and a B-centered pseudo-orthorhombic cell are shown. The labels (n,z) designate molecule type number (1 or 2) and the z-coordinate of atom C(1n).

The erroneous conclusion concerning the molecular orientation appears to have arisen because in all the ESR measurements the magnetic field direction lay in the monoclinic symmetry plane, or in one of the pseudosymmetry planes **b-c** or **b-a×b**. Hence the spectra of at least two radicals were observed throughout as coincident or nearly coincident.

Thermal Motion. — The two nonequivalent molecules of glycolic acid are shown in the stereographic drawing[64] in Fig. 9.11, in which the atoms are represented by ellipsoids enclosing 50% of normally distributed thermal displacements. These drawings suggest that the molecules undergo oscillation and libration as nearly rigid bodies restrained by the hydrogen bonds. The motion has been analyzed by application of a computer program of C.K. Johnson[65] on the basis of the theory of rigid-body motion of Schomaker and Trueblood,[66] in which the motion is described in terms of three tensors of the second rank: **T**, describing translational motion, **L**, describing librational motion, and **S**, describing the interaction of translation and libration. The two hydrogen atoms attached to oxygen atoms were excluded from the rigid bodies,

[64] C. K. Johnson, *ORTEP: A Fortran Thermal Ellipsoid Plot Program for Crystal Structure Illustrations*, ORNL-3799 (Revised) (June 1965).

[65] C. K. Johnson, *Chem. Div. Ann. Progr. Rept. May 20, 1967*, ORNL-4164, p. 127.

[66] V. Schomaker and K. N. Trueblood, *Acta Cryst.* B24, 63 (1968).

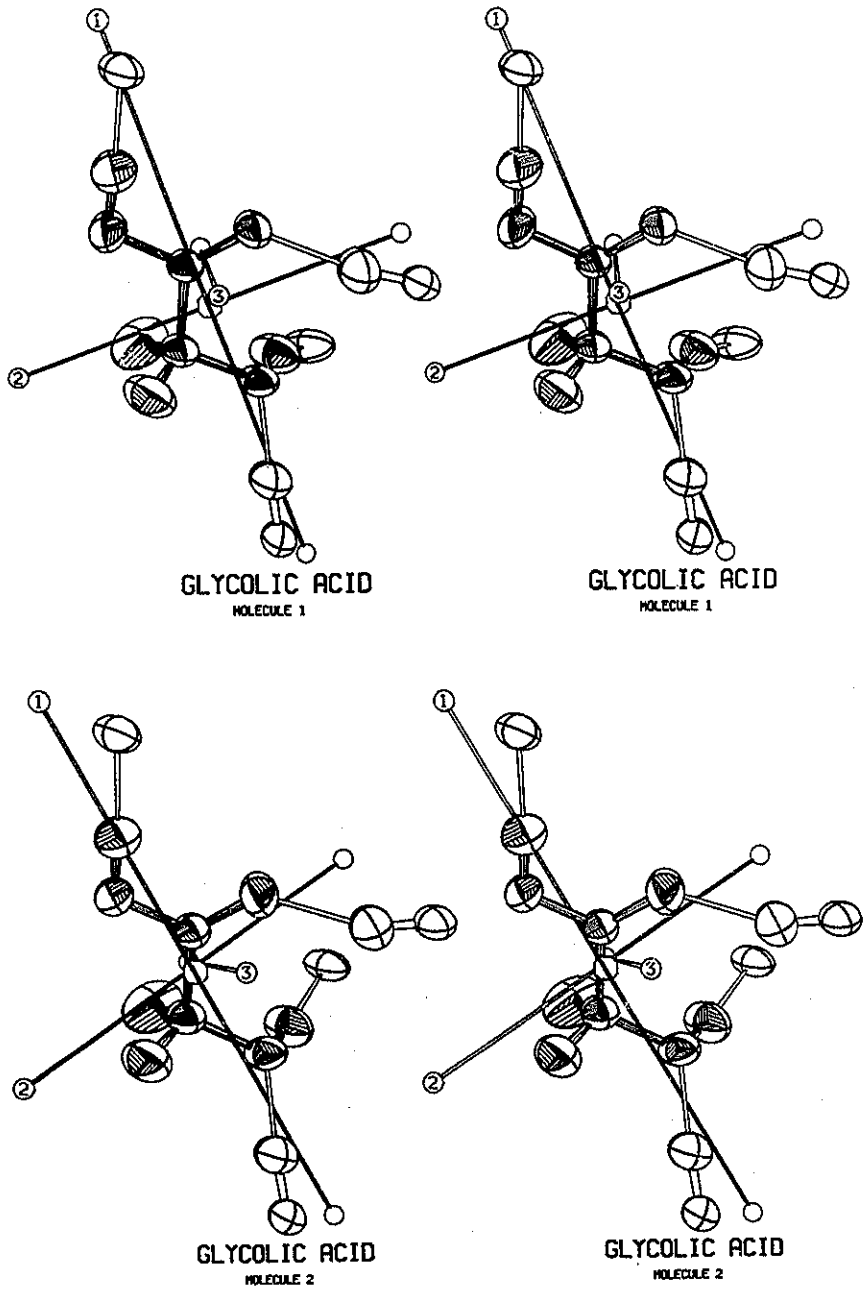

Fig. 9.11. Stereoscopic Drawings of the Two Crystallographically Distinct Molecules of Glycolic Acid. Atoms are represented by 50% probability ellipsoids. Unshaded ellipsoids represent hydrogen-bonded atoms of adjacent molecules. The nonintersecting helical libration axes are shown. For identification of the individual atoms, compare Fig. 8.18 of ref. 62.

since their displacements are substantially affected by internal rotation about the C–O single bonds. The thermal parameters of the aliphatic hydrogen atoms were first reduced by estimated values of their internal vibrational mean-square amplitudes, deduced from the frequencies of the normal modes[67] of the methylene chloride molecule; these are[68] 0.00578 A^2 along and 0.01369 A^2 perpendicular to the C–H bond. The fit of the rigid-body model to the observed thermal displacements is considered to be quite satisfactory for both molecules: the standard errors of fit are 0.0015 and 0.0016 A^2 for molecules 1 and 2, respectively, considering only the seven atoms included in the rigid bodies. The largest principal-axis components of the residual tensors are 0.0037 and 0.0031 A^2 respectively.

As shown by Schomaker and Trueblood,[66] the result of the rigid-body analysis may be interpreted as the superposition of six independent simple motions: three helical librations about a set of unique nonintersecting axes parallel to the principal axes of libration, and three translations. Parameters of these six independent motions are listed in Table 9.7 and are presented pictorially in Figs. 9.11 and 9.12. The wedge-cut cylinders

[67] T. Shimanouchi and I. Suzuki, *J. Mol. Spectry.* 8, 222 (1962).

[68] Computed with a program by M. D. Danford, which is a modification of one reported by J. H. Schachtschneider, *Vibrational Analysis of Polyatomic Molecules. III, Vibrational Secular Equation Programs*, Shell Development Co. Tech. Report 263-62 (1962).

Table 9.7. Interpretation of the Rigid-Body Thermal Motion of Glycolic Acid in Terms of Independent Simple Motions

		Molecule 1 Axis K			Molecule 2 Axis K		
		1	2	3	1	2	3
Helical motions (about nonintersecting axes)							
Rms amplitude, radians		0.187	0.091	0.046	0.186	0.087	0.047
Pitch,[a] A/radian		0.000	−0.192	0.768	0.075	−0.528	0.636
Direction[b]	$J = 1$	−0.251	−0.612	−0.750	0.437	0.793	−0.423
	2	0.940	−0.339	−0.038	−0.894	0.433	−0.112
	3	−0.231	−0.714	0.661	0.095	0.427	0.899
Center of reaction,[c] A		0.168	−0.652	0.332	−0.027	0.667	−0.075
Axis displacements,[d] A	$J = 1$		−0.146	0.579		0.057	−0.197
	2	0.011		−0.179	0.025		−0.385
	3	0.072	−0.305		0.025	−0.115	
Reduced translation[a,e]							
Rms amplitude, A		0.199	0.167	0.151	0.201	0.178	0.169
Direction[b]	$J = 1$	0.246	0.968	0.044	0.661	0.666	0.346
	2	0.034	0.036	−0.999	−0.096	0.532	−0.841
	3	−0.969	0.247	−0.025	−0.744	0.523	0.416

[a] Based on the arbitrary constraint trace $S = 0$.

[b] Columns are direction cosines of principal axis K with respect to Cartesian axes J parallel to a, b, and a × b, respectively.

[c] Referred to the Cartesian system of b with origins at atom C(11) for molecule 1 and C(22) for molecule 2.

[d] Columns are components of displacement of helical axis K along helical axes J from center of reaction.

[e] Defined in Eq. (20) of Schomaker and Trueblood (ref. 66).

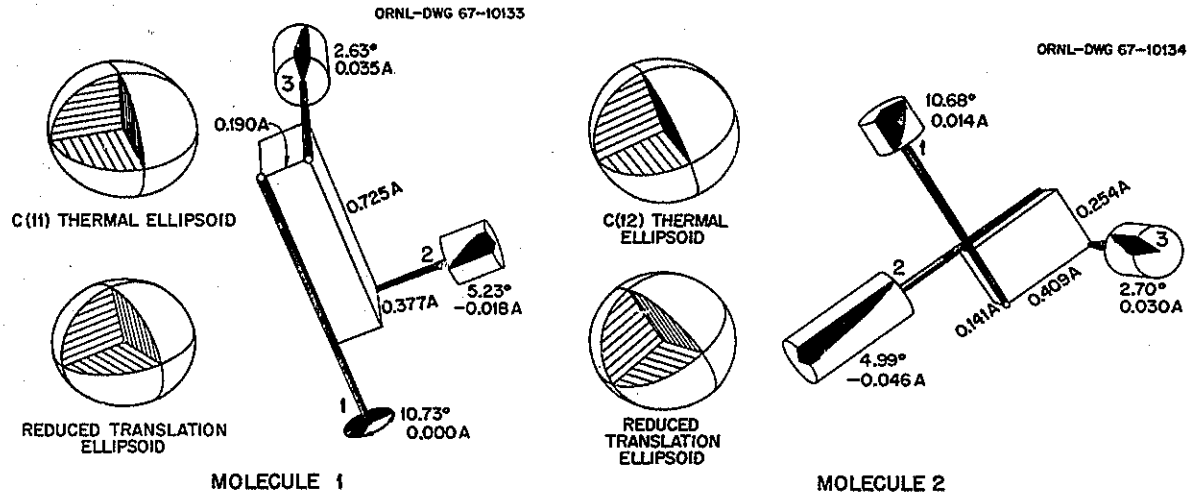

Fig. 9.12. Pictorial Display of the Rigid-Body Thermal Parameters of Glycolic Acid Molecules. For each molecule, the accented edges of the box represent the nonintersecting helical libration axes. The lengths of the attached cylinders represent the screw translations and the wedge cuts the angular rms amplitudes. The ellipsoids are for 50% probability and represent the reduced translation tensors, and for comparison the observed total displacement tensor of C(1) for each molecule. The angular amplitudes are magnified by a factor of ten; the scale for the screw translations is ten times that for the ellipsoids and the separation of axes. The orientation is the same as in Fig. 9.11.

in Fig. 9.12 have angles proportional to the respective principal root-mean-square librational amplitudes $L_{II}^{1/2}$ and lengths proportional to the associated screw-translations $S_{II}/L_{II}^{1/2}$. Also shown is the reduced translation ellipsoid[69] (50% probability surface) in correct orientation with respect to the molecule. For comparison, the observed atomic displacement ellipsoids[70] for the carboxyl carbon atoms C(11) and C(12) are shown.

It is of interest to examine the characteristics of the helical motions in relation to the inertial parameters of the molecules and the disposition of restraining hydrogen bonds. Helical axis 1, of largest angular amplitude, lies about 9° and 4° from the line connecting the α-hydroxyl oxygen atom to the carboxyl carbon atom, the O(21)–C(11) and O(22)–C(12) directions of the two molecules. This direction appears to be one of low moment of inertia; the corresponding libration only slightly distorts the two stronger hydrogen bonds O(1*n*)–H(1*n*)... O(2*n*) and O(2*n*)... H′(1*n*)–O′(1*n*) (*n* = 1, 2 refers to the molecule number) which lie in the chains parallel to **b**, and it produces mostly bending distortion of the two remaining, weaker, cross-linking hydrogen bonds. This placement is thus consistent with the relatively large angular amplitude and small screw components of this libration mode. In contrast, rotations about axes 2 and 3, with larger moments of inertia, produce marked distortions of all hydrogen bonds, and the corresponding libration amplitudes are smaller. Rotation about axis 2 produces marked stretching of hydrogen bonds O(2*n*)–H(2*n*)... O′(3*m*) and O(3*n*)... H′(2*m*)–O′(2*m*) ($n \neq m = 1, 2$); this distortion in both bonds is reduced by the left-handed helical component. Rotation about axis 3 appears to produce some stretching distortion of all four hydrogen bonds formed by each molecule, and

[69] For purpose of illustration, the reduced translation tensor is taken as

$$^{r}T'_{IJ} = T_{IJ} - \sum_{K=1}^{3} S_{KI}S_{KJ}/L_{KK}, \quad I, J = 1, 2, 3,$$

which differs from Eq. (20) of Schomaker and Trueblood (see ref. 66) by subtraction of the quantities S_{II}^2/L_{II} from the diagonal elements, in keeping with the notion of screw motion. In evaluating these quantities, the recommended constraint trace S = 0 was applied.

[70] For the labeling of the atoms, see ref. 62.

the distortion of each seems to be relieved by the right-handed helical component.

Since the rigid-body analysis of thermal motion gives a satisfactory fit and has a reasonable interpretation, the libration tensors were judged to be sufficiently reliable to be the basis for estimating bond length corrections. The corrected values were computed from the expression

$$\bar{S} = |\mathbf{S}_0| \{1 + (1/4\pi^2)[\text{trace}\,(2\pi^2\mathbf{L}\mathbf{g}) - \mathbf{S}_0^t\mathbf{g}(2\pi^2\mathbf{L})\mathbf{g}\,\mathbf{S}_0/\mathbf{S}_0^t\,\mathbf{g}\mathbf{S}_0]\}$$

where $\bar{S}$ represents the mean separation of two atoms, $\mathbf{S}_0$ is the interatomic distance vector, expressed in oblique crystal coordinates, $\mathbf{L}$ is the matrix of the libration tensor, also expressed in crystal oblique coordinates[71] and $\mathbf{g}$ is the matrix of the metric tensor whose elements are $\mathbf{a}_i \cdot \mathbf{a}_j$, the scalar products of the unit-cell translations. This expression is a generalization of one derived by Busing and Levy[72] and is equivalent to the dyadic expression, Eq. (22), of Schomaker and Trueblood.[66] In the case of the bonds from carbon to aliphatic hydrogen atoms, an additional correction was made for the internal motion, considering that in each case the hydrogen atom rides on carbon; the expression for the corrected value is

$$\bar{S}' = \bar{S} + (1/4\pi^2|\mathbf{S}_0|)[\text{trace}(\beta\mathbf{g}) - \mathbf{S}_0^t\mathbf{g}\,\beta\,\mathbf{g}\,\mathbf{S}_0/\mathbf{S}_0^t\mathbf{g}\,\mathbf{S}_0],$$

where β is the tensor for the internal motion, again expressed in oblique crystal coordinates. The tensors involved are listed in Table 9.8. In the case of the O—H bonds, which are influenced by internal rotations about C—O, the empirical riding model correction[72] (Busing and Levy, 1964) seems to be the best available. The corrected distances are listed in Table 9.9.

[71] The expression of L in crystal oblique coordinates was chosen for ease in programming the correction, since now $2\pi^2\mathbf{L}$ enters computationally as β does in the riding correction (see ref. 72). The components of L in the crystal oblique coordinates have dimensions radians^2/A^2.

[72] W. R. Busing and H. A. Levy, *Acta Cryst.* 17, 142 (1964).

Crystal and Molecular Structure of Rhenium Iron Carbonyl, $Re_2Fe(CO)_{14}$

P. A. Agron R. D. Ellison
H. A. Levy

The crystal structure[73] of the trinuclear metal carbonyl $Mn_2Fe(CO)_{14}$, reported briefly[74] in the

[73] P. A. Agron, R. D. Ellison, and H. A. Levy, *Acta Cryst.* 23, 1079 (1967).

[74] P. A. Agron, R. D. Ellison, and H. A. Levy, *Chem. Div. Ann. Progr. Rept. May 20, 1967*, ORNL-4164, p. 133.

Table 9.8. Rigid-Body and Internal Vibration Parameters for Glycolic Acid

	$ij = 11$	$ij = 22$	$ij = 33$	$ij = 12$	$ij = 13$	$ij = 23$
	Libration Tensor, $2\pi^2 L^{ij} \times 10^4$, Crystal Oblique Coordinates					
	L^{ij} in radians^2/A^2					
Molecule 1	30	57	28	−19	25	−15
Molecule 2	38	52	14	−24	15	−5
	Internal Vibration, $\beta^{ij} \times 10^4$					
H(31)	25.90	22.45	53.46	−5.16	22.12	0.76
H(41)	40.57	23.70	26.50	−0.46	16.54	−3.76
H(32)	24.87	21.60	39.42	−6.49	4.69	−6.13
H(42)	40.91	24.18	29.79	−0.06	21.28	0.97

Table 9.9. Intramolecular Interatomic Distances, A, in Glycolic Acid and Their Corrections for Thermal Motion

From	To	Molecule 1		Molecule 2		Model for Correction[b]
		Uncorrected[a]	Corrected	Uncorrected[a]	Corrected	
C(1)	O(1)	1.314(1)	1.329	1.310(1)	1.323	ML
	O(3)	1.205(1)	1.227	1.202(2)	1.225	ML
	C(2)	1.503(1)	1.514	1.505(1)	1.519	ML
C(2)	O(2)	1.403(1)	1.420	1.406(2)	1.420	ML
	H(3)	1.081(3)	1.115	1.084(2)	1.117	ML + IV
	H(4)	1.080(3)	1.115	1.083(3)	1.118	ML + IV
O(1)	H(1)	1.003(2)	1.007	1.001(2)	1.011	RM
O(2)	H(2)	0.970(3)	0.998	0.971(3)	0.988	RM

[a]Least-squares standard error in least-significant digit given in parentheses.

[b]ML = molecular libration; IV = internal vibration; RM = riding model.

1967 annual report, showed this molecule to be linear and symmetric, without bridging carbonyl groups. Two crystallographically nonequivalent molecules in the structure are closely similar, except for an apparent difference in Mn-Fe bond length of 0.03 A.

To extend this study to the analogous compound of rhenium, and to assess further the significance of the bond length variation, the crystal structure of the compound $Re_2Fe(CO)_{14}$ has been determined. The sample was furnished by Prof. R. Sheline of Florida State University.

Like the manganese analog, $Re_2Fe(CO)_{14}$ crystallizes in space group[75] $C2/m$ with cell dimensions of $a = 12.0620(8)$ A, $b = 14.6793(10)$ A, $c = 11.8164(5)$ A, $\beta = 97.310(5)°$ as determined from x-ray measurements and least-squares refinement. X-ray intensity measurements were made on 1932 independent reflections (Mo $K\alpha$ radiation) with the Oak Ridge Computer-Controlled Diffractometer[76] by the usual θ-2θ and ω scan techniques.

Examination of the Patterson function showed the structure to be closely similar to that of the manganese analog. The structural parameters, including the components of the anisotropic temperature factors, were refined by the method of least squares; the values of the usual measures of agreement are: $R_F = 0.0658$, $R_{F^2} = 0.0523$, $\sigma_1 = 1.0981$. Values of the molecular bond distances and some bond angles are listed in Tables 9.10 and 9.11; for identification of the atoms, compare Fig. 8.26 of ref. 74.

Like the manganese compound, molecules of $Re_2Fe(CO)_{14}$ are linear and chemically symmetric, of point symmetry $2/m$, without bridging carbonyl groups. The apparent difference in metal-to-metal bond length again appears; since in the present case the techniques of measurement were the standard ones, different from those employed[74] for the manganese compound, the hypothesis[73] that the difference arises from unusual systematic errors in data is ruled out. However, as in the former case, the two nonequivalent molecules are so similar in conformation and in chemical environment as to make highly implausible the possibility that the difference represents a real difference in molecular bond length.

We have examined the thermal motion parameters of the crystal for a possible explanation of the discrepancy. The pertinent data, listed in Table 9.12, are estimates of the mean separation[77] of iron and rhenium for the two nonequivalent mole-

[75]The designation on p. 133 of ref. 74 is in error.

[76]W. R. Busing, R. D. Ellison, H. A. Levy, S. P. King, and R. T. Roseberry, *The Oak Ridge Computer-Controlled X-Ray Diffractometer*, ORNL-4143 (January 1968).

[77]W. R. Busing and H. A. Levy, *Acta Cryst.* 17, 142 (1964).

Table 9.10. Bond Distances[a] in Rhenium Iron Carbonyl

Molecule 1		Molecule 2	
Bond	Distance (A)	Bond	Distance (A)
Fe(1)–Re(1)	2.8758(6)	Fe(2)–Re(2)	2.8493(6)
Fe(1)–C(1,1)	1.753(18)	Fe(2)–C(2,1)	1.735(17)
Fe(1)–C(1,2)	1.785(19)	Fe(2)–C(2,2)	1.769(14)
Re(1)–C(1,3)	1.983(11)	Re(2)–C(2,4)	1.987(12)
Re(1)–C(1,4)	1.876(17)	Re(2)–C(2,3)	1.932(16)
Re(1)–C(1,5)	1.990(11)	Re(2)–C(2,5)	1.992(11)
C(1,1)–O(1,1)	1.146(17)	C(2,1)–O(2,1)	1.219(17)
C(1,2)–O(1,2)	1.157(18)	C(2,2)–O(2,2)	1.170(15)
C(1,3)–O(1,3)	1.143(11)	C(2,4)–O(2,4)	1.140(12)
C(1,4)–O(1,4)	1.180(17)	C(2,3)–O(2,3)	1.135(16)
C(1,5)–O(1,5)	1.151(12)	C(2,5)–O(2,5)	1.159(12)

[a]Not corrected for thermal motion. For atom designations, see Fig. 8.26 of Ref. 74.

Table 9.11. Some Bond Angles in $Re_2Fe(CO)_{14}$

Molecule 1		Molecule 2	
Bond Angle	Angle (deg)	Bond Angle	Angle (deg)
C(1,1)–Fe(1)–Re(1)	90.4(5)	C(2,1)–Fe(2)–C(2,2)	89.4(6)
Fe(1)–Re(1)–C(1,4)	179.1(4)	Fe(2)–Re(2)–C(2,3)	180.000
Fe(1)–Re(1)–C(1,3)	87.3(3)	Fe(2)–Re(2)–C(2,4)	85.8(3)
Fe(1)–Re(1)–C(1,5)	87.3(3)	Fe(2)–Re(2)–C(2,5)	89.1(3)
C(1,3)–Re(1)–C(1,5)	88.8(4)	C(2,4)–Re(2)–C(2,5)	90.1(4)
C(1,3)–Re(1)–C(1,3)′	89.9(6)	C(2,4)–Re(2)–C(2,5)′	89.8(4)
C(1,5)–Re(1)–C(1,5)′	92.0(6)	C(2,4)–Re(2)–C(2,4)′	171.5(6)
C(1,3)–Re(1)–C(1,5)′	174.3(4)	C(2,5)–Re(2)–C(2,5)′	178.2(5)

Table 9.12. Mean Separation[a] of Rhenium and Iron in $Re_2Fe(CO)_{14}$ for Several Assumed Models of the Thermal Motion

Model	Molecule 1	Molecule 2
Uncorrected	2.8758(6)	2.8493(6)
Lower bound	2.8760(6)	2.8497(6)
Riding model	2.8795(7)	2.8543(6)
Independent motion	2.9106(7)	2.8786(6)
Upper bound	2.9453(10)	2.9074(9)

[a]See ref. 77.

cules, based on several assumed models for the correlation function of displacements for the two atoms. The two limiting cases, lower bound and upper bound, both correspond to completely correlated, and highly improbable, atomic motions; the middle range, encompassing the riding and independent motion models, represents the physically acceptable possibilities. It may be seen that if the motion of molecule 1 conforms to something like the riding model and that of molecule 2 to an approximation to independent motion, the discrepancy is removed to within the precision of the structure determination.

A difference in molecular motion of this sort would of necessity arise from differences in the molecular environment. Although the environments of the two molecules are chemically quite similar, they are of course crystallographically distinct. Examination of the van der Waals contacts between oxygen atoms indicates that such a difference in motion is not implausible: the motion of the central $Fe(CO)_4$ group is more strongly limited by these contacts in molecule 2, while that of the terminal $Re(CO)_5$ groups is more limited in molecule 1. In fact a rather short (2.80 A) end-on contact between apical oxygen atoms of adjacent molecules 2 would encourage lateral displacements of the end groups of this molecule; no analogous short contact occurs with molecule 1. Furthermore, in molecule 1, the mean-square displacements of iron perpendicular to the metal-metal bond are greater than those of rhenium, while the reverse is true in molecule 2. Thus in molecule 1 the iron atom is relatively free to follow the restrained thermal displacements of rhenium, in good approximation to riding motion, but in molecule 2, since motion of rhenium is promoted and motion of iron is restrained, the distribution of relative displacements may be expected to approach that described by the independent motion model.

Crystal Structures of Two Stereoisomeric Photodimers of Isophorone

C. K. Johnson A. Vos[78]

Photodimers are receiving considerable attention in the biological literature because of the photodimerization of thymine in DNA. Recent crystallographic work[79] in the ORNL Biology Division has elucidated the crystal structures of several different thymine photodimers. Another compound which undergoes photodimerization in ultraviolet light is isophorone, I. The photodimerization of

ORNL-DWG. 68-6655

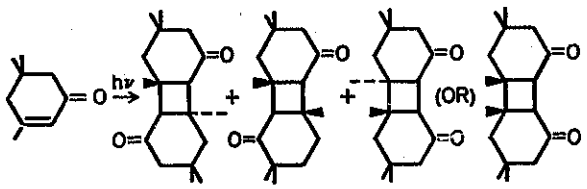

I II III IVa IVb

isophorone has been under study by V. F. Raaen[80] of this division for several years. Features in common between the two photodimer systems include the two methyl groups on the cyclobutane ring, a carboxyl group adjacent to the cyclobutane ring, and the possibility of four distinct stereoisomers. Crystals of the isophorone photodimers are completely stable, while the thymine photodimers are quite susceptible to radiation damage during the diffraction experiment.

[78] Visiting scientist from the Laboratory of Structural Chemistry, Rijksuniversiteit Groningen, the Netherlands, supported in part by fellowships from the American Association of University Women and the North Atlantic Treaty Organization.

[79] J. R. Einstein, J. L. Hosszu, J. W. Longworth, R. O. Rahn, and C. H. Wei, *Chem. Commun.*, p. 1063 (1967).

[80] V. F. Raaen, "Photodimerization of Isophorone," this report.

Table 9.13. Photodimers of Isophorone

	II, Head-to-Tail, *cis-anti-cis*	III, Head-to-Tail, *cis-syn-cis*	IV, Head-to-Head, *cis-anti-cis* or *cis-syn-cis*
Melting point	214–215°	114°	187°
Space group	$P\bar{1}$	$P2_1/a$	*Aa* or *A2/a*
a[a]	8.084 A	15.476 A	16.09 A
b	9.092 A	11.312 A	17.37 A
c	5.859 A	10.911 A	12.48 A
α	103.58°		
β	74.28°	116.93°	106.4°
γ	94.90°		
z	1	4	8

[a] A more accurate determination of the cell parameters for the three crystals remains to be done.

The three crystalline photodimers[80] isolated by V. F. Raaen during his study of the irradiation products of isophorone were examined by diffraction methods and the crystal structures determined for two of the three compounds. A crystal structure analysis[81] of derivative IV is currently under way at Iowa State University using material from an independent study by O. L. Chapman of that university. The melting points, cell parameters, and space groups of the three crystalline derivatives II, III, and IV are given in Table 9.13. The configurations of II and III were determined in this study and are shown in Figs. 9.13 and 9.14.

The crystal structure of II was solved from 2836 independent three-dimensional neutron dif-

[81] T. A. Beineke, private communication (1968).

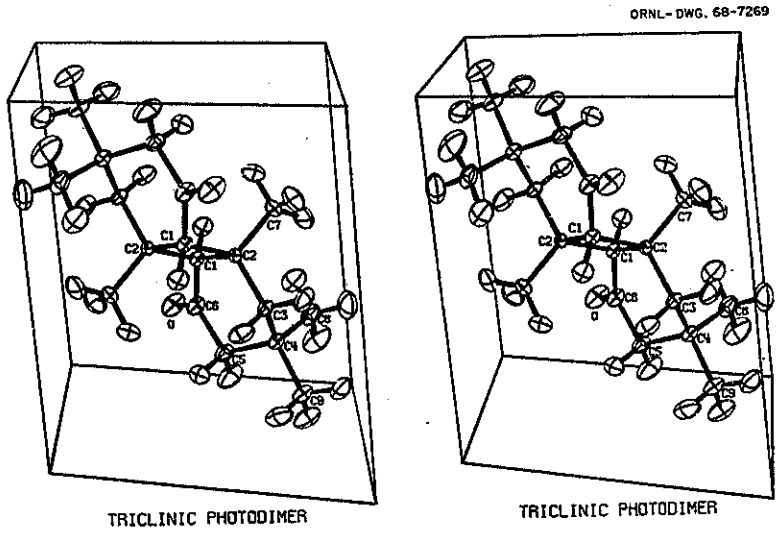

Fig. 9.13. Stereoscopic Drawing of the *cis-anti-cis* Head-to-Tail Photodimer II of Isophorone with Thermal Ellipsoids. Structure was determined from neutron diffraction data.

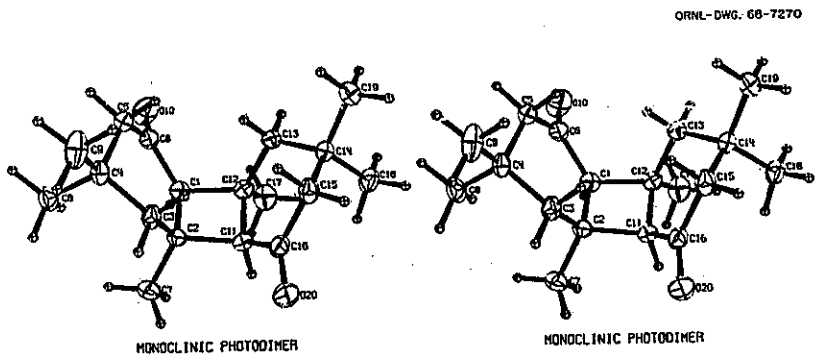

Fig. 9.14. Stereoscopic Drawing of the *cis-syn-cis* Head-to-Tail Photodimer III of Isophorone with Thermal Ellipsoids for Carbon and Oxygen Atoms. Hydrogen atoms are drawn as small spheres. Structure was determined from x-ray diffraction data.

fraction intensities collected from a 70-mg crystal. The automatic diffractometer at the ORR was used with neutrons of wavelength 1.077 A. Corrections for absorption were made and the usual methods for data reduction applied. The statistical distribution of the intensities strongly indicated a centrosymmetric space group, which was confirmed by the structure analysis. The carbon and oxygen atom positions were determined from a three-dimensional Patterson synthesis. There are no translational parameters involved in positioning the molecule in the unit cell since the centrosymmetric molecule lies on an inversion center. The analysis was not strongly hampered by the occurrence of the negative peaks representing the vectors between hydrogen and carbon (or oxygen) atoms. All hydrogen atom positions, including those on the three different methyl groups, were located from an F_0 Fourier synthesis based on the positions of the carbon and oxygen atoms found from the Patterson synthesis.

Refinement by the method of least squares proceeded smoothly until rather severe effects of extinction became evident. A correction term based on the new theoretical treatment for extinction by Zachariasen[82] was then coded into the least-squares structure-factor program, giving an additional adjustable parameter. The resulting correction for extinction produced excellent results, and the structure refined to an R value of 0.056 (based on F^2) for all data.

The crystal structure of III was solved from 3345 independent x-ray diffraction intensities collected with our computer-controlled x-ray diffractometer.[83] Copper $K\alpha$ radiation was used, and the usual data reduction techniques, including corrections for absorption, were applied to the intensity data. A computer program[84] which automates the symbolic addition method[85] was used to solve the phase problem. Of the seven symbols initially assigned, three were eliminated by arbitrarily choosing three signs for appropriate sym-

[82] W. H. Zachariasen, *Acta Cryst.* 23, 558 (1967).

[83] W. R. Busing, R. D. Ellison, H. A. Levy, S. P. King, and R. T. Roseberry, *The Oak Ridge Computer-Controlled X-Ray Diffractometer*, ORNL-4143 (January 1968).

[84] E. B. Fleischer, A. L. Stone, and R. B. K. Dewar, *MAGIC—Multiphase Automatic Generation from Intensities in Centric Crystals*, FORTRAN program, University of Chicago (1966).

[85] J. Karle and I. H. Karle, *Acta Cryst.* 21, 849 (1966).

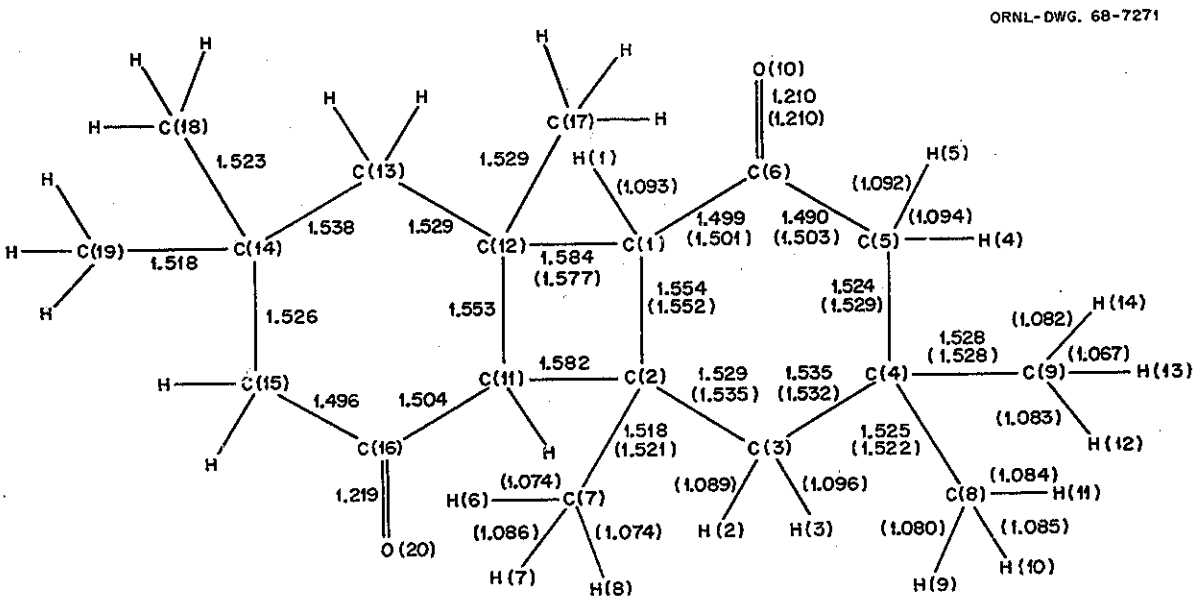

Fig. 9.15. Bond Lengths in the Head-to-Tail Photodimers of Isophorone. Values in parentheses are from the neutron diffraction study of the *cis-anti-cis* isomer II. Values not in parentheses are from the x-ray diffraction study of the *cis-syn-cis* isomer III.

ORNL-DWG. 68-7272

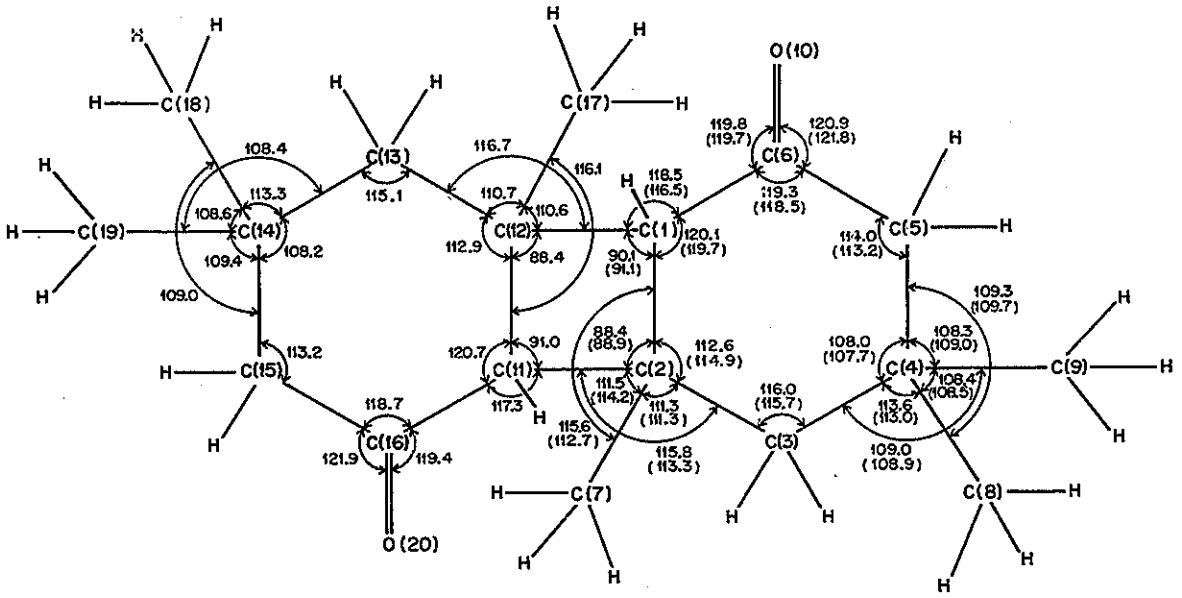

Fig. 9.16. Bond Angles in the Head-to-Tail Photodimers of Isophorone. Values in parentheses are from the neutron diffraction study of the *cis-anti-cis* isomer II. Values not in parentheses are from the x-ray diffraction study of the *cis-syn-cis* isomer III.

bols to fix the position of the origin. This procedure gave $2^4 = 16$ possible structures. Three-dimensional Fourier syntheses were calculated for 4 of the 16 sign combinations having the greatest probability of being correct. The positions of the 20 independent carbon and oxygen atoms were easily found from one of the four Fourier maps. Later it was found that 74 of the 602 reflections used in calculating the preliminary Fourier map had incorrect signs, but this did not affect the progress of the structure determination appreciably. The 28 hydrogen atoms, including those on all six unique methyl groups, were found with a difference Fourier synthesis with phases based on the positions of the heavy atoms. Although the refinement is not yet complete, the present R factor (based on F^2) is 0.056, which is the same as that for photodimer I. Near the end of the refinement, anisotropic temperature factors for the hydrogen atoms were estimated by a rigid-body-motion analysis of the thermal parameters for the heavy atoms and were not varied in the subsequent least-squares cycles.

The stereochemical configuration and thermal ellipsoids of the two structures are illustrated with stereoscopic drawings in Figs. 9.13 and 9.14. Figures 9.15 and 9.16 show the bond lengths and valence angles for the heavy atoms of the two isomers. No major differences are observed between corresponding distances and angles. The C–C bonds of the four-membered ring are relatively long (1.555 to 1.582 A), and those bordering the C=O groups are the shortest (1.490 to 1.503 A). Bond length corrections for thermal motion have not been applied.

Preparation and Crystal Structure of CfOF

J. H. Burns J. R. Peterson

See p. 41.

Crystal and Molecular Structure of Cesium Tetrakishexafluoroacetylacetonatoeuropate(III) and -Americate(III)

J. H. Burns M. D. Danford

See p. 42.

Preparation and Properties of Some Rare-Earth and Americium Chelates

M. D. Danford J. H. Burns

See p. 44.

X-Ray Diffraction Studies of Liquids

A. H. Narten

Diffractometer. – The diffractometer for liquid samples has been in continuous operation for 265 days of the year. With an average counting time of 38 days (24 hr/day) for an experiment, seven complete diffraction patterns were measured. Reliability of the diffractometer and stability of its electronic components are prerequisites for these long experiments. The resulting diffraction data are of a precision that is unequaled and limited only by the inherent difficulties associated with radiation scattering from liquid systems. The available computing facilities make it possible to extract from these data detailed information on the average atomic and molecular arrangement in the liquid state.

Benzene. – Earlier work on the structure of some simple nonpolar liquids has been supplemented with a study of liquid benzene, from which a structural model has been proposed. In this model, the benzene ring is a regular hexagon with a C–C distance of 1.41 A,[86] in good agreement with gas diffraction results. In the liquid, each molecule "sees" 12 neighboring molecules in preferred orientations, surrounded by a random distribution of distances. The molecular arrangement, illustrated in Fig. 9.17, is surprisingly similar to that of the solid. The molecule pairs

[86] A. H. Narten, *Chem. Div. Ann. Progr. Rept. May 20, 1967*, ORNL-4164, p. 135.

ORNL-DWG. 67-9464

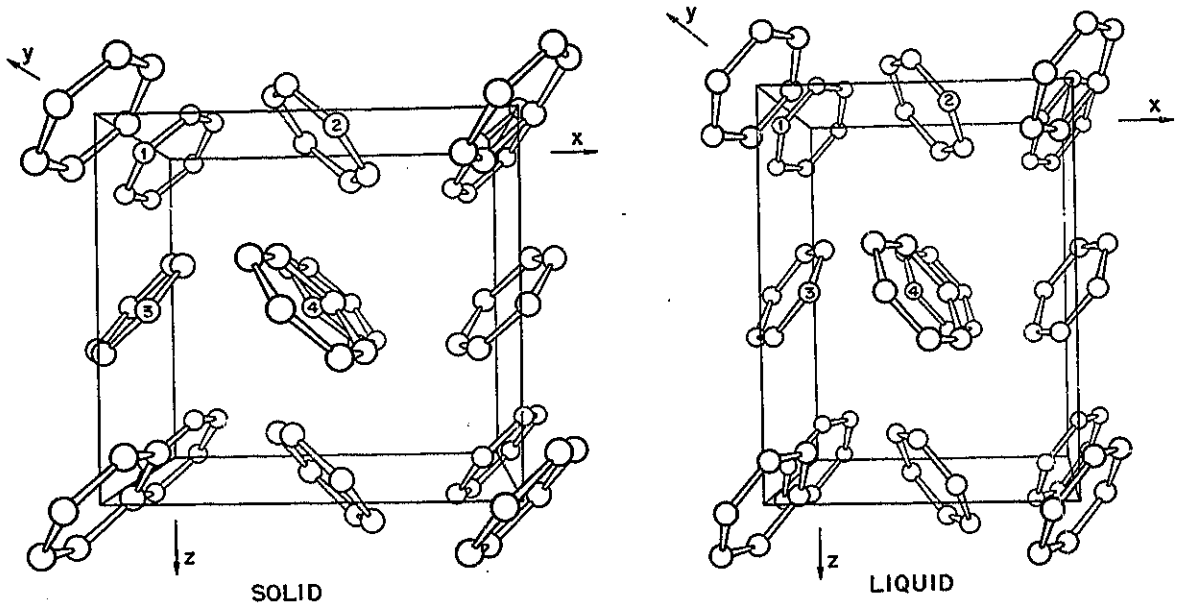

Fig. 9.17. Structure of Benzene. Solid at –3°C, liquid at 25°C. (Only carbon atoms shown).

1 and 2 (or 3 and 4) fit together like six-toothed bevel gear wheels whose axes are almost at right angles, and the molecules so related form corrugated sheets perpendicular to the *c* axis of the crystal. The axes of molecules 1 and 3 are inclined at 41° (26° in the solid), and they are not intermeshed. The planes of molecules 1 and 4 are inclined at 64° (84° in the solid), and the extension of the plane of 4 passes close to the center of 1. Since the molecules of types 1 and 2 bind the structure more tightly in the *a* and *b* directions than do molecules of types 1 and 4 which extend in the *b* and c directions, the large expansion of the liquid in the *c* direction of the crystal, found for the model, appears plausible. The computed radial distribution function for the model is compared with that observed for the real liquid in Fig. 9.18.

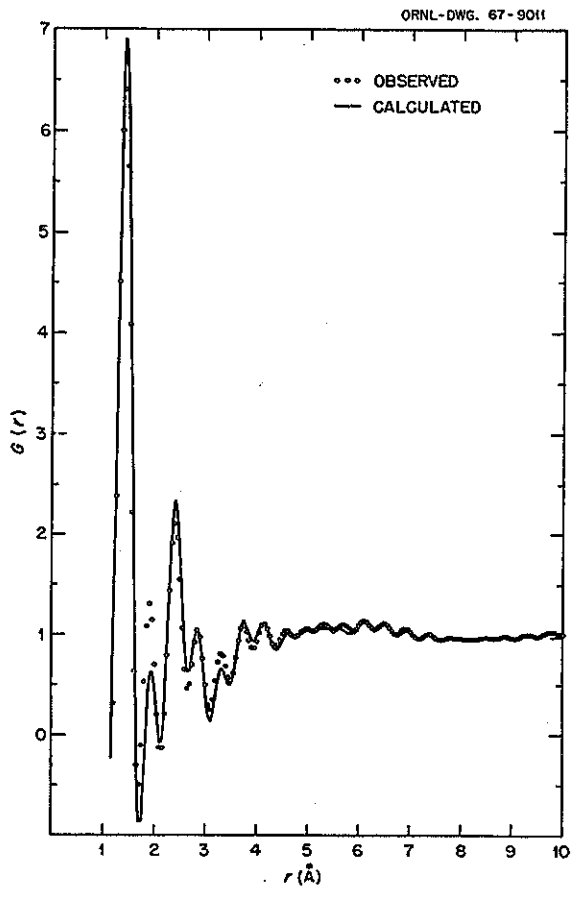

Fig. 9.18. Radial Distribution in Liquid Benzene at 25°C.

Methanol. – The diffraction pattern of liquid methanol has been measured at 20°C. Both the intramolecular distances and the associated rms displacements derived from this study are identical with values obtained from gas diffraction experiments[87] (1.42_8 and 0.049 A, respectively, for the C – O interaction). This result indicates that the precision of liquid diffraction data can be comparable with the high precision achieved in electron diffraction experiments with gaseous molecules.

Studies of other aliphatic alcohols are planned to obtain information on the conformation of hydrogen-bonded straight-chain molecules in the liquid state.

Aqueous Solutions. – The structure of water and aqueous solutions continues to be the subject of controversy. We have shown[88] that a model based on a modified ice I structure (ice I model) explains the observed diffraction pattern of liquid water from 4 to 200°C quantitatively.

The gas hydrate model for pure water (originally proposed by Pauling[89]) was again investigated in detail. As stated previously,[88,90] this model or any reasonable modification of it yields radial distribution functions which do not agree with those derived from experiment (Fig. 9.19). A critical review of other water models for which agreement with diffraction data has been claimed is under way. In the meantime, a study of simple 1-1 electrolyte solutions has yielded considerable information on the influence of these solutes on water structure. The ice I model, with proper adjustment of its parameters, is capable of explaining the diffraction patterns of all systems that have been studied.

Butylammonium Fluoride. – Aqueous alkylammonium halide solutions have thermodynamic properties which are unusual in many respects. It is thought that the large cations promote structure in water,[91] possibly in the form of clathrate

---

[87] K. Kimura and M. Kubo, *J. Chem. Phys.* 30, 151 (1959).

[88] A. H. Narten, M. D. Danford, and H. A. Levy, *Discussions Faraday Soc.* 43, 97 (1967).

[89] L. Pauling, p. 1 in *Hydrogen Bonding*, ed. by D. Hadzi, Pergamon, New York, 1959.

[90] M. D. Danford and H. A. Levy, *J. Am. Chem. Soc.* 84, 3965 (1962).

[91] S. Lindenbaum, *Chem. Div. Ann. Progr. Rept. May 20, 1967*, ORNL-4164, p. 67.

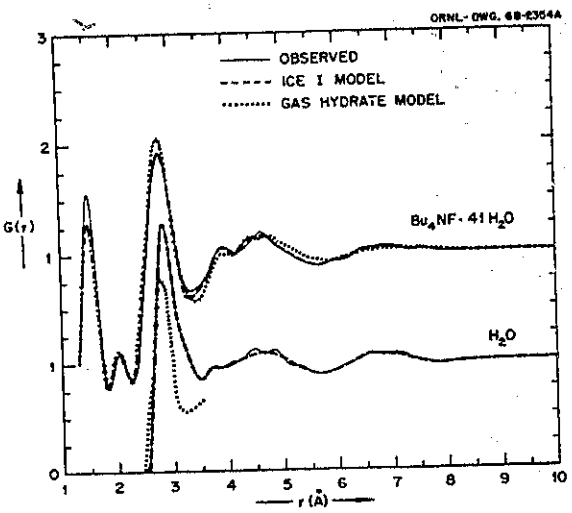

Fig. 9.19. Radial Distribution Functions for a Saturated Solution of Tetra-*n*-butylammonium Fluoride in Water at 25°C.

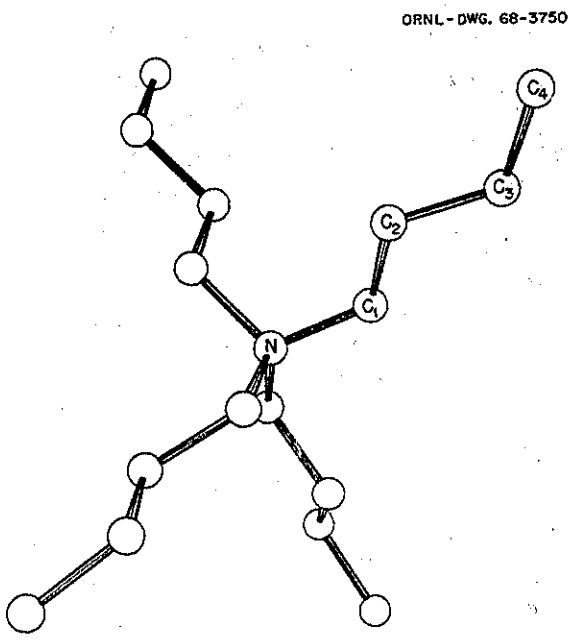

Fig. 9.20. Tetra-*n*-butylammonium Ion.

cages around the alkyl chains (gas hydrate model), as is known to be the case for the solid hydrates.[92] A saturated solution of tetra-*n*-butylammonium fluoride in water was studied at 25°C. The radial distribution function for this system (Fig. 9.19) is surprisingly similar to that of pure water, except for the pronounced peak at 1.52 A, which represents the covalent C–C and C–N bond of the cation (Fig. 9.20). Radial distribution functions calculated for the ice I model are in quantitative agreement with experiment. However, the gas hydrate model cannot be ruled out in this case (Fig. 9.19). In both models the butyl chains of the cation (Fig. 9.20) were assumed to be located in the respective cavities which, though of different size and shape, are typical for both structures (Figs. 9.21 and 9.22). The parameters for both models indicate that all of the water molecules are in network positions, and the nearest-neighbor distances are significantly shorter than found in pure water. This is in agreement with the hypothesis that butylammonium ions promote water structure.

Ammonia. – Work on the system water-ammonia at 4°C has been completed.[93] The ice I model (Fig. 9.21) explains the diffraction data quantitatively (Fig. 9.23). The changes in the model parameters from pure water to the highest ammonia concentration studied are small but significant. In the solutions, as in pure water, about half the available cavities are occupied by "interstitial" molecules. Each water or ammonia molecule has one neighbor at 2.8 A and three others at a distance which increases from 2.91 A in water to 3.00 A in $NH_3 \cdot 2.51H_2O$. The parameters for pure ammonia are quite different from those of the solutions, and most of these changes (Fig. 9.23) seem to occur at high NH_3 concentrations (not studied because of experimental difficulties). In pure ammonia, each molecule has one neighbor at 3.48 A and three others at 3.31 A; about 76% of the cavities in the ice I model are occupied by ammonia molecules. The amplitudes associated with

[92] G. A. Jeffrey and R. K. McMullan, *Progr. Inorg. Chem.* 8, 43 (1967).

[93] A. H. Narten, *J. Chem. Phys.*, to be published.

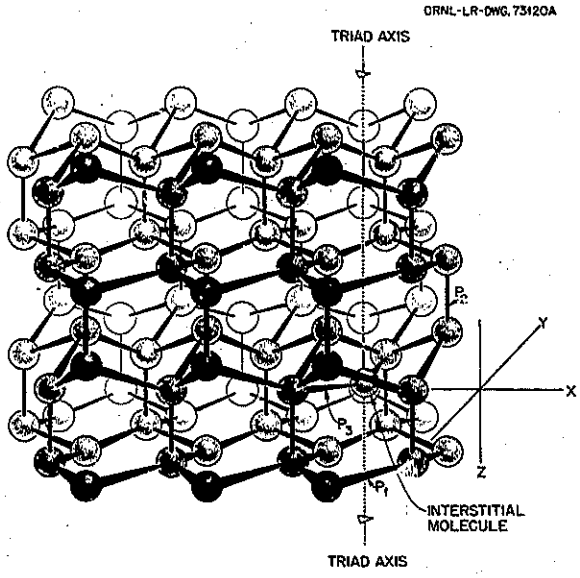

Fig. 9.21. Ice I Model. The balls represent oxygen atoms, the sticks hydrogen bonds. P_1, P_2, and P_3 are independently variable distances of the model. Occupancy of cavities by "interstitial" molecules is constrained by density.

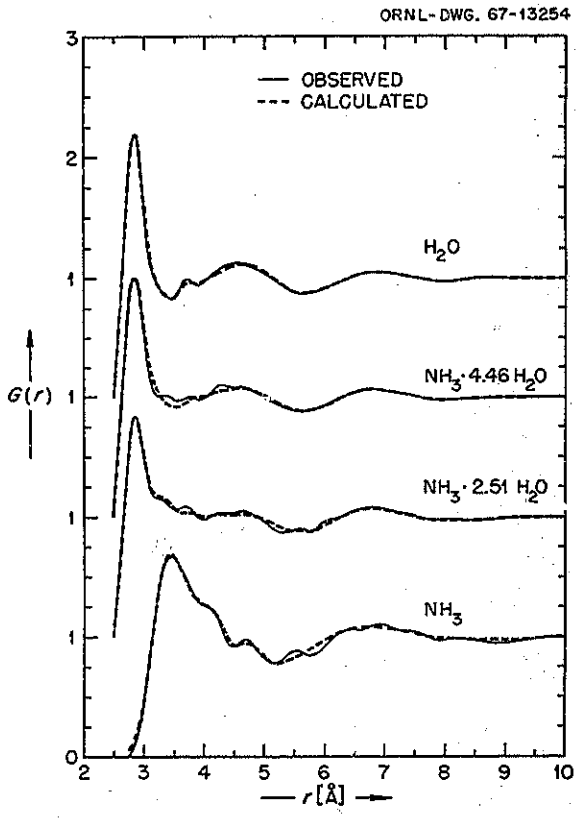

Fig. 9.23. Radial Distribution Functions for the Water-Ammonia System. Calculated curves are for ice I model (Fig. 9.21).

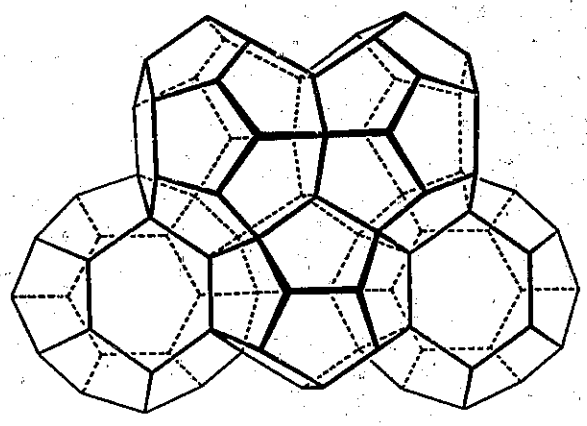

Fig. 9.22. Gas Hydrate Model. Oxygen atoms located at the corners of the polyhedra. Occupancy of cavities by "interstitial" molecules is constrained by density.

the near-neighbor distances for liquid ammonia are nearly alike, making the qualitative distinction between network and cavity molecules (which makes the model for water and the solutions, in a sense, a clathrate) disappear.

Ammonium Halides. – The properties of the ammonium ion are very similar to those of a water molecule. Solutions of the ammonium halides in water are therefore suitable for a study of the influence of halide ions on water structure. The diffraction patterns of concentrated fluoride,[94] chloride, bromide, and iodide solutions have been measured. Analysis of these data is under way.

[94] M. D. Danford, *Diffraction Pattern and Structure of Aqueous Ammonium Fluoride Solutions*, ORNL-4244 (June 1968).

In a similar manner, alkali fluoride solutions are suitable for a study of the influence of alkali metal ions on water structure, and this has been planned for the near future.

MOLECULAR BEAM STUDIES

Vibrational Excitation and Fragmentation of Molecular Hydrogen from Potassium Ionic and Atomic Collisions

Peter F. Dittner Sheldon Datz

Inelastic energy losses arising from knock-on collisions of K^+ with H_2 and D_2 molecules have been determined by time-of-flight measurements of the K^+ velocity following collision with a target molecule. The apparatus is pictured in Fig. 9.24. Surface ions of K^+ formed on an indirectly heated cathode are accelerated and pulsed on for 1 μsec. The pulsed beam is bent and passed through an oven, which may be used for charge exchange when a fast neutral beam is desired. Following its path through the liquid-nitrogen-cooled scattering chamber and a flight tube, the particle impinges on an electron multiplier, which initiates a "start" pulse in a time-to-pulse-height converter. The "stop" pulse is obtained through a delay line from the beam pulser. Beam currents are adjusted so that less than one ion per pulse is measured at the detector (else only the fastest ion in the pulse is measured). Total flight times range from 27 μsec at 320 ev to 70 μsec at 50 ev. For the experiments reported here the detector aperture was directly in line with the primary beam, so that ions backscattered through center-of-mass angles between 170 and 180° were detected. Particles backscattered from inelastic collisions will lose velocity in the center-of-mass system and thus will appear with higher velocities in the forward (lab) direction than elastic events.

Time-of-flight spectra were obtained for K^+ scattered by H_2, D_2, and He with initial center-of-mass energies ranging from 2.5 to 10 ev for H_2, 10 to 30 ev for D_2 and He. With helium only elastic scattering was observed, and the spectra obtained

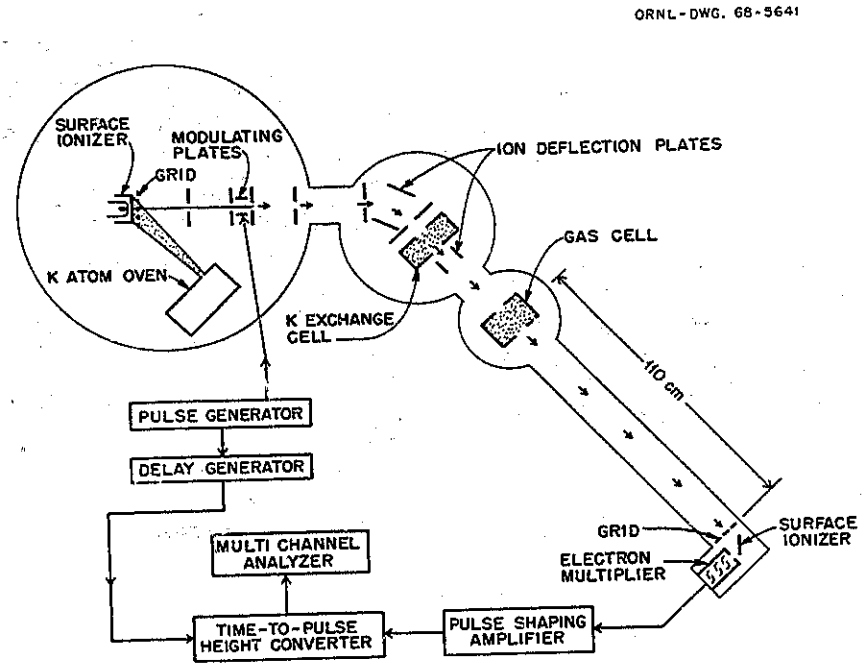

Fig. 9.24. Schematic of the Time-of-Flight Apparatus.

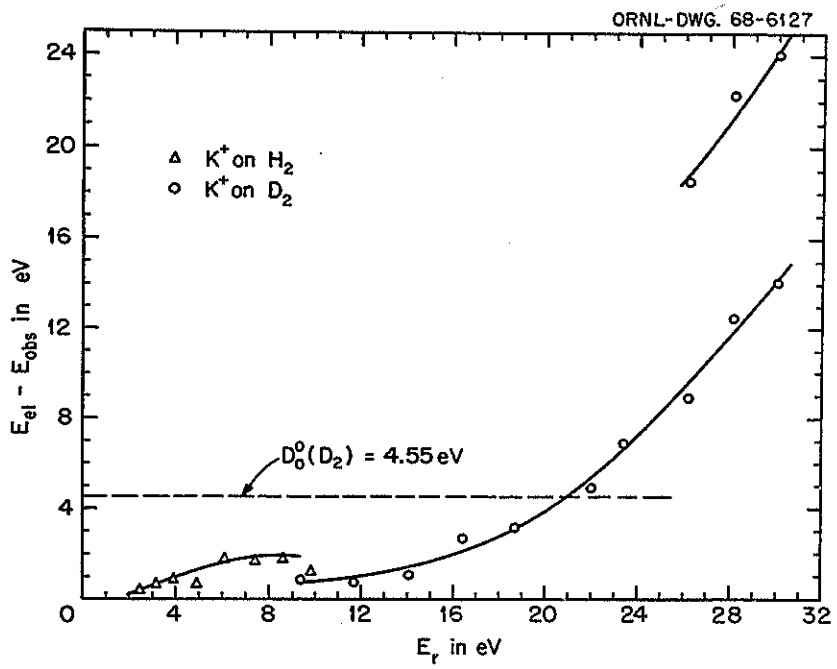

Fig. 9.25. Center-of-Mass Energy of the Elastically Back-Scattered K^+ Ions, E_{el} (Obtained from He Scattering) Minus the Observed Energy of K^+ Back-Scattered from H_2 (Δ) and D_2 (O) vs the Relative Collision Energy E_r.

were used as model peaks for stripping the data obtained with D_2 and H_2. With H_2 and D_2 the back-scattered K^+ peak was relatively narrow and showed an inelastic energy loss which increased with increasing relative energy (Fig. 9.25).

Inelastic energy losses below the dissociation limit correspond to vibrational-rotational excitation of the molecule. However, at the small impact parameters required for backward scattering, it is expected that the degree of rotational excitation is small. The cross section for back-scattering into the detector aperture was $\sim 10^{-18}$ cm^2. Thus if we assume a hard-sphere interaction and a spherically symmetric potential the maximum rotational excitation would amount to only 0.2% of the relative energy. Above ~20 ev the inelastic loss exceeded the 4.5-ev molecular dissociation limit, and the slope of the loss curve increased. The peak shape remained relatively sharp, but a second energy loss peak appeared which increased in relative population with increasing energy. The difference in energy loss between the two peaks was 10 ev. The possibility that one of these peaks arises from KD^+ is eliminated on the basis of kinematics. The velocity of any KD^+ formed depends only upon the initial conditions and the kinetic endothermicity of the ion-molecule reaction. Assuming any reasonable value for the KD^+ binding energy from 0 to 2.5 ev gives velocities which fall between the two groups. Since the peak separation corresponds closely to the $n = 1$ to $n = 2$ spacing in the deuterium atom, we ascribe the higher energy loss peak to the dissociation of a D_2 molecule accompanied by electronic excitation of a D atom.

Pulsed fast K atom beams have been formed by charge exchange and detected by surface ionization on cold platinum and tungsten. Backscattering from He and H_2 and D_2 has been observed, and measurements of inelasticity in the neutral atom system are under way.

Crossed-Molecular-Beam Studies of Reactions of Atomic Deuterium with Halogen Molecules

George E. Moore Sheldon Datz

The successful observation of product DBr by means of reasonably high-resolution mass spectrometry from a crossed-molecular-beam study of the reaction of deuterium atoms with Br_2 (refs. 95 and 96) stimulated a similar interest in the analogous reaction of $D + F_2$. Since, however, with the apparatus used for both reactive chemical systems, signal-to-noise ratios of 1/100 or smaller for the product species were obtained, a redesign of the detection system was judged necessary. Such redesign would permit a less ambiguous kinematic analysis in the $D\text{-}Br_2$ system, since even a crude velocity analysis of the product DBr should be possible and, in addition, should open up new possibilities of reactive systems.

The new system retains the previously used source and scattering chambers[95,96] but now includes an improved detecting system on which initial tests have been completed. The system incorporates a bakeable, differentially pumped (ion/sublimation pumping) chamber capable of maintaining pressures in the 10^{-10} torr range, a quadrupole mass filter and power supply of improved design which permit increased transmission still with good resolution, and an ion source of proven efficiency. Enhancement in the signal-to-noise ratio is anticipated both through the attainment of ultrahigh vacuum, which will lower the background in the mass range of interest (1–100 amu), and through improved sensitivity in signal detection.

Crossed-Molecular-Beam Studies of Bimolecular Association and Unimolecular Decomposition Reactions

R. E. Minturn Sheldon Datz

By using modulated crossed molecular beams and mass spectrometric detection, we made an intensive effort to detect vibrationally excited products from reactions of the type:

$$R-NH_2 + BF_3 \longrightarrow [R-NH_2-BF_3]^*,$$

where R is an organic radical and where the asterisk denotes vibrational excitation. Since the minimum excess energy in the product, equal to the sum of the initial relative kinetic energy and the heat of the reaction, is known, the lifetime of the activated product can supposedly be calculated from unimolecular decomposition rate theory. For example, 2-ethylhexylamine boron trifluoride, formed as above with no collisional deexcitation, should have an average lifetime of about 1.1×10^{-3} sec. We see no such product, however, and this may be due to one or more of the following reasons:

1. The reaction cross section is very small, that is, below 10^{-17} cm^2. This seems unlikely from other evidence.
2. The excited product yields, under electron bombardment in our detector, a cracking pattern so different from that of the ground-state product that it cannot be identified.
3. The excited product does not live as long as the calculations would indicate. This would suggest either that the excess energy in the boron-nitrogen bond does not transfer rapidly to other oscillators or that not all oscillators in the product are equally effective as energy sinks.

The data collected on these systems do suggest, however, elastic scattering into large angles, and experiments are presently under way to determine the nature of the intermolecular forces causing this large-angle scattering.

---

[95] S. Datz, T. W. Schmidt, and G. E. Moore, *Chem. Div. Ann. Progr. Rept. May 20, 1967*, ORNL-4164, p. 136.

[96] S. Datz and T. W. Schmidt, *V Intern. Conf. Phys. Electronic and Atomic Collisions*, Leningrad, U.S.S.R., July 17–23, 1967, p. 247, "Nauka" Publ. House.

MASS SPECTROMETRY AND RELATED TECHNIQUES

Radiolysis of Methane in a Wide-Range Radiolysis Source of a Mass Spectrometer. I. Individual and Total Cross Sections for the Production of Positive Ions, Negative Ions, and Free Radicals by Electrons[97]

P. S. Rudolph C. E. Melton[98]

The abundance of, and the total and individual cross sections for, primary products (positive ions, neutral species, and negative ions) resulting from elementary reactions induced by the absorption of energy by CH_4 from ionizing radiation (100-ev electrons) have been measured. This was accomplished with the dual electron-beam section of our wide-range radiolysis source.[99] The results (Table 9.14) show that positive ions and free radicals are produced in nearly equal abundances, 45 and 55% respectively. On the other hand, negative ions are less abundant by about four orders of magnitude. The total cross section for positive ionization (σ_I) by 100-ev electrons is 3.8×10^{-16} cm^2, and that for the formation of neutral species (σ_N) is 4.7×10^{-16} cm^2. Our values of individual and total cross sections for positive ionization agree very well with those of Adamczyk *et al.*[100] except for the cross section for H^+. In this instance our value is about one-third of theirs.

The average of seven literature values for the total cross section for positive ionization of CH_4 is 3.3×10^{-16} cm^2 (range 2.2 to 4.5×10^{-16} cm^2). This agrees well with our value of 3.8×10^{-16} cm^2.

To independently test the reliability of the dual electron-beam ion source, the total and individual cross sections for ionization of argon by 100-ev electrons were measured for comparison with published values. Our value for the total cross sec-

[97] C. E. Melton and P. S. Rudolph, *J. Chem. Phys.* 47, 1771 (1967).

[98] Present address: Department of Chemistry, University of Georgia, Athens.

[99] P. S. Rudolph and C. E. Melton, *Chem. Div. Ann. Progr. Rept. May 20, 1967*, ORNL-4164, p. 140.

[100] B. Adamczyk, A. J. H. Boerboom, B. L. Schram, and J. Kistemaker, *J. Chem. Phys.* 44, 4640 (1966).

Table 9.14. Individual Cross Sections for Initial Products Produced by the Irradiation of CH_4 with 100-ev Electrons at a Pressure of 6×10^{-6} Torr

Positive Ions			Neutral Species			Negative Ions		
Ion	Per Cent of Total Products	σ_I (cm^2)	Neutral	Per Cent of Total Products	σ_N[a] (cm^2)	Ion	Per Cent of Total Products	σ_I (cm^2)
		$\times 10^{-16}$			$\times 10^{-16}$		$\times 10^{-5}$	$\times 10^{-21}$
H^+	0.47	0.04	·H	28.24	2.4	H^-	82.42	7.9
H_2^+	0.24	0.02	H_2	9.41	0.8			
C^+	0.59	0.05	·C	0.001		C^-	8.38	0.81
CH^+	1.65	0.14	·CH	1.18	0.1	CH^-	6.6	0.64
CH_2^+	3.29	0.28	$\cdot CH_2$	2.35	0.2	CH_2^-	2.5	0.24
CH_3^+	17.65	1.5	$\cdot CH_3$	14.12	1.2	CH_3^-	0.09	0.008
CH_4^+	21.18	1.8						
	45	3.8		55	4.7		100	9.6

[a] These values determined by the use of the following cross sections (in units of 10^{-16} cm^2) for ionization of the neutrals by 100-ev electrons: H, 0.6; CH, 1.1; CH_2, 1.4; and CH_3, 1.8.

tion (σ_T) of 3.2×10^{-16} cm^2 is in satisfactory agreement with those reported by other workers, whose values range from 2.8 to 3.6×10^{-16} cm^2.

Acetylene Production by the Radiolysis of Methane[101]

P. S. Rudolph C. E. Melton[102]

The production of acetylene as a final product in the radiolysis of methane is a controversial issue in the literature. Using our wide-range radiolysis source[103] and employing flow, electric fields, and relatively low pressure (10^{-2} torr) we found C_2H_2 as a final product with $G_{C_2H_2} = 0.7$ for 100-ev electrons.

Acetylene represented over 19% of all observed hydrocarbon products, being exceeded only by C_2H_4. This is contrary to reported results, wherein C_2H_6 is the predominant hydrocarbon. Cahill *et al.*,[104] using a single very short and very high-intensity pulse of high-energy electrons in a static system, found $G_{C_2H_2} = 0.5$. Even in this work C_2H_6 had a higher yield. The results of previous workers obtained in flow systems or where an attempt was made to remove products by condensation showed appreciably larger yields of unsaturated hydrocarbons, including C_2H_2, than results in static systems, although still in toto showing the saturated hydrocarbon yield greater than the unsaturated hydrocarbon yield. This would imply that unsaturated hydrocarbons are products of the radiolysis of CH_4 but subsequently react with CH_4 or other products to yield saturated hydrocarbons. This is in agreement with our observations.

Our results indicate that 27% of the C_2H_2 is produced by ion-molecule reactions. The yield-energy curves (Fig. 9.26) indicate that CH_4^+ and CH_2^+ are the ionic precursors of C_2H_2.

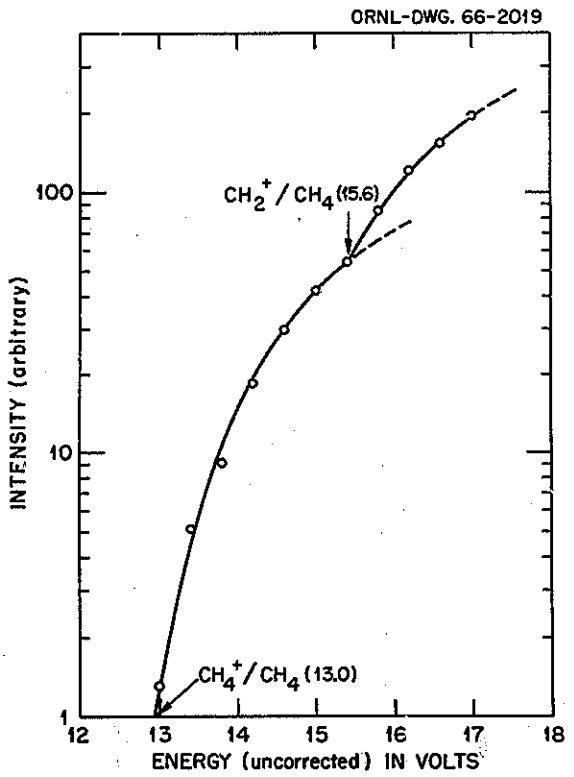

Fig. 9.26. Dependence of Yield of Acetylene on Electron Energy in Radiolysis of Methane. The marked increase in the yield curve for C_2H_2 at 13.0 and at 15.6 ev (the appearance potentials of CH_4^+ and CH_2^+ from CH_4 respectively) indicates that C_2H_2 is formed from these primary products (CH_4^+ and CH_2^+).

Two-Stage Mass Spectrometer

Russell Baldock L. E. Idom

The primary application of the two-stage mass spectrometer is the measurement of isotopic abundance ratios in support of the neutron cross-section measurement program of the Chemistry Division. During the past year the measurement of more than 80 isotopic analyses which were required for measuring the burnup of ^{233}U were completed. The problem of sample contamination, discussed in last year's annual report,[105] was

[101] P. S. Rudolph and C. E. Melton, *J. Phys. Chem.* 71, 4572 (1967).

[102] Present address: Department of Chemistry, University of Georgia, Athens.

[103] P. S. Rudolph and C. E. Melton, *Chem. Div. Ann. Progr. Rept. May 20, 1967*, ORNL-4164, p. 140.

[104] R. W. Cahill, A. K. Seeler, and R. A. Glass, *J. Phys. Chem.* 71, 4564 (1967).

[105] *Chem. Div. Ann. Progr. Rept. May 20, 1967*, ORNL-4164, p. 143.

satisfactorily overcome by electroplating the submicrogram samples of uranium on 6-mil platinum wire. Small sections of wire, about 5 mm in length, are readily inserted in the self-heated ovens which are employed to vaporize the samples.

CHARGE SPECTROMETRY: USES OF ELECTRON SPECTROSCOPY IN CHEMICAL PROBLEMS[106]

Thomas A. Carlson

Multiple ionization and excitation in the photoelectron process has been studied by means of electron spectroscopy. Gases at low pressure are irradiated with x rays of characteristic energy, and the electrons ejected as the result of the photoelectron process are measured with an electrostatic analyzer. In addition to the principal photoline, discrete satellite lines and continua are observed at lower energies and are interpreted as arising respectively from transitions to excited and ionized states. Results on the rare gases have been successfully interpreted in terms of the sudden approximation. Studies have now been extended to a variety of simple molecules: N_2, O_2, CO, NO, CO_2, CF_3Cl, and CF_4. In addition to photoelectron results, Auger electrons have been measured; and, in a separate investigation, the relative abundances and recoil energies of the fragment ions were determined. Some of the results (e.g., on the Freons) have been successfully interpreted in terms of atomic Hartree-Fock wave functions. Others will require a more sophisticated approach.

Recently, a substantial modification of the spectrometer has been carried out: the housing has been fashioned completely iron-free, and three pairs of Helmholtz coils have been constructed to cancel the earth's and stray magnetic fields. In addition, the double-focusing electrostatic plates have been completely rebuilt. The new spectrometer will have a resolution of better than 0.05% full width at half maximum in energy and will be able to measure electrons from a few kilo-electron volts to a few electron volts. In addition to continuing our program on multiple ionization and excitation we shall initiate programs on a variety of other chemical problems. Specifically, we shall study the nature of chemical bonding by measuring the shifts in the inner atomic binding energies as a function of chemical environment. Also, the electronic structure of the valence shell will be studied by photoelectron emission as a function of the angle between the x ray and the ejected electrons.

---

[106] Research sponsored jointly with the Physics Division.

Publications

NUCLEAR CHEMISTRY

L. L. Riedinger,[1] N. R. Johnson, and J. H. Hamilton,[2] "Band Mixing in ^{152}Sm and ^{154}Gd," *Phys. Rev. Letters* **19**, 1243 (1967).

N. R. Johnson, L. L. Riedinger,[1] and J. H. Hamilton,[2] "Monopole Matrix Elements for $E0$ Transitions in ^{152}Sm and ^{154}Gd," Proceedings of the International Conference on Nuclear Structure, Tokyo, *J. Phys. Soc. Japan* (Suppl.) **24**, 172 (1968).

A. V. Ramayya,[2] J. H. Hamilton,[2] B. van-Nooijen,[3] and N. R. Johnson, "Search for Members of the Two-Phonon Triplets in ^{80}Se and ^{80}Kr," *Phys. Rev.* **157**, 1015 (1967).

J. K. Dickens[4] and E. Eichler, "The ^{91}Zr$(d,p)^{92}$Zr Reaction at $E_d = 6.25$ MeV," *Nucl. Phys.* **A101**, 408 (1967).

J. K. Dickens,[4] G. R. Satchler,[5] and E. Eichler, "The ^{90,92,94}Zr(p,p') Reactions at 12.7 MeV," *Phys. Rev.* **168**, 1355 (1968).

M. F. Roche,[6] "The Independent Yield of ^{112}Ag and the Cumulative Yield of ^{115}Pd in Thermal-Neutron Induced ^{233}U and ^{235}U Fission," Ph.D. thesis, University of Missouri, January 1968.

CHEMISTRY AND PHYSICS OF TRANSURANIUM ELEMENTS

A. H. Wapstra,[7] "Actinide Fingerprints," *Actinide Rev.* **1**, 39 (1967).

C. D. Cornwell[8] and L. J. Nugent, "Matrix Elements of $(\lambda P_x + \mu P_y + \gamma P_z)^n$ for Slightly Asymmetric Top Molecules," *J. Mol. Spectry.* **24**, 363 (1967).

R. L. Hahn, "Angular Distributions of the Recoil Nuclei from the Reactions ^{12}C$(^3$He$,\alpha)^{11}$C and ^{12}C$(^3$He$,d)^{13}$N," *Nucl. Phys.* **A101**, 545 (1967).

R. L. Hahn, K. S. Toth,[9] and T. H. Handley,[10] "Alpha Decay of Holmium Nuclei; New Isotope, ^{154}Ho," *Phys. Rev.* **163**, 1291 (1967).

---

[1] ORAU Predoctoral Fellow from Vanderbilt University.

[2] Vanderbilt University.

[3] Visiting scientific staff member from the University of Delft, Netherlands.

[4] Neutron Physics Division.

[5] Physics Division.

[6] ORAU Predoctoral Fellow from the University of Missouri, Columbia.

[7] Present address: Instituut voor Kernphysisch Onderzoek, Amsterdam, Netherlands.

[8] Department of Chemistry, University of Wisconsin, Madison.

[9] Electronuclear Division.

[10] Analytical Chemistry Division.

R. L. Hahn, "The Recoil Technique and Its Possible Use in Activation Analysis," *Anal. Chem.* **40**, 219 (1968).

A. Chetham-Strode, Jr.,[11] R. J. Silva, J. R. Tarrant, and I. R. Williams,[12] "The Decay of ^{251}Cf," *Nucl. Phys.* **A107**, 645 (1968).

J. H. Burns, A. C. Tennissen,[13] and G. D. Brunton,[14] "The Crystal Structure of α-Li_3AlF_6," *Acta Cryst.* **B24**, 225 (1968).

ISOTOPE CHEMISTRY

G. M. Begun and A. A. Palko, "Raman and Infrared Spectra of $^{10}BF_3$ and $^{11}BF_3$ Complexes with Dimethyl Sulfide and the Isotopic Exchange of This Complex with BF_3," *J. Chem. Phys.* **47**, 967–70 (1967).

J. S. Drury, "Chemistry of Nuclear Reactors, Isotope Separation," p. 85 in *Encyclopedia of Chemical Technology*, 2d ed., vol. 14, Wiley, 1967.

A. A. Palko and J. S. Drury, "Fractionation of Boron Isotopes Between Boron Trifluoride and Its Molecular Addition Compounds," *J. Chem. Phys.* **47**, 2561–66 (1967).

G. M. Begun and A. C. Rutenberg, "Vibrational Frequencies and Force Constants of Some Group IVa and Group Va Hexafluoride Ions," *Inorg. Chem.* **6**, 2212–16 (1967).

L. L. Brown and J. S. Drury, "Exchange and Fractionation of Nitrogen Isotopes Between NO_2^- and NO_3^-," *J. Chem. Phys.* **48**, 1399 (1968).

L. L. Brown and J. S. Drury, "Exchange and Fractionation of Nitrogen Isotopes Between NO and NO_2^-," *J. Chem. Phys.* **48**, 1400 (1968).

RADIATION CHEMISTRY

J. W. Boyle, J. F. Riley,[15] J. A. Ghormley, and C. J. Hochanadel, "Flash Photolysis of Water Above 1800 Å, Formation of the Hydrated Electron, Absorption Spectrum of the Hydrated Electron Down to 2100 Å and the Absorption Spectrum of the Hydroxyl Radical," *Radiation Res.* **31**, 582 (1967).

J. A. Ghormley, "Enthalpy Changes and Heat-Capacity Changes in the Transformations from High-Surface-Area Amorphous Ice to Stable Hexagonal Ice," *J. Chem. Phys.* **48**, 503 (1968).

H. A. Mahlman and T. J. Sworski, "On the Nature of the Precursor of Molecular Hydrogen in the Radiolysis of Water," p. 259 in *The Chemistry of Ionization and Excitation*, Taylor and Francis Ltd., London, England, 1967.

F. T. Jones[16] and T. J. Sworski, "Radiation Chemistry of Gaseous Ammonia, Part 1. – Radical and Molecular Product Yields," *Trans. Faraday Soc.* **63**, 2411 (1967).

F. T. Jones[16] and T. J. Sworski, "Radiation Chemistry of Gaseous Ammonia, Part 2. – Hydrazine Formation," *Trans. Faraday Soc.* **63**, 2426 (1967).

G. E. Boyd and Q. V. Larson, "Chemistry of ^{82g}Br Recoils in Neutron-Irradiated Crystalline Alkali Metal Bromates," *J. Am. Chem. Soc.* **90**, 254 (1968).

---

[11] Deceased.

[12] Present address: Knoxville College, Knoxville, Tenn.

[13] Lamar State College of Technology, Beaumont, Tex.; ORAU Summer Participant, 1966.

[14] Reactor Chemistry Division.

[15] Present address: Lockheed Palo Alto Research Laboratory, Palo Alto, Calif.

[16] Stevens Institute of Technology, Hoboken, N.J.; ORAU Summer Participant, 1965.

T. G. Ward, Jr.,[17] G. E. Boyd, and R. C. Axtmann,[17] "γ-Radiolysis of Molten Lithium Nitrate: Dose Rate Effects," *Radiation Res.* **33**, 447 (1968).

T. G. Ward, Jr.,[17] R. C. Axtmann,[17] and G. E. Boyd, "Neutron-Induced Radiolysis of Lithium Nitrate: LET and Phase Change Effects," *Radiation Res.* **33**, 456 (1968).

H. W. Kohn, "The Radiation Chemistry of Surfaces," chapter in *Actions Chimiques et Biologiques des Radiations*, ed. by M. Haissinsky, vol. 11, Masson, Paris, 1967.

E. H. Taylor, "The Effects of Ionizing Radiation on Solid Catalysts," chapter in *Advances in Catalysis*, vol. 18, pp. 111–258, Academic, New York, 1968.

ORGANIC CHEMISTRY

C. J. Collins and M. H. Lietzke, "Molecular Rearrangements. XXIV. A Mechanistic Analysis of Available Isotopic Data for Solvolyses of 2-exo-Norbornyl and 2-(Δ^3-Cyclopentenyl)ethyl Esters," *J. Am. Chem. Soc.* **89**, 6565 (1967).

C. J. Collins, V. F. Raaen, B. M. Benjamin, and I. T. Glover,[18] "Anomalous Behavior of 3-*endo*-Hydroxy-3-*exo*-phenyl-2-*endo*-norbornylamine During Deamination," *J. Am. Chem. Soc.* **89**, 3940 (1967).

H. Kwart,[19] R. W. Spayd,[20] E. N. Givens,[20] and C. J. Collins, "Rearrangements of α-Triketones," *Chem. Commun.* **530** (1967).

C. J. Collins, review of book *Electrophilic Additions to Unsaturated Systems* by P. B. D. De La Mare, *J. Am. Chem. Soc.* **89**, 2510 (1967).

V. F. Raaen, G. A. Ropp,[21] and H. P. Raaen,[10] book *Carbon-14*, McGraw-Hill, New York, 1968.

C. E. Higgins and W. H. Baldwin, "The Thermal Decomposition of Tri-sec-butyl Phosphate," *J. Org. Chem.* **33**, 1065 (1968).

CHEMISTRY OF AQUEOUS SYSTEMS

M. H. Lietzke and J. O. Hall,[22] "The Thermodynamics of Aqueous Silver Sulphate–Lanthanum Sulphate Solutions," *J. Inorg. Nucl. Chem.* **29**, 1249 (1967).

M. H. Lietzke, Richard Shea,[23] and R. W. Stoughton, "Correlation of Sea Salt Concentration with EMF Response of a Cation-Sensitive Glass Electrode, *J. Tenn. Acad. Sci.* **42**, 123 (1967).

M. H. Lietzke and R. W. Stoughton, "Electromotive Force Studies in Aqueous Solutions at Elevated Temperatures. IX. The Thermodynamic Properties of HCl-$GdCl_3$ Mixtures, *J. Phys. Chem.* **72**, 257 (1968).

M. H. Lietzke, R. W. Stoughton, and R. M. Fuoss,[24] "A Two Structure Model for Electrolytic Solutions," *Proc. Natl. Acad. Sci.* **59**, 39 (1968).

J. S. Johnson and R. M. Rush, "Osmotic Coefficients of Tungstosilicic Acid," *J. Phys. Chem.* **72**, 360 (1968).

---

[17] Department of Chemical Engineering, Princeton University, Princeton, N.J.

[18] Present address: Oak Ridge Associated Universities, Special Training Division.

[19] University of Delaware.

[20] ORAU Predoctoral Fellow.

[21] Coker College, Hartsville, S.C.

[22] Graduate Student, University of Tennessee.

[23] Co-op Student, University of Tennessee.

[24] Yale University.

R. M. Rush and J. S. Johnson, "Isopiestic Measurements of the Osmotic and Activity Coefficients for the Systems $HClO_4$-$LiClO_4$-H_2O, $HClO_4$-$NaClO_4$-H_2O, and $LiClO_4$-$NaClO_4$-H_2O," *J. Phys. Chem.* **72**, 767 (1968).

R. M. Rush and R. A. Robinson,[25] "A Reevaluation of the Activity Coefficients in the System NaCl-KCl-H_2O," *J. Tenn. Acad. Sci.* **43**, 22 (1968).

G. E. Boyd, F. Vaslow, and S. Lindenbaum, "Thermodynamic Quantities in the Exchange of Zinc with Sodium Ions in Variously Cross-Linked Polystyrene Sulfonate Cation Exchangers at 25°," *J. Phys. Chem.* **71**, 2214 (1967).

G. E. Boyd and J. Schubert,[26] "The First Use of Organic and Inorganic Ion Exchangers for Separating Plutonium from Uranium and the Fission Products," *Process Chemistry*, vol. IV, Pergamon, New York, 1968.

G. E. Boyd, F. Vaslow, A. Schwarz,[27] and J. W. Chase,[28] "Thermodynamic Properties at 25° of Aqueous Solutions of *p*-Ethylbenzenesulfonic Acid and Its Alkali Metal Salts. Comparisons with Cross-Linked Polystyrenesulfonate Type Cation Exchangers," *J. Phys. Chem.* **71**, 3879 (1967).

G. E. Boyd and Q. V. Larson, "The Binding of Quaternary Ammonium Ions by Polystyrenesulfonic Acid Type Cation Exchangers," *J. Am. Chem. Soc.* **89**, 6038 (1967).

G. E. Boyd, "Thermal Effects in Ion-Exchange Reactions: Heats of Ion Exchange," *Analytical Calorimetry*, Advances in Chemistry Series (1968).

S. Lindenbaum, "Osmotic Coefficients of Aqueous Solutions of Tri-*n*-alkylsulfonium Halides at 25°," *J. Phys. Chem.* **72**, 212 (1968).

G. E. Boyd, review of books, "The Chemistry of Rhenium and Technetium" by R. Colton, and "The Chemistry of Technetium and Rhenium," by R. D. Peacock, *Am. Scientist* **54**(4), 444A (1966).

G. E. Boyd, review of book, "Insoluble Monolayers at Liquid-Gas Interfaces" by G. L. Gaines, Jr., *J. Am. Chem. Soc.* **89**, 3087 (1967).

F. Vaslow, "Changes in Slope of the Apparent Molal Volume Curves of Lithium Chloride Solutions," *J. Phys. Chem.* **71**, 4585 (1967).

*J. R. Kuppers,[29] A. E. Marcinkowsky,[30] K. A. Kraus, and J. S. Johnson, "Hyperfiltration VIII. Filtration of Organic Solutes by Dynamically-Formed Membranes," *Separation Sci.* **2**, 617 (1967).

*K. A. Kraus, A. J. Shor,[14] and J. S. Johnson, "Hyperfiltration Studies X. Hyperfiltration with Dynamically Formed Membranes," *Desalination* **2**, 243 (1967).

*J. J. Perona,[31] F. H. Butt,[32] S. M. Fleming,[33] S. T. Mayr,[33] R. A. Spitz,[33] M. K. Brown,[33] H. D. Cochran,[33] K. A. Kraus, and J. S. Johnson, "Hyperfiltration IX. Processing of Pulp-Mill Sulfite Wastes with a Membrane Dynamically Formed from Feed Constituents," *Environ. Sci. Technol.* **1**, 991 (1967).

---

*Based on work performed in the Chemistry Division under the Water Research Program.

[25]Consultant, Washington, D.C.

[26]University of Pittsburgh, Pittsburgh, Pa.

[27]Deceased; formerly of the Soreq Nuclear Research Center, Yavne, Israel.

[28]Present address: Eastman Kodak Co., Rochester, N.Y.

[29]University of North Carolina at Charlotte; ORAU Summer Participant, 1966.

[30]Present address: Technical Center, Union Carbide Corp., South Charleston, W. Va.

[31]Chemical Technology Division.

[32]IAEA Fellow, Pakistani AEC.

[33]MIT School of Chemical Engineering Practice.

*A. J. Shor,[14] K. A. Kraus, J. S. Johnson, and W. T. Smith, Jr.,[34] "Hyperfiltration VII. Concentration Polarization in Tubular Systems with Dynamically-Formed Membranes," *Ind. Eng. Chem., Fundamentals* **7**, 44 (1968).

*K. A. Kraus, J. S. Johnson, Jr., and A. J. Shor,[14] "Humic Acid as an Additive in the Process of Forming a Salt-Rejection Membrane," U.S. Pat. 3,344,928 (Oct. 3, 1967).

*A. J. Shor,[14] "Hyperfiltration Properties of Dynamically Formed Hydrous Zr(IV) Oxide Membranes," Ph.D. thesis, University of Tennessee, March 1968.[35]

*R. J. Raridon, W. H. Baldwin, and K. A. Kraus, "Properties of Organic-Water Mixtures. VI. Activity Coefficients of Sodium Chloride in Saturated Water-Pyridine Mixtures at 5 and 25°," *J. Phys. Chem.* **72**, 925 (1968).

*A. E. Marcinkowsky,[30] H. O. Phillips, and K. A. Kraus, "Properties of Organic-Water Mixtures. VII. Self-Diffusion Coefficients of Na^+ in Ethylene Glycol–Water and Glycerol-Water Mixtures at 25°," *J. Phys. Chem.* **72**(4), 1201 (1968).

*K. A. Kraus and H. O. Phillips, "Processes for Removal and/or Separation of Metals from Solutions," U.S. Pat. 3,317,312 (May 1967).

ELECTROCHEMICAL KINETICS AND ITS APPLICATION TO CORROSION

*T. Morozumi[36] and F. A. Posey, "Application of the Electrochemical pH-Stat to the Study of Hydrolysis of Metal Ions," *Denki Kagaku* **35**, 633 (1967).

*F. A. Posey and E. G. Bohlmann,[14] "Pitting of Titanium Alloys in Saline Waters," *Desalination* **3**, 269 (1967).

NONAQUEOUS SYSTEMS AT HIGH TEMPERATURES

A. S. Dworkin and M. A. Bredig, "Diffuse Transition and Melting In Fluorite and Anti-Fluorite Type of Compounds: Heat Content of Potassium Sulfide from 298° to 1260°K," *J. Phys. Chem.* **72**, 1277 (1968).

M. A. Bredig, "Immiscibility Diagrams of Molten Sodium Bromide–Sodium Polyborates at 800° and 980°C," *J. Chem. Eng. Data* **13**, 295 (1968).

CHEMICAL PHYSICS

W. C. Waggener, A. J. Weinberger, and R. W. Stoughton, "Effects of Temperature on the Near-Infrared Absorption Spectra of Molecules in the Condensed States. I. Carbon Dioxide," *J. Phys. Chem.* **71**, 4320 (1967).

R. W. Holmberg and Ralph Livingston, "Paramagnetic Resonance Study of NO_2 in Irradiated KNO_3 at 4°K," *J. Chem. Phys.* **47**, 2552 (1967).

Henry Zeldes and Ralph Livingston, "Paramagnetic Resonance Study of Liquids During Photolysis. IV. Free Radicals from Acetaldehyde, Diacetyl, and Acetoin," *J. Chem. Phys.* **47**, 1465 (1967).

---

[34]Department of Chemistry, University of Tennessee.

[35]Work performed in Chemistry Division.

[36]Faculty of Engineering, Hokkaido University, Sapporo, Japan.

Ralph Livingston and Henry Zeldes, "Paramagnetic Resonance Study of Liquids During Photolysis. V. Acid Amides and an Imide," *J. Chem. Phys.* **47**, 4173 (1967).

P. A. Agron, R. D. Ellison, and H. A. Levy, "The Crystal Structure of Dimanganese Iron Carbonyl, $Mn_2Fe(CO)_{14}$," *Acta Cryst.* **23**, 1079 (1967).

J. H. Burns, R. D. Ellison, and H. A. Levy, "The Crystal Structure of $Na_7Zr_6F_{31}$," *Acta Cryst.* **B24**, 230 (1968).

A. H. Narten, "Diffraction Pattern and Structure of Liquid Benzene," *J. Chem. Phys.* **48**, 1630 (1968).

G. M. Brown, "Misuse of the 'Riding' Model in Correcting Bond Lengths for Effects of Thermal Motion," *Acta Cryst.* **B24**, 294 (1968).

Dick van der Helm,[37] J. P. Glusker,[37], C. K. Johnson, J. A. Minkin,[37] N. E. Burow,[37] and A. L. Patterson,[11,37] "X-Ray Crystal Analysis of the Substrates of Aconitase. VIII. The Structure and Absolute Configuration of Potassium Dihydrogen Isocitrate Isolated from *Brophyllum calycinum*," *Acta Cryst.* **B24**, 578 (1968).

A. H. Narten, M. D. Danford, and H. A. Levy, "Structure and Intermolecular Potential of Liquid Carbon Tetrachloride Derived from X-Ray Diffraction Data," *J. Chem. Phys.* **46**, 4875 (1967).

A. H. Narten, M. D. Danford, and H. A. Levy, "An X-Ray Diffraction Study of Liquid Water in the Temperature Range 4–200°C," *Discussions Faraday Soc.* **43**, 97 (1967).

W. R. Busing, R. D. Ellison, H. A. Levy, S. P. King,[38] and R. T. Roseberry,[39] "The Oak Ridge Computer-Controlled X-Ray Diffractometer," ORNL-4143 (January 1968).

J. A. O'Malley[40] and A. H. Narten, "X-Ray Diffraction Data on Liquid Benzene," ORNL-4166 (July 1967).

A. H. Narten, "X-Ray Diffraction Data on the System Carbon Tetrachloride–Neopentane at 0°C," ORNL-4203 (October 1967).

A. H. Narten, "X-Ray Diffraction Data on the System Water-Ammonia at 4°C." ORNL-4221 (December 1967).

S. Datz, G. Leibfried,[41] H. O. Lutz,[42] and C. Erginsoy,[43] "Motion of Energetic Particles in Crystals," *Ann. Rev. Nucl. Sci.* **17**, 129 (1967).

S. Datz and T. W. Schmidt,[44] "A Crossed Molecular Beam Study of the Reaction of Atomic Deuterium with Bromine," *Proc. Fifth Intern. Conf. Electronic and Atomic Collision Phenomena*, p. 247, Leningrad, USSR, "Nauka" Leningrad, 1967.

S. Datz, C. D. Moak,[5] H. O. Lutz[42], L. C. Northcliffe,[45] and L. B. Bridwell,[46] "Electron Capture and Loss Processes for Fast (20–150 Mev) Bromine and Iodine Ions in Gases," *Proc. Fifth Intern. Conf. Electronic and Atomic Collision Phenomena*, p. 425, Leningrad, USSR, "Nauka" Leningrad, 1967.

L. B. Bridwell,[46] L. C. Northcliffe,[45] S. Datz, C. D. Moak,[5] and H. O. Lutz,[42] "Stopping Powers for Iodine Ions at Energies up to 200 Mev," *Phys. Rev.* **159**, 276 (1967).

---

[37]Institute for Cancer Research, Philadelphia, Pa.

[38]Mathematics Division.

[39]Instrumentation and Controls Division.

[40]Drexel Institute of Technology, Philadelphia; ORAU Summer Participant, 1966.

[41]Technische Hochschule, Aachen, West Germany.

[42]Solid State Division.

[43]Brookhaven National Laboratory; deceased.

[44]ORAU Predoctoral Fellow from the University of Tennessee.

[45]Texas A.&M.

[46]ORAU Summer Participant, Murray State University, Murray, Ky.

C. E. Melton[47] and P. S. Rudolph, "The Mass Spectrometer as a Research Laboratory," *Naturwissenschaften* **54**, 297 (1967).

C. E. Melton[47] and P. S. Rudolph, "Radiolysis of Methane in a Wide-Range Radiolysis Source of a Mass Spectrometer. I. Individual and Total Cross Sections for the Production of Positive Ions, Negative Ions, and Free Radicals by Electrons," *J. Chem. Phys.* **47**, 1771 (1967).

P. S. Rudolph and C. E. Melton,[47] "Acetylene Production by the Radiolysis of Methane," *J. Phys. Chem.* **71**, 4572 (1967).

T. A. Carlson, "The Role of Auger Processes and Electron Shake-Off in the Chemical Consequences of Radioactive Decay," *Nippon Genshiryoku Gakkaishi* **9**, 259 (1967).

T. A. Carlson, "Double Electron Ejection Resulting from Photo-Ionization in the Outermost Shell of He, Ne, and Ar, and Its Relationships to Electron Correlation," *Phys. Rev.* **156**, 142 (1967).

M. O. Krause[5] and T. A. Carlson, "Vacancy Cascade in the Reorganization of Krypton Ionized in an Inner Shell," *Phys. Rev.* **158**, 18 (1967).

T. A. Carlson, C. W. Nestor, Jr.,[38] T. C. Tucker,[38] and F. B. Malik,[48] "Calculation of Electron Shake-Off for Elements from $Z = 2$ to 92 with the Use of Self-Consistent-Field Wave Functions," *Phys. Rev.* **169**, 27 (1968).

T. A. Carlson, P. Erman,[49] and K. Fransson,[49] "Dependence of Internal Conversion in ^{169}Tm on the Chemical Environment and Its Application to the Mössbauer Isomer Shift," *Nucl. Phys.* **A111**, 371 (1968).

---

[47]Present address: Department of Chemistry, University of Georgia, Athens.

[48]Physics Department, Yale University, New Haven, Conn.

[49]Research Institute for Physics, Stockholm, Sweden.

Papers Presented at Scientific and Technical Meetings

NUCLEAR CHEMISTRY

N. R. Johnson, "Monopole Strength Parameters for $E0$ Transitions from β-Bands of Deformed Nuclei," Gordon Research Conference on Nuclear Chemistry, New London, N.H., June 19–23, 1967 (invited).

N. R. Johnson, L. L. Riedinger,[1] and J. H. Hamilton,*[2] "Monopole Matrix Elements for $E0$ Transitions in ^{152}Sm and ^{154}Gd," International Conference on Nuclear Structure, Tokyo, Sept. 7–13, 1967.

L. L. Riedinger,*[1] N. R. Johnson, and J. H. Hamilton,[2] "Nonadiabatic Properties of ^{152}Sm and ^{154}Gd," Meeting of the American Physical Society, Washington, D.C., Apr. 22–25, 1968.

M. F. Roche,*[3] R. L. Ferguson, and D. E. Troutner,[4] "Charge Distribution in Symmetric Fission: Yields of ^{112}Ag and ^{115}Pd in Thermal-Neutron Fission of ^{235}U and ^{233}U," 154th National Meeting, American Chemical Society, Chicago, Sept. 10–15, 1967.

S. C. Burnett,*[5] R. L. Ferguson, F. Plasil,[6] and H. W. Schmitt,[6] "An Indirect Measurement of Neutron Emission in Proton-Induced Fission of ^{233}U," American Physical Society Meeting, Washington, D.C., Apr. 22–25, 1968; *Bull. Am. Phys. Soc.* 13, 604 (1968).

R. L. Ferguson,* S. C. Burnett,[5] Frances Pleasonton,[6] F. Plasil,[6] and H. W. Schmitt,[6] "Fragment Energy Correlation Measurements in the Fission of ^{233}U, ^{235}U, and ^{238}U by 7- to 13-MeV Protons," American Physical Society Meeting, Washington, D.C., Apr. 22–25, 1968; *Bull. Am. Phys. Soc.* 13, 605 (1968).

J. K. Dickens,*[7] E. Eichler, F. G. Perey,[7] P. H. Stelson,[6] J. Ashe,[8] and D. O. Nellis,[8] "^{14}N$(n,n'\gamma)$ Reaction for $5.8 < E_n < 8.6$," Second Conference on Neutron Cross Section and Technology, Washington, D.C., Mar. 4–7, 1968.

B. H. Ketelle* and A. R. Brosi, "The Decay of ^{136}Nd and ^{137}Nd," Meeting of the Nuclear Division of the American Physical Society, Madison, Wis., October 1967.

---

*Speaker.

[1]ORAU Predoctoral Fellow from Vanderbilt University.

[2]Vanderbilt University.

[3]ORAU Predoctoral Fellow from the University of Missouri.

[4]University of Missouri.

[5]ORAU Predoctoral Fellow from the University of Tennessee.

[6]Physics Division.

[7]Neutron Physics Division.

[8]Texas Nuclear Corp., Houston, Tex.

CHEMISTRY AND PHYSICS OF TRANSURANIUM ELEMENTS

R. L. Hahn,* M. F. Roche,[9] and K. S. Toth,[9] "New Neptunium Isotopes: ^{230}Np and ^{229}Np," American Physical Society Meeting, Washington, D.C., Apr. 22–25, 1968.

M. F. Roche,[9] K. S. Toth,[9] R. L. Hahn, C. E. Bemis, and T. H. Handley,[10] "Investigation of γ Rays in the Decay Chain ^{172}Hf → ^{172}Lu → ^{172}Yb," American Physical Society Meeting, Washington, D.C., Apr. 22–25, 1968.

O. L. Keller, Jr.,* D. E. Ferguson,[11] and J. P. Nichols,[11] "Prospects of Transuranium Isotopes as Neutron Sources," Medical Symposium: "Radioisotopes in Medicine. In Vitro Studies," Oak Ridge, Tenn., Nov. 13–16, 1967 (invited).

L. J. Nugent,* J. R. Tarrant, J. L. Burnett, R. D. Baybarz,[11] G. K. Werner,[6] and O. L. Keller, Jr., "Intra-Molecular Energy-Transfer in Actinide Beta-Diketones. Exchange of Lanthanide and Actinide Ions in a Convenient Method of Scanning Actinide Complexes for Application to Liquid Lasers," Symposium on Macroscopic Studies of the Actinides, 155th National Meeting, American Chemical Society, San Francisco, Apr. 1–5, 1968.

J. H. Burns,* H. A. Levy, and O. L. Keller, "The Crystal Structure of $RbPaF_6$," American Crystallographic Association Summer Meeting, Minneapolis, Minn., Aug. 20–25, 1967.

ISOTOPE CHEMISTRY

G. M. Begun* and A. A. Palko, "Vibrational Frequencies and Force Field Calculations for BF_3 Addition Compounds Using ^{10}B and ^{11}B Isotopes," Gordon Research Conference on Chemistry and Physics of Isotopes, Crystal Mountain, Wash., July 10–14, 1967.

A. A. Palko* and L. Landau, "A New System for the Separation of Carbon Isotopes," 155th National Meeting, American Chemical Society, San Francisco, Apr. 3, 1968.

RADIATION CHEMISTRY

G. E. Boyd, "Chemistry of Halogen Atom Recoils in Neutron-Irradiated Crystalline Halates and Perhalates," 155th National Meeting, American Chemical Society, San Francisco, Mar. 31–Apr. 5, 1968.

CHEMISTRY OF AQUEOUS SYSTEMS

G. E. Boyd, "Thermal Effects in Ion-Exchange Reactions," Symposium on Analytical Calorimetry, 155th National Meeting, American Chemical Society, San Francisco, Mar. 31–Apr. 5, 1968 (invited).

†J. S. Johnson, "Hydrolysis, from Solutions to Hyperfiltration," Gordon Research Conference on Inorganic Chemistry, The New Hampton School, New Hampton, N.H., Aug. 7, 1967 (invited).

†J. S. Johnson, "Hyperfiltration," session on Inorganic Ion Exchangers of the Gordon Research Conference on Ion Exchange, Colby Junior College, Colby, N.H., Aug. 21, 1967 (invited).

†K. A. Kraus, "Dynamic Hyperfiltration Membranes," 21st Conference Blood Research Institute, Boston, Mass., Nov. 8, 1967 (invited).

---

[9]Electronuclear Division.

[10]Analytical Chemistry Division.

[11]Chemical Technology Division.

†Based on work performed in the Chemistry Division under the Water Research Program.

†J. S. Johnson* and K. A. Kraus, "Hyperfiltration by Dynamically Formed Membranes," Symposium on Saline Water Conversion, 155th National Meeting, American Chemical Society, San Francisco, Apr. 2, 1968 (invited).

†A. J. Shor,[12] K. A. Kraus, J. S. Johnson,* and W. T. Smith, Jr.,[13] "Salt Rejection Properties of Dynamically Formed Hydrous Zr(IV) Oxide Membranes," 155th National Meeting, American Chemical Society, San Francisco, Apr. 5, 1968.

†R. J. Raridon, "Some Thermodynamic and Transport Properties of Multicomponent Systems," Conference on Properties of Solutions Sponsored by the Office of Saline Water, Cornell University, Ithaca, N.Y., Aug. 14–16, 1967 (invited).

ELECTROCHEMICAL KINETICS AND ITS APPLICATION TO CORROSION

G. H. Cartledge, "The Role of the Molybdate Ion in Passivation," Symposium on Electrode Processes and Inhibition, National Association of Corrosion Engineers, Cleveland, Ohio, Mar. 18–21, 1968 (invited).

NONAQUEOUS SYSTEMS AT HIGH TEMPERATURES

A. S. Dworkin* and M. A. Bredig, "Diffuse Transition and Melting in Fluorite and Anti-Fluorite Type of Compounds: Heat Content of Potassium Sulfide from 298° to 1260°K," 22nd Annual Calorimetry Conference, Thousand Oaks, Calif., June 20–22, 1967.

H. R. Bronstein, "Electromotive Force Studies in Molten Rare Earth Metal–Metal Halide Solutions," Gordon Research Conference on Chemistry of Molten Salts, Meriden, N.H., Aug. 28–Sept. 1, 1967.

CHEMICAL PHYSICS

A. H. Narten, "Some Recent X-Ray Diffraction Studies of a Variety of Liquids with Interpretation in Terms of Models," American Physical Society Meeting, Berkeley, Calif., Mar. 18, 1968 (invited).

G. M. Brown, "The Crystal Structure of 6-Mercaptopurine Monohydrate," American Crystallographic Association Summer Meeting, Minneapolis, Minn., Aug. 20–25, 1967.

W. R. Busing, "An Aid to the Analysis of Interionic and Intermolecular Forces in Crystals," American Crystallographic Association Winter Meeting, Tucson, Ariz., Feb. 4–7, 1968.

W. R. Busing, "Computers, Chemists, and Crystallography," Conference on Computers in Chemistry, University of California, San Diego, June 26–30, 1967 (invited).

L. H. Hall*[14] and G. M. Brown, "The Crystal Structure of Isoboldine Hydrobromide," American Crystallographic Association Winter Meeting, Tucson, Ariz., Feb. 4–7, 1968.

C. K. Johnson, "Information on Molecular Motion Derived from Anisotropic Temperature Factor Coefficients," 2d Materials Research Symposium on Molecular Dynamics and Structure of Solids, Gaithersburg, Md., Oct. 15–19, 1967.

C. K. Johnson, "Segmented-Body Thermal-Motion Analysis: An Extension of the Rigid-Body Approach," American Crystallographic Association Summer Meeting, Minneapolis, Minn., Aug. 20–25, 1967.

---

[12]Reactor Chemistry Division.

[13]Department of Chemistry, University of Tennessee.

[14]ORAU Summer Participant 1966 from Florida Atlantic University, Boca Raton, Fla.; present address, Department of Chemistry, Eastern Nazarene College, Quincy, Mass.

Ralph Livingston,* Henry Zeldes, and Cheryl Voelker,[15] "Paramagnetic Resonance Study of Liquids During Photolysis," The Eighth International Symposium on Free Radicals, Novosibirsk, U.S.S.R., July 29, 1967.

Ralph Livingston, "Electron Spin Resonance Studies of Liquids During Photolysis," Southeastern Section of the American Physical Society, Clemson, South Carolina, Nov. 3, 1967 (invited).

P. F. Dittner* and Sheldon Datz, "Collisional Excitation and Dissociation of Molecular Hydrogen with Slow K^+ Ions," American Physical Society Meeting, Washington, D.C., April 1968 (invited).

L. D. Ellsworth,*[16] L. B. Bridwell,[17] L. C. Northcliffe,[18] C. D. Moak,[6] B. R. Appleton,[19] and Sheldon Datz, "Stopping Power of Gases for ^{127}I and ^{79}Br Ions," American Physical Society Meeting, Washington, D.C., April 1968 (invited).

Sheldon Datz, "Channeled Ion Energy Loss Spectra," American Physical Society, Berkeley, Calif., March 1968 (invited).

---

[15] ORAU Summer Student Trainee from South Dakota State University.

[16] Kansas State University; ORAU Summer Participant, 1967.

[17] Murray State University, Murray, Ky.; ORAU Summer Participant, 1967.

[18] Texas A&M.

[19] Solid State Division.

Lectures

NUCLEAR CHEMISTRY

L. L. Riedinger,[1] "Electric Monopole Strengths for Transitions from the Beta Bands in ^{152}Sm and ^{154}Gd," Physics Seminar, Vanderbilt University, May 22, 1967.

L. L. Riedinger,[1] "Band Mixing in ^{152}Sm and ^{154}Gd," Thermonuclear Division Seminar, Oak Ridge National Laboratory, Feb. 8, 1968.

E. Eichler, "Nuclear Spectroscopy in the $A = 90$ Region," Nuclear Chemistry Seminar, Purdue University, Dec. 4, 1967 (ORAU Traveling Lecture).

G. D. O'Kelley, "Scientific Experiments on Returned Lunar Samples," Department of Physics Seminar, Vanderbilt University, Oct. 13, 1967 (ORAU Traveling Lecture).

RADIATION CHEMISTRY

H. A. Mahlman, "Radiation Chemistry," Academic Year Institute, ORAU, May 3, 1968.

ORGANIC CHEMISTRY

C. J. Collins, "Multiple Isotope Experiments for Determining Carbonium Ions," East Tennessee State University, Johnson City, Tenn., Feb. 6, 1968.

C. J. Collins, "Hydride Shifts During Carbonium Ion Reactions," Pennsylvania State University, University Park, Jan. 29, 1968.

C. J. Collins, "Isotopic Studies on Carbonium Ions. The Mechanism of Hydride Shift," Clemson University, Clemson, S.C., Nov. 17, 1967 (ORAU Traveling Lecture).

C. J. Collins, "The Mechanism of Hydride Shift," Binghamton, Poughkeepsie, Albany, Syracuse, and Canton, N.Y., Mar. 18–22, 1968 (American Chemical Society Lecture Tour).

C. J. Collins, "The Use of Isotopes to Study Organic Reactions," Orange County Section of the American Chemical Society, Anaheim, Calif., May 16, 1968.

C. J. Collins, "The Use of Isotopes to Study Carbonium Ions," University of California, Irvine, May 17, 1968.

C. J. Collins, "Hydride Shift in Norbornyl Compounds," Temple University, Apr. 11, 1968.

B. M. Benjamin, "Rotational Isomerism of Allyl Compounds," Grambling College, Grambling, La., Mar. 11, 1968.

---

[1] ORAU Predoctoral Fellow from Vanderbilt University.

CHEMISTRY OF AQUEOUS SYSTEMS

M. H. Lietzke, "A Two Structure Model for Electrolytic Solutions," University of Georgia, Athens, Feb. 9, 1968.

M. H. Lietzke, "Recent Developments in Aqueous Solution Theory," St. John's University, Queens, N.Y., Apr. 5, 1968.

M. H. Lietzke, "Recent Developments in Aqueous Solution Chemistry," Colgate University, Hamilton, N.Y., Apr. 10, 1968.

*M. H. Lietzke, "Desalination," Augusta, Ga.; Hampton, S.C.; Kinston, N.C.; Charlotte, N.C.; Gaffney, S.C.; Winston-Salem, N.C.; Chapel Hill, N.C.; Norfolk, Va.; Charlottesville, Va.; and Blacksburg, Va.; Mar. 12–23, 1968 (American Chemical Society Lecture Tour).

*M. H. Lietzke, "Desalination" (30-min television lecture), WSJK-TV, Aug. 8, 1967, and Oct. 10, 1967.

*A. E. Marcinkowsky,[2] "Desalination and Filtration with Dynamically Formed Membranes," University of Alabama, Research Institute, Huntsville, Aug. 14, 1967.

*K. A. Kraus, "Hyperfiltration," Parma Research Center, Union Carbide Corp., Cleveland, Ohio, Oct. 30, 1967.

*J. S. Johnson, "Hyperfiltration with Dynamically Formed Membranes," American Machine and Foundry, Stamford, Conn., Mar. 8, 1968.

*K. A. Kraus, "Hyperfiltration," Savannah River Laboratory, Mar. 1, 1968.

*R. J. Raridon, "Desalination," St. Fidelis College, Herman, Pa., Nov. 1, 1967; Pennsylvania Military Colleges, Chester, Nov. 2, 1967; Georgetown College, Georgetown, Ky., Nov. 21, 1967 (ORAU Traveling Lecture); Florida Southern College, Lakeland, Mar. 3, 1968; Rollins College, Winter Park, Fla., Mar. 13, 1968.

*R. J. Raridon, "Use of Isotopes in Chemical Research," Stetson University, De Land, Fla., Mar. 12, 1968; Rollins College, Winter Park, Fla., Mar. 13, 1968.

*R. J. Raridon, "ORNL Water Research Program," University of Delaware, Newark, Nov. 2, 1967.

CHEMICAL PHYSICS

R. A. Gilbert, "Some Calorimetric Equipment, Techniques, and Studies in the ORNL Chemistry Division," Grambling College, Grambling, La., May 13, 1968; Louisiana Polytechnic Institute, Ruston, May 14, 1968 (ORAU Traveling Lecture).

R. W. Holmberg, "The Study of Chemical Free Radicals by Electron Spin Resonance," University of Miami, Coral Gables, Fla., Sept. 25, 1967; Indiana State University, Terre Haute, Nov. 15, 1967; University of Missouri, Kansas City, Dec. 14, 1967; Duquesne University, Pittsburgh, Pa., Feb. 13, 1968 (ORAU Traveling Lecture).

Ralph Livingston, "Etude de l'Effet des Irradiations UV dans les Liquides par la Méthode de Résonance Paramagnétique," Centre d'Etudes Nucléaire de Grenoble, Grenoble, France, July 11, 1967.

Ralph Livingston, "Paramagnetic Resonance Study of Liquids during Photolysis," Hahn-Meitner-Institut für Kernforschung, Berlin, Germany, July 14, 1967.

---

*Based on work performed in the Chemistry Division under the Water Research Program.

[2]Present address: Technical Center, Union Carbide Corp., South Charleston, W.Va.

Ralph Livingston, "Paramagnetic Resonance Study of Photolyzed Liquids," Radiation Research Laboratories, Mellon Institute, Pittsburgh, Pa., Oct. 16, 1967.

Ralph Livingston, "Paramagnetic Resonance Studies of Short-Lived Free Radicals Formed in Liquids by Photolysis," Department of Chemistry, University of Virginia, Charlottesville, Apr. 11, 1968; Department of Chemistry, Baylor University, Waco, Tex., Apr. 19, 1968.

P. A. Agron, "Crystal Chemistry of Polynuclear Iron Carbonyls," Brookhaven National Laboratory, Upton, N.Y., July 13, 1967.

C. K. Johnson, "Stereoscopic Drawings Illustrating the Three-Dimensional Structure of a Protein," University of Virginia, Charlottesville, Feb. 12, 1968.

Sheldon Datz, "Recent Developments in Molecular Beam Studies of Chemically Reactive Collisions," University of Freiburg, Freiburg, West Germany, July 1967; Institute for Atomic and Molecular Physics, Amsterdam, Netherlands, July 1967; University of Washington, Chemistry Colloquium, March 1968.

Sheldon Datz, "Channeling of Ions in Crystals," University of Aarhus, Aarhus, Denmark, Physics Colloquium, July 1967; Institute for Atomic and Molecular Physics, Amsterdam, Netherlands, July 1967; University of Washington, Physics Colloquium, March 1968; University of Virginia, Aerospace Engineering Colloquium, May 1968.

Sheldon Datz, "Interactions of Energetic Particles with Solid Surfaces," Short Course in Gas-Surface Interactions, University of Tennessee Space Institute, Tullahoma, May 1968.

E. H. Taylor, "Application of Molecular Beam Techniques to Chemical Kinetics," Department of Chemistry, University of Virginia, Charlottesville, Mar. 7, 1968.

R. E. Minturn, "Molecular Beam Studies in Physical Chemistry," Lehigh Valley Sectional Meeting of the American Chemical Society, Palmerton, Pa., September 1967.

Russell Baldock, "The Relevance of Isotopes in the Development of the Atomic Theory," Auburn University, Auburn, Ala., Nov. 10, 1967 (ORAU Traveling Lecture).

Russell Baldock, "The Mass Spectrometer as a Tool in Research," Glenville State College, Glenville, W.Va., May 1, 1968; West Virginia Institute of Technology, Montgomery, May 2, 1968 (ORAU Traveling Lecture).

Russell Baldock, "Isotopes," Glenville State College, Glenville, W.Va., May 1, 1968; West Virginia Institute of Technology, Montgomery, May 2, 1968 (ORAU Traveling Lecture).

T. A. Carlson, "Multiple Ionization and Its Relationship to the Many-Body Problem in Atoms," Atomic Physics Seminar, Yale University, Dec. 13, 1967.

T. A. Carlson, "Dependence of Internal Conversion on the Chemical Surroundings," Chemical Physics Seminar, Indiana University, Mar. 14, 1968.